

CONSTANT-VOLUME CARBONIZATION OF BIOMASS

A THESIS SUBMITTED TO THE GRADUATE DIVISION OF THE
UNIVERSITY OF HAWAI'I AT MĀNOA IN PARTIAL FULFILLMENT
OF THE REQUIREMENTS FOR THE DEGREE OF

DOCTOR OF PHILOSOPHY

IN

MECHANICAL ENGINEERING

AUGUST 2018

By

Maidier Legarra Arizaleta

Dissertation Committee:

Scott Q. Turn, Chairperson
Charles M. Kinoshita
Stephen M. Masutani
Trevor J. Morgan
Gérard C. Nihous

Keywords: Pyrolysis, Carbonization, Biomass, Constant-Volume

To Dr. Michael J. Antal

Acknowledgements

In September 2014, after four years of research work under the supervision of Dr. Michael Antal, I was given an opportunity beyond my imagination: becoming a PhD student.

During the years we worked together, my gratitude and admiration to Dr. Antal only grew with time as he became my mentor, inspiration and made me dream deeper, farther and higher than I could have ever imagined.

My appreciation also extends to Dr. Scott Turn and Dr. Trevor Morgan who supervised me after Dr. Antal's loss. Special thanks for their patience and support in this difficult time in my life, for their flexibility and for providing me with the opportunity to complete this PhD. Thanks also to Lloyd Paredes, our scientific Lab technician, for filling the Lab with Aloha spirit and for his invaluable work (many times not noticeable but essential) maintaining and repairing the Lab equipment. Our team in Hawaii gratefully acknowledges support from SINTEF Energi Research AS (Award Number 006356-00003) in Norway under the BioCarb+ Project and the U.S. Office of Naval Research (Award Number N00014-14-1-054). The Norway team acknowledges the financial support from the Research Council of Norway and a number of industrial partners through the project BioCarb+ ("Enabling the Biocarbon Value Chain for Energy", grant number 228726/E20).

And finally, to wrap this up, many thanks to my family and fiancé for their unconditional love, help, serenity and encouragement throughout this PhD.

ABSTRACT

Carbonization in constant-volume reactors has received little attention in current biomass pyrolysis research. In this conversion process, volatiles linger in close proximity to the carbonaceous solid material resulting in long vapor residence times and high partial pressures. The formation of additional secondary charcoal through heterogeneous reactions between the pyrolyzing charcoal and the tarry vapors is therefore greatly enhanced minimizing carbon losses in the form of gases and liquids. The result is the relatively quick formation of a charcoal product with a higher fixed-carbon yield and a lower content of volatiles compared to charcoals derived from conventional, hydrothermal carbonization or flash carbonization processes.

This work presents the effect of processing conditions (pressure, temperature, heating rate, reaction time, biomass loading) and fuel properties (biomass type and particle size) on product yields and char properties in constant-volume carbonization processes. Raising the pre-test system pressure with an inert gas from 0 to 2.17 MPa did not significantly affected product yields or char proximate analysis. It seems that the volatiles partial pressures, rather than the total system pressure, accounts for the dominant effect on the high yields and fixed-carbon contents reported for constant-volume carbonization processes. Raising the reaction time from 30 to 190 minutes and the temperature in a 300-550°C range improved fixed-carbon contents and reduced volatiles while maintaining fixed-carbon yields near theoretical limiting values. In contrast with flash-carbonization or traditional carbonization

observations which showed a beneficial effect of the use of larger particles, constant-volume carbonization manifested higher fixed-carbon contents and yields (or similar under certain conditions) when using smaller biomass particles, offering possibilities for smaller, lower-grade biomass to produce a charcoal high in fixed-carbon.

A fascinating phenomenon has been reported from certain constant-volume carbonization experiments. Under specific heating rate, pressure and temperature conditions, the particulate biomass seems to exhibit a transient plastic phase that converts it into a single solid piece of char. The roles of pressure, temperature, heating rate, particle size and mass loading in the formation of this transient liquid phase are briefly summarized.

Table of Contents

Acknowledgements.....	ii
ABSTRACT.....	iii
LIST OF TABLES.....	x
LIST OF FIGURES.....	xii
LIST OF ABBREVIATIONS AND SYMBOLS.....	xix
CHAPTER 1. INTRODUCTION	1
1.1 Motivation.....	1
1.2 Pyrolysis processes. A brief overview	3
CHAPTER 2. OBJECTIVES.....	12
CHAPTER 3. LITERATURE REVIEW	13
3.1. Effect of a Closed Vessel versus an Open Vessel.....	13
3.2. Effect of Pressure and Gas Flow	15
3.3. Effect of Heat Treatment Temperature	22
3.4. Effect of Heating Rate.....	30
3.5. Effect of Particle Size.....	34
3.6. Effect of Mass Loading.....	38
3.7. Effect of Solid Residence Time	40
3.8. Effect of Feedstock	45

3.8.1. Effect of cellulose, hemicellulose and lignin ratios	46
3.8.2. Effect of mineral matter or ash.....	52
3.9. Kinetic schemes and heat of reaction of biomass pyrolysis	58
CHAPTER 4. MATERIALS AND METHODS	64
4.1. Apparatus Evolution	64
4.2. Materials and Experimental Procedure.....	71
CHAPTER 5. STUDY OF REPRODUCIBILITY, EXPERIMENTAL PROFILE AND EXPERIMENTAL DESIGN	78
5.1. Experimental Profile	78
5.2. Study of Reproducibility.....	84
5.3. List of Experiments and Parity Plot.....	88
CHAPTER 6. RESULTS AND DISCUSSION	104
6.1. Effect of a Closed Vessel versus an Open Vessel.....	104
6.2. Effect of Pressure	106
6.3. Effect of Heat Treatment Temperature	114
6.4. Effect of Heating Rate.....	121
6.5. Effect of Particle Size.....	125
6.6. Effect of Mass Loading.....	130
6.7. Effect of Solid Residence Time or Immersion Time	139
6.8. Effect of Feedstock	143

CHAPTER 7. MODELING EFFORT.....	152
7.1. CVC model 1 (employing kinetic scheme of Shafizadeh and Chin with secondary reactions).....	153
7.2. CVC model 2 (employing kinetic scheme of Koufopoulos et al. with secondary reactions).....	179
7.3. Conclusions from the CVC models	195
CHAPTER 8. CONCLUSIONS.....	197
CHAPTER 9. FUTURE WORK.....	203
APPENDIX A. PRESSURE TERMS.....	205
A.1. Design Pressure.....	205
A.2. Allowable Working Pressure or Maximum Allowable Working Pressure (MAWP)	207
A.2.1. How does Swagelok calculate the Allowable Working Pressure?.....	210
A.2.2. How does Swagelok calculate the Derating Temperature Factors?.....	214
A.3. Catastrophic Failure Pressure and Safety Factor	214
A.4. Allowances for Pressure.....	216
A.5. Burst Diaphragm Rupture Pressure.....	219
A.6. Hydrostatic Testing Pressure	220
A.7. Leak Testing Pressure	221
APPENDIX B. ASME ALLOWABLE STRESS.....	222

APPENDIX C. MULTIPOINT AND HOSE CLAMP THERMOCOUPLES	224
APPENDIX D. SOP and JSA 1: Milling Biomass Material into Finely Divided Particles with a Fritsch Universal Cutting Mill “Pulverisette 19”	226
APPENDIX E. SOP and JSA 2: Assembly, Loading and Leak Testing of the Wall Heated Tubing Bomb.....	233
APPENDIX F. SOP and JSA 3: Analysis of Feed Moisture Content	254
APPENDIX G. SOP and JSA 4: Gas Chromatograph Operation.....	261
APPENDIX H. SOP and JSA 5: Water Displacement Vessel Operation	277
APPENDIX I. SOP and JSA 6: Volume Evaluation of the Wall Heated Tubing Bomb	289
APPENDIX J. SOP and JSA 7: Performing an Experiment, Unloading and Disassembly of the Wall Heated Tubing Bomb.....	299
APPENDIX K. SOP and JSA 8: Analysis of the Charcoal Moisture Content.....	319
APPENDIX L. SOP and JSA 9: Proximate Analysis	326
APPENDIX M. SOP and JSA 10: Replacing and Operating Gas Cylinders.....	334
APPENDIX N. Proximate Analysis Reproducibility Study.....	340
APPENDIX O. MATLAB code CVC model 1	355
APPENDIX P. Temperature, pressure and product distribution history profiles at various heat transfer coefficients predicted by CVC model 1.....	357
APPENDIX Q. MATLAB code CVC model 2	359

APPENDIX R. Temperature, pressure and product distribution history profiles at various heat transfer coefficients predicted by CVC model 2.....	361
BIBLIOGRAPHY	363

LIST OF TABLES

Table 1.1. Typical ranges of operating parameters for torrefaction, hydrothermal carbonization, gasification and pyrolysis (flash pyrolysis, fast pyrolysis, slow pyrolysis and constant-volume carbonization) processes.	5
Table 1.2. Average properties of charcoals for some common applications. Bold numbers indicate required values for a specific application.	9
Table 3.1. Summary of kinetic schemes of biomass pyrolysis proposed in the literature. Data taken from Haseli's Ph.D. thesis. ¹⁸⁵	60
Table 4.1. Moisture content, elemental and proximate analysis, higher heating value, and cellulose, hemicellulose and lignin composition of Norwegian spruce, birch, cellulose, oak and rice husk feedstock.....	72
Table 4.2. Schedule of SOP use during performance of WHTB experiments (number in parentheses reflects number of SOP in list above).	74
Table 5.1. Conditions and results for Wall Heated Tubing Bomb experiments. Superscripts meanings shown in footnotes at the bottom of the table.	89
Table 7.1. References used in the literature models for kinetic and enthalpy data for kinetic scheme of Shafizadeh and Chin. ¹⁶³	156
Table 7.2. Kinetic data and property values applied to constant-volume carbonization (CVC) model 1. Superscripts meanings shown in footnotes at the bottom of the table.....	170
Table 7.3. References used in the literature models for kinetic and enthalpy data for kinetic scheme of Koufopoulos et al. ¹⁷⁸ with secondary reactions.....	181
Table 7.4. Kinetic data and property values applied to constant-volume carbonization (CVC) model 2. Superscripts meanings shown in footnotes at the bottom of the table.....	187
Table A.1. Fractional Stainless Steel Seamless tubing. Allowable working pressures are calculated from an S value of 20 000 psi (137.8 MPa) for ASTM A269 tubing at -20 to 100°F (-28 to 37°C), as listed in ASME B31.3, except as noted. For welded and drawn tubing, a derating factor must be applied for weld integrity:	209
Table A.2. Derating temperature factors.	209
Table A.3. Swagelok Chart of factors for use in calculating allowable working pressures of tubing. Allowable working pressure=Factor x Allowable stress value in psi. Based on ANSI B31.3-1993.	212
Table A.4. Chart of factors calculated with Duffill equation (see Equation A.1).	212

Table A.5. Chart of factors calculated with Lamé equation (see Equation A.2).....	213
Table A.6. Chart of factors calculated with Barlow equation (see Equation A.4).....	213
Table A.7. WHTB catastrophic failure pressure in ksi calculated with data from Swagelok. The unit kilopound per square inch (ksi) is a scaled unit derived from psi, equivalent to a thousand psi.	215
Table B.1. ASME basic allowable stresses in tension for metals	222
Table N.1. Outline of the experimental conditions and goal for the proximate analysis reproducibility study.....	341
Table N.1. Outline of the experimental conditions and goal for the proximate analysis reproducibility study (Continued).	342
Table N.2. Results of moisture content analysis of Kiawe charcoal loaded in two different types of crucibles.....	343
Table N.3. Results of proximate analysis tests of Kiawe charcoal analysed using several methods.....	347
Table N.4. Results of nine proximate analysis tests of Kiawe charcoal analyzed simultaneously.....	349
Table N.5. Results of proximate analysis tests of various mass loadings of Kiawe charcoal.	351
Table N.6. Results of proximate analysis tests of Kiawe charcoal analysed in Ni-Cr crucibles.....	352
Table N.7. Results of proximate analysis tests of various mass loadings of certified reference coal materials.....	354

LIST OF FIGURES

Figure 1.1. Comparison of product yields from different carbonization techniques. CVC: Data from constant volume carbonization experiments at an initial pretest pressure of 0.1 MPa. FC: Data from Flash Carbonization experiments calculated from ⁵² . FAO: Data calculated from the Food and Agriculture Organization (FAO) ⁴⁰ . FAO provided theoretical reference values, method and biomass species were not specified. Fuwape: Data of carbonization in a conventional furnace calculated from ⁵³ . HTC: Data of hydrothermal carbonization calculated from ³³	11
Figure 3.1. On the left, cellulose biochar powder from constant-volume carbonization at initial N ₂ pressure of 0.1 MPa and heat treatment temperature of 300°C. On the right, cellulose biochar from constant-volume carbonization at an initial N ₂ pressure of 2.38 MPa and a heat treatment temperatures of 300-400°C. Figure taken from ⁵⁸	21
Figure 3.2. Schematic representation of effect of secondary reactions on pyrolysis yields at different temperatures. Figure reproduced from Kosstrin. ⁷⁹ Solid line: yields with secondary reactions as in fluidized bed pyrolysis. Dashed line: yields without secondary reactions, indicating only primary decomposition or pyrolysis.....	24
Figure 4.1. Schematic of the Wall Heated Tubing Bomb (WHTB) reactor.....	65
Figure 4.2. Sand bath equipment and protective structure	69
Figure 4.3. Secondary Lexan protective shield	70
Figure 5.1. Temperature and pressure profile of a constant-volume carbonization experiment with birch as the feedstock, a heat treatment temperature of 300°C and an initial nitrogen pressure of 0.1 MPa. (a) Profile of reactor body 1 and (b) Profile of reactor body 2. ● Axis temperature. ■ Sand bath temperature. ▼ Stem temperature. ▲ Wall temperature. -- Pressure.....	80
Figure 5.2. Temperature and pressure profile of a constant-volume carbonization experiment with birch as the feedstock, a heat treatment temperature of 550°C and an initial nitrogen pressure of 0.1 MPa. (a) Profile of reactor body 1 and (b) Profile of reactor body 2. ● Axis temperature sensor 1. ▲ Axis temperature sensor 2. ▼ Axis temperature sensor 3. ■ Sand bath temperature. ▼ Stem temperature. ▲ Wall temperature. -- Pressure.....	81
Figure 5.3. Reproducibility study on the yields of char, condensates and gas products from the constant-volume carbonization of spruce at a heat treatment temperature of 300°C and an initial nitrogen pressure of 0.1 MPa. Negligible free tars were recovered in the experiments. Liquid yield mainly represents water content of the final moist charcoal.	84
Figure 5.4. Comparison between product yields from spruce constant-volume carbonization experiments in the single and dual Wall Heated Tubing Bombs at a heat treatment temperature of 300°C and an initial nitrogen pressure of 0.1 MPa.....	85

Figure 5.5. Reproducibility study on the proximate analysis of charcoals derived from the constant-volume carbonization of spruce at a heat treatment temperature of 300°C and an initial nitrogen pressure of 0.1 MPa. 87

Figure 5.6. Comparison between proximate analyses of charcoals derived from the constant-volume carbonization of spruce in the single and dual Wall Heated Tubing Bombs at a heat treatment temperature of 300°C and an initial nitrogen pressure of 0.1 MPa..... 87

Figure 5.7. Parity plot displaying the experimental fixed carbon yield from Wall Heated Tubing Bomb pyrolysis experiments vs the theoretical values. Shape of the symbols indicate biomass type: ●Oak, ▲Spruce■Birch. Colours represent heat treatment temperature: ■300°C and reactor open to the atmosphere, ■300°C, ■370°C, ■400°C, ■500°C, ■and 550°C. Size represents immersion times: smaller symbols represent short experiments (25-60 min) and larger symbols represent long experiments (70-300 min). Symbol fillings represent special experimental conditions: □ small biomass particles, ◐ use of volume compensation, ◑ under initial nitrogen pressure, ◒ low heating rate, star symbol *on top of a symbol indicates high loading. 102

Figure 5.8. Close-up of the top right corner of Figure 5.7. Shape of the symbols indicate biomass type: ●Oak, ▲Spruce■Birch. Colours represent heat treatment temperature: ■300°C and reactor open to the atmosphere, ■300°C, ■370°C, ■400°C, ■500°C, ■and 550°C. Size represents immersion times: smaller symbols represent short experiments (25-60 min) and larger symbols represent long experiments (70-300 min). Symbol fillings represent special experimental conditions: □ small biomass particles, ◐ use of volume compensation, ◑ under initial nitrogen pressure, ◒ low heating rate, star symbol *on top of a symbol indicates high loading 103

Figure 6.1. Effect of sealing the Wall Heated Tubing Bomb reactor on the product yields from the pyrolysis of oak sawdust (0.149-0.425 mm) at a heat treatment temperature of 300°C. Liquid yield on the open reactor experiment and gas yields on both experiments were not measured. 105

Figure 6.2. Effect of sealing the Wall Heated Tubing Bomb reactor on the proximate analysis of charcoal from the pyrolysis of oak sawdust (0.149-0.425 mm) at a heat treatment temperature of 300°C. 105

Figure 6.3. Effect of initial nitrogen pretest pressure on the product yields from the constant-volume carbonization of oak sawdust (0.149-0.425 mm) under immersion times of 21-134 minutes at a heat treatment temperature of 300°C. 107

Figure 6.4. Effect of initial nitrogen pretest pressure on the proximate analysis of charcoal from the constant-volume carbonization of oak sawdust (0.149-0.425 mm) under immersion times of 21-134 minutes at a heat treatment temperature of 300°C. 107

Figure 6.5. Effect of initial nitrogen pretest pressure on the product yields from the constant-volume carbonization of birch sawdust (<2 mm) under an immersion time of 190 minutes at heat treatment temperatures of 300 and 400°C. 108

Figure 6.6. Effect of initial nitrogen pretest pressure on the proximate analysis of charcoals from the constant-volume carbonization of birch sawdust (<2 mm) under an immersion time of 190 minutes at heat treatment temperatures of 300 and 400°C.	109
Figure 6.7. Effect of nitrogen pressure on the theoretical product distribution of the constant-volume carbonization of birch predicted by FactSage.....	110
Figure 6.8. On the left, oak biochar powder from constant-volume carbonization at an initial N ₂ pressure of 0.1 MPa and a heat treatment temperature of 300°C. On the right, oak biochar from constant-volume carbonization at an initial N ₂ pressure of 2.69 MPa and a heat treatment temperatures of 300-370°C.....	111
Figure 6.9. (a) Scanning electron microscopy image of birch charcoal from constant-volume carbonization at a heat treatment temperature of 300°C and an initial nitrogen pressure of 0.1 MPa, (b) and (c) higher magnification views of selected areas in (a).	112
Figure 6.10. (a) Scanning electron microscopy image of birch charcoal from constant-volume carbonization at a heat treatment temperature of 300°C and an initial nitrogen pressure of 2.17 MPa, (b) higher magnification view of selected area in (a).....	112
Figure 6.11. (a) Scanning electron microscopy image of birch charcoal from constant-volume carbonization at a heat treatment temperature of 400°C and an initial nitrogen pressure of 0.1 MPa, (b) and (c) higher magnification views of selected areas in (a).	113
Figure 6.12. (a) Scanning electron microscopy image of birch charcoal from constant-volume carbonization at a heat treatment temperature of 400°C and an initial nitrogen pressure of 2.17 MPa, (b) - (e) higher magnification views of selected areas in (a).....	113
Figure 6.13. Effect of heat treatment temperature on the yields of char, condensate and gas from the constant-volume carbonization of oak at an initial N ₂ pressure of 4.79 MPa and at various immersion times.....	114
Figure 6.14. Effect of heat treatment temperature on the proximate analysis of charcoal from the constant-volume carbonization of oak at an initial N ₂ pressure of 4.79 MPa and at various immersion times.....	115
Figure 6.15. Effect of heat treatment temperature on the yields of char, condensate and gas from the constant-volume carbonization of birch and spruce at an initial N ₂ pressure of 0.1 MPa and 190 min immersion time.	115
Figure 6.16. Effect of heat treatment temperature on the proximate analysis of charcoals from the constant-volume carbonization of birch and spruce at an initial N ₂ pressure of 0.1 MPa and 190 min immersion time.	116
Figure 6.17. Effect of temperature on the theoretical product distribution from the constant-volume carbonization of birch predicted by FactSage.	117

Figure 6.18. (a) Scanning electron microscopy image of birch charcoal from constant-volume carbonization at a heat treatment temperature of 500°C and an initial nitrogen pressure of 0.1 MPa, (b) -(d) higher magnification views of selected areas in (a), (e) higher magnification view of selected area in (d)..... 119

Figure 6.19. (a) Scanning electron microscopy image of birch charcoal from constant-volume carbonization at a heat treatment temperature of 550°C and an initial nitrogen pressure of 0.1 MPa, (b)-(d) higher magnification views of selected areas in (a)..... 119

Figure 6.20.(a) Birch charcoal produced under constant-volume carbonization at a heat treatment temperature of 550°C, an initial nitrogen pressure of 0.1 MPa, particle size <2 mm, standard loading of 130 g/L and an immersion time of 190 minutes. (b) Birch charcoal produced under constant-volume carbonization at a heat treatment temperature of 300°C, an initial nitrogen pressure of 0.1 MPa, particle size <0.2 mm, higher loading of 240 g/L and an immersion time of 190 minutes. (c) Oak charcoal produced under constant-volume carbonization at a heat treatment temperature of 300-400°C, an initial nitrogen pressure of 2.69 MPa, a coarse particle size, loading of ~120 g/ L and an immersion time of 55 minutes. (d) Cellulose charcoal produced under constant-volume carbonization at a heat treatment temperature of 300-400°C, an initial nitrogen pressure of 2.4 MPa, particle size 50-180 µm, loading of ~200 g/ L and an immersion time of 85 minutes..... 120

Figure 6.21. Effect of heating rate on the product yields from the constant-volume carbonization of birch (<2 mm) at an initial N₂ pressure of 0.1 MPa. 122

Figure 6.22. Effect of heating rate on the proximate analysis of charcoals from the constant-volume carbonization of birch (<2 mm) at an initial N₂ pressure of 0.1 MPa. 123

Figure 6.23. (a) and (c) Scanning electron microscopy images of birch charcoal from constant-volume carbonization at an initial nitrogen pressure of 0.1 MPa, a heat treatment temperature of 300°C and at a “slow” heating rate (b) and (d) higher magnification views of selected areas in (a) and (c) 124

Figure 6.24. (a) Scanning electron microscopy images of birch charcoal from constant-volume carbonization at an initial nitrogen pressure of 0.1 MPa, a heat treatment temperature of 500°C and at a “slow” heating rate. (b) and (c) higher magnification views of selected areas in (a). (d) and (e) higher magnification views of selected areas in (c) ... 124

Figure 6.25. Effect of particle size on the yields of char, condensates and gas from the constant-volume carbonization of spruce and birch at 300°C and at an initial N₂ pressure of 0.1 MPa..... 127

Figure 6.26. Effect of particle size on the proximate analysis of charcoals from the constant-volume carbonization of spruce and birch at 300°C and at an initial N₂ pressure of 0.1 MPa..... 128

Figure 6.27. Charcoals from constant-volume carbonization of spruce at an initial N₂ pressure of 0.1 MPa, immersion time of 190 min and a heat treatment temperature of 300°C at particle sizes of <2 mm (on the left) and <0.2 mm (on the right). 129

Figure 6.28. (a) Scanning electron microscopy image of birch (<0.2 mm) charcoal from constant-volume carbonization at a heat treatment temperature of 300°C and an initial nitrogen pressure of 0.1 MPa, (b) higher magnification view of selected area in (a).	129
Figure 6.29. Effect of mass loading on the yields of char, condensates and gas from the constant-volume carbonization of birch, spruce, cellulose and oak at 300°C and at an initial N ₂ pressure of 0.1 MPa.....	132
Figure 6.30. Effect of mass loading on the proximate analysis of charcoals from the constant-volume carbonization of birch, spruce, cellulose and oak at 300°C and at an initial N ₂ pressure of 0.1 MPa.....	133
Figure 6.31. Effect of adding a dead volume on the yields of char, condensates and gas from the constant-volume carbonization of birch and spruce at an initial N ₂ pressure of 0.1 MPa.....	135
Figure 6.32. Effect of adding a dead volume on the proximate analysis of charcoals from the constant-volume carbonization of birch and spruce at an initial N ₂ pressure of 0.1 MPa.	135
Figure 6.33. Effect of mass loading on the theoretical product distribution from the constant-volume carbonization of birch at 300°C predicted by FactSage	136
Figure 6.34. (a) Scanning electron microscopy image of charcoal from constant-volume carbonization of birch grains of particle size <0.2 mm at a mass loading of 165 g/L, at a heat treatment temperature of 300°C and an initial nitrogen pressure of 0.1 MPa, (b), (c) and (d) higher magnification views of selected areas in (a), (b) and (c) respectively.....	138
Figure 6.35. (a) Scanning electron microscopy image of charcoal from constant-volume carbonization of birch grains of particle size <0.2 mm at a mass loading of 240 g/L, at a heat treatment temperature of 300°C and an initial nitrogen pressure of 0.1 MPa, (b), (c), (d) and (e) higher magnification views of selected areas in (a), (b), (c) and (d) respectively.	138
Figure 6.36. Effect of immersion time on the yields of char, condensates and gas from the constant-volume carbonization of spruce and birch at an initial N ₂ pressure of 0.1 MPa..	140
Figure 6.37. Effect of immersion time on the proximate analysis of char from the constant-volume carbonization of spruce and birch at an initial N ₂ pressure of 0.1 MPa.	141
Figure 6.38. (a) Scanning electron microscopy images of charcoal from constant-volume carbonization of birch grains of particle size <0.2 mm at a mass loading of 240 g/L, at a heat treatment temperature of 300°C, an initial nitrogen pressure of 0.1 MPa and a short immersion time of around 30 min, (b), (c) and (d) higher magnification views of selected areas in (a), (b), (c) respectively.	143

Figure 6.39. Effect of feedstock on the yields of char, condensates and gas from constant-volume carbonization at an initial N ₂ pressure of 0.1 MPa, immersion time of 190 minutes and mass loading of 130 g/L.	144
Figure 6.40. Effect of feedstock on the proximate analysis of char from constant-volume carbonization at an initial N ₂ pressure of 0.1 MPa, immersion time of 190 minutes and mass loading of 130 g/L.	145
Figure 6.41. Effect of feedstock on the yields of char, condensates and gas from constant-volume carbonization at an initial N ₂ pressure of 0.1 MPa and a heat treatment temperature of 300°C.....	146
Figure 6.42. Effect of feedstock on the proximate analysis of charcoals from constant-volume carbonization at an initial N ₂ pressure of 0.1 MPa and a heat treatment temperature of 300°C.....	146
Figure 6.43. Parity plot displaying the experimental fixed carbon yields from CVC vs the theoretical values predicted by FactSage for cellulose, rice husk, oak, birch and spruce at a heat treatment temperature of 300°C and a pretest pressure of 0.1 MPa.	149
Figure 6.44. Effect of small changes in the birch elemental analysis (provided by two laboratories) on the theoretical product fixed-carbon yield from the constant-volume carbonization of birch at 300°C predicted by FactSage.	151
Figure 7.1. Kinetic scheme of Shafizadeh and Chin ¹⁶³ with secondary reactions.....	154
Figure 7.2. History profile of wood, char and volatile yields predicted by CVC model 1 assuming constant-volume carbonization of biomass at a heat treatment temperature of 300°C and an initial pretest pressure of 0.1 MPa.	173
Figure 7.3. History profile of temperature and pressure predicted by CVC model 1 assuming a constant-volume carbonization of biomass at a heat treatment temperature of 300°C and an initial pretest pressure of 0.1 MPa	173
Figure 7.4. Effect of heat treatment temperature on the yields of char and gas predicted by CVC model 1.	176
Figure 7.5. Kinetic scheme of Koufopoulos et al. ¹⁷⁸ with secondary reactions.....	180
Figure 7.6. History profile of wood, char and volatile yields predicted by CVC model 2 assuming constant-volume carbonization of biomass at a heat treatment temperature of 300°C and an initial pretest pressure of 0.1 MPa.	189
Figure 7.7. History profile of temperature and pressure predicted by CVC model 2 assuming a constant-volume carbonization of biomass at a heat treatment temperature of 300°C and an initial pretest pressure of 0.1 MPa.	189

Figure 7.8. History profile of wood, char and volatile yields predicted by CVC model 2 assuming constant-volume carbonization at a heat treatment temperature of 300°C and an initial pretest pressure of 0.1 MPa. The primary and secondary fractions of char and volatile yields are shown.	190
Figure 7.9. Effect of heat treatment temperature on the yields of char and volatiles predicted by the CVC model 2 using deposition factors of 1.45 and 2.....	192
Figure A.1. Allowable working pressure with temperature for a 1” outer diameter Swagelok tube with a wall thickness of 0.21 cm (0.083”).....	208
Figure C.1. Multipoint Thermocouple.....	224
Figure C.2. Hose Clamp Thermocouple D6-16-U for Reactor Walls and D6-6-U for Reactor Arms.....	225
Figure P.1. History profiles of product yields (Left) and pressure and temperature (Right) predicted by CVC model 1 using a heat transfer coefficient of 10^{-3} kW/K. The rest of the model parameters are given in Table 7.2.....	357
Figure P.2. History profiles of product yields (Left) and pressure and temperature (Right) predicted by CVC model 1 using a heat transfer coefficient of 10^{-4} kW/K. The rest of the model parameters are given in Table 7.2.....	357
Figure P.3. History profiles of product yields (Left) and pressure and temperature (Right) predicted by CVC model 1 using a heat transfer coefficient of 10^{-5} kW/K. The rest of the model parameters are given in Table 7.2.....	358
Figure R.1. History profiles of product yields (Left) and pressure and temperature (Right) predicted by CVC model 2 using a heat transfer coefficient of 10^{-3} kW/K. The rest of the model parameters are given in Table 7.4.....	361
Figure R.2. History profiles of product yields (Left) and pressure and temperature (Right) predicted by CVC model 2 using a heat transfer coefficient of 10^{-4} kW/K. The rest of the model parameters are given in Table 7.4.....	361
Figure R.3. History profiles of product yields (Left) and pressure and temperature (Right) predicted by CVC model 2 using a heat transfer coefficient of 10^{-5} kW/K. The rest of the model parameters are given in Table 7.4.....	362

LIST OF ABBREVIATIONS AND SYMBOLS

A_i : Preexponential factor of reaction i for Arrhenius equation

Bi: Biot number

COP: Conference of the Parties

$c_{p,i}$: Specific heat capacity of component i . Component i can refer to wood w , charcoal c , total volatiles g , non-condensable gas G and tar T

CVC: Constant-Volume Carbonization

daf: Dry ash free

db: Dry basis

DTG: Derivative Thermogravimetric

E : Energy

E_i : Activation energy of reaction i for Arrhenius equation

FAO: Food and Agriculture Organization

fC: fixed-Carbon

FC: Flash Carbonization

fCC: fixed-Carbon Content

GROT: GRenar Och Toppar. Norwegian acronym for branches and treetops

h_i : Specific enthalpy of component i . Component i can refer to wood w , charcoal c , total volatiles g , non-condensable gas G and tar T

h_{rad} : Heat transfer coefficient

HHV: Higher Heating Value

HNEI: Hawaii Natural Energy Institute

HTC: Hydrothermal Carbonization

HTT: Heat Treatment Temperature

IEA: International Energy Agency

JSA: Job Safety Analysis

k_i : Kinetic constant of reaction i

k : Thermal conductivity

k_{SS} : Thermal conductivity of stainless steel

L: Length

L_c : Characteristic length

m_{bio} : Dry mass of biomass feedstock

m_{char} : Dry mass of charcoal

M_i : Mass of component i . Component i can refer to wood w , charcoal c , total volatiles g , non-condensable gas G and tar T

MC: Moisture Content

NA: Not Available

NTNU: Norwegian University of Science and Technology

P: Pressure

P_o : Initial reactor pressure

PAHs: Polycyclic Aromatic Hydrocarbons

PCB: Polychlorinated Biphenyls

PhD: Philosophiae Doctor. Latin acronym for doctor of philosophy

\dot{Q} : Heat rate

r_k : Rate of reaction k

R_o : Ideal gas constant

Rad: Radio

R³Lab: Renewable Resources Research Laboratory

SEM: Scanning Electron Microscopy

SINTEF: Stiftelsen for INdustriell og TEknisk Forskning. Norwegian acronym for the foundation for scientific and industrial research

SOP: Standard Operating Procedure

t: time

T : Temperature

T_o : Initial reactor temperature

T_s : Sand bath temperature

TC: Thermocouple

TGA: Thermogravimetric Analysis

TPP: Transient Plastic Phase

t_w : Wall thickness reactor

U : Internal energy

u_i : Specific internal energy of component i . Component i can refer to wood w , charcoal c , total volatiles g , non-condensable gas G and tar T

V : Reactor volume

v_i : Specific volume of component i . Component i can refer to wood w , charcoal c , total volatiles g , non-condensable gas G and tar T

VM: Volatile Matter

VOC: Volatile Organic Compounds

V_{wo} : Initial volume occupied by the solid in the reactor

wb: Wet basis

WHTB: Wall Heated Tubing Bomb

W_i : Molecular weight of component i . Component i can refer to wood w , charcoal c , total volatiles g , non-condensable gas G and tar T

wt: Weight

y_{char} : Charcoal yield

y_{fc} : fixed-Carbon yield

Δh_k : Heat of reaction k

ρ_i : Apparent density of component i . Component i can refer to wood w , charcoal c , total volatiles g , non-condensable gas G and tar T

CHAPTER 1. INTRODUCTION

This chapter provides an overview of the importance of renewable energy and biocarbon production on the world stage and the contributions HNEI has made to this area of research.

1.1 Motivation

On June 1, 2017, U.S. President Donald Trump announced that the United States would no longer participate in the Paris Agreement.¹ The agreement, reached at the Paris climate conference (COP21) in December 2015, united 195 countries on “the first-ever universal, legally binding global climate deal” with the long-term goal of limiting the global temperature rise well below 2°C.²

Understandably, international reactions to Trump’s announcement from the whole political spectrum came fast. Some were supportive, especially the ones coming from coal executives, who seem to largely benefit from Trump’s decision.³ But overwhelmingly, reactions were critical bringing up concerns about the impacts for the U.S. and global economies, for the climate and for political international cooperation.^{3,4} In response to President Trump’s announcement, several nations such as China and India, the European Union, and even mayors and governors of several U.S. cities reiterated their own commitment to the mitigation of climate change.^{3,5} Critics often claimed that, regardless of President Trump’s strategy, with governments facing difficult

decisions to tackle economic crises, increasing prices for fossil-derived energy and rising costs related to health impacts, the transition from fossil fuel energy towards renewables is unstoppable.^{3,5-7}

The potential of an international bioenergy market has already been assessed by a number of studies. However, one major obstacle for development of bioenergy production is a lack of information on market conditions both regionally and globally. In order to develop efficient policies and measures to encourage the uptake of renewable energy, knowledge of the market region and its main characteristics of supply, demand, trade and market prospects are essential.

The 2009 IEA Bioenergy Task 40-Country report for Norway by Trømborg and Leistad gives an overview of the situation regarding bioenergy in Norway for the year 2007.⁸ With a national target of increasing bioenergy use to 50 pJ by 2020 (i.e. doubling the 2007 production), the Norwegian government launched a strategic plan in 2008 that outlined the necessary measures to reach this bioenergy target. Since less than half of the annual growth of round wood in Norway is harvested annually, the report recognized forest resources as the major potential source for increasing bioenergy production in Norway. However, the sustainable potential use of biomass for energy production is uncertain. Øyvind Skreiberg reported that high quality (and expensive) woody biomass is currently the main expected contributor for the Norwegian bioenergy future but emphasized that Norway possesses major unexploited low-grade energy resources of waste wood in the form of branches and treetops – known in their Norwegian acronym as GROT– as well as straw, sewage sludge and other agricultural residues that would most likely go unused as

a resource. “*Upgrading such challenging fuels to biocarbon will dramatically change this picture*”.^{9,10}

The Norwegian ferroalloy industry is one of the sectors that have taken interest in this project. At present, they use fossil coal and coke as reductants in the smelting process, producing about 3 Tg of CO₂ emissions a year.¹¹ Substituting biocarbon for coal and coke will reduce these emissions considerably, and “*Norway is funding a major study of wood carbonization for metallurgical and fuel applications based on a collaboration between the Hawaii Natural Energy Institute (HNEI), the Norwegian University of Science and Technology (NTNU), and SINTEF (Norway)*”.¹² As part of this research effort, Norwegian biomass is imported to the R³Lab at the HNEI in its raw form, where it is transformed from a low-value fuel into a more valuable, high-energy biocarbon.

1.2 Pyrolysis processes. A brief overview

During the mid-19th century, there was a major transition of energy sources that was propelled by the technological advances of the industrial revolution.¹³ Prior to it, mankind energy needs were met by muscle power combined with animal power, and by combustion of biomass resources, mainly wood and peat, for light and heat generation.^{14,15} Ever since the industrial revolution took off, the consumption of more powerful, reliable and apparently inexhaustible energy resources started to grow exponentially until present times. Its effects, not noticeable in the origins, became clear many years later. Fossil fuels are non-renewable, their primary reserves

will eventually be depleted and their consumption is widely associated with causing extensive damage to environmental health. Governments began to tap and invest in alternative, renewable and clean energy sources. Biomass and other green energy sources recaptured interest and made headlines as potential options.¹⁶

Biomass is a carbon-neutral, plentiful and cheap fuel but has a low energy density. Its energy can be directly released in the form of heat via combustion or can be harnessed by converting the biomass into more energy dense biofuels. Torrefaction, liquefaction, pyrolysis or gasification technologies have focused on capturing the energy in biomass as solid, liquid or gaseous biofuels.

The pyrolysis of biomass has been receiving a lot of attention in recent years. Pyrolysis is the thermal break-down of carbon-based materials in the absence of an oxidizer. The composition and relative amounts of the final solid (biocarbon), liquid (water and oil/tar) and gas (CO_2 , CO , CH_4 , H_2) pyrolytic products are determined by the composition of the original biomass and the pyrolysis method and conditions. Pyrolysis processes can be optimized for the production of liquids (oil/tar) which operate at high heating rates and short residence times known as fast pyrolysis. Conventional or slow pyrolysis is used to maximize solid biocarbon products by operating with slow heating rates and long residence times, often termed as carbonization processes. More recently other carbonization processes have been developed to improve the yield and/or quality of the solid products such as Flash CarbonizationTM, hydrothermal carbonization (HTC) and constant-volume carbonization (CVC), which is the focus of this PhD.

Table 1.1 displays a typical range of operating parameters for torrefaction, hydrothermal carbonization, gasification and pyrolysis processes. Bold numbers on the product yields indicate the desired product for a specific process.

Table 1.1. Typical ranges of operating parameters for torrefaction, hydrothermal carbonization, gasification and pyrolysis (flash pyrolysis, fast pyrolysis, slow pyrolysis and constant-volume carbonization) processes.

Process	Temperature (°C)	Solid residence time (s)	Heating rate (°C/s)	Particle size (mm)	Vapor residence time (min)	Product yield (wt.%)		
						Solid	Liquid	Gas
Gasification ¹⁷⁻¹⁹	>800 ¹⁹ 800-1000 ^{a,17,18}	<0.5 ¹⁷⁻¹⁹	>1000 ¹⁷⁻¹⁹	<0.2 ^{18,19} Dust ¹⁷	<1 ¹⁹	10 ¹⁹	5 ¹⁹	85 ¹⁹
Fast pyrolysis	~500 ¹⁹ 600-1000 ^{17,18}	0.5-10 ^{18,19} 0.5-5 ¹⁷	200- 1000 ¹⁹ 10- 200 ^{17,18}	<1 ^{18,19}	<2 ¹⁹	12 ¹⁹ 15- 25 ²⁰	75 ¹⁹ 60 - 75 ²⁰	13 ¹⁹ 10- 20 ²⁰
Slow pyrolysis ¹⁷⁻¹⁹	300-700 ^{17,18} 400-660 ¹⁹	Minutes ¹⁸ to hours ^{17,19}	0.1-1 ¹⁷⁻¹⁹	5-50 ¹⁷⁻¹⁹	5-30 ¹⁹	35 ¹⁹	30 ¹⁹	35 ¹⁹
Flash carbonization ²¹⁻²⁴	400-750 ^{21,23}	Minutes to hours ¹⁷⁻¹⁹	~1 ²¹	<100 ²¹ <200 ²²	NA ^b	30 - 50 ¹⁷⁻¹⁹	NA ^b	NA ^b
Constant-volume carbonization ²⁵⁻²⁷	300-550 ^{c,25-27}	Minutes to hours ²⁵⁻²⁷	<1 ²⁷	<2 ²⁵⁻²⁷	Minutes to hours ²⁵⁻²⁷	55 ²⁵⁻²⁷	30 ^{d,25-27}	15 ²⁵⁻²⁷
Torrefaction ²⁸⁻³⁰	200-300 ²⁸⁻³⁰	Minutes to hours ²⁸⁻³⁰	<1 ^{29,30}	<2 ²⁸ <30 ²⁹ <40 ³⁰	<1 ^e	80 ^{28,29}	15 ^{28,29}	5 ^{28,29}
Hydrothermal carbonization ³¹⁻³⁵	150-300 ³¹⁻³⁵	Minutes ³³ - Hours 31,32,34,35	<5 ^f	<6 ³¹ <~0.3 ^{33,35} <3 ³⁴	Minutes ³³ - Hours ^{31,32,34,35}	50 - 80 ³¹⁻³⁶	5- 20 ^{31,32}	2- 5 ^{31,32}

^a Up to 2000°C with solar furnaces¹⁷

^b Not Available (NA)

^c Previous work in constant-volume carbonization in the Lab tested temperatures up to 400°C. This work will present results at temperatures up to 550°C

^d Negligible free tars are recovered from constant-volume carbonization. Liquid yield represent water content mainly present on the final moist charcoal

^e Torrefaction is usually performed under atmospheric conditions. In these processes, volatiles escape as they get released from the solid matrix. Some processes operate under pressure³⁷ which will increase the vapor residence time

^f Heating rate calculated from history profile in ³¹

The final biocarbon product derived from carbonization processes has a wide range of applications including use as: fuel for cooking and barbecuing, fuel for heat and power generation; a reductant in the metallurgical industry; an adsorbent for removing pollutants from air or water streams; production of advanced carbon materials; supercapacitors; hydrogen storage; and a natural soil amendment to sequester carbon and enhance soil quality for bedding plants and commercial crops.³⁸

During the carbonization processes, the virgin biomass is heated in the absence of oxygen to a certain temperature, driving off a major part of its volatile matter leaving its carbon behind and, hence, increasing the relative carbon content, fixed-carbon content and calorific value.

Traditional charcoal production has relied principally on lighting wood-stacks inside earth mounds or excavated pits. Part of the wood is combusted to generate the heat necessary for pyrolyzing the remainder. These methods are still widely used in many countries despite the inherent lack of control over the process conditions or the final charcoal properties (uneven quality and low conversion efficiencies with long reaction times of hours or days) and the negative impact on the environment.³⁹ Traditional methods have reported efficiencies of around 25 wt.%,⁴⁰ expressed as the yield of charcoal, $y_{\text{char}} = m_{\text{char}}/m_{\text{bio}}$, where m_{char} and m_{bio} are the dry masses of charcoal and biomass feedstock respectively. These low charcoal yields have a direct impact on deforestation and substantial carbon emissions when collecting and processing the wood necessary for charcoal production.⁴¹

Over the past 200 years, the development of industrial production technology has offered a deeper understanding of the basic phenomena that govern pyrolytic processes and has permitted a greater control over them. Surprisingly, despite these advances, charcoal production methods have barely changed since ancient times and modern versions of traditional methods have improved efficiencies to just 25-37 wt%.⁴² Finally, new carbonization methods (HTC, CVC or flash carbonization) have successfully reported higher yields of around 50 wt%.

Achieving an increased charcoal yield has little value unless charcoal quality parameters are specified and maintained.⁴³ The properties of a “good-quality” charcoal are defined by its intended end use. Table 1.2 lists the average properties of charcoals for some common applications. Required values are given in bold. For example, metallurgical industries can demand charcoals with fixed-carbon contents above 70%⁴⁴ or above 85%⁴⁵. The fixed-carbon (fC) content of charcoal, along with its volatile matter (VM) content and ash content are estimated by proximate analysis. The fixed-carbon content is determined on a dry basis by subtracting the sum of ash and volatile matter percentages from 100%, that is to say, %fC = 100 – %VM – %ash. This property has been identified as the main one for metallurgical grade charcoal since it is the fixed-carbon that determines the charcoals effectiveness as a reductant.⁴⁶ Hence, there are strict demands from the metallurgical industry regarding the charcoals fixed-carbon content.

The domestic market is more flexible; a charcoal with lower fixed-carbon and more volatiles is preferred since charcoal with these properties is harder to break and easier to ignite.⁴⁵ Charcoals

intended for soil conditioning, or biochar, require different criteria. A good biochar is characterized by a high content of elemental carbon, low volatile matter content, a low content of heavy metals, and a high surface area and porosity. In this way, the retention of nutrients and water, and the growth of beneficial microorganisms are promoted. The fixed-carbon content, although not needed to be specified in biochars, has been proved to be related to the char aromaticity and the stability of the biochar in soil.^{47–49} This area of research is still in its infancy and more research on biochar applied as a soil amendment is required to understand the ideal charcoal properties for soil amendment applications, to demonstrate its benefits and to prove economic viability and sustainability.

With the aim of creating a more meaningful definition of efficiency for biocarbon production, Antal and Grønli³⁹ used the charcoal yield and fixed-carbon content parameters to define a new parameter, the fixed-carbon yield (y_{fC}). It is determined by multiplying the charcoal yield (y_{char}) by the relative purity of the carbon created from the dry ash-free feedstock as $y_{fC} = y_{char} \cdot \%fC / (100 - \%ash_{feed})$.

Table 1.2. Average properties of charcoals for some common applications. Bold numbers indicate required values for a specific application.

Domestic	fCC ^a : 60-80% Balance VM ^b : 20-40% ⁴⁵ Ash: 0.5-5% ⁴⁵ MC ^c : 3-15% ,Up to 15% with high volatiles ⁴⁵ HHV ^d : 28-33MJ/kg ⁴⁵ Bulk density: 250-400 kg/m ³ . ⁴⁵
Metallurgy	fCC^a: >70% ⁴⁴ , >80% ⁵⁰ , 85-90% ⁴⁵ VM ^b : 10-30% Balance Ash: 0.5-5% ⁴⁵ MC ^c : 3-5% ⁴⁵ HHV ^d : 28-33MJ/kg ⁴⁵ High fracture resistance for blast furnace charcoals ⁴⁶
Charcoal for Activated carbon production	fCC^a: >82% ⁴⁶ VM ^b : 10% ⁴⁶ Ash: 4% ⁴⁶ MC ^c : 4% ⁴⁶ pH=4-10 (Acidity test of a water extract of the charcoal) ⁴⁶
Soil amendment	Carbon content>50% ⁵¹ H/C_{org} molar ratio<0.7 ⁵¹ O/C_{org} molar ratio<0.4 ⁵¹ Respect thresholds on heavy metals (Pb, Cd , Cu ,Ni, Hg, Zn, Cr), polycyclic aromatic hydrocarbons (PAHs), polychlorinated biphenyls (PCB), dioxins and furans listed on ⁵¹ . No limits were imposed on the following properties but their values must be listed: Volatile Organic Compounds (VOC), pH, bulk density, water content, ash content, specific surface area and the biochar nutrient contents with regard to nitrogen, phosphorus, potassium, magnesium and calcium. Usually, a biochar with an alkaline pH, a high surface area (>150m ² /g), low in water, low in ash, and a high biochar nutrient content is preferred
^a Fixed-carbon content (fCC) ^b Volatile matter (VM) ^c Moisture Content (MC) ^d Higher Heating Value (HHV)	

The following chapter presents the accumulated knowledge regarding the effect of pressure, gas flow, heat treatment temperature (HTT), heating rate, particle size, mass loading, solid residence time and feedstock on biomass carbonization. The vast majority of studies in literature investigated the carbonization process in a variety of reactor set-ups wherein the pyrolytic vapor products are partially or totally swept away from the vicinity of the hot carbonaceous solid—configurations referred to in the present work as “open” reactors.

Carbonization in constant-volume reactors has received little attention in literature despite the promising results that have been reported. CVC permits a better control of the carbonization process and the resultant charcoals are characterized by higher fixed-carbon yields in comparison to other carbonization processes such as conventional carbonization, hydrothermal carbonization or flash carbonization (see Figure 1.1). This work investigates the effect of process variables on product distributions and char properties from CVC. The ultimate goal is to gain understanding of the CVC process in order to be able to tailor the charcoals properties to those required by specific processes.

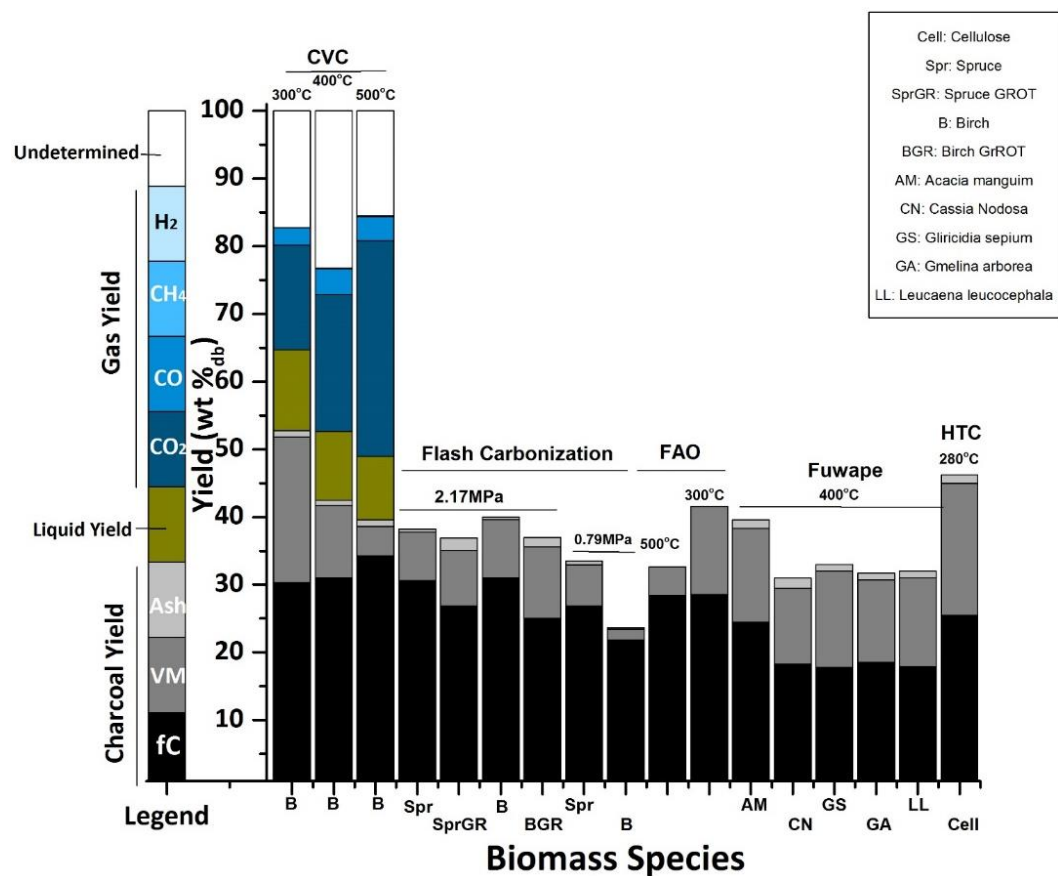


Figure 1.1. Comparison of product yields from different carbonization techniques. CVC: Data from constant volume carbonization experiments at an initial pretest pressure of 0.1 MPa. FC: Data from Flash Carbonization experiments calculated from⁵². FAO: Data calculated from the Food and Agriculture Organization (FAO)⁴⁰. FAO provided theoretical reference values, method and biomass species were not specified. Fuwape: Data of carbonization in a conventional furnace calculated from⁵³. HTC: Data of hydrothermal carbonization calculated from³³.

CHAPTER 2. OBJECTIVES

Carbonization in sealed vessels has opened up a potential field for the rapid production of charcoal with remarkably high fixed-carbon yields when compared to conventional methods. Eight factors will be investigated - (i) closed vessel versus open vessel, (ii) initial reactor pressure, (iii) HTT, (iv) particle size, (v) heating rate, (vi) mass loading, (vii) immersion time and (viii) biomass type-- with the objective of understanding the effects of operating parameters on the yields of the final products, the proximate analysis, elemental composition, morphology and energy density of the final charcoals manufactured from CVC.

The experimental campaign includes a total of 49 experiments to explore the effects of these parameters. Details are provided in Chapter 5. In Chapter 6, experimental yields, char proximate analysis and char morphology trends obtained from CVC were compared with results from other carbonization methods and from theoretical values predicted by thermodynamics. Finally, Chapter 7 developed two models for CVC based on literature modelling data from “open” carbonization configurations and evaluated them against experimental results.

CHAPTER 3. LITERATURE REVIEW

The literature review serves as the basis for the research proposed in this document. It summarizes the effects of pressure, gas flow, HTT, heating rate, particle size, mass loading, solid residence time and biomass feedstock on carbonization. The review on the vast knowledge accumulated on carbonization in “open” reactors is expanded with limited information found on past CVC studies. Given the promising results and the large number of unknowns revealed during the preliminary CVC studies, experimental research on CVC has continued at HNEI. Chapter 6 “Results and Discussion”, as and when required, provides additional comparisons of experimental results obtained in the present study with relevant work from the literature.

3.1. Effect of a Closed Vessel versus an Open Vessel

The beneficial effect on carbonization when using a closed vessel versus an open vessel was first observed by Violette⁵⁴ in the 1800’s. When Violette heated a wood sample in a sealed glass tube, he observed a substantial rise in pressure and temperature during the carbonization process and a remarkable increase of the final charcoal yield that went from 29.7 to 78.7%. The importance of pressure during carbonization is widely recognized. Most of the work in the literature regarding carbonization under pressure utilizes what we will refer to as “open” reactors, i.e. processes with openings or with gas flows that sweep reaction products from the reaction zone. Few researchers have followed Violette’s pioneering work on CVC by using completely sealed vessels.

Dr. Antal's research group in Hawai'i focused on the study of pyrolysis under elevated pressure including some work using sealed vessels. Their findings regarding CVC started in the late 1990's with Mok et al.⁴² confirming the positive influence on the final charcoal yields when a sealed reactor was used (i.e. that lacked a flow of an inert gas). In addition, Várhegyi et al.⁵⁵ performed research using sealed crucibles with small pinholes (strictly speaking, not CVC). The results showed that the increase in char yield is accompanied by a higher production of H₂O, CO, and CO₂. Unfortunately, none of Mok or Várhegyi charcoals was subjected to proximate analysis therefore the effect on fixed-carbon yield was not determined.

Proximate analysis on charcoals from a wide diversity of lignocellulosic substrates was conducted during later pyrolytic work with a thermogravimetric analyzer and a constant-pressure reactor (Note, none of this work was CVC). The thermogravimetric analysis research reported higher fixed-carbon yields from closed crucibles with pinholes than from open crucibles.⁵⁶ Likewise, chars manufactured in a pressurized vessel at 1.0 MPa revealed higher fixed-carbon yields than chars from an open retort,⁵⁷ remarkably the yields from the pressurized reactor approached the equilibrium fixed-carbon yield predicted by thermodynamic calculations.

Proximate analysis of the final chars derived from the pyrolysis of cellulose in open (at constant atmospheric pressure) and closed (CVC) batch reactors were reported more recently.^{25,58} The reactor, referred to as the Wall Heated Tubing Bomb (WHTB), can be hermetically sealed and can withstand high pressures and temperatures.^{25,58} Completely closing the reactor during pyrolysis produced fixed-carbon yields close to the equilibrium limiting values whereas leaving

the WHTB reactor open to the atmosphere resulted in a considerable loss of carbon during pyrolysis leaving a charcoal whose fixed-carbon yield is far from the theoretical maximum predicted at equilibrium.^{25,58} The improvement on the properties of the char manufactured under elevated pressures is explained by the higher residence times and/or partial pressures of the tars within and surrounding the carbonaceous particles. These two parameters have been discerned to be key to the enhancement of secondary, heterogeneous charring reactions between the hot reacting charcoal and the tarry vapors.^{39,42,59–62} Due to the promising initial results on CVC, work with the WHTB has been continued using mainly oak, spruce and birch woods as feedstocks. A comparison of experimental results obtained from carbonization of oak in a sealed reactor versus an open reactor is provided in Section 6.1.

3.2. Effect of Pressure and Gas Flow

In a review paper describing the role of process conditions during pyrolysis, Antal and Grønli³⁹ recognized the noticeable improvement of charcoal yields by using high pressure and low gas flows during biomass pyrolysis. Higher pressures and lower sweep gas flow rates have been acknowledged to increase the residence times and partial pressure of volatiles in the reaction zone leading to increased amounts of secondary reactions^{39,59–62} that form more char at the expense of tar yield.^{59,60} For instance, Mok and Antal⁶³ observed a doubling in the char yields when they combined elevated pressures and low carrier gas flow rates in a fixed bed reactor.

Likewise, Zaror and co-workers⁶⁴ more than doubled the char recovered during cellulosic pyrolysis when a flowing gas stream was interrupted in a Gray-King retort. In contrast, studies on carbonization under pressure with high flows of carrier gas in fixed bed and hot-rod reactors conducted by Palmer,⁶⁵ Frolich et al.⁶⁶ and Kandiyoti and co-workers⁶⁷—mentioned in Antal and Grønli's paper³⁹— did not observe a pressure influence on char yields. The studies suggest that if the gas flow rate employed is high enough so that tarry vapors spend an insignificant amount of time in contact with the rest of the pyrolysis products, secondary charring reactions are minimized or inhibited. The results obtained by Shafizadeh and co-workers⁶⁸ regarding carbonization under vacuum can also be explained by the suppression of these secondary charring reactions.

An external inert gas can be used to decouple the effects of the volatiles partial pressure from the total reactor pressure during constant-volume carbonization. Adding an inert gas to the reactor prior to sealing the system and conducting biomass carbonization increases the total system pressure while keeping the volatile vapor pressure unchanged. Mok et al.⁴² were the first to envision this idea when they added dry ice and cellulose inside closed crucibles prior to heating during pyrolysis experiments. They found that increasing the total system pressure with CO₂ did not influence the yield of charcoal (fixed-carbon content was not measured) or the amount of heat released. Additionally, increasing the initial cellulose mass loading resulted in greater charcoal yields and faster, more exothermic reactions that originated at lower temperatures. Thus, Mok et al. identified the volatile partial pressure—instead of the total system pressure—as the prevailing parameter which affects the char yield and amount of heat released.

Proximate analysis on the final charcoals produced from recent CVC experiments on cellulose confirmed the lack of influence of an inert gas pressure on the product yields.⁵⁸ Nonetheless, the fixed-carbon contents showed a slight improvement with higher inert pressures.⁵⁸ For example, when the initial nitrogen pressure was increased from 0.1 to 4.79 MPa, the fixed-carbon content improved from 54 to 58%. Nevertheless, the increased carbon mass balance (from 92 to 101.5%) may indicate that these differences in fixed-carbon content are not significant, this finding was later revisited by conducting CVC of oak and birch under various pressures in the WHTB (see Section 6.2 for details).

The lack of influence of inert gas pressure on fixed-carbon contents and product yields further supported the conclusion that the concentration of volatiles and/or their increased residence time, not the total system pressure, dictates the product yields and charcoal proximate analysis values. This finding is in agreement with thermochemical equilibrium calculations on the CVC processes which predicts a negligible effect of pressure on the final fixed-carbon yields and presents solid carbon as the major product, followed by gaseous byproducts of carbon dioxide, water, methane, and traces of carbon monoxide and hydrogen (see Section 6.2). Using equilibrium calculations as a basis, the lack of influence from increasing pressure on theoretical product yields and the product distribution of the constant-pressure pyrolysis (not CVC) of cellulose at 400°C were reported by Antal et al.⁶⁹

In conclusion, partial pressure and/or residence time of the tarry vapors within and surrounding the solid appear to play a crucial role on the charcoal yields and the chemical properties of the

final charcoal during pyrolysis. The effect of elevating the system pressure through the addition of an external gas to the system is strongly dependent on the reactor set-up. In “open” reactors where the tarry vapors are partially or totally evacuated from the solid matrix by a reactor opening or an external gas flow, the total system pressure and gas flow has a strong effect on the vapor pressure and residence time of volatiles. In this case, higher pressures and lower gas flows increase cross-linking reactions which ultimately enhances the formation of secondary char and reduces tar yields. In addition, if the gas flows employed are high enough that tarry vapors quickly escape the reaction zone (even when operating at elevated pressure), secondary reactions are minimized and consequently, pressure appears to have an insignificant effect on the yields. On the other hand, increasing the system pressure in a sealed batch reactor lacking an external gas flow by the pre-addition of an inert gas does not significantly affect the partial pressure and residence times of volatiles. Therefore, yields and fixed-carbon contents remain roughly constant.

The processing conditions employed during pyrolysis also play a key role on the morphology of the final charcoal produced. Experimental observations have demonstrated the formation of a transient plastic phase (TPP) under particular conditions. Lédé et al. observed a lubricating effect when wood was exposed to compression forces against hot mobile disks or found charcoal structures with smooth surface areas when cellulose was subjected to fast pyrolysis.^{70,71} The formation of a liquid intermediate phase has also been verified by high speed photography during ablative pyrolysis at 700 °C.^{72,73}

In “open” reactors, pressure, as well as temperature and heating rate (see Sections 3.3 and 3.4 for details) seem to affect the plastic behavior of biomass.^{74,75} In wire mesh reactors operating at high heating rates and HTTs of 800-1000°C, Cetin et al.⁷⁴ reported that increasing pyrolytic pressures from 1 to 20 bar lead to chars characterized by smaller and smoother surface areas with larger pores. They explained the effect of pressure by the entrapment of volatiles in the solid, which promotes char melting and consequently closes micropores but opens larger pores through the release of bubbles. Their results also showed a decrease in char apparent gasification reactivity values with higher pressures. Possible explanations for this behavior were attributed to changes in the char chemical structure or intrinsic reactivity rather than to char surface areas.

In an entrained flow reactor, Newalkar et al.⁷⁵ observed the existence of an intermediate optimum pressure of around 10 bar that resulted in a more graphitic char with a more pronounced molten stage, a lower oxygen content and a reduced surface area characterized by larger cavities and less micropores. Making use of coal analogies, Newalkar et al.⁷⁵ depicted lignocellulosic char structural changes in detail. Below the optimum pressure, as pressure was raised (from 5 to 10 bar in their case), volatiles try to escape the solid matrix causing a promotion of larger-sized pores due to big gas bubbles evolving inside the char. The result is an expansion and melting of the char that consequently rearranged itself into a more graphitic solid with a reduced number of micropores and lower surface area. In addition, the discharge of volatiles released oxygen from the char structure and further promoted graphitization by restricting the creation of stable oxygen-containing linkages in the solid. Above 10 bar, raising the outer pressure restricted the release of volatiles and blocked particle swelling. Being a larger

molecule than hydrogen, oxygen was preferentially retained in the char matrix leaving behind carbon-oxygen bonds and a less graphitic solid with a more open surface structure.

Newalkar et al. emphasized that the effects of pressure and temperature on char morphology cannot be studied independently. Their scanning electron microscopy (SEM) images displayed more intense changes of char morphology with pressure when the temperature was raised in a 600-800°C range. Temperatures from 800 to 1000°C produced a lesser pressure effect. A phenomenon called shrinkage provided an explanation to this behavior (see Section 3.3). Illerup and Rathmann⁷⁶ also reported a negligible pressure effect on char gasification reactivity at high temperatures that ranged between 700 and 900°C during the CO₂ gasification of biomass.

In sealed reactors, the addition of a pretest inert gas pressure has been shown to have no effect on product yields and char proximate analysis (see above). Nevertheless, it did show a fascinating phenomenon on the char morphology. Figure 3.1 (duplicated from reference⁵⁸) shows the appearances of two CVC charcoals. One was produced under an initial atmospheric pressure and a HTT of 300°C, while the other was produced under elevated pressure at a HTT of 300-400°C. The visual observations and SEM images appear to reveal a TPP that produce a single solid piece of char above a certain pretest pressure and HTT.⁵⁸

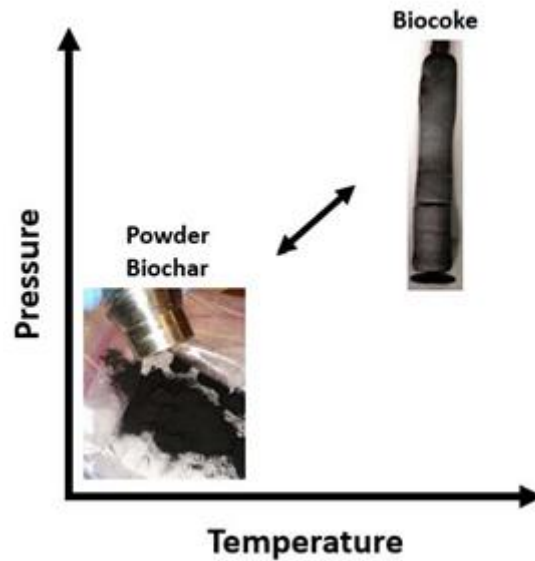


Figure 3.1. On the left, cellulose biochar powder from constant-volume carbonization at initial N₂ pressure of 0.1 MPa and heat treatment temperature of 300°C. On the right, cellulose biochar from constant-volume carbonization at an initial N₂ pressure of 2.38 MPa and a heat treatment temperatures of 300-400°C. Figure taken from ⁵⁸.

The use of elevated pressures has also been reported to have a beneficial effect on expediting the whole carbonization process, which appears to be the result of an enhancement of the heat transfer of the gases contained in pyrolysis reactors.⁷⁷ Antal et al.⁵⁷ shortened the pyrolysis processing time by days by using pressurized reactors with a gas flow versus carbonization in Missouri kilns (conventional pyrolysis), and concluded that this advantageous feature may be regarded by the manufacturer as a more decisive variable than the improvements observed on charcoal yields.^{39,45}

3.3. Effect of Heat Treatment Temperature

While there is general consensus on the critical role of temperature on biomass pyrolysis, the biomass temperature is not a uniform value through time and space during the carbonization process. This makes direct comparisons between researchers difficult or impossible. The temporal and spatial temperature gradients within the biomass, especially intense during the heating period, are related to a number of factors such as grain size, heating rate, biomass type, grain orientation, bed packing density, and reactor geometry. For example, analogous external heating rates or temperature readings may occur in distinct temporal and spatial temperature gradients within the char particle. These internal temperature gradients can heavily affect the product yields and properties of the final charcoal produced. Despite disparities in product yields reported in literature, some features are usually common. Raising the temperature above 280°C typically leads to lower char yields,^{39,40,53,78} higher gas yields⁷⁸⁻⁸⁰ and a greater char devolatilization resulting in char products with a higher content of fixed-carbon and less volatiles.^{39,40,53}

The Food and Agriculture Organization (FAO) of the United Nations⁴⁰ and Fuwape⁵³ tabulated typical char yields and proximate analysis measurements for different biomass materials at various carbonization temperatures. For example, at 300°C, the FAO⁴⁰ reported a typical char yield of 42% - not counting the wood which was burned to provide heat to the process (the pyrolysis process is not specified but is assumed to be slow pyrolysis). The charcoal produced has approximately 68% fixed-carbon and 31% volatile matter. At 500°C, the char yield reduced to 33% and the charcoal devolatilized resulting in values of fixed-carbon and volatile matter of

85% and 13% respectively. In a conventional furnace, Fuwape⁵³ reported the same trends of decreasing char yield, increasing fixed-carbon and decreasing volatile matter with increasing carbonization temperature. However, some values are considerably different from those reported by FAO. For example, the pyrolysis of five varieties of wood at 500°C resulted in char yields between 20 and 32% (versus a value of 33% reported by FAO), fixed-carbon contents ranging from 62 to 72% (versus a 85% fixed-carbon content reported by FAO) and volatile matters from 23 to 31% (versus a 13% volatile matter content reported by FAO).

Kosstrin⁸⁰ presented a fast pyrolysis model over the temperature range of 425 to 925°C in a bubbling fluidized bed. Figure 3.2 (reproduced from Kosstrin) illustrates qualitative changes in char, oil (tar) and gas yields with temperature. The product distributions occur in such a way that the total mass of the three components (tar, char and gas) remains constant and equal to the original feedstock mass. The solid curves depict product yields from the pyrolytic bed and the dashed curves exemplify yields assuming complete elimination of both tar-cracking and charring secondary reactions (it is implied this means a zero residence time for the volatiles). Both cases show that increasing the temperature leads to lower char yields and higher gas yields. The tar yield curves show distinct behaviors with temperature. Increasing the temperature in the absence of secondary reactions results in an increased production of tar, whereas the tar yield exhibits a maximum peak when secondary reactions are included. Dissimilarities between the curves demonstrate the impact of secondary reactions. Accounting for secondary reactions - versus assuming an absence of them - results in the formation of more char and gas at the expense of tar yield. The extent of these secondary reactions appears to escalate with increasing temperature. The asymmetric bell-shaped curves of tar yields with temperature are usually displayed by

fluidized beds.⁵⁹ Tar release increases with temperature until reaching a critical temperature. Above this, thermal cracking occur resulting in a decline of tar as temperature increases.

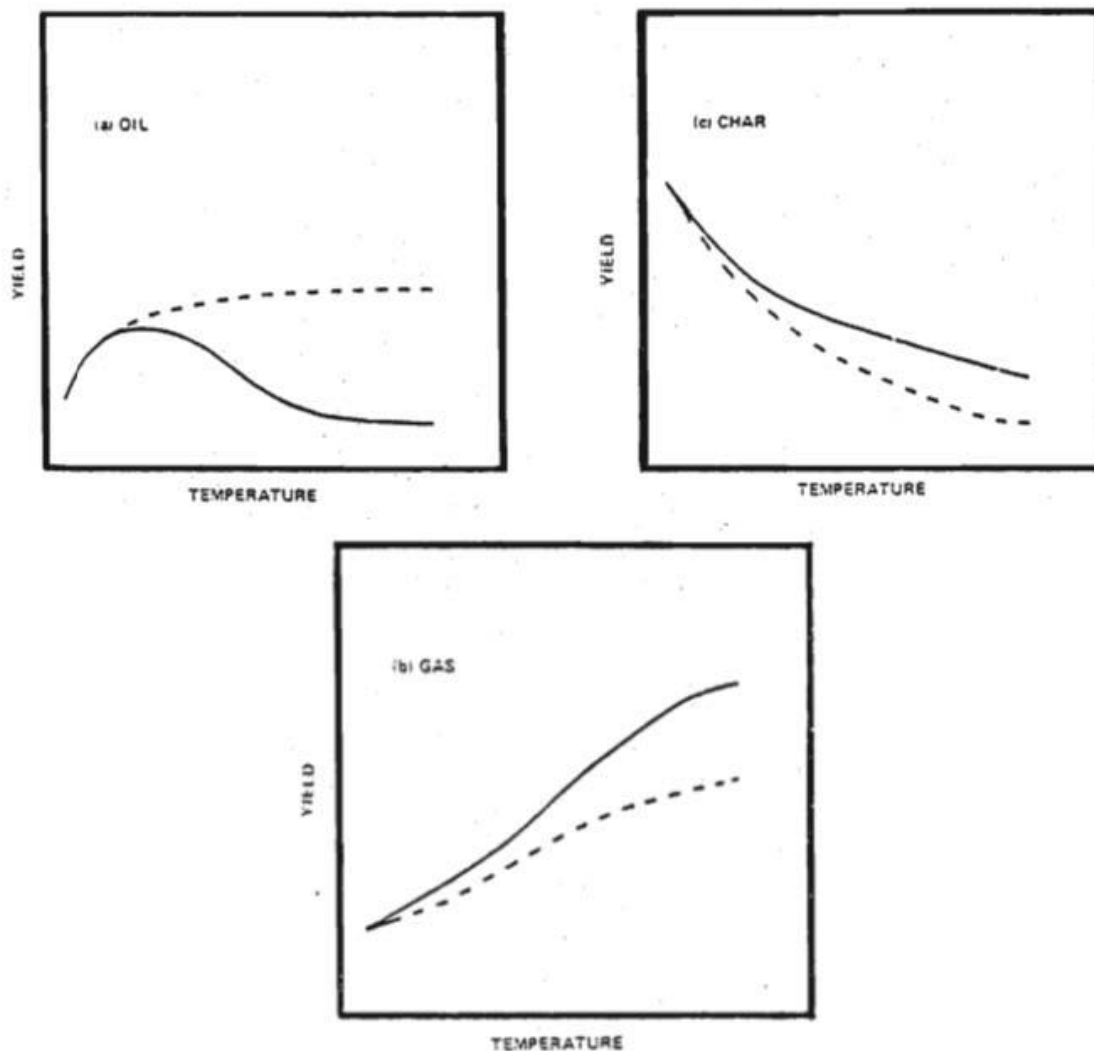


Figure 3.2. Schematic representation of effect of secondary reactions on pyrolysis yields at different temperatures. Figure reproduced from Kosstrin.⁷⁹ Solid line: yields with secondary reactions as in fluidized bed pyrolysis. Dashed line: yields without secondary reactions, indicating only primary decomposition or pyrolysis.

Stiles and Kandiyoti⁶⁰ and Morgan and co-workers^{81,82} experimentally confirmed the findings from Kosstrin concerning the effect of temperature and residence time on the tar yields. Stiles and Kandiyoti⁶⁰ reported the tar yields recovered from a fluidized bed reactor with variable

freeboard height and a constant nitrogen flow. They observed diminishing amounts of tar derived from biomass and coal when the tar residence time was increased. The role of increasing temperature initially increased the tar yield until a maximum was reached; above this temperature vapor tar cracking reactions lead to diminished oil/tar yields. Raising the temperature from 600 to 700°C lessened the tar yield by ~30 wt%. Additionally, extending the residence time from 0.25 s to 3.5 s at 600°C reduced the tar yield by about ~30 wt% (daf cellulose). Morgan and co-workers^{81,82} pyrolyzed banagrass in a fluidized bed reactor over a temperature range from 400 to 600°C and over a range of residence times from 1 to 12 s. The char yield declined with increasing temperature and the tar yield exhibited a maximum at ~450°C at a residence time of 1 s. An increase in temperature above ~450°C and residence time >1 s resulted in the production of more gas and light volatiles with the loss of oil/tar.

The composition of tars recovered from fast-pyrolysis has been described in literature. The tar liquid product consists of a complex mixture of condensable hydrocarbons covering a wide range of molecular weights. A detailed description of tar properties can be found elsewhere.^{83,84} A considerable fraction of these compounds present high molecular weights and low stabilities.⁸⁵ Different theories have been reported as an attempt to explain the origin of the heavier species present in the tarry liquid condensed from pyrolytic processes.⁸⁶ One theory explains the formation of high molecular weight species by weak chemical bonds between lighter volatiles. A second explanation is derived from the true volatile composition, which includes heavy aerosols, i.e. a gas mixed with liquid and solid whose product distribution is influenced by the reactor configuration. Peacocke⁸⁷ observed that ablative reactors produced a lighter tar than fluidized bed reactors. *“This is consistent with the formation of a liquid intermediate (issued from biomass*

*depolymerization) undergoing further cracking or vaporisation on the hot surface of ablative reactors, but being directly ejected into the gas/vapour phase on fluidized beds”.*⁸⁶

Piscorz et al.⁸⁸ demonstrated aerosol to be a direct intermediate of a significant fraction of the final pyrolytic products. There is a wide diversity of opinion regarding the aerosol formation.⁸⁶ Its origin can be explained by an incomplete condensation of volatiles in the gas product, by the capture of the liquid intermediate in the char solid structure or by being directly ejected into the gas-phase due to micro explosions of water vapor and the liquid intermediate.⁸⁶ The tar composition is heavily influenced by the pyrolytic temperature as well. Raising the temperature to around 800°C appears to intensify tar-cracking reactions which results in a shift of tar composition to products with lower molecular weight.^{75,89} Further increasing the temperature, i.e. 900°C, led to an agglomeration and combination of these cracked species which causes the formation of heavier tertiary products such as polycyclic aromatic hydrocarbons, often reported for gasification processes.^{60,89,90}

Similar to the experimental observations made in regard to “open” reactors, raising the temperature from 300 to 400°C during CVC reduced the charcoal yield and volatile matter content, while increasing the fixed-carbon content and gas yield mainly as CO₂ evolution.^{27,58} Typically, applying more severe carbonization conditions, e.g. increasing the temperature, improves the fixed-carbon content of the charcoal but sacrifices some fixed-carbon yield. For example, charcoal from *Leucaenaleucocephala* produced by Fuwape in a conventional furnace at 250°C had a fixed-carbon content of 29% and a fixed-carbon yield of 28%. Increasing the

carbonization temperature to 400°C was able to greatly improve its fixed-carbon content to 56% but suffered the loss of around 9% (absolute) of its fixed-carbon yield. Raising the temperature to 700°C further improved the fixed-carbon content up to 70% and produced a charcoal with a fixed-carbon yield comparable to that obtained at 400°C.

Raising the CVC HTT produced a final solid product rich in fixed-carbon content and low in volatiles while maintaining the fixed-carbon yield near-theoretical values.^{27,58} All these are attractive properties for both char suppliers and customers. Nonetheless, operating the CVC batch processes at industrial scale may be costly due to the high-pressure conditions. One of the aims of the on-going research is to generate the data required to estimate production costs at larger scales to determine whether the process is viable at commercial scale.

The HTT used to drive the carbonization process plays a key role on the morphology of the final char. In “open” reactors, the appearance of a TPP has been observed on chars manufactured at temperatures above 550-600°C^{74,75,89} under fast heating rates ($\sim 500^\circ\text{C/s}$ ⁷⁴– $\sim 10^4^\circ\text{C/s}$ ^{74,75,91}). Fast heating results in an interaction of a volatile release effect and a simultaneous char softening effect.^{75,91} This interaction heavily influences the resultant char morphology.

Jarvis et al.⁸⁹ provided a detailed description of the morphology evolution of a char produced in a laminar entrained flow reactor at temperatures from 450 to 950°C and heating rates of $\geq 1000^\circ\text{C/s}$. At 450°C, devolatilization causes chemical and physical changes in the char. the physical cell wall thickness of the char significantly reduces and the final char structure becomes

a skeleton of the parent material. At 550°C, the cell walls fragmented developing a microporous structure while the first signs of bubble formation appear. Char begins to soften while volatile release continues and the gases trapped in the char begin to generate gas-filled pockets. As the temperature increases and approaches a value of 850°C, the char softening intensifies and bubbles increase in size. These two factors cause the micropores to close while at the same time the char swells like a balloon and large cavities are opened on the char surface due to the bursting of bubbles.^{75,91} The chars produced present a cenospheric morphology. Within this temperature range, the formation of primary volatiles seems to end at 650°C, at this point gas evolution continues through secondary and tertiary tar-cracking. Above 650°C, char circularity plateaus and the char becomes progressively more brittle. Finally, at temperatures above 850°C, the cenosphere particles appear to rupture releasing the trapped gases and reduce in size. This phenomenon is referred to as shrinkage (see below).⁷⁵

Newalkar et al.⁷⁵ reported a similar description of char morphology profile with temperature during the fast-pyrolysis of biomass in an entrained flow reactor in a temperature range between 600 -1000 °C and pressures between 5 and 20 bar. They confirmed that increasing the temperature until 800°C developed char melting and swelling which typically resulted in a more graphitic char with surface areas characterized by less micropores and more meso- and macropores and with lower ratios of H/C and O/C. The only exception to this trend was observed by chars produced at 600 and 800°C at the highest pressure of 20 bar. In this case, the 800°C material presented a lower degree of graphitization and a higher O/C ratio. They explained this deviation in the behavior by a pressure influence. At the elevated pressure, the O molecule could be retained longer in the char structure compared to the small and light hydrogen molecule

giving rise to the formation of stable oxygen-containing bonds that limit graphitization and leaves the structure more open. Chars produced at temperatures above 800°C can manifest shrinkage.⁷⁵ The elevated temperatures provoke the rupture of carbon-oxygen linkages which in turn, closes micropores, reduces the char surface area and leads to char collapse.⁹² A number of models have included this shrinkage effect during pyrolysis in order to improve predictions of conversion times and product yields.⁷³ Some linearly correlate the particle size reduction with the biomass composition (one-dimensional models), and others take into account reaction evolution as well as calculate local collapse of the particle volume (two-dimensional models).⁷³

In CVC experiments, the appearance of a TPP has been observed at much lower temperatures and heating rates than in “open” reactors.^{27,58} For example, molten phases have been reported in a constant-volume reactor that contained birch at initial room conditions of pressure and temperature that was subsequently heated to 400°C under a heating rate of around 1°C/s,²⁷ or when carbonizing cellulose where the initial N₂ pressure was 2.40 MPa at room temperature before heating to 260°C or higher under a similar heating rate.⁵⁸ When elevated pressures are used, it appears that the tars captured within the char evolve (react and/or interact) during the CVC process to enhance char plasticization and shift the char softening point to relatively low temperatures. Increasing the temperature and pressure appear to intensify the molten stage of char and can transform the charcoal from a grainy structure to a single coke-looking product that adopts the shape of the reactor vessel.^{27,58}

3.4. Effect of Heating Rate

In a review paper, Morgan and Kandiyoti⁵⁹ compiled experimental measurements of char yields from cellulose pyrolysis in various “open” reactor designs and processing conditions. A trend of increasing char yield with decreasing heating rate was observed. When a wire-mesh reactor with a heating rate of $\sim 1000^{\circ}\text{C}/\text{s}$ was used to pyrolyze cellulose at 600 and 900°C ,⁹³ or when using a fluidized-bed reactor with a heating rate above $200^{\circ}\text{C}/\text{s}$ and a HTT of 500°C ,⁶⁰ negligible amounts of char were produced; in both of these examples small particles were used ($<152\ \mu\text{m}$). In the same way, Pindoria et al⁶⁴ recovered almost no char when fine wood particles ($<100\ \mu\text{m}$) were flash-heated to temperatures above $550\text{--}600^{\circ}\text{C}$. The char yield dramatically increased when using a McBain thermogravimetric balance to pyrolyze a thin ($100\ \mu\text{m}$) cellulosic layer with a slower heating rate of $14^{\circ}\text{C}/\text{min}$ and a HTT of 480°C or when using a Gray-King retort (fixed-bed) with a $5^{\circ}\text{C}/\text{min}$ heating rate to the same temperature for the same feedstock.

Martin et al.⁹⁴ observed a decrease in char yields with an increase in fixed-carbon contents as the heating rate increased from 0.98 to $9.44^{\circ}\text{C}/\text{min}$ when pyrolyzing oak chips in an atmospheric pressure batch reactor heated to temperatures up to 490°C . Likewise, Angin⁹⁵ reported the same pattern of lower char yields and higher fixed-carbon contents in biochars produced in a fixed-bed reactor with a flow of inert gas at heating rates of 10 , 30 and $50^{\circ}\text{C}/\text{min}$ (the reactor pressure was not specified). Chen et al.⁹⁶ studied the pyrolysis of bamboo in a thermogravimetric analyzer and a fixed-bed reactor at a HTT of 700°C using heating rates between 5 and $30^{\circ}\text{C}/\text{min}$. A significant effect of the heating rate was observed on the kinetic parameters and product yields with preferential secondary decomposition of volatiles in the fixed-bed reactor leading to greater char

yields. Activation energy and gas yields increased with the heating rate while char and liquid yields decreased. The final charcoals presented similar fixed-carbon contents.

Quantitatively, Chan and co-workers⁹⁷ developed a polynomial model that correlated the product yields to particle size, moisture content, heating rate and grain orientation for the pyrolysis of pinewood in a reactor subjected to temperatures as high as 1000°C where volatiles were removed by a stream of helium while maintaining the reactor pressure at 1 atm absolute pressure. The heating rate was identified as the dominant variable on the resultant yields. Antal et al.⁹⁸ concluded that decreasing the heating rate seems to cause the char yield to reach an asymptotic maximum value. Conversely, a minimum char yield was not detected. Negligible char, if any, was observed when a high enough heating rate was used in combination with small particles of biomass (<100-152 μm).^{57,99} Notice that to achieve fast-pyrolysis, small particles are also a requirement since large particles pose an impediment to rapid internal heating.

Shafizadeh¹⁰⁰ provided an explanation regarding the effect of heating rate on the yield of char derived from cellulose. Below 300°C, the main pyrolytic reaction is the dehydration of cellulose into a more stable species (anhydrocellulose) which results in a higher yield of the final char. At temperatures above 300 °C, a more unstable levoglucosan is formed which tends to depolymerize into primary tar resulting in lower char yields. When rapid heating rates are used, the time period the biomass is exposed to lower temperatures is reduced which inhibits the formation of charcoal.

Reed and co-workers¹⁰¹ explained the influence of the heating rate on the product yields. They considered that the biomass initially decomposes into a solid that subsequently melts and, if the temperature is high enough, vaporizes. Un-vaporized tar molecules, present at lower temperatures, combine into larger molecules by forming more stable bonds that finally produce char. Higher heating rates promote the rapid vaporization of tar which reduces the amount of char formation. Lewellen et al.¹⁰² hypothesized that lower temperatures and larger particles increase the residence time of volatiles within the particle which favors the production of secondary char through reactions between primary volatiles and the pyrolyzing solid mass. Bradbury et al.¹⁰³ measured the effect of temperature on the volatile and char yields. At 300°C, a volatile/char ratio of two was determined versus a ratio of fifty at 600°C. In conclusion, slow heating rates offer additional time at lower temperatures which enhance repolymerization reactions between tar molecules and with the solid matrix. Whereas rapid heating can cause biomass and cellulose to completely breakdown into volatiles.

All these literature findings regarding the role of heating rate on biomass pyrolysis pertain to “open” reactor set-ups. To our knowledge, the effect of heating rate in sealed reactors has not been reported. In CVC, volatiles that would be swept away when using “open” reactors remain in the reaction zone and interact with the pyrolyzing char, and consequently produce additional secondary char. As a result, the production of high solid yields in CVC processes may not be limited, as observed in “open” reactors, to a slow release of volatiles which is attained by slow heating but could be also extended to a faster volatile release related to higher heating rates. See Section 6.4 for details of the heating rate effect on experimental product yields and properties of char from the CVC of biomass.

The heating rate has also been found to greatly influence the evolution of the char structure in both “open” and sealed reactors. In “open” reactors, slow heating causes the particle to lose the majority of its volatile matter prior to softening (around 600°C).⁷⁵ Consequently, the final char basically retains the skeleton structure of the virgin biomass. Fast-heating ($\sim 500^\circ\text{C}/\text{s}$ ⁷⁴- $\sim 10^4^\circ\text{C}/\text{s}$ ^{74,75,91}) enables the interaction between volatile release and char softening,⁷⁵ which results in changes to the char morphology. The chars seem to experience TPPs that lead to final smoother structures with rounder voids.^{74,75,91} Cetin et al.⁷⁴ observed that lignocellulosic chars manufactured under faster heating rates seem to improve the char gasification reactivity. A possible explanation was the larger surface areas found on these chars.

Likewise, Zanzi et al.¹⁰⁴ observed that fast devolatilization of chars produced under fast pyrolysis in a free-fall reactor at temperatures up to 1100°C enhances the formation of more porous and more reactive chars than the ones produced in a thermobalance under slow pyrolysis conditions. In the same way, Biagini et al.⁹¹ also observed an increase in reactivity of chars produced in drop tube furnaces at temperatures of 400-800°C and fast heating rates (not specified) in comparison to chars produced in thermogravimetric balance under less severe conditions.

In contrast, Biagini and Tognotti¹⁰⁵ noticed a lower reactivity of chars pyrolyzed in platinum filaments under higher temperatures (1400°C) and longer residence times of 100 s than of chars manufactured from thermogravimetry under slower pyrolysis and milder conditions. They reported that both the high temperature and the extended time in the platinum reactor contributed

to form a collapse structure characterized by a higher plasticity, lower porosity and higher degree of graphitization.⁹¹ Cetin et al.⁷⁴ also noted that slow pyrolysis may disperse catalytic metal oxide agents which would lessen the char reactivity.

In line with findings reported on “open” configurations, closed reactors (CVC) also reported the appearance of molten structures when the carbonization heating rate was increased. These TPPs have been observed, nonetheless, at considerably lower heating rates and carbonization temperatures than the ones reported for carbonization in “open” reactors. A study of the effect of heating rate on the morphology of char produced in CVC is provided in Section 6.4.

3.5. Effect of Particle Size

There is a strong link between the particle size of biomass, the internal heating rate and the residence time of volatiles within the char particle. Larger particle sizes slow heat transfer across the char particle and retard release of volatiles from the pyrolyzing char matrix.^{39,106–109} Thus, an increase in particle size would have a similar effect to that of slower heating rates combined with an increase in pressure or a reduced gas flow. All these effects favor char-forming secondary reactions in “open” reactors.

Di Blasi¹¹⁰ theoretically proved the strong linkage between particle size and internal heating rate. She developed a computer model that accounted for primary and secondary reactions, as well as

for heat and mass transfer phenomena in reactors equipped with gas flows. Under the same external heating rate of 15°C/s, the model predicted a decrease in the char yield with decreasing particle sizes at all pyrolysis temperatures. Larger particles experience a thermally thick regime, i.e. spatial temperature gradients were governed by both external and internal heat transfer processes, whereas particle sizes below a critical value only experienced a thermally thin regime, i.e. spatial temperature gradients were just governed by external heat transfer. Internal heat transfer and therefore, the temperature gradients across the particle became negligible.

The relation between particle size and heating rate was experimentally proved by Pindoria et al.⁶⁷ When using wood particle sizes below 100 µm and a rapid heating rate, negligible char yield was recovered. When larger particle sizes were pyrolyzed under the same external heating rate, the char yield increased to 10-30 wt. % of the original wood feedstock (dry-ash-free basis). The char yield varied within this range depending on the residence time of volatiles across the reactor. In a batch reactor, Demirbas¹¹¹ observed an increase in charcoal yield with an increase in particle size for agricultural residues ground and sieved into particle sizes ranging from <0.5 to >2.2 mm. The gas flow in the batch reactor was not specified.

Beaumont and Schwob¹¹² found that the pyrolysis of coarser particles in a reactor equipped with a sweep gas at temperatures of ~300-500°C resulted in larger char and gas yields and less tar. The gas composition also varied with the particle size whereas the tar composition was unaffected. When the process changed to a slower pyrolysis regime, the biomass particle size did not alter the experimental observations. Therefore, they attributed the experimental results to the

change in the particle internal heating rate. Várhegyi et al.¹¹³ studied the effect of particle size on the devolatilization of biomass charcoals by thermogravimetry. They reported a decline in volatiles yield when larger grains were pyrolyzed at temperatures under $\sim 520^{\circ}\text{C}$, and hypothesized that volatiles suffered secondary reactions during diffusion from the interior of the carbon matrix resulting in higher yields of char. At temperatures greater than 550°C , the particles exhibited remarkably similar derivative thermogravimetric (DTG) curves, revealing that secondary formation of char was suppressed at high temperatures.

In another thermogravimetric study, Bennadji et al.¹¹⁴ pyrolyzed three varieties of wood using particle sizes from $250\ \mu\text{m}$ to $3.81\ \text{cm}$. An increase in the particle size from $250\ \mu\text{m}$ to $2.54\ \text{cm}$ at HTT of $\sim 425^{\circ}\text{C}$ resulted in significant increases in char yields (from $\sim 17\ \text{wt.}\%$ to $\sim 23\ \text{wt.}\%$ of the dry feedstock). Further increase of the particle diameter did not show a significant effect on the char yield. Kandiyoti et al.¹⁰⁸ provided an explanation for this asymptotic behavior of char yield with particle size. As particle size increase, the extent of secondary reactions between the hot char solid and the volatiles that diffuse across this char intensifies. As a consequence, char yield increase and volatile yields exhibit an initial pronounced drop.¹⁰⁸ The plateau in volatile and char yields that follows was explained by the lack of subsequent secondary reactions when particle sizes exceed a critical value. The remaining tar molecules are likely to be lighter (lower molecular weight) and be more stable, therefore, they are less prone to reactions with the char matrix.¹⁰⁸

The theories presented in the literature regarding the effect of particle size on product yields are based on the use of “open” reactor vessels. In these cases, volatiles are removed from the reaction zone and the pyrolyzing carbon matrix, resulting in different vapor residence times depending on the pyrolysis conditions and reactor. The final char yield from pyrolysis in the “open” reactor is related to particle size, where smaller particles produce less char.

In contrast, when a sealed reactor is used, the released pyrolytic vapors stay in close proximity to the solid char enhancing secondary char-forming reactions and limiting carbon partitioning to the gas and oil/tar phases. The pyrolysis of cellulose powder (50-180 μm) in the WHTB gave hope to the possibility of producing a charcoal high in fixed-carbon content and yield from small particles.⁵⁸

Consequently, the effect of particle size on wood carbonization was studied in greater detail. Section 6.5 presents the results of this study. The results show that decreasing the particle size in CVC does not have any detrimental effect. If anything, it has a positive effect on the process which demonstrates that the WHTB is a good option for charcoal manufacturing from small particles. This study is of special relevance as small particles of biomass (i.e. sawdust, grasses, agricultural residues) that were previously impractical for use in charcoal production could be used to produce charcoals with high fixed-carbon contents and fixed-carbon yields. Particle size reductions in the case of large biomass sizes, nevertheless, may be compromised by increased investment costs and energy requirements.¹¹⁵

3.6. Effect of Mass Loading

The effect of mass loading (dry sample mass per unit reactor volume) on yields and properties of products from biomass pyrolysis is a topic that few authors have focused on. In “open” reactor set-ups, its study is complicated since it cannot be easily isolated from the influence of other variables. For example, in a constant-pressure reactor, the impact of mass loading on product yields and properties is interrelated with the reactor gas flow. Higher mass loadings in constant-pressure reactors would release a greater amount of volatiles and therefore, higher outlet gas flows would be needed to keep the reactor pressure constant. As a result, both variables will play a role in the final results complicating the pyrolytic studies. The use of sealed reactors removes the effect of gas flow rate and facilitates the decoupling of the mass loading effect from other variables.

In sealed crucibles, Mok et al.⁴² studied the effect of mass loading on the differential scanning calorimetric curves and char yields of biomass pyrolysis. They reported that higher mass loadings raised the concentration of volatiles in the reactor which led to increased exothermic heats of reaction, expedited reaction rates, reduced reaction onset temperatures and improved charcoal yields. Mok et al. were able to decouple mass loading effects from absolute mass effects and system pressure effects (since mass loading is directly related to increases on both volatile partial pressure and total system pressure). A couple of experiments were performed in reactors with distinct volumes but equal mass loadings, as well as an additional experiment with a pre-added inert gas. The results revealed that improved char yields and heats of reaction were the result of a mass loading effect—which increases the volatile partial pressure—rather than an

absolute mass effect or a total system pressure effect. Várhegyi et al.¹¹⁶ developed a mathematical model that explained Mok et al.'s experimental results. The model described the pyrolytic process by initial hydrolysis reactions that are followed by decomposition reaction. Intermediate products formed in the later reactions and kept captive in the sealed vessel further react to eventually produce char, water and gases.

In studies using thermogravimetric analyzers, Wang et al.^{56,117} confirmed the attainment of higher yields of charcoal and fixed-carbon when larger sample masses of wood were pyrolyzed in open and closed crucibles with pinholes. It was concluded that the increased yields were due to greater extents of secondary charring reactions.

Based on the work from previous authors, Bai and Xue¹¹⁸ also provided insight regarding the mass loading role during biomass pyrolysis. Their focus, nonetheless, was put on the production of bio-oil (not charcoal), particularly on the production of levoglucosan. Levoglucosan is the main product from primary reactions of cellulose pyrolysis. It has a low enough boiling point (339°C) to be able to leave the hot reaction zone and later be condensed as liquid tar.

Theoretically, a 100% levoglucosan yield could be recovered from cellulose pyrolysis as long as depolymerization was the sole pyrolytic reaction.¹¹⁹ In practice, depending on the reactor configuration, yields between a few per cent and a 70% have been reported from cellulose pyrolysis.¹¹⁸

Secondary reactions that involve primary levoglucosan explain the reduction in the final bio-oil yield. Levoglucosan destruction can result from two competing reaction pathways of polymerization and evaporation.^{120–122} The experimental findings suggest that the evaporated fraction can be condensed into bio-oil, whereas the polymerized fraction gets entrapped in the pyrolyzing zone and eventually undergoes secondary reactions that produce light volatiles and char. Increasing the mass loading of levoglucosan during pyrolysis in sealed reactors revealed a shifting of the product distribution in favor of char and light volatiles formation.^{121,122} When 0.1 mg of levoglucosan was pyrolyzed in a sealed reactor at 400°C for a time period somewhere between 1 and 20 minutes, Hosoya et al.¹²² primarily found CO and CO₂ and no char. Increasing the levoglucosan loading up to ~10 mg resulted in the production of char and low molecular weight condensates.

3.7. Effect of Solid Residence Time

In a pyrolytic process, the residence time can refer to that of either solid or gaseous products, and usually indicates the period of time the char or gas stays in the reaction zone. In “open” reactors, the residence time generally refers to the gaseous one which is often calculated as the ratio of reactor volume to carrier gas flow, whereas solid residence time, when specified, is usually measured as the reaction time. In sealed reactors; solid, liquid and gaseous products stay in the reaction zone during the whole pyrolysis process and their residence times coincide with the reaction time.

Volatile residence times inside and in the vicinity of the char particle, although different, are closely related to gaseous residence times. They cannot be experimentally measured but they can be indirectly modified by varying gas reactor flows, reactor pressures, and/or particle sizes.

As widely pointed out in literature, prolonging the volatile residence times enhance secondary char-forming reactions at the expense of tar yield.^{39,59-62} If combined with slow heating, the residence time at lower temperatures of both solid and volatiles is expanded which further favors repolymerization reactions into char.¹⁰⁰⁻¹⁰³ In order to ensure high bio-oil yields, flash or fast pyrolysis processes operate at short gaseous residence times and high heating rates. In contrast, conventional pyrolysis operates at long residence times combined with slow heating rates with the aim of maximizing char yields.

Ningbo et al.¹²³ studied the effect of HTT and solid residence time in a screw reactor that continuously fed biomass at a 1.47 kg/h rate and purged the system with a continuous N₂ stream. At a pyrolysis temperature of 600°C, the solid residence time was varied between 3 to 7 minutes. The results showed a decrease of the char yield with increasing residence time. Gas yield presented a minimum when the system was operated with a 4 minute residence time and liquid yield was maximum at 6 minute residence time. As the solid residence time increased within the 3-7 minute range, char fixed-carbon content increased and volatile matter declined. A clear trend of fixed-carbon yield was not observed. Based on their results, the process was divided into three stages. In the first one (3-4 minutes), secondary reactions are absent and the product yields are the result of primary reactions. In the second one (4-6 minutes), secondary cracking start to be

significant leading to an increase on both bio-oil and gas yields. After 6 minutes, in the third and last stage, primary reactions are complete while secondary cracking dominates. The result is a decline of the bio-oil yield and an increase in gas yield.

In a fixed-bed reactor that pyrolyzed empty fruit bunch at $\sim 450^\circ\text{C}$ at a ramp rate of $50^\circ\text{C}/\text{min}$ under a 2 bar N_2 gas flow, Mohamed et al.¹²⁴ showed a very minor decline of char yields (considered insignificant by the authors) with increasing holding time in a 6-12 minute range, and minor fluctuations in the gas and liquid yields. Mayor and Williams¹²⁵ investigated the effect of varying the residence time between 10 and 120 s on product yields and char calorific values from fast pyrolysis of Loblolly pine biomass at a HTT of 400°C . The experiments were performed in a microreactor exposed to heating rates above $100^\circ\text{C}/\text{s}$. Lengthening the residence time resulted in higher bio-oil and gas yields, and lower char yields but with improved lower heating values. A study of the kinetics revealed the incompatibility of applying kinetic parameters and models obtained from conventional thermogravimetric analysis (TGA) processes and concluded that fast and slow pyrolysis present distinct kinetics.

The pyrolysis of a variety of biomass feedstocks in a muffle furnace under limited oxygen concentrations was performed by Wang et al.¹²⁶ in two steps at a rate of $5^\circ\text{C}/\text{min}$ to final temperatures of 500 or 700°C . The results generally showed (although there were some exceptions to this trend) a reduction on the char yields and an increase on BET surface areas as the holding time at temperature was prolonged from 4 to 8 to 16 hours. Retention time did not show much of an effect on the char pH and its content of elemental carbon.

Ling et al.¹²⁷ studied the effect of residence time (30, 60 and 90 minutes) and temperature (between 300 and 600°C) on the pyrolysis of two types of biomass: oil palm trunks and empty fruit bunches. During the process, volatiles were continuously removed from the reaction zone to a condenser. The focus of this study was on bio-oil product. The results showed an improvement to the bio-oil yield and calorific value as the residence time was prolonged. Char yields declined with residence time for the empty fruit bunch biomass while the pyrolysis of the oil palm trunk did not present clear char yield trends.

Lin et al.¹²⁸ performed slow pyrolysis of tobacco stems in an “open” fixed-bed reactor under various conditions of temperature (between 350 and 600°C), residence times (between one and five hours) and heating rates (between 5 and 25°C/min). Bio-oil yields lowered with retention time while gas yield usually increased and char yields presented some fluctuations. In most cases, the fixed-carbon contents improved and the volatile contents decreased as the HTT, retention time and heating rate increased. Notice the long time scales of these processes in comparison to fast pyrolysis processes.

In slow pyrolysis processes at a 0.1 MPa constant-pressure and a continuous nitrogen flow, Antal et al.⁵⁷ reported an increase on the fixed-carbon yields of various biomass feedstocks when the heating time and solid soaking time at temperature were simultaneously prolonged. For example, pine wood pyrolysis characterized by a HTT of 450 °C, a 90 min-heating period plus a 10 min-soaking, resulted in a 20.2% fixed-carbon yield and a 69.6% fixed-carbon content. When

the heating and soaking were extended to 4 hours and 60 minutes respectively, the fixed-carbon yield and content increased to 24.0% and 74.6% respectively. Further prolonging the soaking time to 4 hours (but maintaining the heating time fixed at 4 hours) appeared to improve the fixed-carbon content to 78.6% and maybe slightly increased the fixed-carbon yield to 25.0%.

Ronsse et al.¹²⁹ slowly pyrolyzed various biomass feedstocks in a fixed-bed reactor at a heating rate of 17°C/min to temperatures ranging between 300 and 750°C under a continuous nitrogen flow of 800 ml/min. Lengthening the solid residence time after heating from 10 to 60 minutes or raising the HTT appeared to maintain the fixed-carbon yields constant but increased fixed-carbon contents and char HHVs while reducing volatile matters. Prolonging the time also led to a decline in the BET char surface area. A possible explanation offered was the filling of char pores with time due to ash fusion.

In conclusion, it appears that longer solid residence times especially benefit slow pyrolysis systems where secondary reactions are enhanced. The resultant chars appear to present lower yields but improved values of fixed-carbon contents, without sacrificing the valuable fixed-carbon yields.

Newalkar et al.⁷⁵ described the char morphology history profile in both high and low heating rates set-ups (see Section 3.4). In slow heating set-ups, decomposition reactions occur well before the char starts melting. The char structure becomes increasingly lighter as it releases volatiles but retains the skeleton structure of the original biomass feedstock. Under quick

heating, the char suffers radical morphological transformations. Decomposition reactions of the solid occur at the same time as the char begins to melt. Chars formed in a pressurized entrained flow reactor subject to heating rates as high as 10^3 – 10^4 °C/s presented an amorphous structure at a 15 s solid residence time. As the residence time was lengthened, volatiles tried to escape the solid matrix while the char melted. The result was an improved realignment of the char structure and an expansion of the solid due to gases being trapped within. By 28 s, the char has become significantly more graphitic and swollen. Further prolonging the time expands the char micropores to generate a mesoporous surface, probably due to the release of internal gases. As the time extends, Newalkar et al.⁷⁵ also observed the formation of heavier products (polynuclear aromatic hydrocarbons) through combination reactions between gas compounds.

3.8. Effect of Feedstock

This section is divided into two subsections. The first one compiles the literature findings regarding the effect of the major structural components of biomass feedstocks (cellulose, hemicellulose and lignin) on pyrolysis processes. While the second one analyzes the influence of the mineral matter on pyrolysis.

3.8.1. Effect of cellulose, hemicellulose and lignin ratios

Plant biomass is composed mainly of three basic structural organic polymers: cellulose, hemicellulose and lignin. The degree of association and the ratio between these components depend on the biomass type. For example, woody biomass species, having grown at a slow pace, consist of tightly bound fibers. Whereas herbaceous biomass, typically perennial, is composed of loosely-bound fibers, a sign that indicates a lower lignin content.¹³⁰ Hardwoods are described as biomass species characterized by higher cellulose contents in comparison to wheat straw and leaves, which contain greater hemicellulose amounts.¹³¹

Within a single plant, the relative composition of the constituents also fluctuate in its lifetime with the stage of maturation, soil type, nutrient balance and other factors.^{130,131} Usually, the chief component of biomass is cellulose, constituting around 40–50 wt.% of the material, the other two major components, hemicellulose and lignin, account for around 20-40 wt.% and 10-40 wt.% of the material respectively.^{130,132} Along with these components, biomass also contains trace amounts of inorganics (ash) and extractives. All of these biomass constituents contribute in a greater or lesser degree to the physical and chemical properties, and the pyrolysis characteristics of the lignocellulosic biomass.

In a slow pyrolytic (<100 °C/min)¹³³ process, five distinct stages can be discerned based on the decomposition degree of each of the basic structural components:^{133,134} (i) <100 °C: moisture evolution predominates, (ii) 100-250°C: extractives decomposition begins (many authors do not

mention this zone); (iii) 250-350°C: hemicellulose decomposition predominates; (iv) 350-500°C: cellulose and lignin decomposition predominates; and (v) >500°C: lignin decomposition predominates. These temperature ranges—taken from ¹³⁴—serve as reference values but the reported temperatures can present some variations between authors. The general consensus, nonetheless, is that moisture evaporation represents the first stage of biomass thermal degradation followed by the decomposition of first hemicellulose and subsequently cellulose. And that lignin, characterized by its higher resistance in comparison to cellulose and hemicellulose, decomposes within a larger temperature range.¹³³⁻¹³⁶ For example: Ounas et al.¹³⁵ reported lignin decomposition beginning simultaneously with hemicellulose at 160°C and finalizing at 625°C, considerably after the end of cellulose decomposition at 372°C.

The thermal decomposition of each individual component also results in distinct product yields and composition. Stefanidis et al.¹³² observed that cellulose pyrolysis resulted in a high yield of a tar abundant in levoglucosan plus additional anhydrosugars and a little solid residue. Xylan (representative of hemicellulose) pyrolysis produced large gas and moderate tar yields rich in water, phenols and ketones. Extensive secondary tar-cracking reactions during xylan pyrolysis were speculated to possibly take place at the elevated pyrolytic temperatures employed (500°C), considerably higher than the temperature at which xylan thermal decomposition occurs. Besides, the large amount of ash present in the commercial xylan employed also offered an explanation of the enhancement of gas formation by the sacrifice of tar. Finally, lignin produced little gas, a moderate amount of tar abundant in phenolic groups and the largest amount of char.

In order to predict product distributions and other features of biomass pyrolysis, several attempts have been made to correlate the biomass pyrolysis behavior with that of its basic structural components.¹³⁴ For example, several authors detected no signs of interactions among the individual components during biomass pyrolysis in a thermogravimetric analyser^{133,134,137–142} or a packed-bed pyrolyser.¹³⁴ A biomass pyrolytic global rate was satisfactorily explained by the summation of the rates of the three main biomass constituents, i.e. cellulose, hemicellulose and lignin, and the product distributions by direct cumulative correlations of each component.

Raveendran et al.¹³⁴, Yang et al.¹³³ and several authors also observed that the ash has a considerable effect on the pyrolysis behavior and final product distribution and recommended to include it in the models to improve prediction accuracies (see Section 3.8.2). Stefanidis et al.¹³² conducted thermogravimetric analysis and fast pyrolysis experiments of each of the main biomass components (cellulose, xylan as a hemicellulose representative, and lignin) as well as synthetic biomass produced by combining the components in various proportions. They concluded that in the thermogravimetric analyzer, the final solid residual weight could be accurately predicted by adding the contribution of each of the biomass components. Nonetheless, experimental and calculated DTG curves exhibited some inaccuracies when biomass components were combined. They associated this phenomena to limitations of heat and mass transfer. The fast pyrolysis experiments were specially affected by these limitations. When heat and mass transfer were restricted, the final product distribution appeared to shift in favor of greater charcoal and gas yields at the expense of tar yield.

In line with Stefanidis et al.¹³² findings, Raveendran et al.¹³⁴ pointed out that the good agreement found in the literature models pertained to specific heating rates, each one associated to a particular biomass. When different heating rates were imposed, discrepancies appeared. These inaccuracies were attributed to the heating rate effect on charring reactions. Based on their own experimental studies, they reported that secondary reactions were the reason for the changes in the distribution of final products, and not the interactions between the biomass constituents.

Stefanidis et al.¹³² also reported that the tar extracted from the pyrolysis of synthetic biomass presented a different composition than the one obtained from the individual components. Characteristic chemical tar compounds produced by the isolated biomass components—described above—could be discerned but in different quantities. Stefanidis et al.¹³² experimental observations combined with a literature study led them to conclude that the levoglucosan produced by cellulose via transglycosylation could further react via catalysis to form mostly aromatic hydrocarbons, phenols, furans and polycyclic aromatic hydrocarbons (PAHs). Products derived from xylan, which are characterized by a broader array mainly including phenols and ketones along with some acids, could catalytically react to finally produce aromatic hydrocarbons, phenols and PAHs. Finally, phenolic groups produced from lignin could not be catalytically transformed into other chemical compounds due to their aromaticity.

Contrasting the findings of the authors mentioned previously, some studies have concluded that cellulose, lignin and hemicellulose components do not act independently during pyrolysis and therefore, interactions should not be ignored. Worasuwanarak et al.¹⁴³ reported considerable

cross-linking interactions between cellulose and lignin during biomass pyrolysis in a thermogravimetric analyzer. The result of these interactions was the formation of water and ester groups that resulted in higher char production and lower tar.

During thermogravimetric studies at a temperature of 800°C, Wang et al.¹⁴⁴ reported interactions of both lignin and hemicellulose with cellulose but not obvious interactions between them. The pyrolysis of wood at the same temperature of 800°C performed by Hosoya et al.^{145,146} revealed influences on the final product yields and pyrolytic behavior from both the inorganic matter and interactions between wood polymer components. It appeared that wood is likely to form less levoglucosan and more C₂-C₃ carbonyls and levomannosan than the amounts predicted from the isolated constituents. In consonance with these observations, at temperatures between 350 and 500°C, Wang et al.¹⁴⁷ reported influences between cellulose and lignin that resulted in higher production of 2-furfural and acetic acid, and interactions between cellulose and hemicellulose associated with the formation of phenol and 2,6-dimethoxy.

Regardless of the absence or presence of polymeric interactions, some relations can be found between the biomass composition and charcoal yields or properties. For instance, higher contents of lignin in biomass typically lead to greater yields of charcoal.^{148,149} Due to its higher initial carbon content and the greater tendency to remain in the solid form rather than breaking down to form volatiles, Mackay and Roberts¹⁴⁸ found that lignin, by itself, was able to produce three times more charcoal than cellulose when pyrolyzed at a heating rate of 15°C/min to 500°C under an argon stream.

Shafizadeh and DeGroot¹⁵⁰ acknowledged that after pyrolysis, the biomass energy gets distributed between the different pyrolytic products to distinct degrees dependent on the biomass nature and the pyrolysis conditions. Evaluation of the biomass material through quantitative thermal analysis determined the evolution of mass loss and distribution of heat between the resultant products and showed that a higher lignin content in the biomass leads to a greater fraction of energy captured in the char. Cellulose pyrolysis at 500°C resulted in a mass loss of 92% and in final volatiles that retained 86% of the biomass energy, while lignin pyrolysis lead to a char residue containing 70% of the biomass energy. Volatilization of the fuel was also found to be enhanced by a higher content of carbohydrate and extractives, as well as by higher temperatures.

In terms of proximate analysis, lignin presents a considerably higher amount of fixed-carbon in comparison to cellulose or xylan¹⁵¹ and biomasses with high lignin contents are associated with a higher production of char and a lower release of volatiles. Haykiri-Acma and Yaman¹⁵² concluded that biomass species with higher contents of lignin and ash exhibited enhanced char formation compared to biomass species with higher content of volatile matter, which released more volatiles. Biagini and Tognotti¹⁵³ also observed that biomass species with increased contents of volatile matter exhibited more intense melting, swelling and plastic deformations during fast pyrolysis. The yield of charcoal and its physical properties were also found to be related to the density of the original biomass.¹⁵⁴ In iron industries, charcoals from dense hardwoods have traditionally been more desirable given their greater crushing strength.¹⁵⁴

In terms of elemental analysis, Sonobe and Worasuwannarak¹⁵⁵ observed that biomass species with similar elemental compositions showed different devolatilization behaviors and consequently arrived at the conclusion that biomass cannot be assumed homogeneous but cellulose-hemicellulose-lignin-ash ratios, as well as chemical functional groups and bonds should be considered.

3.8.2. Effect of mineral matter or ash

The ash-forming matter in both coals and biomass is classified by Tumuluru et al.¹⁵⁶ into four categories: easily leachable salts, minerals that form part of the biomass structure, inorganic compounds such as sand, salt or clay, and inorganics associated with the organic material. Raveendran et al.¹⁵⁷ identified that typically, the main inorganic elements in biomass are sodium, potassium, calcium, magnesium, iron, phosphorus, aluminum and silicon; whereas cobalt, chromium, copper, manganese, nickel, sulfur and zinc are also present but in lower concentrations.

A number of studies with demineralized, mineral-treated and/or untreated biomass have investigated the effect of inorganic salts or ash during biomass pyrolysis and have demonstrated that generally, the mineral matter suppresses tar formation and promotes char and gas production.^{149,157-161}

In fast-pyrolysis experiments of demineralized wood at elevated temperatures of ~1000°C, Nik-Azar et al.¹⁶⁰ observed an increase in tar yields and a decline in char and gas yields. The temperature at which tar-cracking reactions became significant was also reduced. A possible justification to this temperature behavior was the swelling of cellulose due to the acid wash pretreatment which caused a reduction on pore sizes and in consequence, restrictions to tar diffusion inside the biomass particles. Shafizadeh et al.¹⁶² also reported an increase of tar yields and levoglucosan content when pure cellulose and wood-derived materials were first prewashed with dilute acid and then pyrolyzed under vacuum at 400°C.

Raveendran et al.¹⁵⁷ confirmed the increase in volatile yields derived from demineralized biomass and reported quicker devolatilization rates and a higher onset temperature of devolatilization. Exceptions to this behavior were biomass samples high in potassium and/or zinc along with high lignin contents. These observations agree with the lignin impact on pyrolytic processes. Shafizadeh and Chin¹⁶³ reported similar effects from the addition of acidic additives to the pyrolysis of isolated cellulose and xylan (i.e. hemicellulose model compound). In these cases, dehydration and charring reactions appear to be enhanced to produce water, char and reduce tars. Furthermore, Tang and Eickner¹⁵⁸ reported a similar influence of inorganic salts on both cellulose or wood pyrolysis, but a less severe impact for lignin pyrolysis.

Conversely, when biomass is mineral-treated and subsequently pyrolyzed, char yields usually become higher and the tar presents a lower yield as well as a reduced molecular weight. The nature of the mineral matter in biomass affects both the distribution and properties of the final products. Fang and McGinnis¹⁶⁴ investigated the pyrolysis of holocellulose from loblolly pine

bark at temperatures ranging from 100 to 600°C in a continuous flow reactor after adding acidic ZnCl₂ and basic NaOH catalysts. In contrast to pyrolysis of a raw sample, char yields increased and the decomposition shifted to lower temperatures when using both catalysts. The concentration of volatiles products considerably varied with the catalytic medium employed. The addition of ZnCl₂ in a catalyst-to-holocellulose ratio of 5% increased the 2-furaldehyde and methanol products. Increasing the ratio in a 5-30% range further reduced the decomposition temperature and increased methanol yield. Furaldehyde concentration did not significantly increase. NaOH addition especially enhanced the production of CO₂ and light hydrocarbons (methane and ethane).

In agreement with these observations, Beaumont and Schwob¹¹² reported different product yields and composition of tar from quick pyrolysis experiments at 350°C using raw wood, and wood impregnated with a basic (5% NaOH) and an acidic (5% FeCl₃) catalyst. Results from both mineral treatments confirmed the suppression of tar yields and the enhancement of char yield in comparison to the untreated biomass, but gas yield behavior changed between catalysts. Compared to the gas yield obtained from the raw biomass, the application of a basic catalyst enhanced the gas yield while the acidic catalyst modestly reduced it. The oil composition also changed. Acidic FeCl₃ raised the furaldehyde content and lowered the hydroxypropanone and furfurylic alcohol. In contrast, the tar derived from the wood pre-treated with basic NaOH contained a higher content of hydroxypropanone and less furaldehyde. They concluded that reaction mechanisms changed with the catalyst employed, acid catalysts favor dehydration and furaldehyde production and basic ones promote gas and char-forming reactions.

Pan and Richards¹⁶⁵ reported that potassium, but not calcium, act as catalytic agents in the production of carbon dioxide and carbon monoxide, acetic and formic acids and methanol during the pyrolysis of wood at an isothermal HTT of 250°C or at progressive heating from 100 to 550°C. They speculated that, as opposed to calcium, potassium is an effective catalyst for the production of formic acid (and maybe methanol) due to its higher alkalinity. Nik-Azar et al.¹⁶⁰ treated raw wood by mineral impregnation before quick-pyrolyzing it and confirmed the catalytic effect of potassium, sodium, and calcium cations (particularly strong for sodium and potassium) on tar-cracking reactions in favor of the production of char and gas.

Gray et al.¹⁶⁶ reported that inserting calcium in woody biomass by ion exchange reduced tar yield, increase the production of water and of hydroxypropanone, acetic acid and furfuraldehyde chemicals. The effects observed from the addition of calcium were reported to be similar to those exerted by ash constituents inherent to the wood material.

During pyrolysis under vacuum of mineral-treated cottonwood, Richards and Zheng¹⁶⁷ observed that K, Li and Ca promoted char formation and reduced the yield of tar characterized by a low content of levoglucosan. Other ions were tested and transition metals (in particular) produced a tar with increased levoglucosan contents. Nassar et al.¹⁶⁸ observed that inorganic salts acted as effective fire-retardants by suppressing the formation of flammable tars, volatiles and gases, and enhancing the formation of char. Catalytic dehydration reactions of cellulose by minerals is a typical mechanism suggested to explain the reduction of depolymerization reactions into flammable tars, such as levoglucosan, in favor of more water and char.^{149,158,159,168} Akhtar and

Saidina Amin¹⁴⁹ also explained that secondary reactions as well as the internal diffusion of tars in the pores of the mineral matter justify the shift in product distribution when applying mineral treatments to the biomass.

Changing the catalyst-to-biomass ratio can also affect the yields and properties of the pyrolysis products. Pütün¹⁶⁹ performed pyrolysis in a tubular fixed-bed reactor at 550°C under various amounts of MgO catalyst in a range from 5 to 20 wt.% of raw material and observed increasing gas and char yields and reducing tar yields were stronger as the catalyst: biomass ratios became higher. Catalytic treatment—versus no treatment—also confirmed the reduction of the oxygen content and the molecular weight of the tar.

Zhou et al.¹⁷⁰ conducted pyrolysis experiments of biomass in a fixed-bed pyrolyzer at 550°C, employing the same catalyst-to-biomass ratios but using ZnO catalyst instead of MgO. They observed analogous trends but a less intense effect from raising the catalyst amount on gas and tar yields. Char yields did not appreciably vary with the catalyst amount added. Catalytic tar, as opposed to non-catalytic tar, also contained lighter compounds and presented a lower viscosity. Based on Pütün's¹⁶⁹ and on their own results, Zhou et al.¹⁷⁰ concluded that ZnO could be a mild catalyst.

Encinar et al.¹⁵⁹ tested several catalysts on biomass pyrolysis and confirmed the effect of the addition of a catalyst on promoting char and gas production and reducing tar production. In

addition, the use of alkaline metals increased the fixed-carbon content. The gas composition also varied with the catalyst type. Iron and especially zinc promoted the formation of hydrogen. It appeared that ZnCl₂-enhanced depolymerization reactions were accompanied with charring and tar-cracking reactions that finally led to hydrogen release. When the ZnCl₂ concentration increased, the effects on product yields were intensified. Demineralizing the biomass by prewashing it with acid lowered char yield but the char presented higher fixed-carbon content and lower ash content.

Catalytic agents have also been added to biomass pyrolysis to improve the quality of the tar produced.¹⁷¹ Tar presents four problematic properties as a fuel: high viscosity due to the presence of large molecules, corrosivity due to the presence of organic acids, instability due to the presence of reactive compounds and low energy content (with a heating value of ~19 MJ/ kg) due to the small amount of elemental hydrogen and large amount of elemental oxygen.¹⁷² A number of technologies have been developed in order to lower the acidity and increase stability and calorific value of tar.^{171,172}

Zeolites catalysts have been shown to produce a tar with a lower yield but with better quality by effectively minimizing oxygenated compounds.^{171,173,174} Studies with ZSM-5, a common zeolite, confirmed the decline of oxygenated aromatic compounds in tar, as well as the increase in aromatic hydrocarbon content.¹⁷³⁻¹⁷⁵ Huang et al.¹⁷⁶ modified a HZSM-5 zeolite catalyst by impregnation with 6% wt. lanthanum and observed that increasing the catalyst-to-biomass ratio

from 0 to 3 increased gas and olefin yields, especially when the ratio varied from 0 to 1.

Increasing the ratio above 3 did not have a significant effect on the olefin yield.

3.9. Kinetic schemes and heat of reaction of biomass pyrolysis

During pyrolysis, the biomass undergoes a complex network of chemical reactions coupled with heat and mass transfer phenomena. The overall mechanism, extremely complex in actual pyrolysis processes with the formation of over a hundred intermediate products, is yet to be fully understood. Nonetheless, a number of authors have discerned patterns and provided useful insights that have resulted in the development of a wide diversity of simplified mathematical models whose reaction rates are based on apparent kinetics.

Literature reaction schemes range from one-step models to more intricate multi-reaction models with sets of parallel reactions. For example, biomass chemistry can be represented with a set of parallel reactions that account for the breakdown of the major structural components: cellulose, hemicellulose and lignin.^{133,134} Other kinetic schemes consider the virgin biomass as a whole, without dividing it into sub-constituents, and represent the thermal decomposition as a set of primary reactions that lead to the production of primary gas, tar and char.^{103,163,177} Some of these kinetic schemes also account for secondary interactions among the products evolved from primary degradation.^{163,178–183} Di Blasi¹⁸⁴ classified the kinetic schemes into three categories:

- a) one-step global models, when a single reaction is used to describe the pyrolytic process.

- b) one-step, multi-reaction models, when the pyrolysis process is represented by several primary reactions, and
- c) two-stage, semi-global models, when primary and secondary reactions are considered.

The main drawback of scheme (a) is that it assumes a constant ratio between the different products and consequently, it cannot be applied to calculate product distributions.

Table 3.1, taken from Haseli's Ph.D. thesis,¹⁸⁵ summarizes kinetic schemes offered in literature and references authors that proposed or applied them. The first four schemes represent primary steps and do not consider vapor-solid secondary reactions. The last two schemes, the models by Shafizadeh and Chin and by Koufopoulos et al., account for secondary interactions from two different points of view. Shafizadeh and Chin¹⁶³ suggested that secondary reactions led to the formation of additional char and light hydrocarbons at the expense of tar. Whereas Koufopoulos et al.¹⁷⁸ proposed that the virgin biomass undergoes primary reactions to decompose into volatiles and gases (reaction 1) and char (reaction 2). These primary pyrolysis products participate in secondary reactions to produce volatiles, gases and char of different compositions (reaction 3).

Pyrolysis mathematical models developed in literature typically predicted product yields by coupling the chemical reactions to heat and mass transfer phenomena. In a recent review, Babu¹⁸⁶ (although not clearly specifying the context of the reaction environment) qualitatively described all these interactions as follows: (i) heat transfer from a heat source to the biomass fuel resulting in hotter internal biomass temperatures; (ii) beginning of pyrolytic reactions as a result of the higher temperatures and the release of volatiles from the fuel and the production of solid

char; (iii) outflow of hot volatiles, leading to heat transfer from the volatiles to the cooler unreacted fuel; (iv) tar condensation in the cooler regions of the fuel; and (v) autocatalytic secondary pyrolysis reactions from the primary products.

Table 3.1. Summary of kinetic schemes of biomass pyrolysis proposed in the literature. Data taken from Haseli's Ph.D. thesis.¹⁸⁵

Model	Kinetic Scheme	Reference
One-step global model	Biomass → Volatiles + Char	187
Three independent reactions model	Cellulose → Volatiles + Char Hemicellulose → Volatiles + Char Lignin → Volatiles + Char	133,134
Broido-Shafizadeh model	Cellulose → Intermediate → Tar → Intermediate → Light gases + Char	177
Model of Koufopoulos et al.	Biomass → Intermediate → Volatiles + Gases → Intermediate → Char	103
Model of Shafizadeh and Chin	Biomass → Light gases Biomass → Tar Biomass → Char	163
Model of Shafizadeh and Chin with secondary reactions	Biomass → Light gases → Tar → Light gases → Tar → Char → Char	163,178–181
Model of Koufopoulos et al. with secondary reactions	Biomass → (Volatiles + Gases) ₁ → Char ₁ (Volatiles + Gases) ₁ + Char ₁ → (Volatiles + Gases) ₂ + Char ₂	178,182,183
Model of Grønli and Melaen with secondary reactions	Biomass → Gases → Tar → Gases → Char	188

A wide range of wood pyrolytic enthalpies for the pyrolytic process have also been reported in the literature varying from endothermic to exothermic as a function of processing conditions. In 1892, Chorley and Ramsay¹⁸⁹ observed that wood distillation became exothermic at a temperature close to 280°C. Around a decade later, Klason and co-workers^{190–192} described wood pyrolysis as an exothermic process at a starting temperature of about 250°C and an end point of

about 350°C. Beyond this temperature, the charcoal was observed to further decompose mainly into gas, with no production of acetic acid or wood alcohol (methanol).

When charring reactions were inhibited, Milosavljevic et al.¹⁹³ reported cellulose pyrolysis to be an endothermic process with a reaction heat of ~538 J/g of volatiles evolved. This endothermic heat was speculated to include reactions' pyrolytic enthalpies associated with the release of volatiles in addition to the latent heat of vaporization of pyrolytic products such as tars. In contrast, when char formation was promoted, the process became exothermic with a heat of reaction of roughly 2kJ/g of char formed. In conclusion, pyrolysis could be driven to the exothermic direction by promoting char-forming reactions (no specification was made between primary and secondary char) versus tar-forming reactions. In an "open" reactor, low heating rates, along with mass transfer restrictions, served to shift pyrolysis towards exothermicity.

In line with these findings, Arseneau¹⁹⁴ observed a very mild, almost indiscernible, endotherm at ~180°C followed by an also almost indiscernible exotherm at ~220°C, and later by a more rapid and clear endotherm starting at ~280°C during the pyrolysis of thin (0.46 mm) cellulose samples by thermogravimetry under a nitrogen flow. The second endotherm was attributed to two phenomena: the depolymerization of residual cellulose and the volatilization of levoglucosan. Restricting the release of levoglucosan by stacking cellulose thin layers to form a cellulose sample 0.9 mm thick, or by placing 25 mg of dried alumina over a thin cellulose sample, produced a drastically clearer exotherm. This behavior was attributed to the breakdown of the primary polymerized product, presumably levoglucosan.

During the pyrolysis of beech and spruce woods in a differential scanning calorimeter, Rath et al.¹⁹⁵ recognized a linear correlation between the heat of reaction and the char yield, which was in turn highly dependent on the conditions of the pyrolytic process. In agreement with Milosavljevic et al.¹⁹³, they speculated that the overall heat of reaction may be a balance between exothermic char-forming processes that compete with endothermic tar-forming processes. Mok and Antal⁶³ arrived at the same conclusion when pyrolyzing cellulose in a tubular flow reactor under pressure embedded in a differential scanning calorimeter. An endothermic process transformed into an exothermic one when tar release was hindered and char formation was promoted by the use of higher pressures and lower gas flows. The endotherm was associated with levoglucosan vaporization while the exotherm was attributed to levoglucosan in-situ carbonization. Antal and Grønli³⁹ recognized that the exothermic nature of secondary reactions could simultaneously provide part of the heat necessary for the carbonization process, improve char yields and reduce the formation of unwanted tars.

A number of authors^{163,178–181} developed mathematical models that applied the kinetic scheme of Shafizadeh and Chin with secondary reactions in Table 3.1. The models attributed an endothermic heat of reaction to the primary formation of tar, but differentiated the formation of primary and secondary char to be endo- and exothermic processes, respectively. DiBlasi¹⁸⁴ pointed out that at low temperatures and brief volatile residence times, only primary (endothermic) reactions occur, while secondary (exothermic) reactions take place at high temperatures and extended residence times.

With respect to the major chemical components of biomass: cellulose, hemicellulose and lignin, pyrolysis of hemicellulose and lignin is generally depicted as an exothermic process. In contrast, cellulose pyrolysis is reported either as an endothermic or exothermic process depending on the experimental conditions.^{193,194,196-198} Kilzer and Broido¹⁹⁹ recognized the existence of at least three distinct processes during cellulose pyrolysis. Two competing endothermic processes associated respectively with the formation of “dehydrocellulose” and levoglucosan (major constituent of the tar), and a third exothermic process attributed to the generation of volatile carbon-containing compounds and hydrogen from "dehydrocellulose" reactions, as well as inter-molecular condensations to produce char. In contrast to these findings, Arseneau¹⁹⁴ and Mok and Antal⁶³ (mentioned above) revealed that the decomposition of levoglucosan, and not the “dehydrocellulose”, was responsible of the exothermicity of cellulose pyrolysis.

Tang and Eickner¹⁵⁸ reported an endothermic net heat of reaction from cellulose pyrolysis and indicated similar heat contributions from dehydration and depolymerization reactions since net heat remained almost unchanged under various catalyst concentrations that will influence the competition between these reactions. Chemical treatment and the presence of lignin showed a reduction of the overall heat, which was consistent with an exothermic heat source contribution coming from secondary charring reactions.

CHAPTER 4. MATERIALS AND METHODS

The following sections describe the experimental apparatus, the materials and the procedures used in the carbonization experiments performed to meet the objectives set forth in Chapter 2 after due consideration of the prior work summarized in the literature review of Chapter 3. The first section of this chapter describes the evolution of the experimental test bed that includes the development of the wall heated tubing bomb (WHTB) reactor and instrumentation used for monitoring reaction conditions and product characterization. And the second section of this chapter describes the steps used to conduct a typical test, the post-test disassembly of the reactor, sample collection and product analyses.

4.1. Apparatus Evolution

The carbonization reactor—referred to as the Wall Heated Tubing Bomb (WHTB)—evolved from the original model presented in references,^{25,26} to an intermediate single reactor model, to an intermediate dual reactor and finally, to the current dual reactor system which is displayed in Figure 4.1.

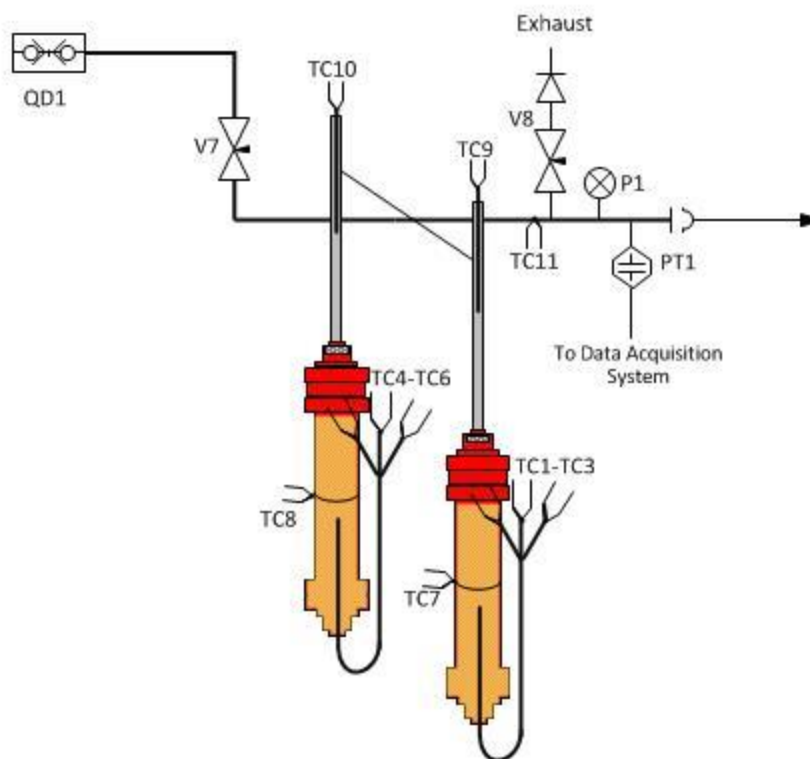
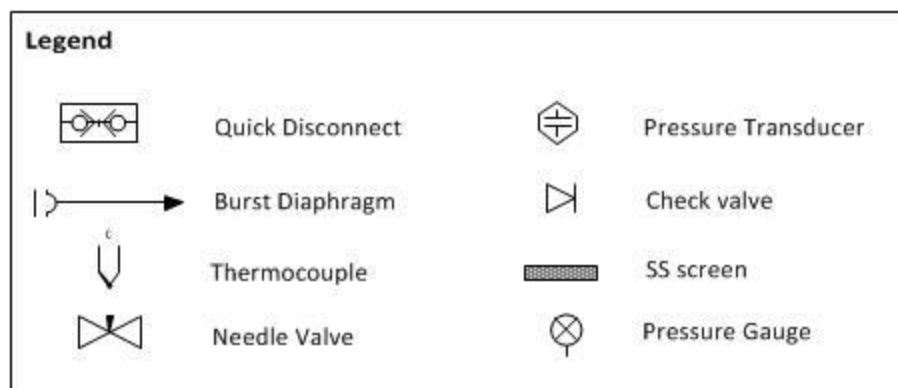


Figure 4.1. Schematic of the Wall Heated Tubing Bomb (WHTB) reactor.

The original model described in references^{25,26} was equipped with a single reactor body that could hold a maximum of 12 g of sawdust. This capacity limited the amount of char manufactured and recovered, and therefore the number of analyses that could be applied to the char. Chars manufactured in the original WHTB were only subjected to proximate analysis and

occasionally to SEM.^{25,26} A greater charcoal mass was desired to allow additional analyses to be performed and thus obtain a better understanding of the carbonization process, the char properties and potential applications.

The intermediate and current versions of the WHTB reactor share the same operating principles, enabling constant-volume pyrolysis in a hermetically-sealed batch reactor able to withstand high temperatures and pressures (up to 16.24 MPa at 537°C). Improvements from the original reactor include a higher loading capacity, enhanced safety, and the ability of acquiring highly reproducible data. The intermediate single reactor model increased the capacity to 14 g of sawdust through internal modifications of the original reactor. This system was equipped with a single reactor body with analogous characteristics to the current WHTB described in this section.

The intermediate dual reactor model doubled the active volume by adding a second reactor body as described in reference ²⁷. Finally, the current reactor system replaced the internal thermocouples from single point to multipoint thermocouples in order to acquire additional data. The burst diaphragm was replaced from the previous model (Oseco STD) rated at 16.20 MPa at 22°C²⁷ to a lighter and smaller model (LaMot) with a superior pressure rating of 21.3 MPa at 22°C. The new burst diaphragm made it possible to operate the reactor at higher temperature and/or pressure (See Appendix A.4 and A.5 for Allowances for Pressure and Burst Diaphragm Rupture Pressure definitions). The burst diaphragm ruptures if its rated pressure is exceeded, protecting the WHTB reactor from experiencing pressures that would result in catastrophic

failure. The outlet of the burst diaphragm vents through a tube into a bucket filled with water that serves as a buffer / shock absorber to dissipate the released energy.

Analysis of the char produced in the dual WHTB reactor designs include proximate and ultimate analysis, higher heating value by bomb calorimetry and SEM imaging. Although beyond the scope of the present work, collaborators anticipate conducting additional analysis including X-ray fluorescence (XRF) spectroscopy, nuclear magnetic resonance spectroscopy (NMR), Fourier transform infrared spectroscopy (FTIR), BET surface area measurements, thermogravimetric analysis under CO₂ and N₂ (TGA-CO₂, TGA-N₂), X-ray diffraction (XRD) and transmission electron microscopy (TEM).

Each reactor body (see the colored sections in Figure 4.1) is constructed from a section of 316 stainless steel tubing that is 17.15 cm long with a 2.54 cm outer diameter and a wall thickness of 2.11 mm. The reactor has an allowable working pressure of 21.37 MPa at room temperature and 16.24 MPa at 537°C. After it is constructed and prior to use, each new reactor is hydrostatically pressure tested at 21.87 MPa. After the reactor is loaded and assembled, a leak test is also performed, prior to each experiment. Swagelok fittings and reducing unions connect the top of each reactor body to a 6.35 mm stainless steel tube referred to as the “stem” of the reactor (rated at 35.26 MPa at room temperature). At the bottom of each reactor body, the unions provide an insertion point for a type K multipoint thermocouple (TC1-TC6 in Figure 4.1, see Appendix C for characteristics of the multipoint thermocouple) whose sensing tips are located on the cylinder axis at 5, 10, 15 cm from the bottom of each reactor body. This new way of inserting and

centering the thermocouple (TC) has improved the reliability and reproducibility of the axis temperature measurements. The original model measured the axis temperature with a TC inserted from the top which required the use of a TC holder (a stainless steel tube inserted through the center of the reactor) that caused problems with the reproducibility of the temperature measurements.^{25,26}

Additional type K thermocouples are positioned internally at the midway point of the reactor stems (TC9 and TC10 in Figure 4.1) and hose clamp thermocouples are placed on the outer reactor walls (TC7 and TC8 in Figure 4.1, see Appendix C for specifications). A union cross connects both stems with 6.35 mm stainless steel tubing side arms. The arms hold an extra outer hose clamp thermocouple (TC11 in Figure 4.1, see Appendix C for specifications), and are connected to the valves, burst diaphragm and other system components as shown in Figure 4.1. The pressure transducer (Omega, model PX 602-5KGV) has a range from 0.1 to 34.58 MPa with a 1.0% accuracy (full scale) which is used in conjunction with a digital readout (Omega, model DP25-S).

Prior to an experiment, the reactor body is filled with a weighed amount of biomass (spruce, birch, oak or cellulose) and a piece of stainless steel mesh is placed on top to retain solids in the reactor. During an experiment, the WHTB colored sections in Figure 4.1 are directly heated by a fluidized alundum sand bath (Techne, model SBL-2D, see Figure 4.2) with a maximum specified temperature rating of 600°C. The heating elements of the sand bath are checked on a routine

basis with a clamp-on amp meter to ensure that they are operating properly (3.43 A per element at 208 V).

A diaphragm pump (Speedaire model No. 26x362) is used to deliver clean dry air to fluidize the sand bath. A rotameter is installed between the pump and the sand bath to regulate airflow (maximum specified air flow of 57 L/min). A digital temperature controller (Omega model CN77R344) maintains the sand bath temperature throughout the experiment. The installation of the pump, rotameter and temperature controller has greatly improved the stability, uniformity and reproducibility of the fluidization conditions and temperature. The whole apparatus (reactor and sand bath) is enclosed in a protective structure built with welded steel tubing and Lexan panels (polycarbonate) (see Figure 4.2). The protective structure is located below a ceiling mounted canopy hood to evacuate heat and fugitive emissions.



Figure 4.2. Sand bath equipment and protective structure

A worm gear winch located on the side of the protective structure is operated with a hand drill to lower the reactor into the sand bath at the start of an experiment or to raise the reactor to terminate an experiment. A blower mounted above the primary protective structure directs cooling air through ducting to the upper arms and pressure sensor during the experiment. This system is also used to cool the reactor after an experiment is complete. Thermocouple wires exit the protective structure from the top. A total of fourteen type K TCs are connected to the WHTB to record the temperatures during an experiment; eleven are shown in Figure 4.1 and three are placed inside the sand bath at different locations to monitor uniformity of the hot fluidized sand bed surrounding the reactor. Data from the TCs and the pressure transducer are collected with a National Instruments SCXI 1303 data acquisition module connected to a computer using LabVIEW software for real time monitoring of the experiment and for data collection. A secondary Lexan shield supported by a wooden structure on wheels (see Figure 4.3) is used to further separate experimenters and the data acquisition computer from the WHTB reactor.



Figure 4.3. Secondary Lexan protective shield

4.2. Materials and Experimental Procedure

Spruce, birch, oak, cellulose and rice husk were subjected to proximate analysis according to ASTM E872-82(2013)²⁰⁰ and ASTM E830-87(1996),²⁰¹ ultimate analysis by ASTM E777-17,²⁰² E775-15²⁰³ and E778-15,²⁰⁴ and to energy density evaluation by bomb calorimetry. These analysis were performed in HNEI laboratories. For these parent materials, three samples were subjected to proximate analysis, two samples to ultimate analysis and one single sample for bomb calorimetry. Uncertainties of the proximate and higher heating value analyses were determined using six replicated samples of a lab-standard charcoal which gave the following values: volatile matter = 21.1%±0.3%, ash= 2.3%±0.1%, fixed carbon = 76.6%±0.2%, and higher heating value = 28.1%±0.2%. All uncertainties are based on absolute percentages.

Prior to each test, a sample of biomass was subjected to moisture content evaluation following ASTM E871-82²⁰⁵ with the following practical modifications: the sawdust stock was too small to supply a 50 g sample for moisture analysis at each WHTB test condition; therefore a 5 to 7 g sample was used instead. Results of the moisture content, proximate, ultimate, and higher heating value analyses are presented in Table 4.1. Values of the contents of structural components taken from elsewhere²⁰⁶ are also provided.

Table 4.1. Moisture content, elemental and proximate analysis, higher heating value, and cellulose, hemicellulose and lignin composition of Norwegian spruce, birch, cellulose, oak and rice husk feedstock.

		Spruce	Birch	Cellulose	Oak ^g	Rice Husk ^g
Moisture content [wt.%, wet basis]		7.8	7.9	5.9	7.5	7.6
Ultimate Analysis ^a [wt.%, dry basis]	C	46.93±0.05	47.4 ±0.3	41.9 ±0.1	45.4 ±0.1	35.1 ±0.3
	H	6.26±0.02	6.32±0.03	6.3±0.1	6.1±0.1	5.20±0.02
	O ^d	46.3	45.43	51.7	47.1	37.4
	N	0.20±0.02	0.20±0.02	0.08±0.04	0.215±0.002	0.366±0.001
	S	0.011±0.001	0.0158±0.001.	0.00	0.017±0.001	0.049±0.001
	Ash ^e	0.36±0.17	0.67±0.02	0.00	1.18±0.05	21.9±0.2
Proximate analysis ^b [wt.%, dry basis]	fCC ^f	14.8±0.1	13.1±0.2	6.0±0.2	14.0±0.7	13.7±1.2
	VM ^g	84.9±0.1	86.2±0.2	94.0±0.2	84.8±0.8	64.4±1.3
	Ash	0.36±0.17	0.67±0.02	0.0±0.0	1.18±0.05	21.9±0.2
Higher heating value [MJ/kg]		18.00	18.50	16.15	17.67	14.17
Contents of structural components[wt.%, dry-ash free basis] ^c	Cellulose	43.6, 47	50.2, 49.1	100	58.4	43.8
	Hemicellulose	27.4, 25.3	32.8, 31.6	0.0	31.4	31.6
	Lignin	29.0, 27.7	17.0, 19.3	0.0	10.2	24.6
	Extractives	1.8, 2.5	3.0	0.0	NA ^h	6.6

^a Average of two samples, uncertainty indicates range of values. Elemental analysis of cellulose closely resembles C 44.4%, H 6.2% and O 49.4% given by its formula (C₆H₁₀O₅)_n

^b Average of three analyses, uncertainty indicates standard deviation.

^c Composition of structural components taken from ²⁰⁶

^d Oxygen by difference.

^e Ash content determined by proximate analysis.

^f Fixed-carbon content (fCC).

^g Volatile matter content (VM).

^hNot Available (NA)

The summary below will briefly describe the steps followed when running a WHTB experiment, this procedure refers to a total of ten Standard Operating Procedures (SOPs) that are presented, in

conjunction with Job Safety Analysis (JSAs), in Appendix D-M. Each SOP presents step-by-step instructions of a routine experimental process, as well as a description of the process hazards and the systems used to prevent and control these hazards. These SOPs are:

1. Milling Biomass Material into Finely Divided Particles with a Fritsch Universal Cutting Mill Pulverisette 19 (Appendix D)
2. Assembly, Loading and Leak Testing of the Wall Heated Tubing Bomb (WHTB) (Appendix E)
3. Analysis of Feed Moisture Content (MC) (Appendix F)
4. Gas Chromatograph (GC) Operation (Appendix G)
5. Water Displacement Vessel (WDV) Operation (Appendix H)
6. Volume Evaluation of the Wall Heated Tubing Bomb (Appendix I)
7. Performing an Experiment, Unloading and Disassembly of the Wall Heated Tubing Bomb (Appendix J)
8. Analysis of the Charcoal Moisture Content (Appendix K)
9. Proximate Analysis (Appendix L)
10. Replacing and Operating Gas Cylinders (Appendix M)

The SOPs used for a typical experiment are summarized in Table 4.2 to provide chronological order helpful in reviewing the SOPs. The SOPs for milling fuel (SOP #1 in the list above) and changing gas cylinders (SOP #10) are used as required.

Table 4.2. Schedule of SOP use during performance of WHTB experiments (number in parentheses reflects number of SOP in list above).

Day 1	Day 2	Day 3
Assemble, load, and leak test WHTB (2)	Start GC (4)	Clean reactor (7)
Start feed MC analysis (3)	Continue feed MC analysis (3)	Continue last week's proximate analysis and begin this week's proximate analyses (9)
Prepare GC (4) and WDV (5)	Continue last week proximate analyses (9)	Begin charcoal MC analysis (8)
Fix leaks (2)	Perform Volume evaluation on WHTB (6)	
Continue last week's proximate analyses (9)	Perform experiment, unload, and disassemble WHTB (7)	

During the reactor assembly process, the feedstock and each reactor piece were weighed and recorded. 12-17 g of oak, ~27 g of cellulose (~20 g in the original reactor)⁵⁸, or 14-26 g of dry spruce or birch were spooned into each reactor body, the reactor bodies were gently tapped during the loading to help fill voids and to loosely compact the biomass (SOP #2). The assembled reactor was pressurized and leak tested with nitrogen. Due to leak issues, WHTB reactors were usually replaced after every 3 experiments. A small sample of biomass was subjected to moisture content evaluation (SOP #3).

Prior to running the experiment, the sand bath was heated until the desired HTT was reached and stabilized (typically to 300, 400, 500 or 550°C). A reactor volume evaluation was performed with nitrogen to determine the gas volume in the WHTB containing the biomass sample (SOP #6), this step also served to flush air from the system. The reactor was pressurized with nitrogen to the desired level specified for the test, and the pressure and temperature sensors were connected to the data acquisition system.

The process employed to heat up the reactor depended on the run. In a typical experiment with birch or spruce biomass fuels, the reactor was immersed into the hot sand bath after it had stabilized at the target temperature of 300, 400, 500 or 550°C. In experiments that studied the effect of slower heating rates, the reactor was immersed in a sand bath heated to 100°C and then subsequently ramped to the desired HTT. In the case of preliminary experiments with cellulose²⁶ and oak biomass fuels that were performed at a HTT of 300 °C (or below), the reactor was heated in the same way as described for birch or spruce above, whereas experiments at HTTs over 300 °C (350, 370 or 400°C), the WHTB was immersed into a 300 °C sand bath that was subsequently ramped to the target temperature. Over the course of a test, data were recorded in LabVIEW every second.

After reaching the planned experimental endpoint, the WHTB was removed from the hot sand bath and cooled down to room temperature with an air stream from the overhead blower. A typical “long” experiment with birch or spruce was terminated 190 minutes after the WHTB was submerged into the hot sand bath, while a typical “short” experiment finishes 10 minutes after the

end of the exotherm, i.e. the exotherm was considered to end once the pressure rise had considerably slowed down. The total experimental time of the short runs was around 30 minutes. Long “slow heating rate” experiments were halted when the reactor remained at the target temperature for a time period similar to the holding time experienced by the typical long experiments (i.e. 190 min of total immersion time minus heating time) whereas short “slow heating rate” experiments were terminated as soon as the sand bath reached the target temperature. Preliminary tests on oak and cellulose at HTT of 300°C were terminated 10 minutes after the exotherm (short experiments) and finally, preliminary tests at HTTs over 300°C were ended when the sand bath reached the target temperature.

Once the reactor was removed and cooled to room temperature, the gas phase contained in the WHTB was depressurized into a water displacement vessel (WDV) and then analyzed by gas chromatograph (SOPs#4 and #5). The amount of water displaced from the WDV was weighed to calculate the final active gas volume using the ideal gas law (for additional details, see ²⁵). After the gases were transferred to the WDV, the reactor was disassembled and the solid product (charcoal) and stainless steel screen were carefully removed (SOP #7). The stainless steel was subjected to a moisture content analysis according to ASTM D1576-13²⁰⁷ at 105°C in a convection oven.

The charcoal moisture content was immediately analyzed using ASTM E1756-08²⁰⁸ in a vacuum oven, instead of the convection oven specified by the standard method- to prevent charcoal combustion (SOP#8). In order to avoid possible errors due to non-representative subsamples of

the charcoal product, a total moisture content analysis was performed on the entirety of the charcoal product recovered from the reactor. This moisture content analysis result has direct influence on the measurements of charcoal yield, mass balance and fixed-carbon yield.

Subsequently, a subsample of the charcoal was ground ≤ 20 mesh (≤ 0.841 mm) using mortar and pestle, loaded into nickel-chromium crucibles and subjected to proximate analysis according to ASTM E872-82(2013)²⁰⁰ and ASTM E830-87(1996)²⁰¹ (SOP #9). A mill was not used to grind samples because of the limited amount of charcoal sample produced from each experiment. Charcoal produced in preliminary experiments with oak or cellulose were subject to proximate analysis by standard ASTM D1762-84.²⁰⁹ A reproducibility study was performed to assess the uncertainty in the results from proximate analysis of certified coal standards and charcoals under various methods and configurations (see Appendix N). It was concluded that standards ASTM E872-82(2013)²⁰⁰ and ASTM E830-87(1996)²⁰¹ provided a more accurate measure of the proximate analysis values of the coal reference materials used to test the methods. Note: if SEM analysis was to be performed, a small amount of un-crushed sample was separated from the bulk sample before grinding. Selected charcoal samples were sent to SINTEF Energy Research for SEM (ZEISS SUPRA-55) analysis.

CHAPTER 5. STUDY OF REPRODUCIBILITY, EXPERIMENTAL PROFILE AND EXPERIMENTAL DESIGN

Experimental profile, conditions and results are reported in this chapter. The first section of the chapter describes the temperature and pressure history observed in typical WHTB experiments. The second section provides a detailed description of a reproducibility study from WHTB data. Experimental errors and data accuracy are determined. The final section of the chapter tabulates a list of experimental conditions and results, and presents a parity plot that depicts theoretical fixed-carbon yields versus experimental values.

5.1. Experimental Profile

Figure 5.1 shows a typical WHTB experimental profile from the dual intermediate reactor (i.e. with the single point internal reactor thermocouple) and Figure 5.2 shows a profile of an experiment with the current reactor (i.e. with the multipoint internal reactor thermocouple). As soon as the reactor enters the sand bath, the outer wall temperatures immediately start to rise followed by the axis temperature. This is expected as the heat flow is from the sand bath to the reactor wall, and then radially inward, through the porous fuel bed, toward the longitudinal axis of the reactor. This initial lag between wall and axis temperature illustrates the temperature gradient across the reactor. Similar to typical heating rates employed in slow pyrolysis (0.1-1°C/s)¹⁷⁻¹⁹ or flash-carbonization ($\sim 1^\circ\text{C/s}$)²¹, the biomass in the CVC reactor experiences rates

of about 0.5-1°C/s. In comparison, flash-pyrolysis reactors employ notably faster rates ranging between 10-1000°C/s.¹⁷⁻¹⁹

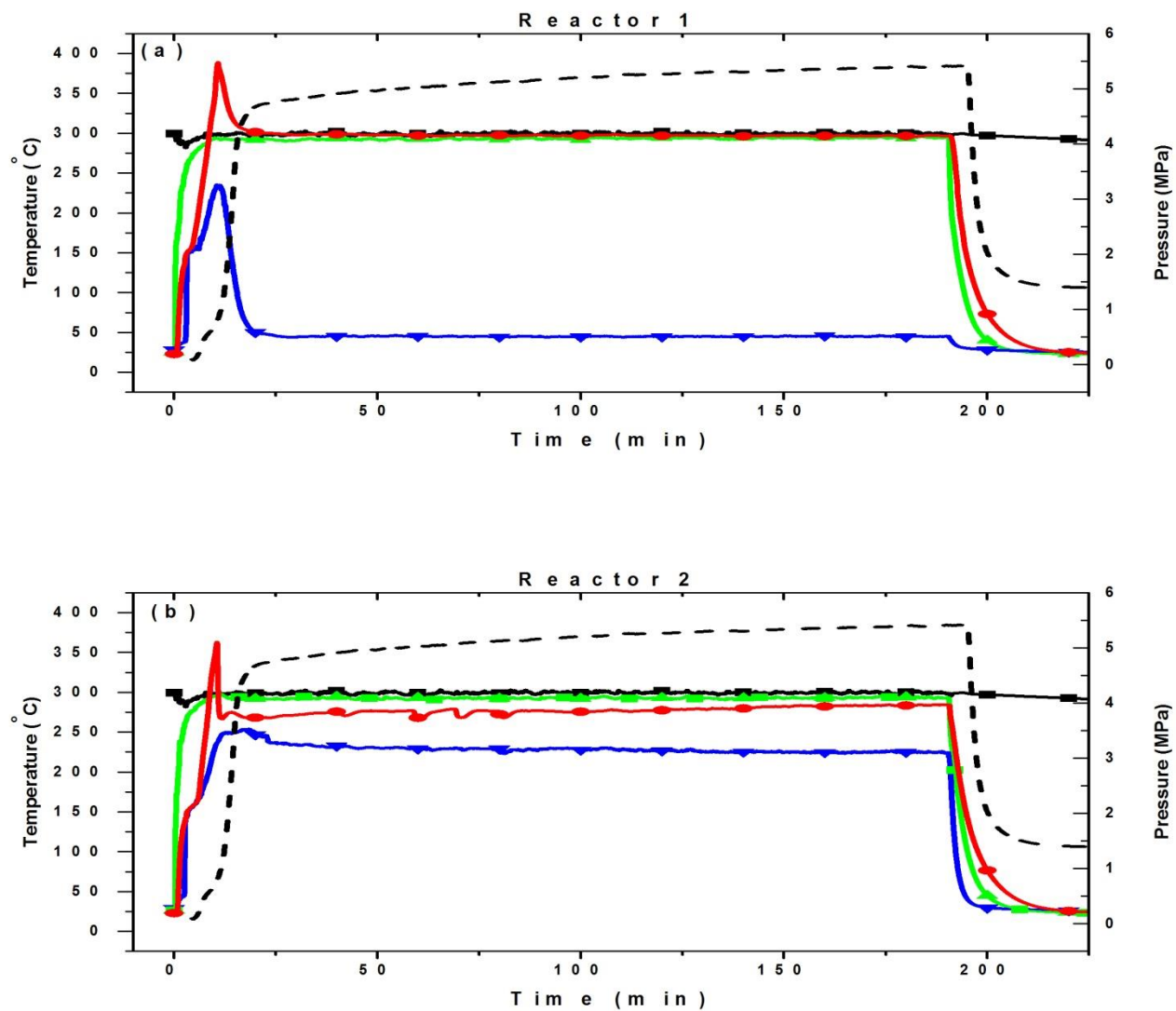


Figure 5.1. Temperature and pressure profile of a constant-volume carbonization experiment with birch as the feedstock, a heat treatment temperature of 300°C and an initial nitrogen pressure of 0.1 MPa. (a) Profile of reactor body 1 and (b) Profile of reactor body 2. ● Axis temperature. ■ Sand bath temperature. ▼ Stem temperature. ▲ Wall temperature. -- Pressure.

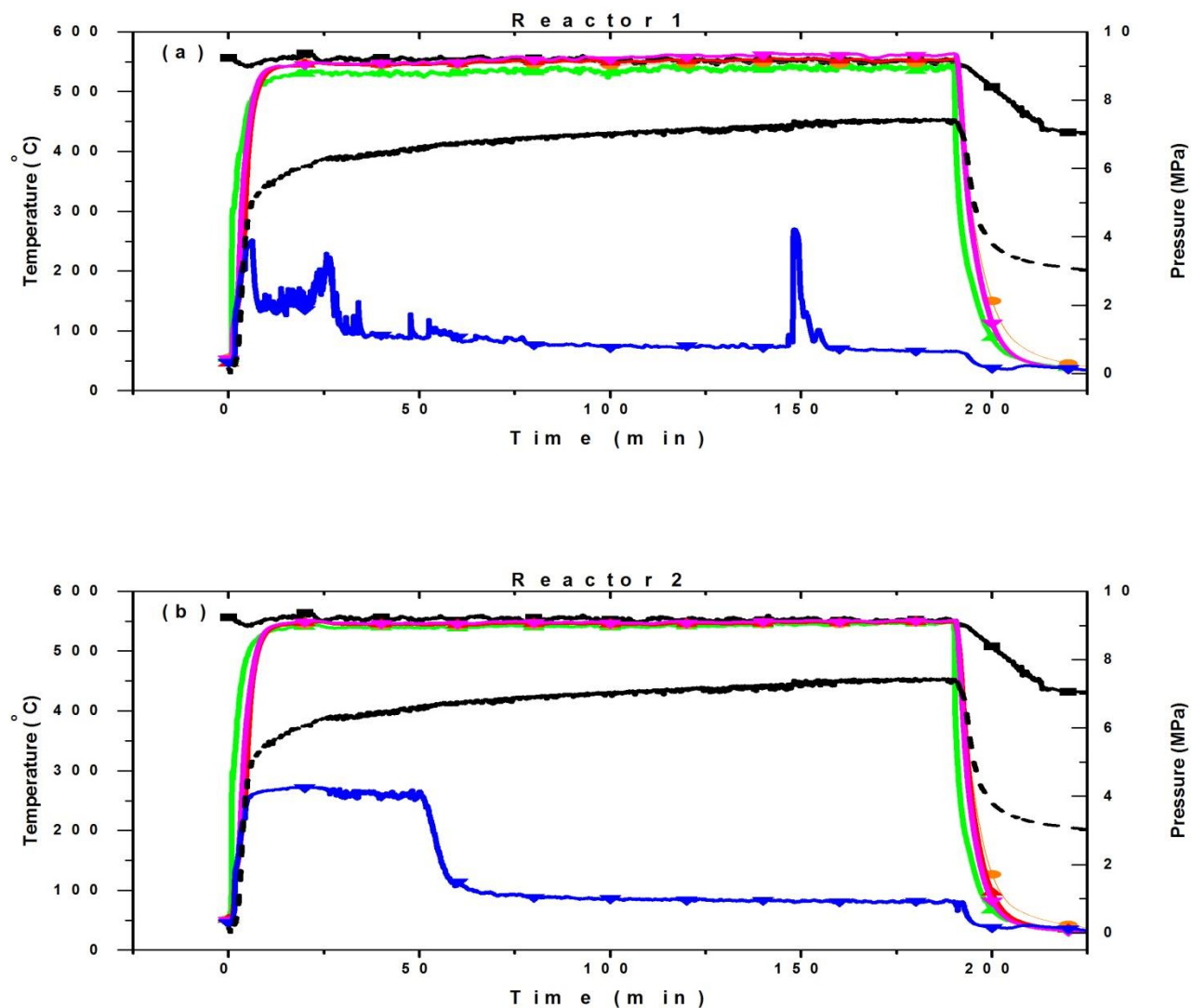


Figure 5.2. Temperature and pressure profile of a constant-volume carbonization experiment with birch as the feedstock, a heat treatment temperature of 550°C and an initial nitrogen pressure of 0.1 MPa. (a) Profile of reactor body 1 and (b) Profile of reactor body 2. ● Axis temperature sensor 1. ▲ Axis temperature sensor 2. ▼ Axis temperature sensor 3. ■ Sand bath temperature. ▼ Stem temperature. ▲ Wall temperature. -- Pressure.

As demonstrated in the experiment at a HTT of 300°C in Figure 5.1, after ~5 minutes the reactor wall temperature approaches the sand bath temperature, the reactor pressure reaches ~0.55 MPa and the axis temperatures is ~165°C. At this point, the rise in pressure and axis temperature accelerates, indicating the dominance of exothermic pyrolytic reactions that causes the axis temperatures to exceed the sand bath and wall temperatures. Figure 5.1 shows exothermic peaks of 363 and 389°C measured in the two reactors. These observations are in line with the description elsewhere of carbonization phenomena,⁴⁰ where above 280°C, wood carbonization became exothermic. Without an external source of heat, this exotherm is not expected to exceed ~400°C. In the experiment at a HTT of 550°C in Figure 5.2, the exotherm effect is masked by the fast heating rates imposed by the sand bath.

In the WHTB, the exothermic temperature peak has been demonstrated to greatly vary with mass loading ($\text{Mass}_{\text{biomass}}/\text{Volume}_{\text{reactor}}$), the feedstock particle size, the HTT and the biomass type. Higher mass loadings, greater HTTs and smaller particles result in greater exothermic peaks and higher final pressures. Increasing the pretest reactor pressure with inert gas appeared to produce no significant changes in the exothermic peaks, char yields or fixed-carbon contents (see Sections 3.6 and 6.6). In line with Mok et al. observations,⁴² it is the partial pressure of volatiles, not the system pressure, that appears to have the dominant effect on the results.

The overall heat of reaction has been widely recognized as the net result of exothermic reactions that favor the formation of char and endothermic reactions that enhance volatile release.^{39,178,184,193,195} Promoting charring reactions shifts the balance in favor of exothermicity.

In a reactor equipped with a gas stream, long vapor residence times, low heating rates and larger particles favor char-forming over tar-forming reactions (see Literature Review for details and references). The current work on CVC has shown an enhancement in char formation-and therefore greater exothermic peaks-when higher mass loadings, greater HTTs and/or smaller particles were employed.

Figures 5.1 and 5.2 suggest that steady state was not attained during the 190 minute experiment as indicated by the continuous rise in pressure observed over the course of the experiment. Most of the experiments presented herein showed a similar temperature and pressure profile.

Exceptionally, an experiment that carbonized small spruce particle sizes seemed to reach stability within 120 minutes indicating that small particles may speed up the carbonization process. In line with these observations, carbonization of small grains of oak sawdust and cellulose performed in the original WHTB reactor appeared to reach stability more quickly (by 10 minutes after the end of the exotherm).

A temperature disparity between the two reactors is evident in Figures 5.1 and 5.2, especially between the stem and wall temperatures. Also, distinctly different char moisture contents were obtained from the two reactors. These differences are generally observed but with some variability between experiments. A preferential condensation path for liquid pyrolytic products (due to one of the reactors being slightly lower than the other) could explain these observations. Nevertheless, these differences in temperature profiles and char moisture contents have a

negligible effect on the char yields (dry basis), char proximate analysis and visual properties of the final char.

5.2. Study of Reproducibility

To study the data reproducibility, five experiments with spruce as the feedstock were performed under the same experimental conditions: a HTT of 300°C, an initial reactor nitrogen pressure of 0.1 MPa, a mass loading of around 100g/L and an immersion time of 190 minutes. The WHTB reactor employed for this part of the study was the intermediate, single-reactor model (see Section 4.1). Figure 5.3 illustrates the product yields from the five replicated experiments performed in the single WHTB.

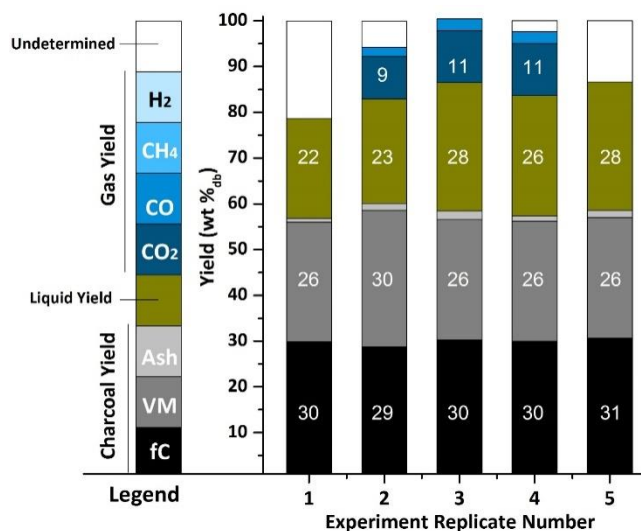


Figure 5.3. Reproducibility study on the yields of char, condensates and gas products from the constant-volume carbonization of spruce at a heat treatment temperature of 300°C and an initial nitrogen pressure of 0.1 MPa. Negligible free tars were recovered in the experiments. Liquid yield mainly represents water content of the final moist charcoal.

To compare results between the intermediate single reactor and the dual WHTB configurations, two additional experiments were carried out under the same conditions with the intermediate dual-reactor model. Figure 5.4 compares the average values of the product yields from the five repeated experiments shown in Figure 5.3 with the yields obtained from the two runs with the intermediate, dual reactor. Error bars are calculated as the standard deviation of the replicates.

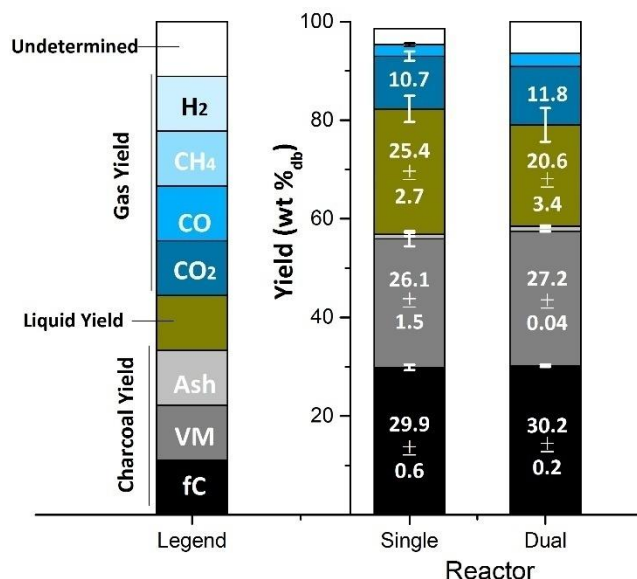


Figure 5.4. Comparison between product yields from spruce constant-volume carbonization experiments in the single and dual Wall Heated Tubing Bombs at a heat treatment temperature of 300°C and an initial nitrogen pressure of 0.1 MPa.

As shown by Figures 5.3 and 5.4, solid and gas yields derived from the single WHTB have good repeatability and were comparable to the yields from the dual reactor. On the other hand, the recovered liquid yields noticeably varied between experiments. This is somewhat expected due to the difficulty in quantifying the amount of liquid produced as it is dispersed throughout the WHTB reactor system. Some of the condensate is located in the reactor tubing or WDV, some is adsorbed on the stainless steel mesh and on the surface of the char, and some is lost due to evaporation during the removal of char and disassembly of the reactor.

Liquid yields are calculated from the weight loss from drying the moist charcoal and the stainless steel mesh. The carbon mass balances are a more reliable measure of product recovery (compared to the liquid yield). The amount of carbon present in the feedstock prior to the experiment was compared to that present in the solid charcoal and in the gas species CO₂, CO and CH₄. The carbon in both feedstock and charcoal was determined by elemental analysis and the gas composition was quantified by gas chromatography. Carbon mass balances revealed that 97.2±0.2% of the carbon weight was recovered in the reproducibility study, indicating that the reported charcoal and gas yields are highly reliable and that carbon in the free-tar accounted for <3% of the total. Nonetheless, tars may condense and adsorb to the surface of the solid charcoal in the cooling period, and would be expected to contribute to higher volatile matter content in the proximate analysis and higher C and H contents in the elemental analysis of the final charcoal product.

If focus is placed on the solid product yields and liquid and gas yields are removed from Figures 5.3 and 5.4, the new figures (Figures 5.5 and 5.6) depict the results of proximate analysis on charcoal. The charcoal product from each reactor body of the dual WHTB was recovered and analyzed separately. As shown in Figure 5.6, charcoals from the dual reactor have similar proximate analysis values as the charcoal produced from the single WHTB reactor.

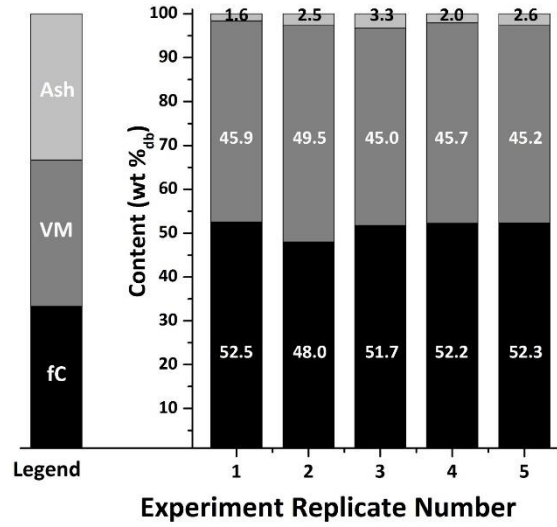


Figure 5.5. Reproducibility study on the proximate analysis of charcoals derived from the constant-volume carbonization of spruce at a heat treatment temperature of 300°C and an initial nitrogen pressure of 0.1 MPa.

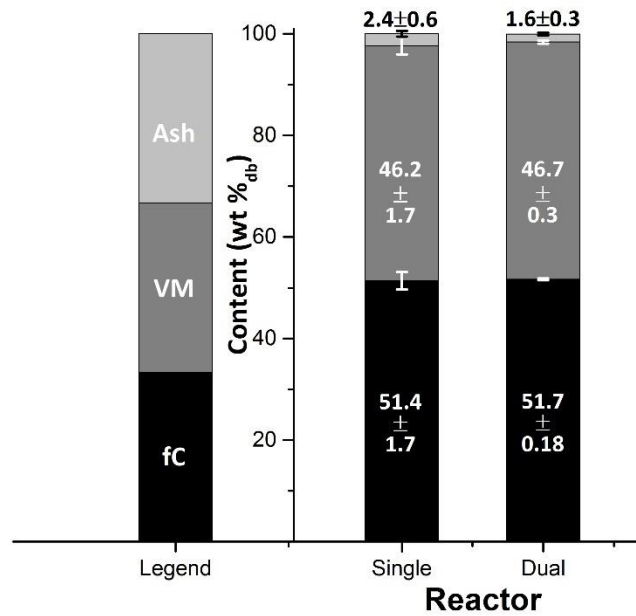


Figure 5.6. Comparison between proximate analyses of charcoals derived from the constant-volume carbonization of spruce in the single and dual Wall Heated Tubing Bombs at a heat treatment temperature of 300°C and an initial nitrogen pressure of 0.1 MPa.

5.3. List of Experiments and Parity Plot

Eight factors -(i) closed vessel versus open vessel, (ii) initial reactor pressure, (iii) HTT, (iv) particle size, (v) heating rate, (vi) mass loading, (vii) immersion time and (viii) biomass type- were investigated with the objective of understanding the effects of operating parameters on the gaseous, liquid and solid product yields, gas composition, and physical and chemical properties (proximate analysis, elemental analysis and energy density) of the final charcoal manufactured from CVC of wood.

Table 5.1 lists the conditions and results of 49 experiments. A factorial experimental design was initially developed, however limitations imposed by operating conditions and safety defined the experimental program shown in the table. Fifteen preliminary experiments studied the effects of factors i to iii (closed vessel versus open vessel, initial reactor pressure, and HTT) with oak biomass as the feedstock in the original reactor. The rest of the experiments that followed this preliminary experimental round used Norwegian birch or spruce wood as the feedstocks (three isolated experiments used oak, cellulose and rice husk) to confirm the observed effects of factors ii and iii (initial reactor pressure and HTT) and to study the roles played by factors iv to viii (particle size, heating rate, mass loading, immersion time and biomass type).

Table 5.1. Conditions and results for Wall Heated Tubing Bomb experiments. Superscripts meanings shown in footnotes at the bottom of the table.

Experiment Number	1	2	3	4	5	6
Date (yymmdd)	151201	151125	150121	141210	150218	150129
Conditions						
Reactor Type	Original	Original	Original	Original	Original	Original
Feedstock	Oak	Oak	Oak	Oak	Oak	Oak
Heat Treatment Temperature[°C]	300	300	300	300	300-400	300-400
Pretest Nitrogen Pressure [MPa]	0.1	0.1	1.48	2.69	2.69	2.69
Immersion Time [min] ^a	34	134	24	38	44	55
Mass Loading [g biomass/L _{reactor}]	~100	~100	~120	~160	~155	~120
Particle size[mm]	0.149- 0.425	0.149- 0.425	0.149- 0.425	0.149- 0.425	<105	Coarse
Reactants						
Moist Mass [g]	12.77	13.63	11.44	16.92	15.63	12.02
Moisture Content [%, wb] ^b	7.68	7.65	7.62	7.49	6.79	7.32
Pyrolysis Reaction						
Axis Peak Temperature [°C]	304	233	294	311	346	379
Wall Peak Temperature [°C]	304	311	292	293	356	388
Peak Pressure [MPa]	0.1	NA ^k	5.18	7.62	9.86	9.38
Solid Products						
Char Moist Mass [g]	8.42	10.15	8.38	11.40	11.37	8.41
Char Moisture Content [%, wb] ^{b, e}	3.34	28.53	30.84	15.50	28.39	29.75
Volatile Matter Content [%, db] ^c	63.1	40.9	49.3	50.8	27.4	27.5
Ash Content [%, db] ^c	1.9	3.6	1.0	0.9	10.8	1.4
Fixed Carbon Content [%, db] ^c	34.4	55.5	49.7	48.3	61.9	71.1
Fixed Carbon Yield [%, db] ^c	23.99	32.52	28.40	30.88	37.54	39.16
Higher Heating Value [MJ/kg]	NA ^k	NA ^k	NA ^k	NA ^k	NA ^k	NA ^k
Gas Products						
Final Gas in V _{Bomb} [mol] ^d	NA ^k	0.054	0.104	0.170	0.194	0.181
Nitrogen [mol %]	NA ^k	12.04	69.84	69.48	66.72	71.64
Oxygen [mol %]	NA ^k	1.55	0.06	0.00	0.00	0.00
Hydrogen [mg/g (Dry Feed)]	NA ^k	NA ^k	0.093	0.061	0.19	0.18
Methane [mg/g (Dry Feed)]	NA ^k	NA ^k	0.031	0.024	0.00	0.00
Carbon Monoxide [mg/g (Dry Feed)]	NA ^k	NA ^k	190	180	210	270
Carbon Dioxide [mg/g (Dry Feed)]	NA ^k	NA ^k	100	120	160	160
Mass Balance						
Gas Products [%, db] ^c	NA ^k	NA ^k	12.37	14.06	18.29	18.98
Char Yield [%, db] ^c	69.80	58.59	56.90	63.61	57.30	54.81
Liquid [%, db] ^c	NA ^k	15.86	26.02	16.67	18.47	19.06
Solid not recovered [%, db] ^{c, f}	NA ^k	NA ^k	NA ^k	NA ^k	NA ^k	NA ^k
Total [%, db]^c	NA^k	NA^k	95.28	94.35	94.06	92.86
Carbon Balance Total [%, db]^c	NA^k	NA^k	NA^k	NA^k	NA^k	NA^k

Table 5.1. Conditions and results for Wall Heated Tubing Bomb experiments (Continued).

Experiment Number	7	8	9	10	11	12
Date (yymmdd)	150115	150909	160114	160120	160126	160209
Conditions						
Reactor Type	Original	Original	Original	Original	Original	Original
Feedstock	Oak	Oak	Oak	Oak	Oak	Oak
Heat Treatment Temperature[°C]	300	300-370	300-400	300-350	300-400	300-370
Pretest Nitrogen Pressure [MPa]	4.79	4.79	3.55	4.79	4.79	2.69
Immersion Time [min] ^a	21	181	84	37	63	120
Mass Loading [g _{biomass} /L _{reactor}]	~120	~145	~145	~145	~155	~155
Particle size[mm]	0.149- 0.425	0.149- 0.425	0.149- 0.425	0.149- 0.425	0.149- 0.425	0.149- 0.425
Reactants						
Moist Mass [g]	12.22	13.26	13.48	13.47	14.38	14.49
Moisture Content [%, wb] ^b	7.73	7.70	7.58	7.58	7.60	7.51
Pyrolysis Reaction						
Axis Peak Temperature [°C]	309	352	364	347	356	351
Wall Peak Temperature [°C]	294	364	387	352	384	359
Peak Pressure [MPa]	10.60	13.06	11.80	13.19	14.36	9.62
Solid Products						
Char Moist Mass [g]	9.61	8.98	9.68	9.72	11.68	9.69
Char Moisture Content [%, wb] ^{b, e}	29.26	32.66	33.57	25.87	41.96	28.93
Volatile Matter Content [%, db] ^c	49.3	28.2	24.3	33.3	25.9	25.3
Ash Content [%, db] ^c	1.3	2.9	3.4	2.9	2.6	2.9
Fixed Carbon Content [%, db] ^c	49.3	68.8	72.4	63.8	71.5	71.8
Fixed Carbon Yield [%, db] ^c	30.79	35.81	34.96	38.35	36.46	38.76
Higher Heating Value [MJ/kg]	NA ^k	NA ^k	NA ^k	NA ^k	NA ^k	NA ^k
Gas Products						
Final Gas in V _{Bomb} [mol] ^d	0.142	0.279	0.211	0.260	0.226	0.173
Nitrogen [mol %]	85.91	80.02	82.98	81.01	77.90	67.83
Oxygen [mol %]	1.38	1.11	0.90	0.26	0.00	0.00
Hydrogen [mg/g (Dry Feed)]	0.071	0.23	0.32	0.142	0.181	0.200
Methane [mg/g (Dry Feed)]	0.053	0.78	0.57	0.00	0.00	0.00
Carbon Monoxide [mg/g (Dry Feed)]	170	180	22	19	20	19
Carbon Dioxide [mg/g (Dry Feed)]	110	170	94	150	170	150
Mass Balance						
Gas Products [%, db] ^c	12.62	18.58	11.66	17.12	18.66	17.08
Char Yield [%, db] ^c	62.09	52.03	48.31	60.10	51.02	53.96
Liquid [%, db] ^c	24.34	30.73	32.82	23.43	28.66	16.79
Solid not recovered [%, db] ^{c, f}						
Total [%, db]^c	99.05	101.34	92.80	100.65	98.34	87.83
Carbon Balance Total [%, db]^c	NA^k	NA^k	NA^k	NA^k	NA^k	NA^k

Table 5.1. Conditions and results for Wall Heated Tubing Bomb experiments (Continued).

Experiment Number	13	14	15	16-20 ^h	21
Date (yyymmdd)	160217	160224	160301	161207-170126	170131
Conditions					
Reactor Type	Original	Original	Original	Single-intermediate	Single-intermediate
Feedstock	Oak	Oak	Oak	Spruce	Oak
Heat Treatment Temperature[°C]	300-400	300-400	300-400	300	300
Pretest Nitrogen Pressure [MPa]	2.69	2.69	0.1	0.1	0.1
Immersion Time [min] ^a	46	37	180	190	190
Mass Loading [g _{biomass} /L _{reactor}]	~130	~145	~145	~100	~125
Particle size[mm]	0.149-0.425	0.149-0.425	0.149-0.425	<2	0.149-0.425
Reactants					
Moist Mass [g]	12.05	13.35	12.56	13.38	16.32
Moisture Content [%, wb] ^b	7.51	7.51	7.56	8.15	7.89
Pyrolysis Reaction					
Axis Peak Temperature [°C]	320	326	391	317	380
Wall Peak Temperature [°C]	372	396	397	296	297
Peak Pressure [MPa]	8.75	8.69	3.00	2.63	3.54
Solid Products					
Char Moist Mass [g]	9.11	9.76	6.66	10.84	12.95
Char Moisture Content [%, wb] ^{b, e}	34.26	34.46	15.32	35.01	40.1
Volatile Matter Content [%, db] ^c	30.5	26.9	27.6	45.7	38.6
Ash Content [%, db] ^c	2.8	3.1	2.8	2.0	3.6
Fixed Carbon Content [%, db] ^c	66.6	70.1	69.6	52.2	57.4
Fixed Carbon Yield [%, db] ^c	38.62	38.06	34.11	29.9	29.6
Higher Heating Value [MJ/kg]	NA ^k	NA ^k	NA ^k	28.92	28.23
Gas Products					
Final Gas in V _{Bomb} [mol] ^d	0.161	0.154	0.063	0.054	0.073
Nitrogen [mol %]	72.93	67.88	9.13	17.70	NA ^k
Oxygen [mol %]	0.00	0.12	0.37	1.60	NA ^k
Hydrogen [mg/g (Dry Feed)]	0.103	0.134	0.203	0.149	NA ^k
Methane [mg/g (Dry Feed)]	0.191	0.00	0.093	0.00	NA ^k
Carbon Monoxide [mg/g (Dry Feed)]	20	20	33	25.88	NA ^k
Carbon Dioxide [mg/g (Dry Feed)]	150	140	140	114.11	NA ^k
Mass Balance					
Gas Products [%, db] ^c	16.56	15.94	17.18	14.01	NA ^k
Char Yield [%, db] ^c	57.95	54.31	49.01	57.32	51.59
Liquid [%, db] ^c	22.76	24.67	3.82	26.32	28.25
Solid not recovered [%, db] ^{c, f}					
Total [%, db]^c	97.27	94.91	70.01	97.66	NA^k
Carbon Balance Total [%, db]^c	NA^k	NA^k	NA^k	97.14	NA^k

Table 5.1. Conditions and results for Wall Heated Tubing Bomb experiments (Continued).

Experiment Number	22	23-24^h		25		26	
Date (yymmdd)	170207	170215, 170309		170313		170316	
Conditions		With dead volume^g					
Reactor Type	Single-intermediate	Dual-intermediate		Dual-intermediate		Dual-intermediate	
Feedstock	Cellulose	Spruce		Spruce		Spruce	
Heat Treatment Temperature[°C]	300	300		300		400	
Pretest Nitrogen Pressure [MPa]	0.1	0.1		0.1		0.1	
Immersion Time [min] ^a	190	190		190		190	
Mass Loading [g biomass/L _{reactor}]	~205	~100		~130		~130	
Particle size[mm]	0.050-0.180	<2		<2		<2	
Reactants		R1 ⁱ	R2 ^j	R1 ⁱ	R2 ^j	R1 ⁱ	R2 ^j
Moist Mass [g]	27.37	13.34	14.01	14.64	13.83	13.99	14.45
Moisture Content [%, wb] ^b	6.49	7.90		7.55		7.93	
Pyrolysis Reaction							
Axis Peak Temperature [°C]	552	310	317	317	336	427	499
Wall Peak Temperature [°C]	310	295	304	285	302	390	405
Peak Pressure [MPa]	7.09	2.72		4.65		7.74	
Solid Products							
Char Moist Mass [g]	13.58	8.87	11.91	10.44	11.21	8.30	7.46
Char Moisture Content [%, wb] ^{b, e}	25.5	15.94	38.07	22.63	34.83	30.15	22.79
Volatile Matter Content [%, db] ^c	28.0	46.2	46.6	46.2	46.9	26.2	23.6
Ash Content [%, db] ^c	0.2	2.1	1.4	1.8	1.7	1.7	1.5
Fixed Carbon Content [%, db] ^c	71.8	51.7	52.0	52.0	51.4	72.1	75.0
Fixed Carbon Yield [%, db] ^c	28.4	30.5	30.6	30.4	30.0	31.84	33.08
Higher Heating Value [MJ/kg]	31.13	28.52	28.77	28.79	30.83	31.92	35.03
Gas Products							
Final Gas in V _{Bomb} [mol] ^d	0.143	0.117		0.119		0.195	
Nitrogen [mol %]	NA ^k	18.22		16.87		12.19	
Oxygen [mol %]	NA ^k	1.04		0.86		0.74	
Hydrogen [mg/g (Dry Feed)]	NA ^k	0.234		0.188		0.612	
Methane [mg/g (Dry Feed)]	NA ^k	0.01		0.00		0.00	
Carbon Monoxide [mg/g (Dry Feed)]	NA ^k	26.41		23.83		43.27	
Carbon Dioxide [mg/g (Dry Feed)]	NA ^k	118.21		127.23		185.68	
Mass Balance							
Gas Products [%, db] ^c	NA ^k	14.49		15.13		22.96	
Char Yield [%, db] ^c	39.53	58.88		58.44		44.14	
Liquid [%, db] ^c	23.24	17.15		16.77		8.50	
Solid not recovered [%, db] ^{c, f}						3.42	
Total [%, db]^c	NA^k	90.52		90.34		79.01	
Carbon Balance Total [%, db]^c	NA^k	99.13		100.30		92.30	

Table 5.1. Conditions and results for Wall Heated Tubing Bomb experiments (Continued).

Experiment Number	27		28		29		30	
Date (yymmdd)	170321		170323		170509		170511	
Conditions	Finish 10 min after exotherm		Finish 10 min after exotherm				Finish 10 min after exotherm	
Reactor Type	Dual-intermediate		Dual-intermediate		Dual-intermediate		Dual-intermediate	
Feedstock	Spruce		Spruce		Spruce		Spruce	
Heat Treatment Temperature[°C]	300		400		300		300	
Pretest Nitrogen Pressure [MPa]	0.1		0.1		0.1		0.1	
Immersion Time [min] ^a	28		18		190		24	
Mass Loading [g biomass/L _{reactor}]	~130		~130		~130		~165	
Particle size[mm]	<2		<2		<0.2		<0.2	
Reactants	R1 ⁱ	R2 ^j	R1 ⁱ	R2 ^j	R1 ⁱ	R2 ^j	R1 ⁱ	R2 ^j
Moist Mass [g]	13.96	13.62	14.60	14.27	13.87	14.48	19.48	17.84
Moisture Content [%, wb] ^b	7.68		7.77		7.52		7.11	
Pyrolysis Reaction								
Axis Peak Temperature [°C]	318	325	408	437	390	419	398	391
Wall Peak Temperature [°C]	290	299	394	395	302	301	294	299
Peak Pressure [MPa]	3.95		7.12		5.62		5.68	
Solid Products								
Char Moist Mass [g]	9.37	11.38	8.96	9.91	9.22	11.81	19.08	11.18
Char Moisture Content [%, wb] ^{b, e}	17.15	35.33	27.30	35.11	22.38	38.03	45.19	3.65
Volatile Matter Content [%, db] ^c	53.3	54.6	32.3	33.1	39.6		47.1	
Ash Content [%, db] ^c	0.9	1.0	1.5	1.3	1.8		1.4	
Fixed Carbon Content [%, db] ^c	45.8	44.4	66.3	65.6	58.6		51.4	
Fixed Carbon Yield [%, db] ^c	27.20	26.39	32.23	31.89	32.27		31.50	
Higher Heating Value [MJ/kg]	31.06	27.81	30.75	30.82	28.82		28.71	
Gas Products								
Final Gas in V _{Bomb} [mol] ^d	0.099		0.173		0.132		0.152	
Nitrogen [mol %]	15.93		6.61		9.09		8.19	
Oxygen [mol %]	1.11		0.00		0.08		0.00	
Hydrogen [mg/g (Dry Feed)]	0.100		0.249		0.177		0.207	
Methane [mg/g (Dry Feed)]	0.00		0.00		0.00		0.00	
Carbon Monoxide [mg/g (Dry Feed)]	23.12		47.29		31.69		28.88	
Carbon Dioxide [mg/g (Dry Feed)]	100.81		171.93		147.03		138.64	
Mass Balance								
Gas Products [%, db] ^c	12.40		21.95		17.89		16.77	
Char Yield [%, db] ^c	59.39		48.62		55.21		61.24	
Liquid [%, db] ^c	15.58		15.04		17.89		19.33	
Solid not recovered [%, db] ^{c, f}	4.76		2.00		3.49		1.63	
Total [%, db]^c	92.14		87.60		94.48		98.96	
Carbon Balance Total [%, db]^c	97.40		96.03		99.54		104.03	

Table 5.1. Conditions and results for Wall Heated Tubing Bomb experiments (Continued).

Experiment Number	31		32		33		34	
Date (yymmdd)	170516		170518		170523		170802	
Conditions	Finish 10 min after exotherm							
Reactor Type	Dual-intermediate		Dual-intermediate		Dual-intermediate		Dual-intermediate	
Feedstock	Spruce		Birch		Birch		Birch	
Heat Treatment Temperature[°C]	300		300		400		300	
Pretest Nitrogen Pressure [MPa]	0.1		0.1		0.1		0.1	
Immersion Time [min] ^a	24		190		190		190	
Mass Loading [g biomass/L _{reactor}]	~130		~130		~130		~130	
Particle size[mm]	<0.2		<2		<2		<0.2	
Reactants	R1 ⁱ	R2 ^j	R1 ⁱ	R2 ^j	R1 ⁱ	R2 ^j	R1 ⁱ	R2 ^j
Moist Mass [g]	14.22	14.01	14.34	14.01	14.62	14.22	14.30	14.38
Moisture Content [%, wb] ^b	7.02		7.88		7.98		7.27	
Pyrolysis Reaction								
Axis Peak Temperature [°C]	408	404	389	363	509	478	299	300
Wall Peak Temperature [°C]	301	299	296	298	392	393	310	299
Peak Pressure [MPa]	4.60		5.42		7.42		5.01	
Solid Products								
Char Moist Mass [g]	8.65	10.58	9.11	9.89	8.74	7.39	9.30	10.43
Char Moisture Content [%, wb] ^{b, e}	19.07	27.88	25.23	29.57	35.02	24.40	22.83	31.41
Volatile Matter Content [%, db] ^c	50.7		40.7		25.0		39.1	
Ash Content [%, db] ^c	1.3		1.8		1.9		3.7	
Fixed Carbon Content [%, db] ^c	48.0		57.4		73.2		57.2	
Fixed Carbon Yield [%, db] ^c	26.76		30.30		31.07		30.84	
Higher Heating Value [MJ/kg]	28.65		30.12		33.02		29.68	
Gas Products								
Final Gas in V _{Bomb} [mol] ^d	0.116		0.129		0.196		0.135	
Nitrogen [mol %]	9.67		9.17		6.15		8.94	
Oxygen [mol %]	0.03		0.00		0.13		0.00	
Hydrogen [mg/g (Dry Feed)]	0.138		0.297		0.655		0.363	
Methane [mg/g (Dry Feed)]	0.068		0.00		0.00		0.00	
Carbon Monoxide [mg/g (Dry Feed)]	28.40		25.60		37.84		28.21	
Carbon Dioxide [mg/g (Dry Feed)]	129.42		154.33		202.20		161.92	
Mass Balance								
Gas Products [%, db] ^c	15.80		18.02		24.07		19.05	
Char Yield [%, db] ^c	55.74		52.75		42.45		53.88	
Liquid [%, db] ^c	11.72		11.95		10.21		14.38	
Solid not recovered [%, db] ^{c, f}	3.87		0.37		2.32		4.50	
Total [%, db]^c	87.14		82.72		79.06		91.82	
Carbon Balance Total [%, db]^c	96.76		93.95		89.62		94.69	

Table 5.1. Conditions and results for Wall Heated Tubing Bomb experiments (Continued).

Experiment Number	35		36		37		38	
Date (yymmdd)	170809		170811		170815		170817	
Conditions					Finish 10 min after exotherm			
Reactor Type	Dual-intermediate		Dual-intermediate		Dual-intermediate		Dual-intermediate	
Feedstock	Birch		Birch		Birch		Birch	
Heat Treatment Temperature[°C]	300		300		300		500	
Pretest Nitrogen Pressure [MPa]	0.1		0.1		0.1		0.1	
Immersion Time [min] ^a	190		190		30		190	
Mass Loading [g biomass/L _{reactor}]	~165		~240		~240		~130	
Particle size[mm]	<0.2		<0.2		<0.2		<2	
Reactants	R1 ⁱ	R2 ^j	R1 ⁱ	R2 ^j	R1 ⁱ	R2 ^j	R1 ⁱ	R2 ^j
Moist Mass [g]	18.74	18.59	25.87	25.86	26.14	26.62	14.12	14.48
Moisture Content [%, wb] ^b	7.31		7.15		7.28		7.83	
Pyrolysis Reaction								
Axis Peak Temperature [°C]	345	415	493	399	399	460	496	505
Wall Peak Temperature [°C]	302	303	314.2	302.3	282	305	486	509
Peak Pressure [MPa]	7.25		9.57		7.96		14.50	
Solid Products								
Char Moist Mass [g]	11.04	12.78	20.22	18.63	22.45	19.43	7.58	7.44
Char Moisture Content [%, wb] ^{b, e}	22.93	30.37	40.38	34.58	36.26	34.15	26.64	34.48
Volatile Matter Content [%, db] ^c	37.1		37.1		48.4		11.1	
Ash Content [%, db] ^c	2.3		1.8		1.8		2.4	
Fixed Carbon Content [%, db] ^c	60.6		61.1		49.8		86.5	
Fixed Carbon Yield [%, db] ^c	31.50		30.82		27.58		34.23	
Higher Heating Value [MJ/kg]	31.00		31.24		29.52		34.52	
Gas Products								
Final Gas in V _{Bomb} [mol] ^d	0.185		0.249		0.199		0.329	
Nitrogen [mol %]	7.80		7.58		9.17		5.20	
Oxygen [mol %]	0.58		0.69		0.00		0.13	
Hydrogen [mg/g (Dry Feed)]	0.287		0.273		0.181		1.386	
Methane [mg/g (Dry Feed)]	0.00		0.00		0.00		0.01	
Carbon Monoxide [mg/g (Dry Feed)]	32.38		27.68		20.36		35.76	
Carbon Dioxide [mg/g (Dry Feed)]	157.15		201.22		133.78		318.33	
Mass Balance								
Gas Products [%, db] ^c	18.98		22.92		15.43		35.55	
Char Yield [%, db] ^c	50.31		50.47		55.41		39.59	
Liquid [%, db] ^c	10.70		23.20		23.27		9.35	
Solid not recovered [%, db] ^{c, f}	1.00		3.28		1.68		1.63	
Total [%, db]^c	80.98		99.88		95.79		86.12	
Carbon Balance Total [%, db]^c	92.96		96.33		95.00		97.10	

Table 5.1. Conditions and results for Wall Heated Tubing Bomb experiments (Continued).

Experiment Number	39		40		41		42	
Date (yymmdd)	170822		170830		171108		171227	
Conditions			Finish 10 min after exotherm		Finish 10 min after exotherm			
Reactor Type	Dual-intermediate		Dual-intermediate		Dual-current		Dual-current	
Feedstock	Birch		Rice husk		Birch		Spruce	
Heat Treatment Temperature[°C]	300		300		300		300	
Pretest Nitrogen Pressure [MPa]	2.17		0.1		0.1		0.1	
Immersion Time [min] ^a	190		28		30		300	
Mass Loading [g biomass/L _{reactor}]	~130		~50		~130		~130	
Particle size[mm]	<2		As received		<0.2		< 2	
Reactants	R1 ⁱ	R2 ^j	R1 ⁱ	R2 ^j	R1 ⁱ	R2 ^j	R1 ⁱ	R2 ^j
Moist Mass [g]	14.44	14.81	7.92	7.60	14.09	14.38	13.26	13.87
Moisture Content [%, wb] ^b	7.83		10.67		7.37		8.00	
Pyrolysis Reaction								
Axis Peak Temperature [°C]	340	320	319	313	313	290	330	334
Wall Peak Temperature [°C]	291	296	297	299	285	299	308	307
Peak Pressure [MPa]	11.05		3.19		5.18		6.38	
Solid Products								
Char Moist Mass [g]	11.64	12.02	7.44	6.49	11.82	11.99	10.18	12.28
Char Moisture Content [%, wb] ^{b, e}	39.38	39.82	34.42	26.12	34.60	38.50	32.42	40.51
Volatile Matter Content [%, db] ^c	40.3		33.4		53.4		42.6	
Ash Content [%, db] ^c	2.1		34.6		2.3		2.0	
Fixed Carbon Content [%, db] ^c	57.6		32.0		44.3		55.4	
Fixed Carbon Yield [%, db] ^c	30.51		22.33		25.38		31.47	
Higher Heating Value [MJ/kg]	31.29		18.83		27.94		29.83	
Gas Products								
Final Gas in V _{Bomb} [mol] ^d	0.335		0.106		0.096		NA ^k	
Nitrogen [mol %]	62.64		27.42		10.67		NA ^k	
Oxygen [mol %]	1.17		2.12		0.23		NA ^k	
Hydrogen [mg/g (Dry Feed)]	0.241		0.0372		0.129		NA ^k	
Methane [mg/g (Dry Feed)]	0.00		0.00		0.000		NA ^k	
Carbon Monoxide [mg/g (Dry Feed)]	14.37		22.21		17.35		NA ^k	
Carbon Dioxide [mg/g (Dry Feed)]	179.74		81.84		114.66		NA ^k	
Mass Balance								
Gas Products [%, db] ^c	19.44		10.41		13.21		NA ^k	
Char Yield [%, db] ^c	53.01		69.78		57.27		56.84	
Liquid [%, db] ^c	26.31		19.11		25.36		24.56	
Solid not recovered [%, db] ^{c, f}	1.46		1.30		2.81		0.24	
Total [%, db]^c	100.21		100.60		98.65		NA^k	
Carbon Balance Total [%, db]^c	97.21		100.88		92.08		NA^k	

Table 5.1. Conditions and results for Wall Heated Tubing Bomb experiments (Continued).

Experiment Number	43		44		45		46	
Date (yymmdd)	180102		180104		180106		180108	
Conditions	Low Heating Rate No holding time		Low heating rate, 180 min holding time				Low heating rate, 120 min holding time	
Reactor Type	Dual-current		Dual-current		Dual-current		Dual-current	
Feedstock	Birch		Birch		Birch		Birch	
Heat Treatment Temperature[°C]	300		300		400		500	
Pretest Nitrogen Pressure [MPa]	0.1		0.1		2.17		0.1	
Immersion Time [min] ^a	53		232		190		350	
Mass Loading [g _{biomass} /L _{reactor}]	~130		~130		~130		~130	
Particle size[mm]	< 2		< 2		< 2		< 2	
Reactants	R1 ⁱ	R2 ^j	R1 ⁱ	R2 ^j	R1 ⁱ	R2 ^j	R1 ⁱ	R2 ^j
Moist Mass [g]	14.13	14.36	14.57	14.29	14.20	14.25	13.96	14.07
Moisture Content [%, wb] ^b	8.07		7.95		7.98		8.07	
Pyrolysis Reaction								
Axis Peak Temperature [°C]	306	301	310	322	405	405	505	505
Wall Peak Temperature [°C]	294	292	306	309	401	405	506	506
Peak Pressure [MPa]	3.84		5.84		17.48		15.10	
Solid Products								
Char Moist Mass [g]	12.28	13.94	12.11	12.12	10.29	10.18	7.54	9.03
Char Moisture Content [%, wb] ^{b, e}	32.07	37.31	40.77	42.23	46.28	45.62	34.42	45.69
Volatile Matter Content [%, db] ^c	61.9		42.4		22.8		12.2	
Ash Content [%, db] ^c	1.5		1.8		2.1		2.1	
Fixed Carbon Content [%, db] ^c	36.6		55.8		75.2		85.8	
Fixed Carbon Yield [%, db] ^c	23.90		29.80		31.77		32.78	
Higher Heating Value [MJ/kg]	24.93		29.86		33.30		34.47	
Gas Products								
Final Gas in V _{Bomb} [mol] ^d	NA ^k		NA ^k		NA ^k		NA ^k	
Nitrogen [mol %]	NA ^k		NA ^k		NA ^k		NA ^k	
Oxygen [mol %]	NA ^k		NA ^k		NA ^k		NA ^k	
Hydrogen [mg/g (Dry Feed)]	NA ^k		NA ^k		NA ^k		NA ^k	
Methane [mg/g (Dry Feed)]	NA ^k		NA ^k		NA ^k		NA ^k	
Carbon Monoxide [mg/g (Dry Feed)]	NA ^k		NA ^k		NA ^k		NA ^k	
Carbon Dioxide [mg/g (Dry Feed)]	NA ^k		NA ^k		NA ^k		NA ^k	
Mass Balance								
Gas Products [%, db] ^c	NA ^k		NA ^k		NA ^k		NA ^k	
Char Yield [%, db] ^c	65.21		53.36		42.26		38.22	
Liquid [%, db] ^c	26.33		29.98		27.39		17.54	
Solid not recovered [%, db] ^{c, f}	2.14		1.92		5.04		3.22	
Total [%, db]^c	NA^k		NA^k		NA^k		NA^k	
Carbon Balance Total [%, db]^c	NA^k		NA^k		NA^k		NA^k	

Table 5.1. Conditions and results for Wall Heated Tubing Bomb experiments (Continued).

Experiment Number	47		48		49	
Date (yymmdd)	180111		180123		180126	
Conditions	Low heating rate, 0 min holding time		With dead volume ^g			
Reactor Type	Dual-current		Dual-current		Dual-current	
Feedstock	Birch		Birch		Birch	
Heat Treatment Temperature[°C]	500		550		550	
Pretest Nitrogen Pressure [MPa]	0.1		0.1		0.1	
Immersion Time [min] ^a	200		190		190	
Mass Loading [g _{biomass} /L _{reactor}]	~130		~100		~130	
Particle size[mm]	< 2		< 2		< 2	
Reactants	R1 ⁱ	R2 ^j	R1 ⁱ	R2 ^j	R1 ⁱ	R2 ^j
Moist Mass [g]	13.98	14.15	14.37	14.26	14.03	14.07
Moisture Content [%, wb] ^b	8.02		7.83		7.99	
Pyrolysis Reaction						
Axis Peak Temperature [°C]	493	494	555	549	556	553
Wall Peak Temperature [°C]	489	490	546	550	546	NA ^k
Peak Pressure [MPa]	10.95		7.49		17.87	
Solid Products						
Char Moist Mass [g]	9.20	10.22	5.06	6.10	6.42	6.84
Char Moisture Content [%, wb] ^{b, e}	40.90	49.00	12.53	28.94	32.68	34.12
Volatile Matter Content [%, db] ^c	17.8		9.2		8.7	
Ash Content [%, db] ^c	1.8		2.1		2.0	
Fixed Carbon Content [%, db] ^c	80.4		88.7		89.3	
Fixed Carbon Yield [%, db] ^c	33.10		29.45		30.51	
Higher Heating Value [MJ/kg]	33.74		34.31		33.64	
Gas Products						
Final Gas in V _{Bomb} [mol] ^d	NA ^k		NA ^k		NA ^k	
Nitrogen [mol %]	NA ^k		NA ^k		NA ^k	
Oxygen [mol %]	NA ^k		NA ^k		NA ^k	
Hydrogen [mg/g (Dry Feed)]	NA ^k		NA ^k		NA ^k	
Methane [mg/g (Dry Feed)]	NA ^k		NA ^k		NA ^k	
Carbon Monoxide [mg/g (Dry Feed)]	NA ^k		NA ^k		NA ^k	
Carbon Dioxide [mg/g (Dry Feed)]	NA ^k		NA ^k		NA ^k	
Mass Balance						
Gas Products [%, db] ^c	NA ^k		NA ^k		NA ^k	
Char Yield [%, db] ^c	41.16		33.20		34.15	
Liquid [%, db] ^c	25.43		1.84		10.33	
Solid not recovered [%, db] ^{c, f}	1.82		5.76		11.72	
Total [%, db]^c	NA^k		NA^k		NA^k	
Carbon Balance Total [%, db]^c	NA^k		NA^k		NA^k	

^a Long experiments ended 190 minutes after the WHTB was submersed into the hot sand bath. Short experiments ended 10 minutes after the end of the exotherm, i.e. the exotherm was considered to end once the pressure rise considerably slowed.

^b Reported on a wet basis (wb).

^c Reported on a dry basis (db).

^d Final gas moles were calculated using the ideal gas law at conditions after cooldown. Final gas volume was measured with the WDV.

^e Weight loss of char product from drying in a vacuum oven at 105°C.

^f Amount of solid adhered on the walls was calculated as the difference between initial and final masses of the empty reactors.

^g Reactor with extended dead volume was employed.

^h Only the results of one of the replica experiments are displayed here.

ⁱ Data for reactor body 1 (R1) of the dual reactor.

^j Data for reactor body 2 (R2) of the dual reactor.

^k Not Available (NA).

The mass balances indicate that product recovery is highly dependent on the experimental conditions used. In some cases up to 21% of the initial biomass on a dry basis was unaccounted for when gas composition data were available. The carbon balance typically shows that more than 95% of the carbon is accounted for in the solid and gaseous products. As mentioned earlier, this indicates that liquid is the main unrecovered product and that measurements of charcoal and gas yields are consistent. Fixed-carbon yields in Table 5.1 were calculated on a dry basis as $y_{FC} = y_{char} \cdot \%fC/100$. As emphasized in the cellulosic work,²⁶ CVC was able to produce a charcoal with a near-theoretical fixed-carbon yield.

The limiting values predicted by thermodynamic and chemical equilibrium were calculated with Stanjan and FactSage. Both simulations agreed on predicted equilibrium yields. In Stanjan, solid carbon, liquid H₂O and gaseous species CO, CO₂, CH₄, H₂, H₂O, NO, NO₂ were user specified as possible equilibrium products. In FactSage, possible products components are selected from a large thermodynamic database based on the elements present in the reactants. "Solution"

databases can also be selected based on the inorganic elements present in the reactants but were not included. A routine that minimizes the Gibb's free energy of the multi-phase mixture calculates the species equilibrium yields. Figures in later sections in Chapter 6 study the effects of pressure, temperature, mass loading and feedstock in the theoretical product yields predicted by FactSage. The thermochemical calculations identify carbon as the preferred pyrolytic product followed by water, CO₂, CH₄ and traces of other gases. Qualitatively agreeing with theoretical predictions, the CVC experiments show solid charcoal—which consists of an ill-defined compound primarily made of carbon, varying quantities of hydrogen and oxygen, along with ash and other impurities—as well as water and CO₂ as the main pyrolytic products. Next is carbon monoxide which is present in considerable amounts but noticeably lower than the three main products, followed by methane and other gases that are present in trace quantities.

The theoretical carbon yields represent maximum limiting values for the experimental fixed-carbon yields,³⁹ whereas gaseous and liquid yields cannot serve as representative quantitative indicators for experimental values in view of the fact that the char product is not pure carbon,⁵⁸ and therefore theoretical and experimental elemental balances would differ considerably.

In order to meaningfully evaluate the efficiency of the carbonization processes, a precise way to measure experimental fixed-carbon yields is essential. Since experimental fixed-carbon yield depends on both the fixed-carbon content (measured by proximate analysis) and charcoal yield, the accuracy of the measured experimental fixed-carbon contents ultimately reflects on the fixed-carbon yields. The fixed-carbon content accuracy is estimated from ultimate analysis of samples

made of just fixed-carbon. In order to obtain such samples, a proximate analysis of a cellulose sample was deliberately interrupted after extracting the volatile matter. Since cellulose contains negligible ash, fixed-carbon would be the only product left behind and therefore, its purity would indicate the accuracy of the reported values. The original proximate analysis technique revealed a “fixed-carbon” of just 94.54 wt.% carbon with the balance comprising O, H, and ash in decreasing amounts (these values were obtained from the resultant charcoal produced in a WHTB experiment with the original reactor and cellulose as the feedstock).⁵⁸ The updated proximate analysis technique, employed for spruce and birch experiments, showed a “fixed-carbon” of 95.27 wt. % carbon.

The use of oak, spruce and birch confirmed the attainment of the theoretical limiting value as illustrated by the parity plot in Figure 5.7. Figure 5.8 shows a close-up of the top right corner of Figure 5.7. It shows that in a constant-volume reactor, pressure does not influence fixed-carbon yields while smaller particles, longer immersion times (at the lower temperature of 300°C) and higher temperatures improve fixed-carbon yields to approach limiting values. The high values obtained with smaller wood particles in this work contrast the fixed-carbon yield of 10% predicted from the pyrolysis of cellulose powder in a TGA under a N₂ flow.²⁶

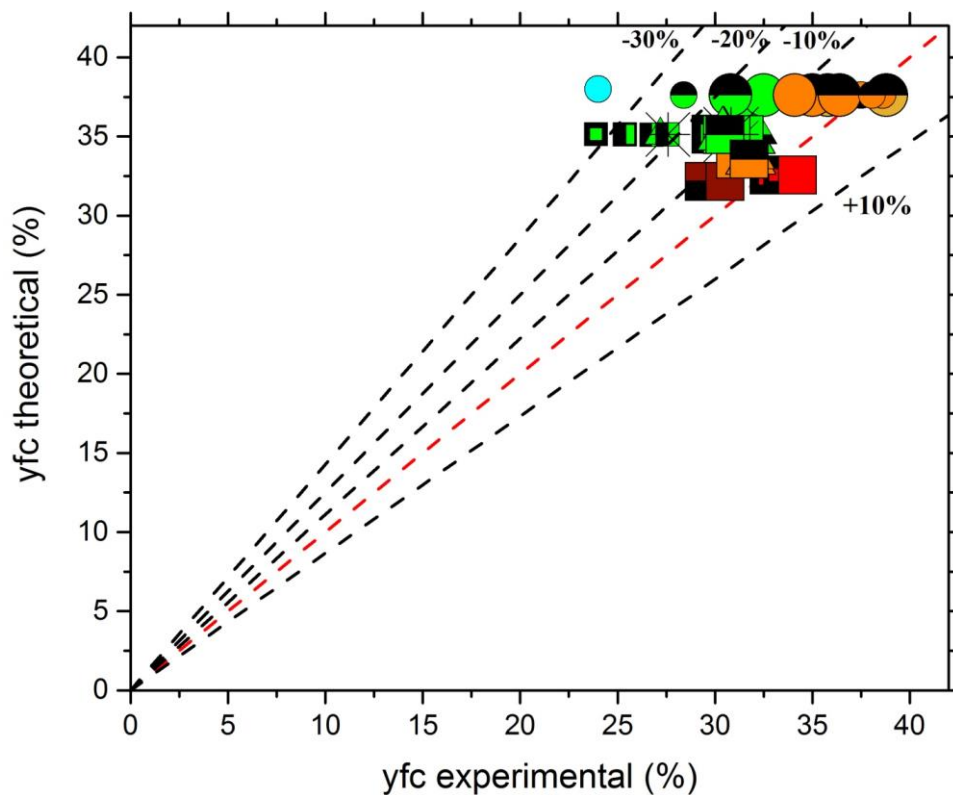


Figure 5.7. Parity plot displaying the experimental fixed carbon yield from Wall Heated Tubing Bomb pyrolysis experiments vs the theoretical values. Shape of the symbols indicate biomass type: ●Oak, ▲Spruce■Birch. Colours represent heat treatment temperature: ■300°C and reactor open to the atmosphere, ■300°C, ■370°C, ■400°C, ■500°C, ■550°C. Size represents immersion times: smaller symbols represent short experiments (25-60 min) and larger symbols represent long experiments (70-300 min). Symbol fillings represent special experimental conditions: □ small biomass particles, ◐ use of volume compensation, ◑ under initial nitrogen pressure, ▨ low heating rate, star symbol * on top of a symbol indicates high loading.

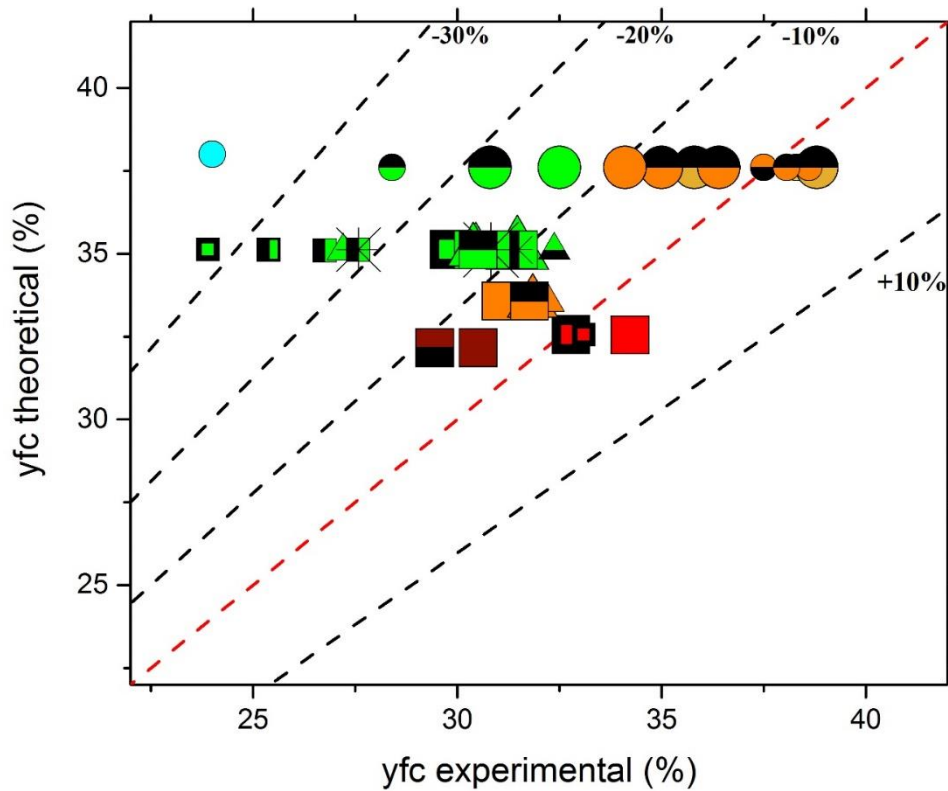


Figure 5.8. Close-up of the top right corner of Figure 5.7. Shape of the symbols indicate biomass type: ●Oak, ▲Spruce■Birch. Colours represent heat treatment temperature: ■300°C and reactor open to the atmosphere, ■300°C, ■370°C, ■400°C, ■500°C, ■and 550°C. Size represents immersion times: smaller symbols represent short experiments (25-60 min) and larger symbols represent long experiments (70-300 min). Symbol fillings represent special experimental conditions: □ small biomass particles, ● use of volume compensation, ● under initial nitrogen pressure, □ low heating rate, star symbol *on top of a symbol indicates high loading.

CHAPTER 6. RESULTS AND DISCUSSION

This chapter presents the most recent experimental CVC results, evaluates the results with literature findings and compares experimental fixed-carbon yields with theoretical values predicted by thermodynamics.

6.1. Effect of a Closed Vessel versus an Open Vessel

Figures 6.1 and 6.2 illustrate the effect of sealing the WHTB reactor on the product yields and proximate analysis from pyrolysis of oak sawdust (0.149-0.425 mm) at a HTT of 300°C. The sealed WHTB did not show an improvement in charcoal yield compared to the open reactor experiment, but actually suffered a reduction from 69.8% to 58.6%, however the fixed-carbon content and fixed-carbon yield dramatically increased. In agreement with literature observations regarding carbonization under pressure (see Section 3.2), both the dramatic increase in partial pressure and residence time of volatiles experienced in the sealed reactor resulted in the higher extent of secondary char formation and the reduction of carbon losses in the form of gases and liquids.

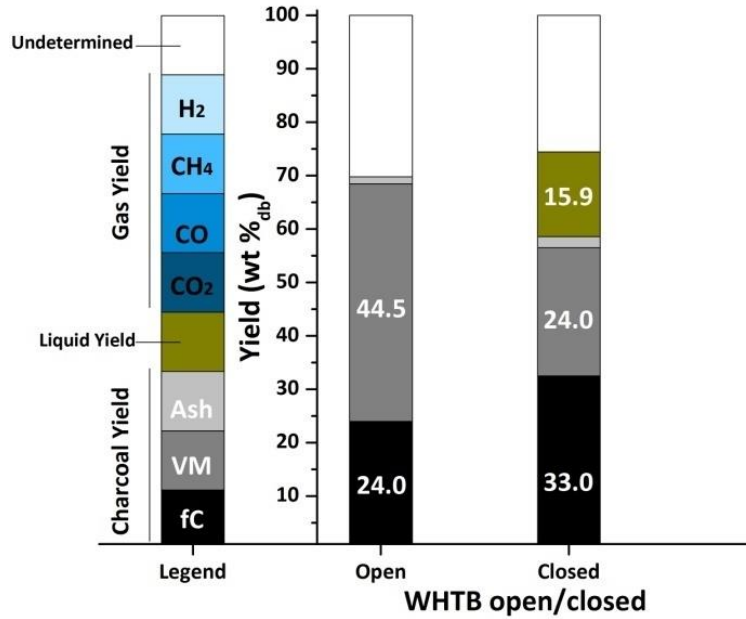


Figure 6.1. Effect of sealing the Wall Heated Tubing Bomb reactor on the product yields from the pyrolysis of oak sawdust (0.149-0.425 mm) at a heat treatment temperature of 300°C. Liquid yield on the open reactor experiment and gas yields on both experiments were not measured.

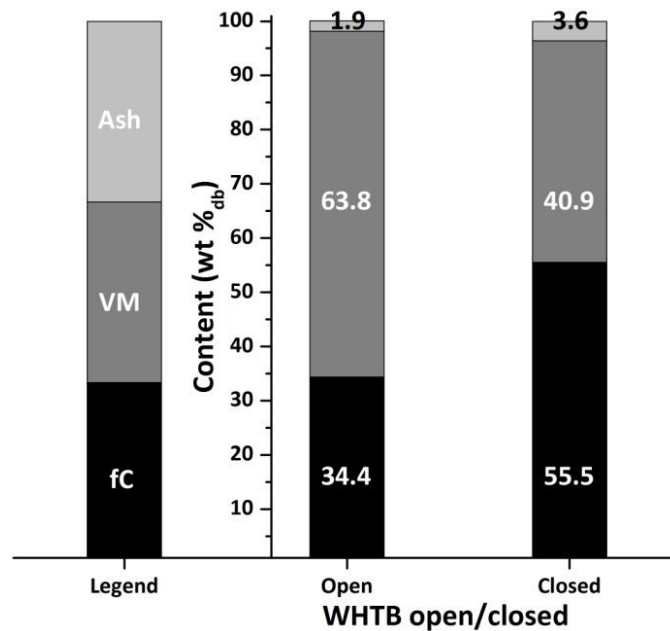


Figure 6.2. Effect of sealing the Wall Heated Tubing Bomb reactor on the proximate analysis of charcoal from the pyrolysis of oak sawdust (0.149-0.425 mm) at a heat treatment temperature of 300°C.

6.2. Effect of Pressure

Figures 6.3 and 6.4 illustrate the effect of changing the initial N₂ pressure of the WHTB on the product yields and the char proximate analysis of oak pyrolysis at a HTT of 300°C in the original reactor. The experimental oak fixed-carbon content and fixed-carbon yield showed an initial decrease when the pretest nitrogen pressure was increased from 0.1 to 1.48 MPa (from 55.5 to 49.7%) and a subsequent plateau with higher pressures. The initial decline of the char fixed-carbon content and yield, however, seem to be the result of a considerably reduction of the immersion time (from 134 to 34 minutes) rather than to a pressure effect (see Effect of Immersion Time).

The results from experiments using similar immersion times (21-38 minutes) with oak that were conducted at elevated pretest pressures (from 1.48 to 4.69 MPa) at a HTT of 300°C help to explain the plateau in fC content and yield observed in earlier tests.

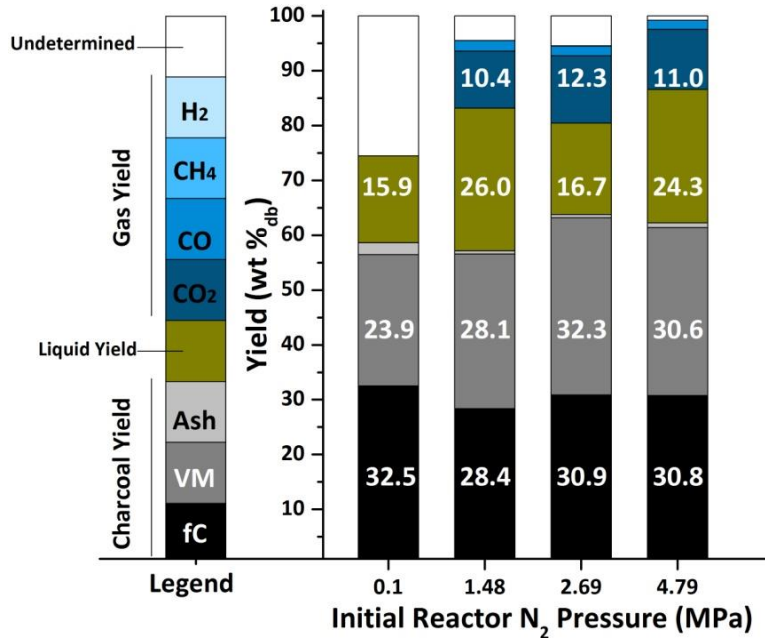


Figure 6.3. Effect of initial nitrogen pretest pressure on the product yields from the constant-volume carbonization of oak sawdust (0.149-0.425 mm) under immersion times of 21-134 minutes at a heat treatment temperature of 300°C.

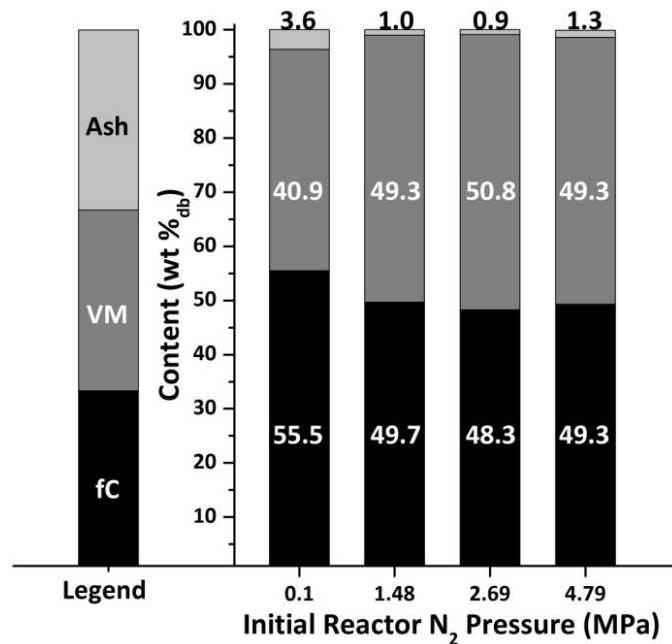


Figure 6.4. Effect of initial nitrogen pretest pressure on the proximate analysis of charcoal from the constant-volume carbonization of oak sawdust (0.149-0.425 mm) under immersion times of 21-134 minutes at a heat treatment temperature of 300°C.

Careful control of the immersion time, and refinements made to the WHTB equipment (see Apparatus Evolution) and to the proximate analysis technique (see Appendix N) permitted the acquisition of more accurate results in later experiments that used birch and spruce feedstocks. Figures 6.5 and 6.6 display the results of product yields and char proximate analysis from birch CVC in the current dual WHTB reactor at pretest pressures of 0.1 and 2.17 MPa and heat treatment temperatures of 300 and 400°C and confirmed the lack of influence of the inert gas pressure on product yields and proximate analysis. The role of temperature will be discussed in Section 6.3.

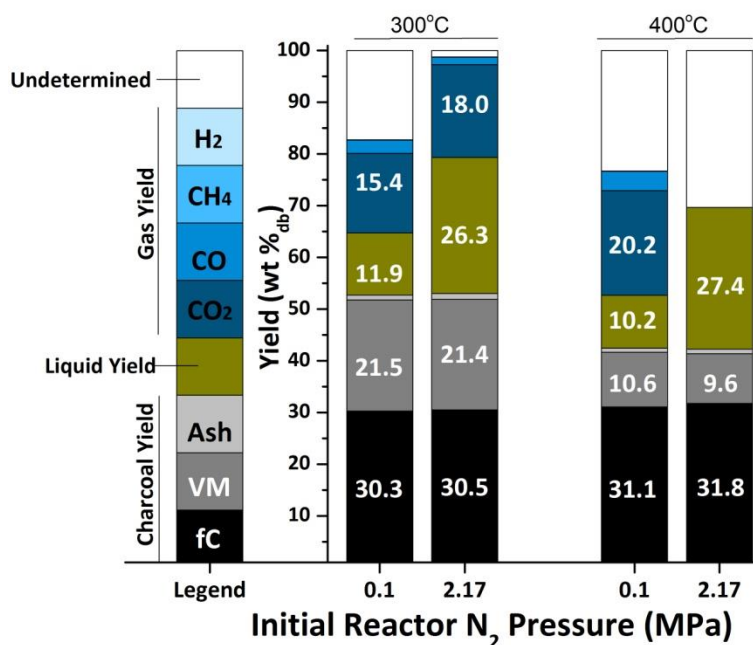


Figure 6.5. Effect of initial nitrogen pretest pressure on the product yields from the constant-volume carbonization of birch sawdust (<2 mm) under an immersion time of 190 minutes at heat treatment temperatures of 300 and 400°C.

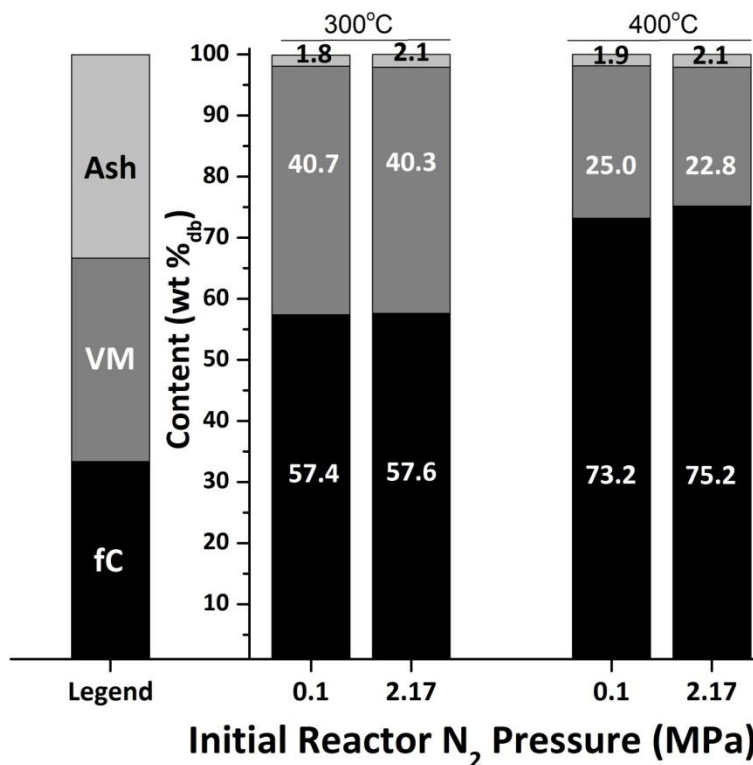


Figure 6.6. Effect of initial nitrogen pretest pressure on the proximate analysis of charcoals from the constant-volume carbonization of birch sawdust (<2 mm) under an immersion time of 190 minutes at heat treatment temperatures of 300 and 400°C.

In agreement with experimental observations, FactSage CVC predictions reflect a negligible pressure effect on theoretical fixed-carbon yields (see Figure 6.7). It appears that it is not the total system pressure, but—as observed in literature—it is the concentration of volatiles and/or their residence time that govern the fixed-carbon contents and yields from biomass carbonization processes.

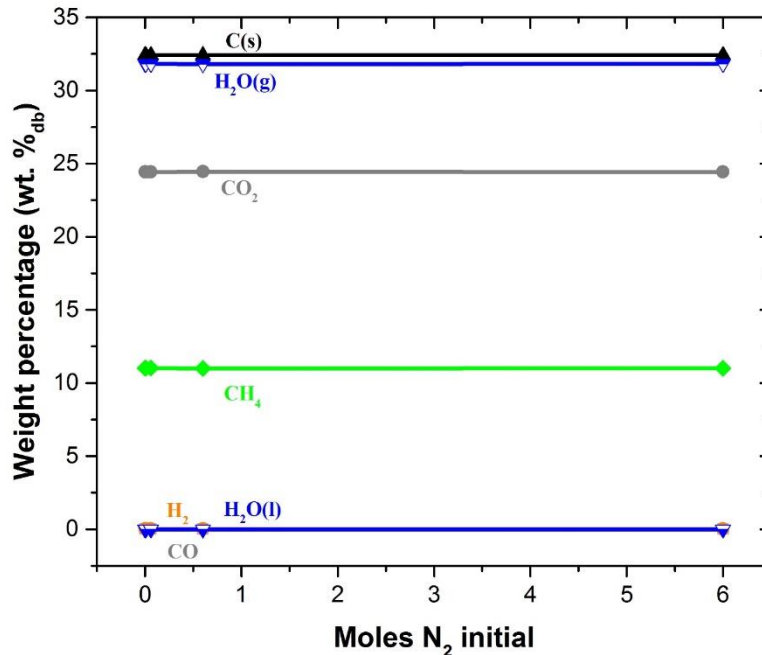


Figure 6.7. Effect of nitrogen pressure on the theoretical product distribution of the constant-volume carbonization of birch predicted by FactSage.

CVC experiments with oak and birch also confirmed the morphological findings observed for chars derived from cellulose. Visual observations (see Figure 6.8) and SEM images of charcoals (see Figures 6.9-6.12) produced at different CVC conditions showed that higher inert pressures—as well as higher temperatures, faster heating rates and possibly smaller particles (see later sections)—produced charcoals that experienced higher stages of melting that later solidified into single pieces that adopted the shape of the reactor container. Note the large differences in the surface morphology of a single molten grain of a birch charcoal produced at a temperature of 400°C and at an elevated pretest pressure of 2.17 MPa displayed in Figure 6.12. It appears that the enhanced contact of volatiles experienced by the CVC chars due to the elevated pressures (internal and external if an inert gas is pre-added to the reactor) throughout the entire process favors the softening of charcoal at much lower temperatures and heating rates than for “open” reactor configurations (see Section 3.3 for details). Volatiles seem to act as plasticizing agents

and adding an inert gas to the constant-volume reactor restricts the release of volatiles from the charcoal structure into the gas phase creating conditions for TPP formation.

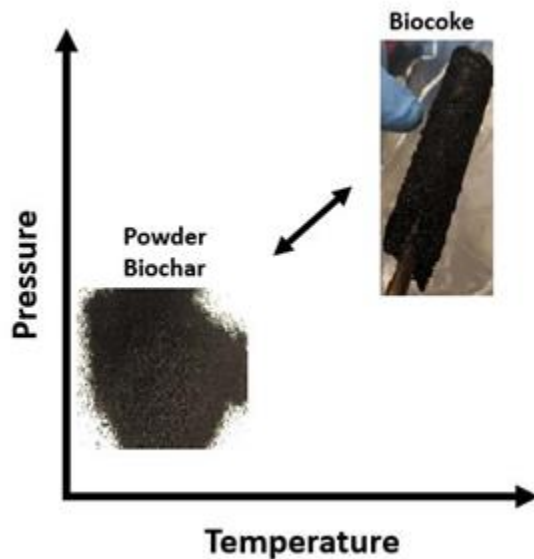


Figure 6.8. On the left, oak biochar powder from constant-volume carbonization at an initial N_2 pressure of 0.1 MPa and a heat treatment temperature of 300°C. On the right, oak biochar from constant-volume carbonization at an initial N_2 pressure of 2.69 MPa and a heat treatment temperatures of 300-370°C.

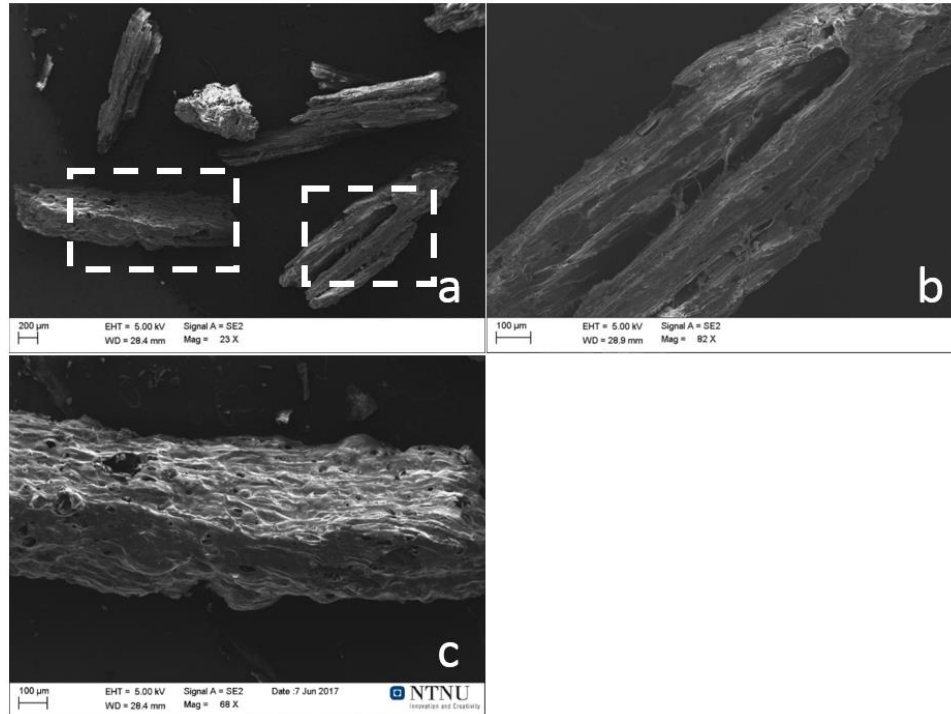


Figure 6.9. (a) Scanning electron microscopy image of birch charcoal from constant-volume carbonization at a heat treatment temperature of 300°C and an initial nitrogen pressure of 0.1 MPa, (b) and (c) higher magnification views of selected areas in (a).

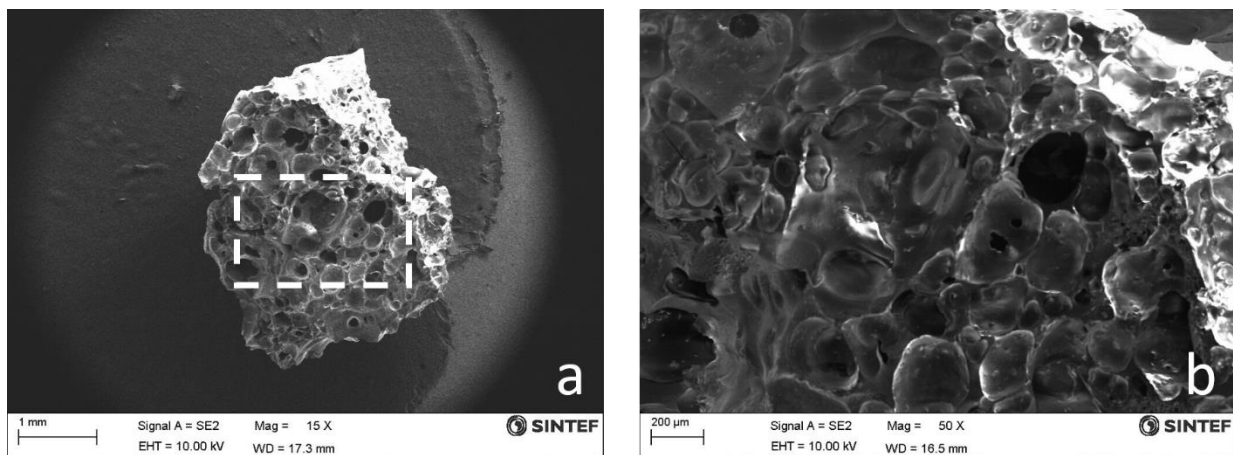


Figure 6.10. (a) Scanning electron microscopy image of birch charcoal from constant-volume carbonization at a heat treatment temperature of 300°C and an initial nitrogen pressure of 2.17 MPa, (b) higher magnification view of selected area in (a).

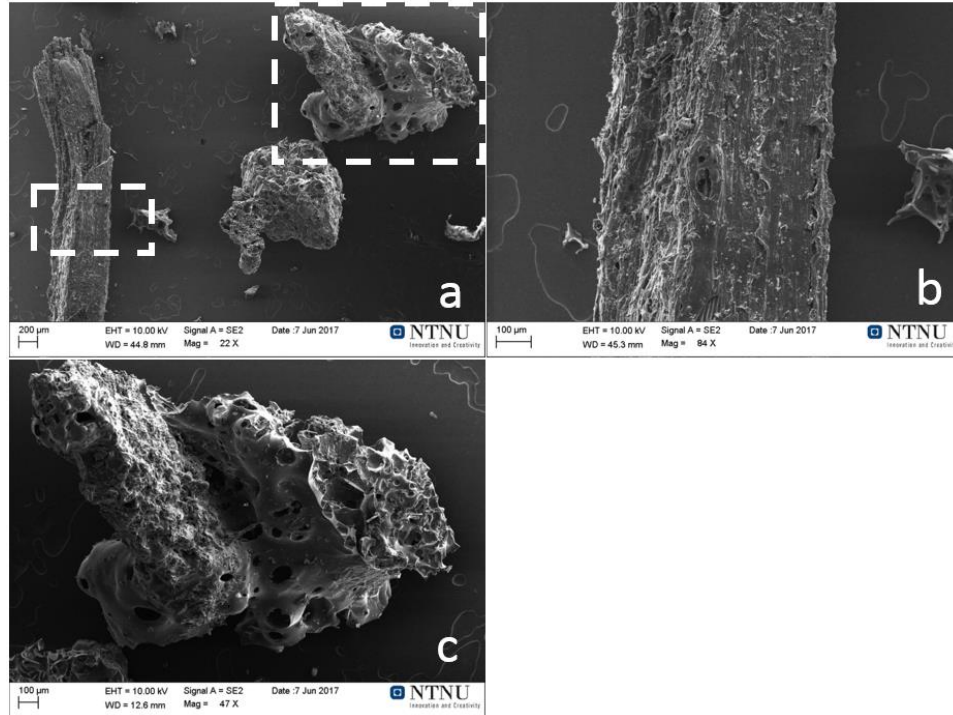


Figure 6.11. (a) Scanning electron microscopy image of birch charcoal from constant-volume carbonization at a heat treatment temperature of 400°C and an initial nitrogen pressure of 0.1 MPa, (b) and (c) higher magnification views of selected areas in (a).

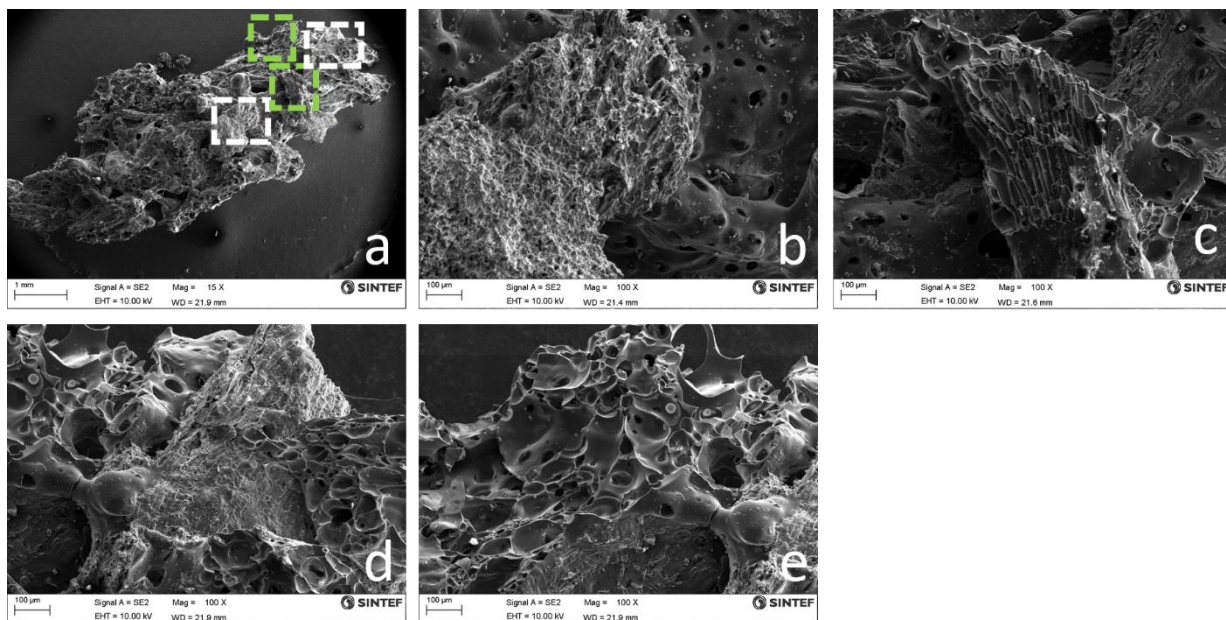


Figure 6.12. (a) Scanning electron microscopy image of birch charcoal from constant-volume carbonization at a heat treatment temperature of 400°C and an initial nitrogen pressure of 2.17 MPa, (b) - (e) higher magnification views of selected areas in (a).

6.3. Effect of Heat Treatment Temperature

Figures 6.13-6.16 display product yields and char proximate analyses from oak, spruce and birch CVC at HTT in a 300-550°C range under an initial nitrogen pressure of 0.1 MPa. Higher temperatures in CVC improved fixed-carbon contents without a concomitant loss in valuable fixed-carbon yields. Raising the temperature lead to a pyrolytic product richer in gas and lower in char, and a solid char with a higher fixed-carbon and less volatile content. As shown in Table 5.1, exothermic temperature peaks and pressures also increased within the temperature range, and char higher heating values (HHV) increased asymptotically.

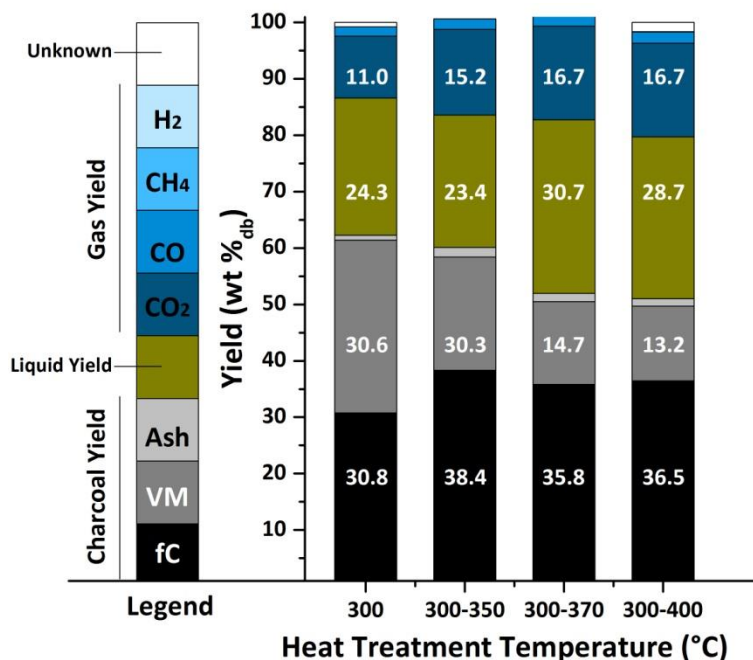


Figure 6.13. Effect of heat treatment temperature on the yields of char, condensate and gas from the constant-volume carbonization of oak at an initial N₂ pressure of 4.79 MPa and at various immersion times.

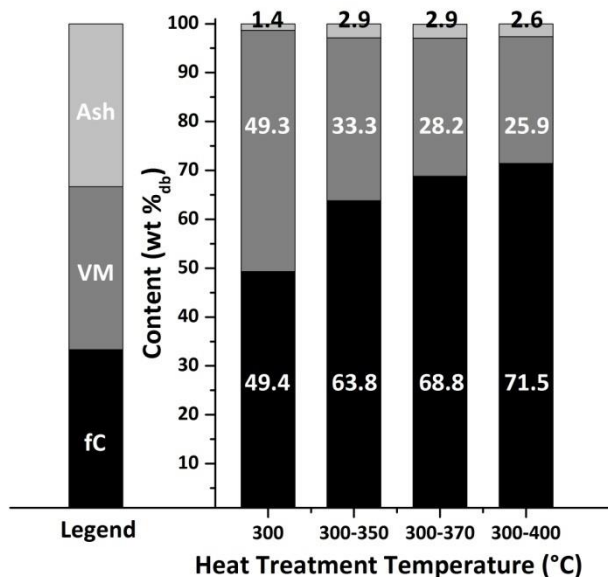


Figure 6.14. Effect of heat treatment temperature on the proximate analysis of charcoal from the constant-volume carbonization of oak at an initial N₂ pressure of 4.79 MPa and at various immersion times.

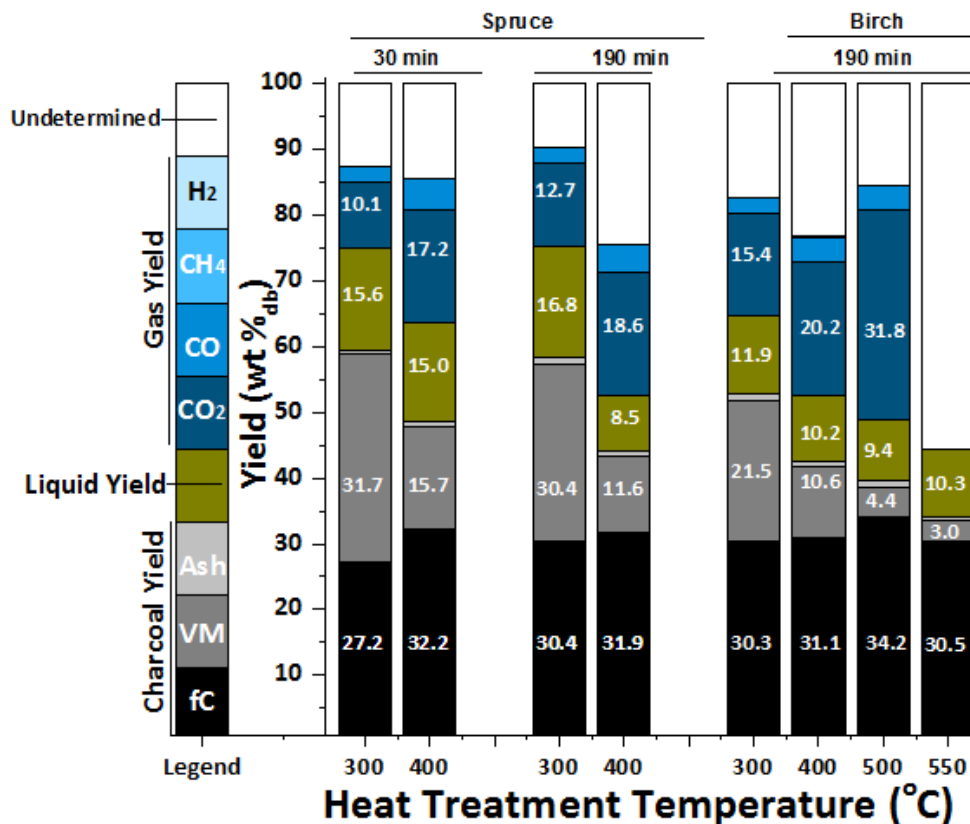


Figure 6.15. Effect of heat treatment temperature on the yields of char, condensate and gas from the constant-volume carbonization of birch and spruce at an initial N₂ pressure of 0.1 MPa and 190 min immersion time.

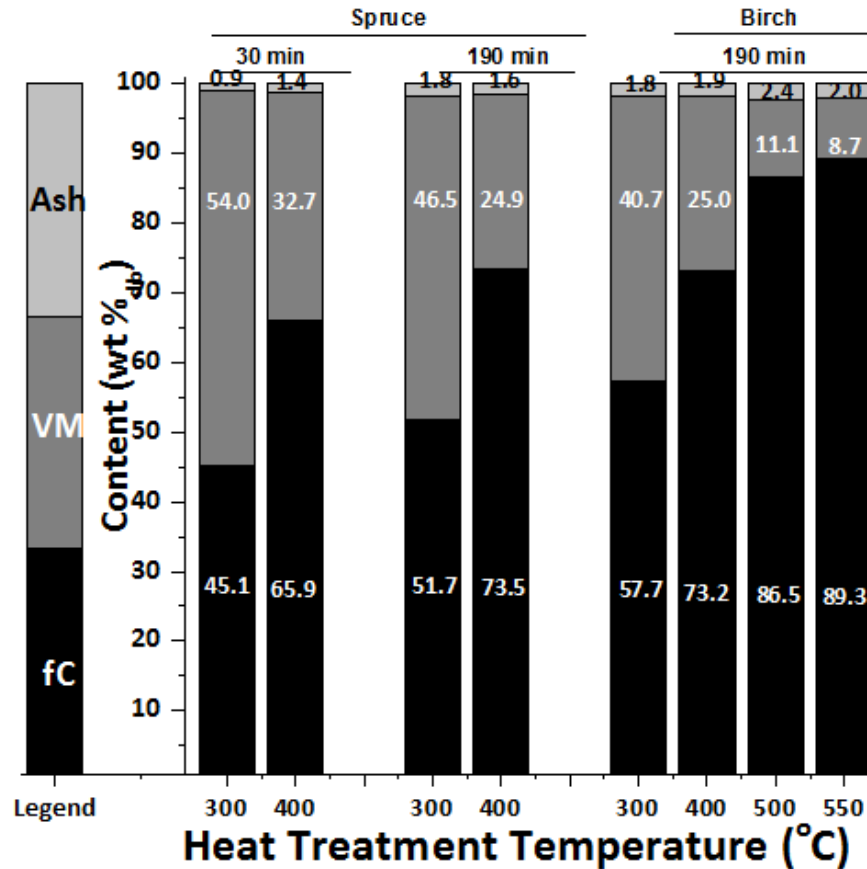


Figure 6.16. Effect of heat treatment temperature on the proximate analysis of charcoals from the constant-volume carbonization of birch and spruce at an initial N₂ pressure of 0.1 MPa and 190 min immersion time.

Figure 6.17 shows theoretical fixed-carbon yields of birch with temperature predicted by FactSage. Both theoretical and experimental trends agree on presenting a minor temperature effect on fixed-carbon yields but show different trends. As observed from the CVC of cellulose²⁶ and the feedstocks presented herein, increasing the temperature from 300 to 400°C slightly improved the experimental fixed-carbon yields. Birch tests under a wider temperature range showed fixed-carbon trends with temperature. From 300 to 400 to 500°C, the birch experimental fixed-carbon yield went from 30.3 to 31.1 to 34.2%. Further increasing the temperature from 500 to 550°C slightly reduced the fixed-carbon yield matching yields obtained at 300°C. Theoretical

trends contrast with the experimental behavior as fixed-carbon yields seem to slightly but continuously decrease with temperature. Both the gas composition predicted by FactSage and the gas composition measured experimentally showed CO₂ as the main gaseous component. Qualitatively, both trends also agreed, showing an increase in CO₂ yields with temperature. A considerable amount of CH₄ and no CO was predicted by equilibrium while experimentally, negligible CH₄ was recovered and a considerable fraction of CO was measured. As explained earlier, gaseous and liquid yields are not representative quantitative indicators for experimental values in view of the fact that the char product is not pure carbon.⁵⁸

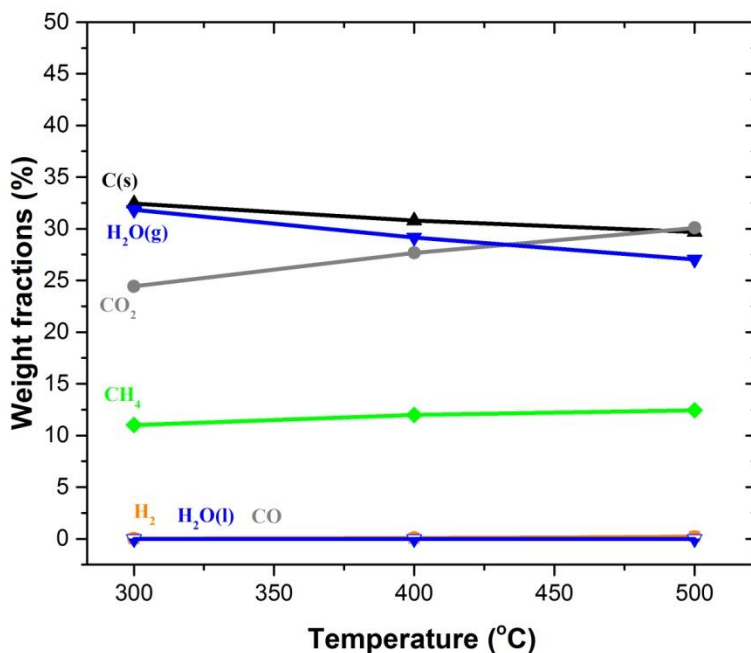


Figure 6.17. Effect of temperature on the theoretical product distribution from the constant-volume carbonization of birch predicted by FactSage.

Incomplete reactions during experiments, as indicated by the continuous rise in pressure during all experiments, may provide an explanation for the differences observed in CVC fixed-carbon yield trends. Also, it appears that, even though equilibrium calculations provide meaningful

limiting values for the fixed-carbon yields,³⁹ complete agreement should not be expected given the observed differences between experimental and theoretical pyrolysis reaction products.

In agreement with morphological observations from cellulose work,²⁶ a more intense TPP was observed as the carbonization temperature was raised. Scanning electron microscopy was used to examine birch charcoal samples. The 300°C-birch charcoal (Figure 6.9) presented a granular appearance that largely retained the structure of the raw wood particles. The char surface was porous, smooth and presented some cracks and openings. The smooth surface shown in Figure 6.9c is probably related to some molten carbon or condensation of tar/pitch on the char surface. In comparison, the 400, 500 and 550°C-birch charcoals revealed both discrete charcoal grains and large size charcoal block aggregates as shown in Figures 6.11, 6.18 and 6.19. Similar to the grains from the 300°C charcoal, some oblong grains partially retained the structure of the raw wood particle, with clear and wide melted zones visible on the surface (see Figures 6.11b and 6.19d). There are also particles with a more spherical shape and round openings on the surface which is partially attributed to release of volatiles from particles as the solid material is softening and melting. Release of volatiles causes swelling of particles and formation of small holes on particle surface. The lack of cell structure and the compact form of these particles indicate a more intense melting and occurrence of plastic transformations as they were carbonized at higher temperatures.

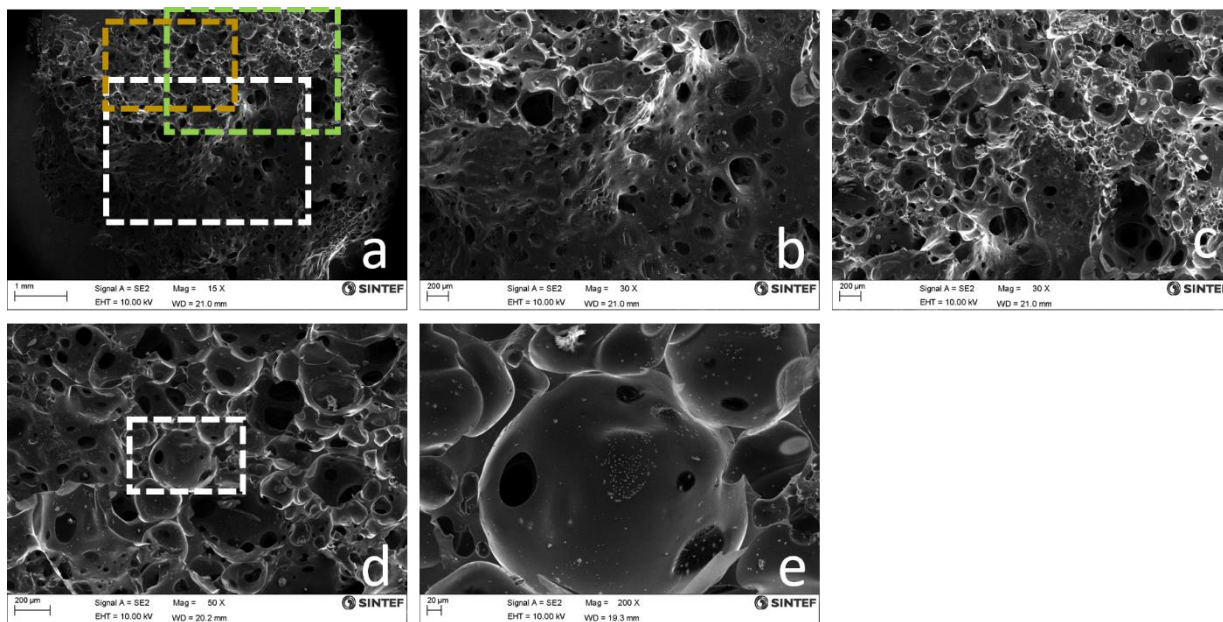


Figure 6.18. (a) Scanning electron microscopy image of birch charcoal from constant-volume carbonization at a heat treatment temperature of 500°C and an initial nitrogen pressure of 0.1 MPa, (b) - (d) higher magnification views of selected areas in (a), (e) higher magnification view of selected area in (d).

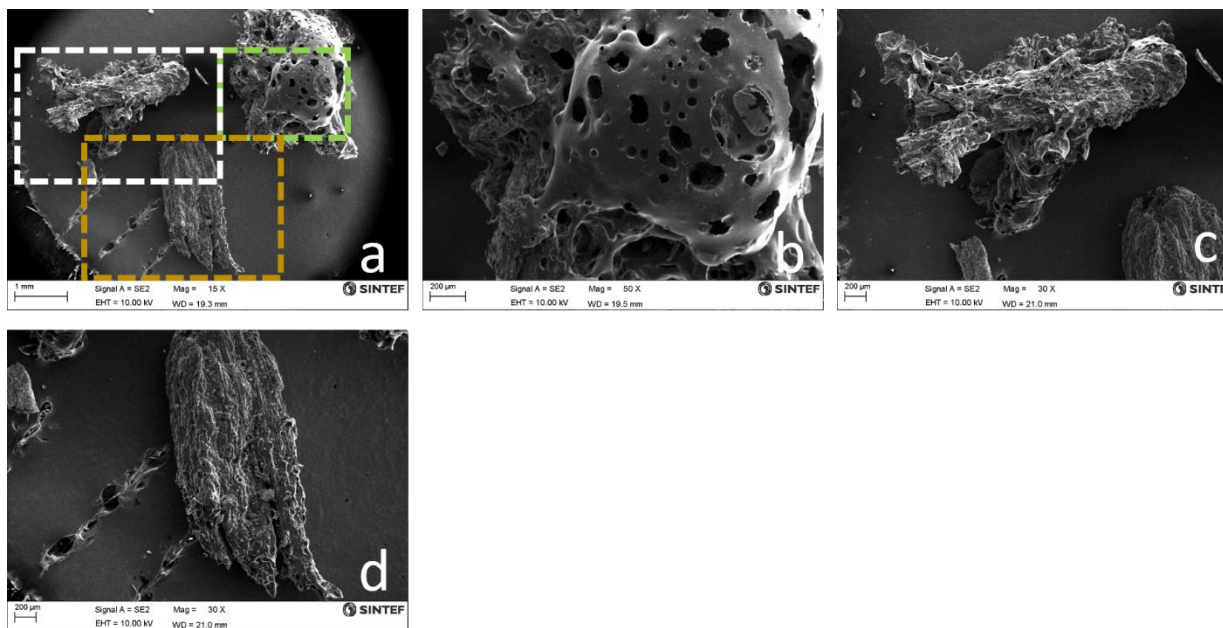


Figure 6.19. (a) Scanning electron microscopy image of birch charcoal from constant-volume carbonization at a heat treatment temperature of 550°C and an initial nitrogen pressure of 0.1 MPa, (b)-(d) higher magnification views of selected areas in (a).

Heating rate, particle size and possibly mass loading also play key roles on the char appearance and microstructure. Higher heating rates and possibly smaller particle sizes favored the formation of a TPP (see following sections). Figure 6.20 shows the contrasting appearances of charcoals from different parent materials and different experimental conditions. The TPP observed from the WHTB experiments is intriguing and requires further study to understand the conditions that govern its formation and how it affects the physical and chemical properties of the product char.

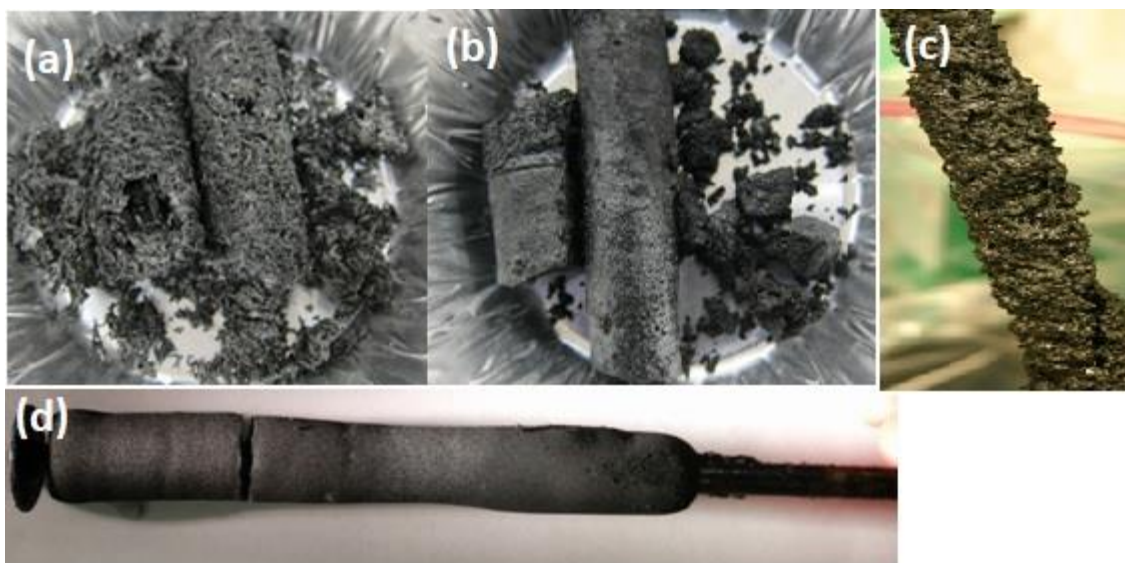


Figure 6.20.(a) Birch charcoal produced under constant-volume carbonization at a heat treatment temperature of 550°C, an initial nitrogen pressure of 0.1 MPa, particle size <2 mm, standard loading of 130 g/L and an immersion time of 190 minutes. (b) Birch charcoal produced under constant-volume carbonization at a heat treatment temperature of 300°C, an initial nitrogen pressure of 0.1 MPa, particle size <0.2 mm, higher loading of 240 g/L and an immersion time of 190 minutes. (c) Oak charcoal produced under constant-volume carbonization at a heat treatment temperature of 300-400°C, an initial nitrogen pressure of 2.69 MPa, a coarse particle size, loading of ~120 g/L and an immersion time of 55 minutes. (d) Cellulose charcoal produced under constant-volume carbonization at a heat treatment temperature of 300-400°C, an initial nitrogen pressure of 2.4 MPa, particle size 50-180 μm , loading of ~200 g/L and an immersion time of 85 minutes.

6.4. Effect of Heating Rate

The WHTB system is not the ideal equipment for studies concerning heating rate effects. The heating method employed, the sand bath, does not allow the experimenter to have a fine control over the heating rate. Thus, precise quantitative studies would require the use of different reactor set-ups. Nonetheless, qualitative studies that test the influence of the heating rate on yields or char properties can nonetheless be performed. Two distinct heating rates, “fast” and “slow”, were obtained in the CVC of birch biomass of particle sizes <2 mm by respectively immersing the reactor in a sand bath already at the carbonization temperature and by immersing the reactor in a ~110°C sand bath that was subsequently ramped to a target temperature.

To decouple the heating rate influence from the immersion time effect, two different soaking times were tested using the “slow” heating rate conditions. In short experiments, the reactor was removed as soon as it reached the target temperature (i.e., null soaking time) while in long experiments, the reactor was removed after the soaking time at carbonization temperature matched the soaking time of the equivalent “fast” heating rate experiment.

Figures 6.21 and 6.22 show that changing the heating rate to reach carbonization temperature does not influence product yields and char proximate analysis as long as the WHTB reactor long soaking time at carbonization temperature (120 minutes at 500°C and 180 minutes at 300°C) is maintained. Reducing the soaking time to 0 minutes lowered fixed-carbon contents and increased the char volatile matter content. The effect was particularly intense in experiments at 300°C but

became minor in “slow” 500°C experiments. This is somehow expected since, due to sand bath heating limitations at high temperatures, “slow” experiments at 500°C required prolonged heating times especially at temperatures close to the carbonization temperature giving time to the charcoal to further devolatilize during the heating period. For example, “slow” 300°C required 50 min of heating (vs. 10 min required in “fast” experiments) whereas “slow” 500°C required 230 min of heating (vs. 70 min required in “fast” experiments). Following this heating period, reactors in long experiments were soaked for time periods of 180 and 120 minutes at respective carbonization temperatures of 300 and 500°C.

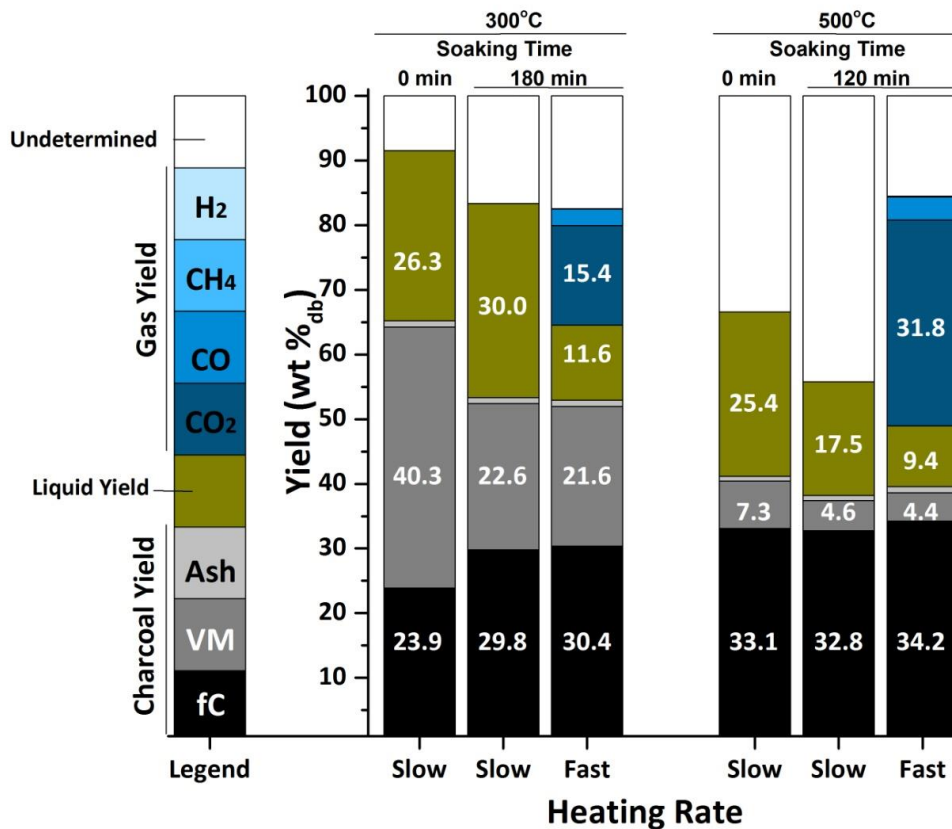


Figure 6.21. Effect of heating rate on the product yields from the constant-volume carbonization of birch (<2 mm) at an initial N₂ pressure of 0.1 MPa.

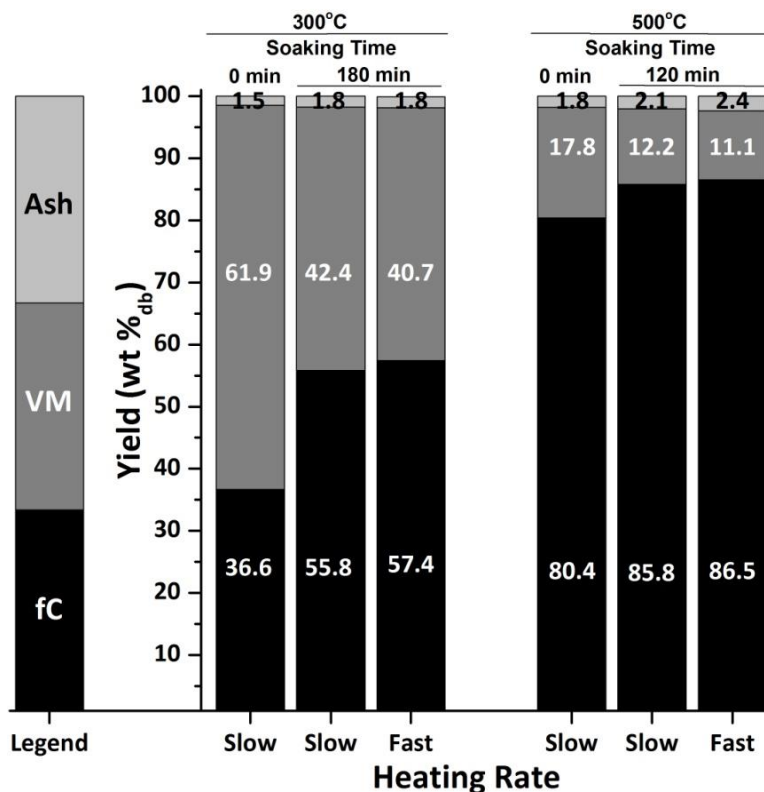


Figure 6.22. Effect of heating rate on the proximate analysis of charcoals from the constant-volume carbonization of birch (<2 mm) at an initial N₂ pressure of 0.1 MPa.

The heating rate also affected the char morphology. At 300°C, no visual signs of TPP were found at both heating rates employed (~0.09 and 0.5°C/s, see Figure 6.23 and 6.9 respectively). Nevertheless, at a HTT of 500°C/s, evidence of some TPP appeared as the heating rate was raised from 0.03°C/s (see Figure 6.24) to 0.09°C/s (see Figure 6.18). As pointed out by Newalkar et al.,⁷⁵ who studied heating rate effects in “open” reactors, raising the heating rate permits interaction between the evolving volatile matter and the solid phase as it approaches its softening point resulting in plastic transformations in the pyrolyzing char.

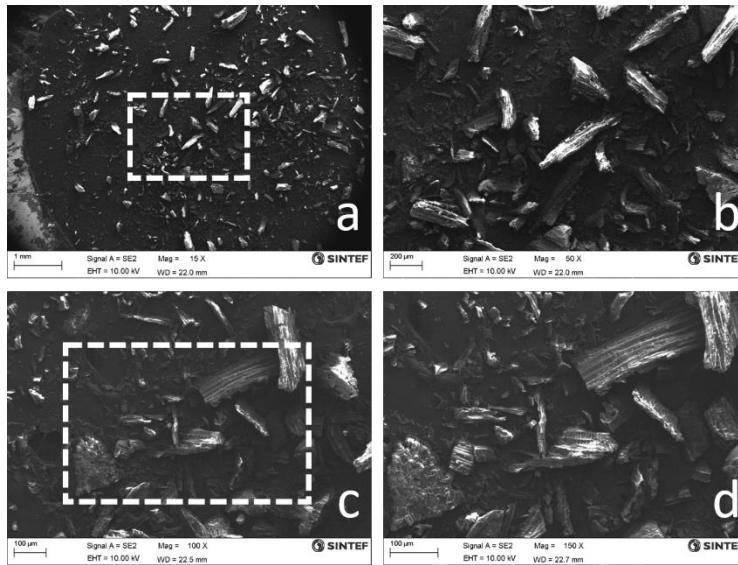


Figure 6.23. (a) and (c) Scanning electron microscopy images of birch charcoal from constant-volume carbonization at an initial nitrogen pressure of 0.1 MPa, a heat treatment temperature of 300°C and at a “slow” heating rate (b) and (d) higher magnification views of selected areas in (a) and (c) .

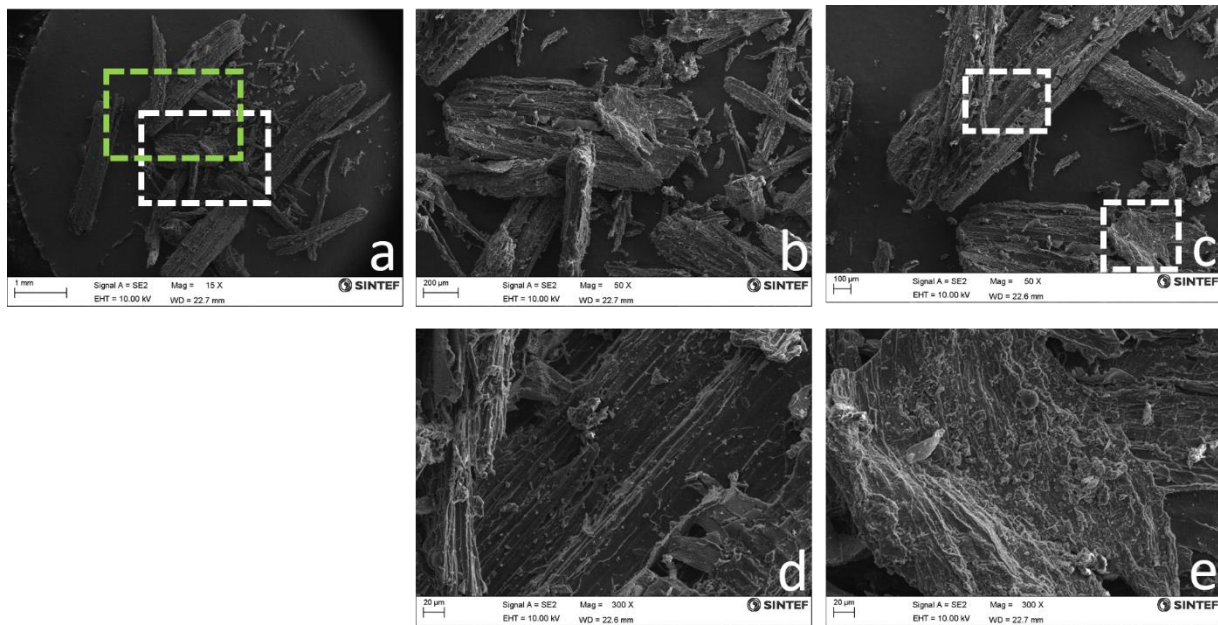


Figure 6.24. (a) Scanning electron microscopy images of birch charcoal from constant-volume carbonization at an initial nitrogen pressure of 0.1 MPa, a heat treatment temperature of 500°C and at a “slow” heating rate. (b) and (c) higher magnification views of selected areas in (a). (d) and (e) higher magnification views of selected areas in (c) .

Present TPPs have been observed at considerably lower heating rates and carbonization temperatures than those reported for carbonization in “open” reactors. For example, CVC enabled the production of molten chars under heating rates as low as $\sim 0.5^{\circ}\text{C}/\text{s}$ at moderate temperatures of 400°C ,^{26,27} as opposed to heating rates of $\sim 500\text{-}10^4^{\circ}\text{C}/\text{s}$ and temperatures of at least 600°C employed in “open” configurations^{74,75,91}. It appears that the large amount of volatiles retained within the char particles in CVC processes intensify plasticization, shifting the occurrence of the TPP to lower temperatures and lower heating rates. Higher initial nitrogen pressures, and possibly smaller particle sizes, can also shift the TPP appearance to even lower temperatures. For example, when the initial pressure in the CVC of cellulose powder was increased from 0.1 to 2.40 MPa, Van Wesenbeeck et al.²⁶ observed TPP signs at temperatures as low as 260°C .

6.5. Effect of Particle Size

CVC has proved that the use of smaller particles does not have a detrimental effect on char yields and properties. This is different from observations from “open” reactors. In CVC, released volatiles remain in contact with the reacting solid which results in an enhancement of secondary charring reactions that would not occur (or to a lesser extent) in reactors where volatiles are removed. The use of larger particles in open reactors provide longer contact times between the char and evolving volatiles and extended opportunity for secondary reactions.

Figures 6.25 and 6.26 illustrate the effect of particle size in product yields and char proximate analysis. Spruce experiments showed that smaller particle sizes (<0.2 mm vs. <2 mm) led to a greater devolatilization of the biomass and resulted in higher pressures, more pronounced exotherms, greater fixed-carbon contents, and greater fixed-carbon yields (increases on fixed-carbon yields become apparent when the carbonization time was extended)²¹⁰. HHV were similar (~30 MJ/kg) across this same range of experimental conditions (see Table 5.1). It is possible that the particle size difference was not large enough to produce a significant difference and that the asymptotic behavior of HHV could not reflect any particle size effect.

The overall rate of reaction also appeared to accelerate with decreasing particle size. When using <0.2 mm spruce particles at a HTT of 300°C and a processing time on 190 min, the pyrolysis process seemed to have reached steady state within 120 minutes as indicated by the stabilized temperature and pressure. When larger particles (<2 mm) were used under the same conditions (mass loading, temperature and processing time) a continuous rise in pressure was observed throughout the course of the experiment which indicates steady state was not achieved during the 190 minute experimental time.

Birch experiments presented similar values of product yields and proximate analysis at the two distinct particle sizes of <0.2 mm and <2 mm. The smaller birch particles—as opposed to spruce—appeared to manifest faster reaction rates since pressure and temperatures stabilized within the first hour. Thus, it is possible that the differences observed on the proximate analysis and yields of spruce at the two particle sizes are the result of reactions not reaching completion at

the larger size (<2 mm) but having terminated or being near completion for the smaller size particles (<0.2 mm). Experiments with the larger spruce grains and immersion times of 30, 190 and 300 min confirmed the continuous improvement of char properties as the time was prolonged. With birch, reactions appeared to be faster so they may be near completion at immersion times of 190 minutes for both the smaller and larger particle sizes resulting in similar birch product yields and proximate analysis. In line with these findings, cellulose powder (50-180 μm) carbonized in the original WHTB required 30-60 minutes to reach steady state. Thereafter, final product yields and proximate analysis remained similar. Differences in reaction rates between spruce and birch could be due to different chemical or physical properties of the feedstocks. For example, larger packing densities (as in the case of birch) appear to lead to improved heat transfer coefficients²¹¹. In the future, it would be interesting to investigate reaction rates in CVC with feedstocks that have been externally compacted prior to carbonization.

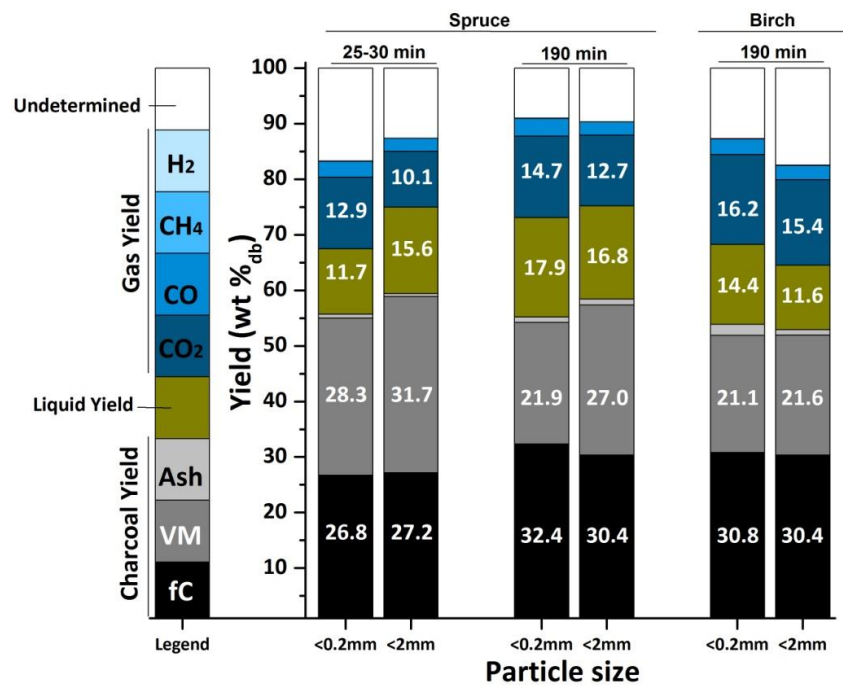


Figure 6.25. Effect of particle size on the yields of char, condensates and gas from the constant-volume carbonization of spruce and birch at 300°C and at an initial N₂ pressure of 0.1 MPa.

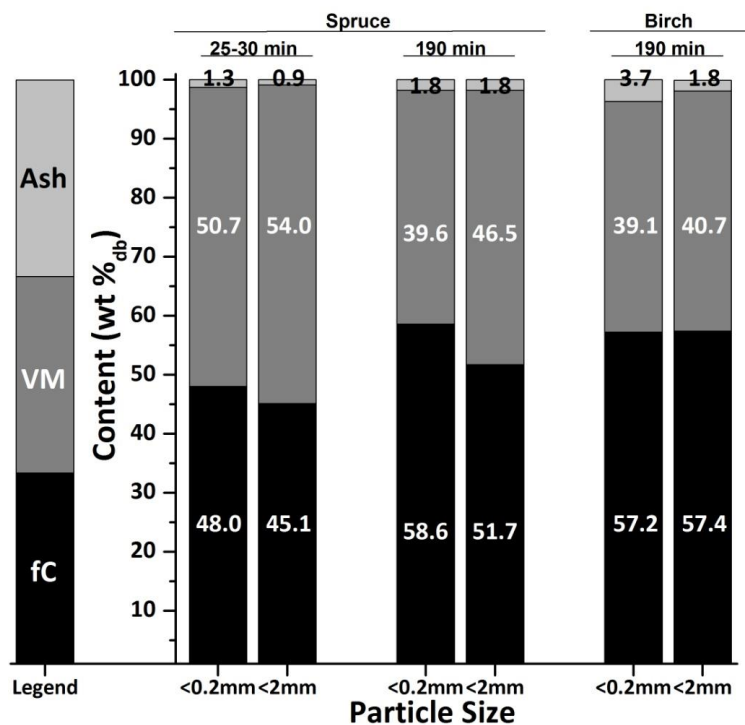


Figure 6.26. Effect of particle size on the proximate analysis of charcoals from the constant-volume carbonization of spruce and birch at 300°C and at an initial N₂ pressure of 0.1 MPa.

Particle size is likely to have an impact on the char morphology. The size of the biomass particle is closely linked to the intraparticle heating rate and intraparticle volatile retention and both are key factors in the evolution of char morphology. The particle size effect is, nonetheless, not intuitive. On the one hand, smaller particles experience higher heating rates which favor TPP formation. On the other hand, smaller particles lead to shorter intraparticle volatile retention which hinders the TPP formation. The only available SEM images (Figures 6.9 and 6.28) from the CVC tests are not that clarifying. The images portray structures of chars produced under CVC at a HTT of 300°C and a pretest pressure of 0.1 MPa. At that pressure and mass loading, TPP evolution in CVC was observed to form at higher temperatures. The visual observations of chars from these two tests (Figure 6.27) and additional observations of chars manufactured from

different feedstocks, each with a different particle size, displayed in Figure 6.20 may indicate that smaller particles appear to have a higher tendency to form TPP.

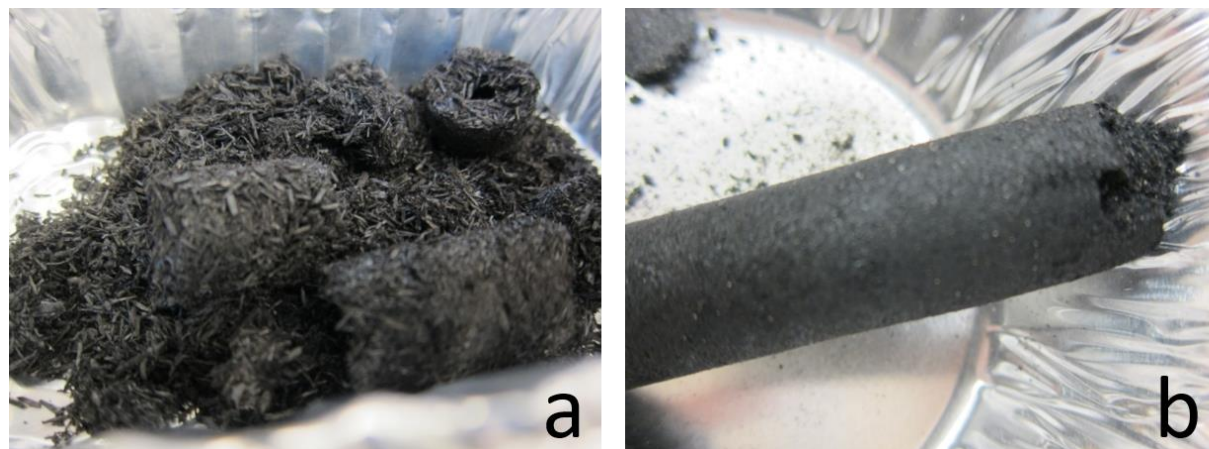


Figure 6.27. Charcoals from constant-volume carbonization of spruce at an initial N_2 pressure of 0.1 MPa, immersion time of 190 min and a heat treatment temperature of $300^\circ C$ at particle sizes of <2 mm (on the left) and <0.2 mm (on the right).

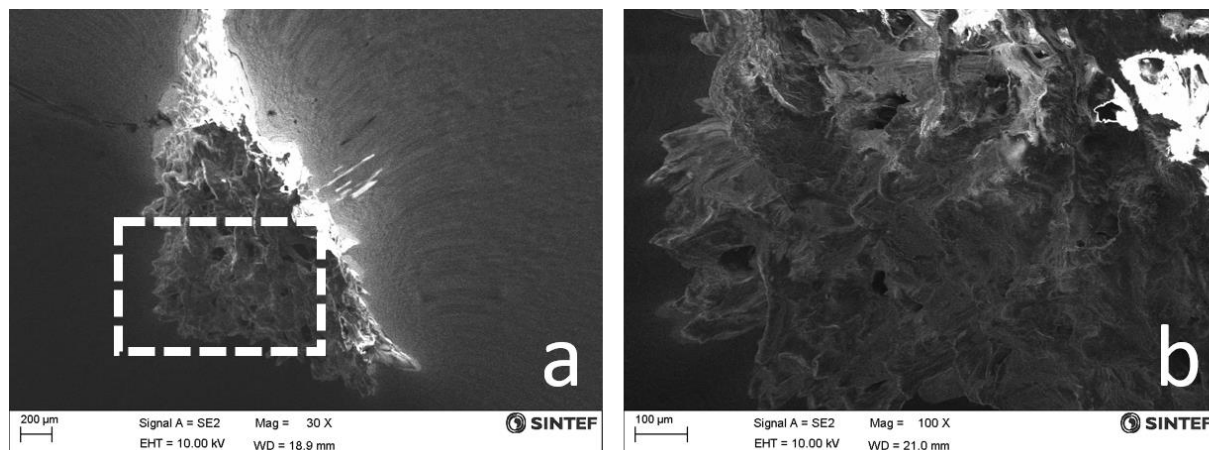


Figure 6.28. (a) Scanning electron microscopy image of birch (<0.2 mm) charcoal from constant-volume carbonization at a heat treatment temperature of $300^\circ C$ and an initial nitrogen pressure of 0.1 MPa, (b) higher magnification view of selected area in (a).

6.6. Effect of Mass Loading

Oak and cellulose experiments were performed in the original and single-intermediate reactors at an initial nitrogen pretest pressure of 0.1 MPa and a HTT of 300°C. The main parameters that changed from the original to the single-intermediate reactor were the mass loading—that went from ~100 to ~125 g/L for oak, and from ~155 to ~205g/L for cellulose—, and in the case of cellulose, the immersion time was prolonged from ~30 to 190 minutes. Going from the original to the single-intermediate WHTB resulted in higher temperature peaks (380 vs. 310°C for oak, and 552°C vs. 365°C for cellulose, notice that temperature differences are partly also related to the change in the temperature measuring technique) and higher pressure peaks (5.7 vs. 4.6 MPa for oak, and ~7.5 MPa vs. 2.3 MPa for cellulose).

Mass loading effects in the WHTB were further explored using spruce and birch wood as feedstocks and the dual WHTB reactor. Birch, compared to spruce, enabled the testing of higher mass loadings due to its greater packing density. Increasing the mass loading showed greater pressure peaks and very similar char HHVs. The similarity in HHVs could be the result of reaching a HHV asymptotic value as the theoretical fixed-carbon yield is approached.

Spruce also showed similar measured temperature peaks (around 400°C). It seems that the increment in spruce mass loadings was not sufficient to present clear temperature differences, in other words the mass loadings tested did not reveal a significant influence on the pyrolytic exotherms and/or differences were masked by the large thermal mass of the sand bath.

Temperature peaks for birch were not representative of biomass temperature at the lower mass loadings since, given birch higher packing density, the thermocouple sensor was not in contact with the biomass.

Figures 6.29 and 6.30 show proximate analysis and product yield trends with mass loadings. Oak and cellulose results of the experiments at the two different mass loadings may be misleading as the proximate analysis measurements followed different methods, as explained earlier in Section 4.2. Nonetheless, in the case of cellulose, the similar fixed-carbon yields but the remarkable increase in the fixed-carbon content with the mass loading (~72% vs. 54%) cannot be solely explained by differences between the proximate analysis measuring techniques or differences in immersion times. This indicates a considerably higher extent of secondary charring reactions when a higher mass loading was tested.

The most recent cellulose experiment proved that attaining a charcoal product high in fixed-carbon and low in volatiles is possible using elevated mass loading at a moderate temperature of 300°C as long as the carbonization reactor is capable of withstanding the high pressures evolved during the pyrolysis reaction. Short experiments with birch and spruce showed a minor increase on the fixed-carbon yields with increased mass loading and a minor increase, if any, on the fixed-carbon contents. The spruce data exhibit a small increase in the fixed-carbon content which is just smaller than the experimental error. For long experiments with birch (long experiments with spruce were not performed), no significant changes to the fixed-carbon yields and contents at the loadings tested were observed. It appears that lengthening the immersion time reduces the

differences in char proximate analysis and product yields, and that there is a limit to the mass loading effect.

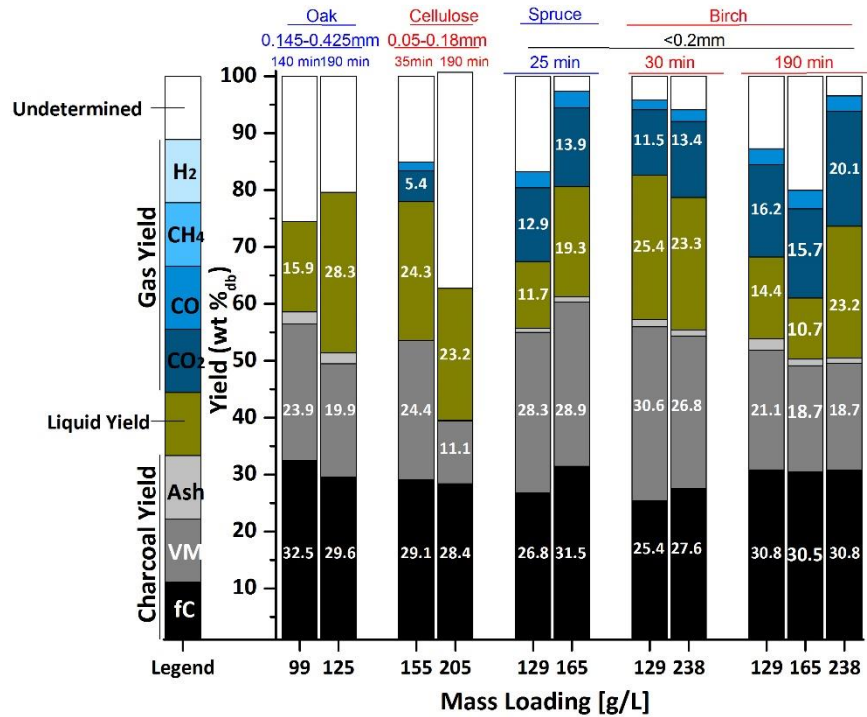


Figure 6.29. Effect of mass loading on the yields of char, condensates and gas from the constant-volume carbonization of birch, spruce, cellulose and oak at 300°C and at an initial N₂ pressure of 0.1 MPa.

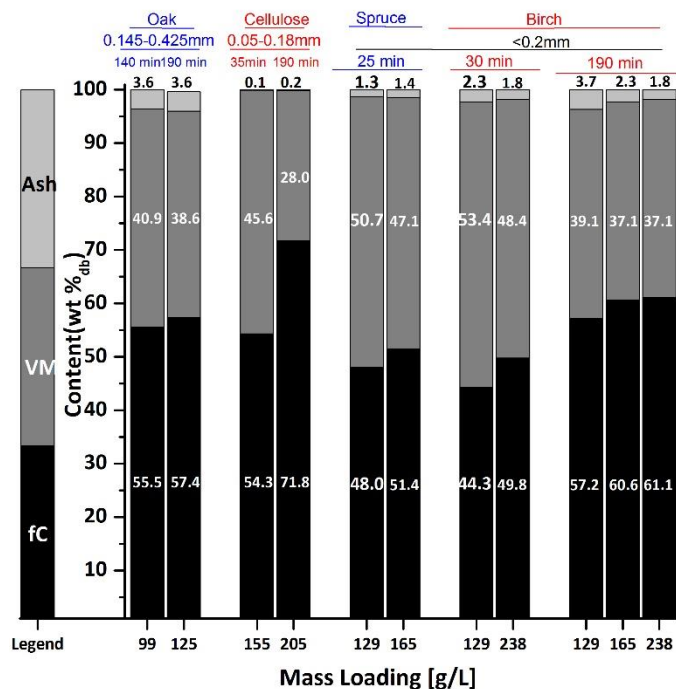


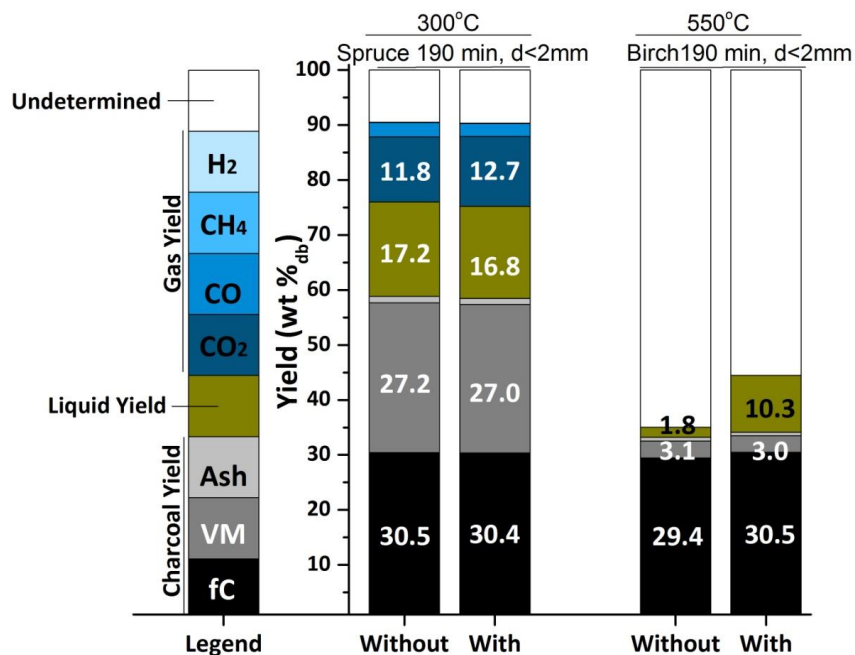
Figure 6.30. Effect of mass loading on the proximate analysis of charcoals from the constant-volume carbonization of birch, spruce, cellulose and oak at 300°C and at an initial N₂ pressure of 0.1 MPa.

To test the mass loading effect, another approach was taken. The mass loading in the WHTB was varied by changing the WHTB dead volume while maintaining the feedstock absolute mass.

Adding a tubing extension to the unheated portion of the reactor system created an incremental WHTB dead volume of 46 mL. The rest of experimental parameters were kept constant, considerably decreasing the peak pressures (from 4.7 to 2.7 MPa at 300°C, and from 17.9 to 7.5 MPa at 550°C) while maintaining char HHVs, fixed-carbon contents and product yields (see Figures 6.31 and 6.32). In contrast to the limited studies in literature that showed a trend of increasing charcoal yields and fixed-carbon contents with the mass loading in sealed vessels, the WHTB experiments indicate that there is a limit to the mass loading effect. Larger mass loadings were tested in the WHTB experiments, in comparison to the loadings reported in literature (for

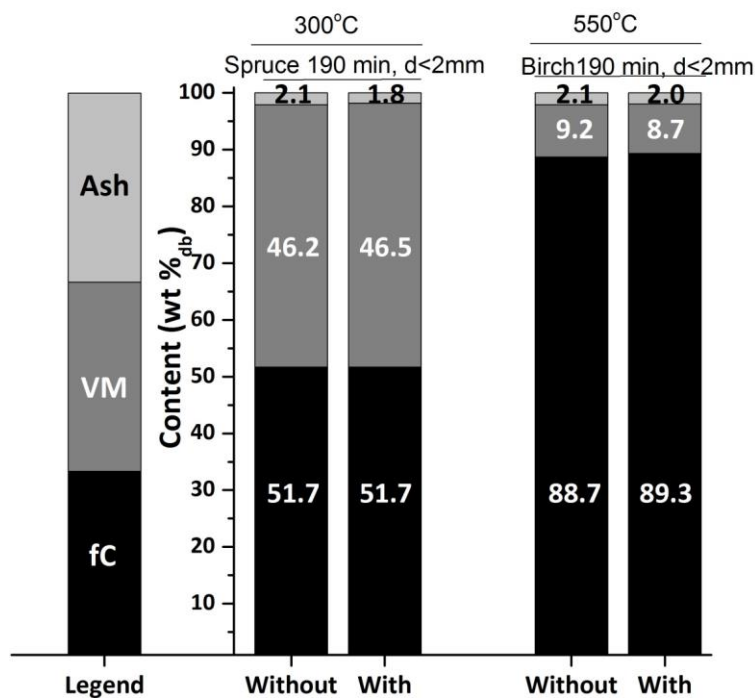
example, Mok et al. varied cellulose mass loadings in a 10-160g/L range while experiments with the most recent WHTB worked in a 130-240 g/L range).

It may be possible that as the loading is increased in a sealed vessel, and therefore, the partial pressure of volatiles and the extent of volatile-char interactions, char yields and proximate values initially improve until a limiting value is approached. Above it, the reactor pressure keeps increasing due to the higher amount of volatiles released but does not improve yields or fixed-carbon. A deeper study is needed to reach definite conclusions that explain the differences observed between literature and experimental trends. The possibility of reducing pressures without affecting char proximate values and yields is particularly interesting since it offers the possibility to produce char of equal qualities in reactors characterized by lower pressure ratings and consequently, requiring lower investment and manufacturing costs.



Additional dead volume compensation of 46 mL

Figure 6.31. Effect of adding a dead volume on the yields of char, condensates and gas from the constant-volume carbonization of birch and spruce at an initial N₂ pressure of 0.1 MPa.



Additional dead volume compensation of 46 mL

Figure 6.32. Effect of adding a dead volume on the proximate analysis of charcoals from the constant-volume carbonization of birch and spruce at an initial N₂ pressure of 0.1 MPa.

Figure 6.33 shows thermodynamic product yield predictions with birch mass loadings calculated by FactSage. Theoretically, an initial plateau on the product yields with the mass loading is predicted until a limiting value is reached. Above it, liquid water is formed, the fixed-carbon yield increases while water vapor, CO₂ and CH₄ yields decline. Oak and cellulose theoretical predictions show similar behaviors. Experimentally, trends differed radically. Experimental mass loadings above the critical theoretical value did not result in any improvements of fixed-carbon yields but a plateau on the yields was observed. Note that the experimental and theoretical results under similar experimentally defined conditions are not completely equivalent. For example, FactSage assumes a constant-volume reactor at a uniform temperature. Experimentally, the constant-volume WHTB has two distinct temperature zones (the hot reaction zone and the cool, near-room-temperature, dead volume) and solid and gaseous volumes keep changing during carbonization. In addition, lots of complex reaction products and intermediates, such as tarry vapors, are not included in theoretical predictions.

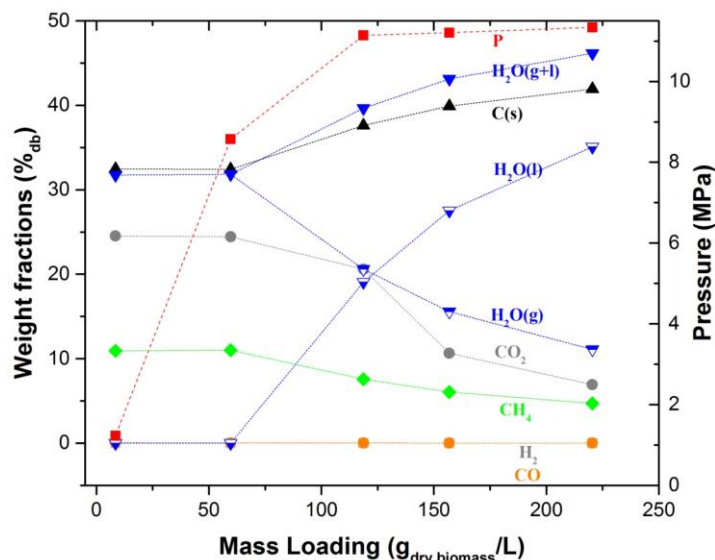


Figure 6.33. Effect of mass loading on the theoretical product distribution from the constant-volume carbonization of birch at 300°C predicted by FactSage

Based on the available SEM images of charcoals derived from birch CVC (0.1 MPa pretest pressure, 300°C HTT and mass loadings of 130, 165 and 240 g/L, see Figures 6.9, 6.28, 6.34 and 6.35), robust conclusions cannot be made regarding the role of mass loading on the char morphology. For example, some TPP formation was observed on chars derived from CVC of small birch particles (<0.2 mm) at a mass loading of 165 g/L (Figure 6.34) whereas no signs of TPP were discerned on chars from CVC of larger birch particles (<2 mm) at a lower mass loading of 130 g/L (see Figure 6.9). Since tests at the higher mass loadings were only performed with smaller birch particles (<0.2 mm), the roles of particle size or mass loading on TPP evolution cannot be isolated.

Intuitively, one could explain both a favorable and a detrimental effect of a decrease in the biomass particle size on the TPP formation (see section 6.5 for details). Similarly, an increase in the mass loading could also have antagonistic impacts on the TPP development. On the one hand, higher mass loadings raise the volatile pressure which most likely benefit the TPP formation. Conversely, higher mass loadings lead to lower heating rates which may jeopardize the TPP development. Thus, the influence of both the mass loading and particle size factors on the evolution of the char morphological structure need further elucidation.

Note that both the mass loading and particle size effects were studied in CVC tests at HTTs of 300°C. This temperature is too modest to observe clear TPP evolution (see section 6.3). Higher temperatures could shed light into the impacts of both factors on the char morphology.

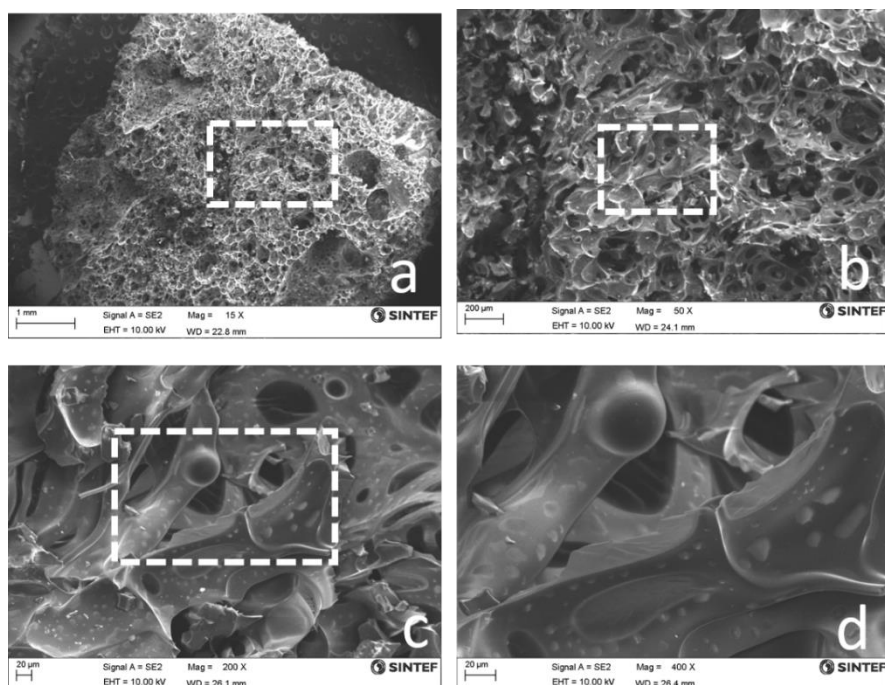


Figure 6.34. (a) Scanning electron microscopy image of charcoal from constant-volume carbonization of birch grains of particle size <0.2 mm at a mass loading of 165 g/L, at a heat treatment temperature of 300°C and an initial nitrogen pressure of 0.1 MPa, (b), (c) and (d) higher magnification views of selected areas in (a), (b) and (c) respectively.

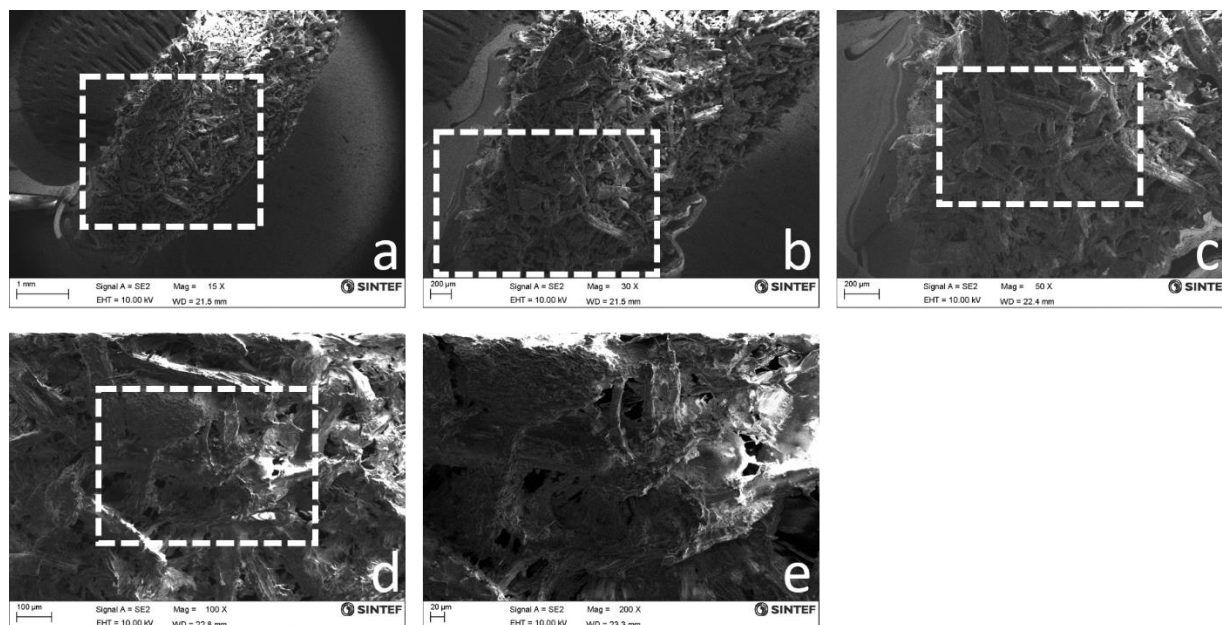


Figure 6.35. (a) Scanning electron microscopy image of charcoal from constant-volume carbonization of birch grains of particle size <0.2 mm at a mass loading of 240 g/L, at a heat treatment temperature of 300°C and an initial nitrogen pressure of 0.1 MPa, (b), (c), (d) and (e) higher magnification views of selected areas in (a), (b), (c) and (d) respectively.

6.7. Effect of Solid Residence Time or Immersion Time

Figures 6.36 and 6.37 show the effects of immersion times on spruce and birch experiments at an initial N₂ pressure of 0.1 MPa. Prolonging the processing times from 30 to 190 minutes led to higher gas yields and pressures and charcoals with a greater degree of devolatilization. Char heating values were similar. At a carbonization temperature of 300°C, fixed-carbon yields improved by more than 10%, relative. At 400°C, however, the longer reaction time did not improve the fixed-carbon yields.

Lengthening the immersion time from 190 to 300 minutes for spruce at 300°C appeared to improve fixed-carbon yield and fixed-carbon content. Keep in mind that spruce feedstock seemed to react more slowly than birch, so it is possible that long experiments with birch presented lower or negligible increases on the fixed-carbon content and yields. Notice that the cold WHTB dead volume wherein tarry vapors can condense could interfere with the reaction rates.

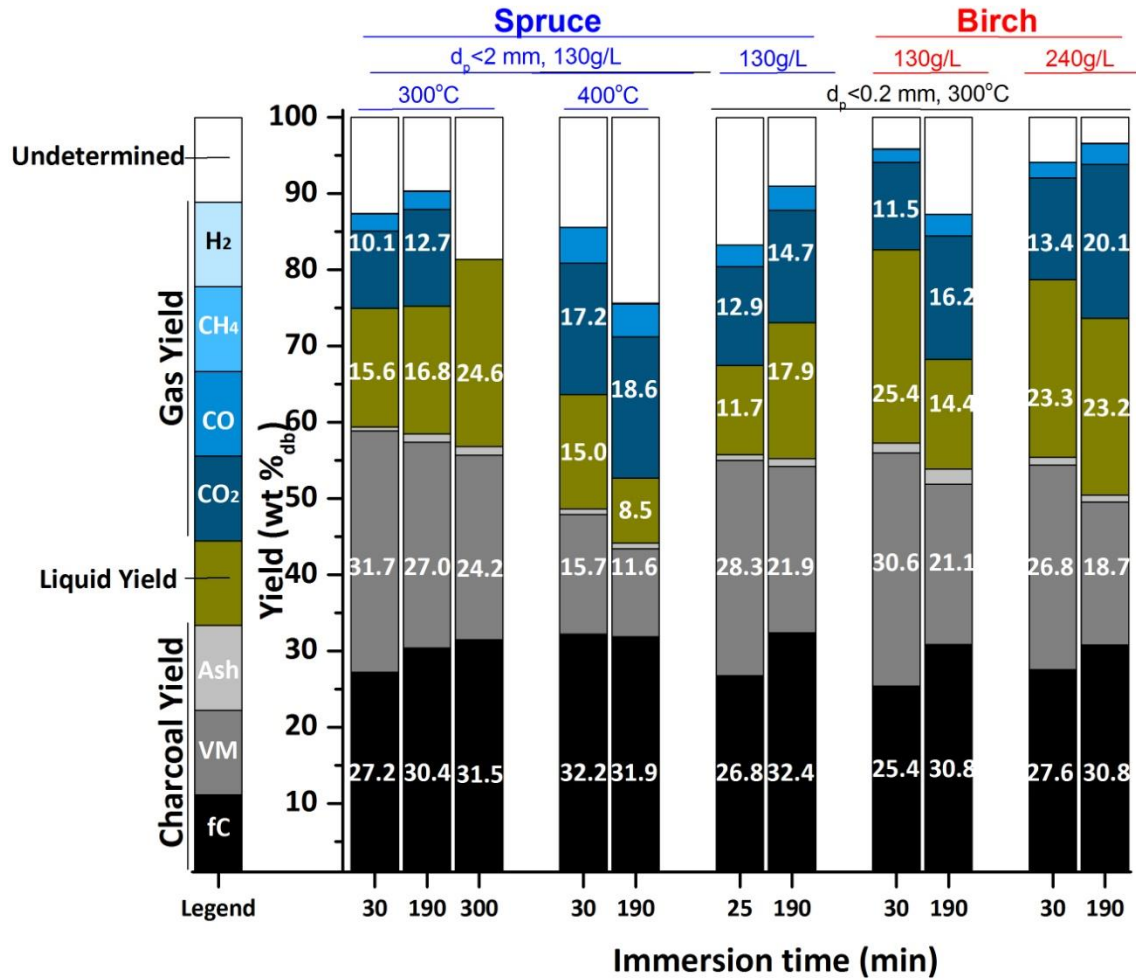


Figure 6.36. Effect of immersion time on the yields of char, condensates and gas from the constant-volume carbonization of spruce and birch at an initial N₂ pressure of 0.1 MPa.

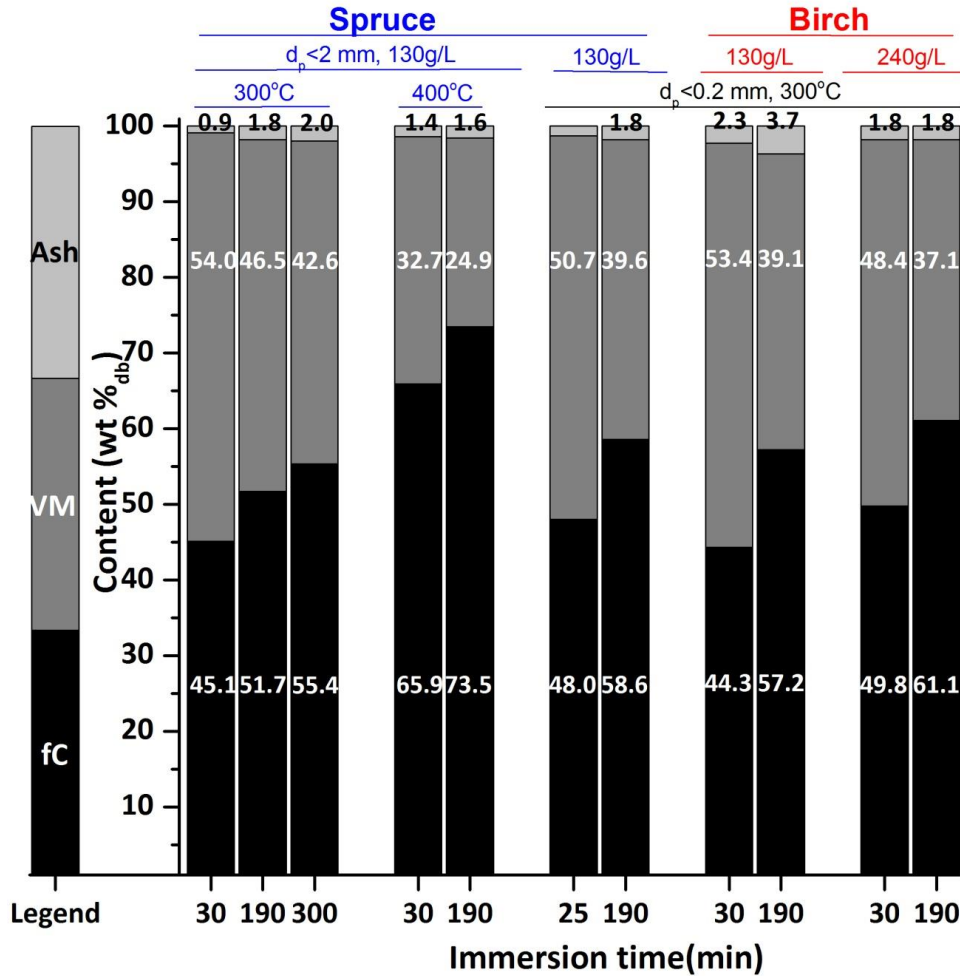


Figure 6.37. Effect of immersion time on the proximate analysis of char from the constant-volume carbonization of spruce and birch at an initial N₂ pressure of 0.1 MPa.

An intriguing aspect of these spruce experiments is their slow rates compared to cellulose experiments in the original WHTB model. For cellulose, immersion time appears to have a lesser effect on the fixed-carbon content, and pressure and temperature stabilized within tens of minutes. Contrary to those observations, spruce and birch carbonization in the current WHTB required hours for the pressure to stabilize which is assumed to indicate that charring reactions are near completion. Pressure and temperature did not stabilize in the majority of the tests. Surprisingly, the long experiment performed with the smallest spruce grains (<0.2 mm) achieved

pressure and temperature stability after about two hours, which indicates the carbonization process is accelerated by the use of smaller particles and may account for the quicker rates observed on cellulose pyrolysis. Particle size, temperature, biomass type, external pressure and mass loading all seem to have an effect on the reaction rates of carbonization. In CVC, rates can be accelerated by the use of smaller particles and higher temperatures. In conventional carbonization processes in “open” reactors, the use of elevated pressures has proved beneficial on reducing times,⁵⁷ while in CVC, the effect of raising the pretest pressure by an external gas, as well as the mass loading, may not be as beneficial due to the self-generated internal pressures experienced by the constant-volume reactor.

Figure 6.38 shows SEM images of a charcoal produced in a short (30 min approx.) carbonization experiment of birch grains of particle size <0.2 mm at 240 g/L mass loading, 0.1 MPa pretest pressure, 300°C HTT and 190 min immersion time. The appearance of some melting can already be appreciated confirming the significance of the early stages of the carbonization process on the morphological evolution of charcoal. This finding was already supported when studying the heating rate effect on the char morphology. The heating path of the biomass proved to be crucial on the evolution of the char structure with fast heating leading to char molten phases and slow heating suppressing the char melting stage.

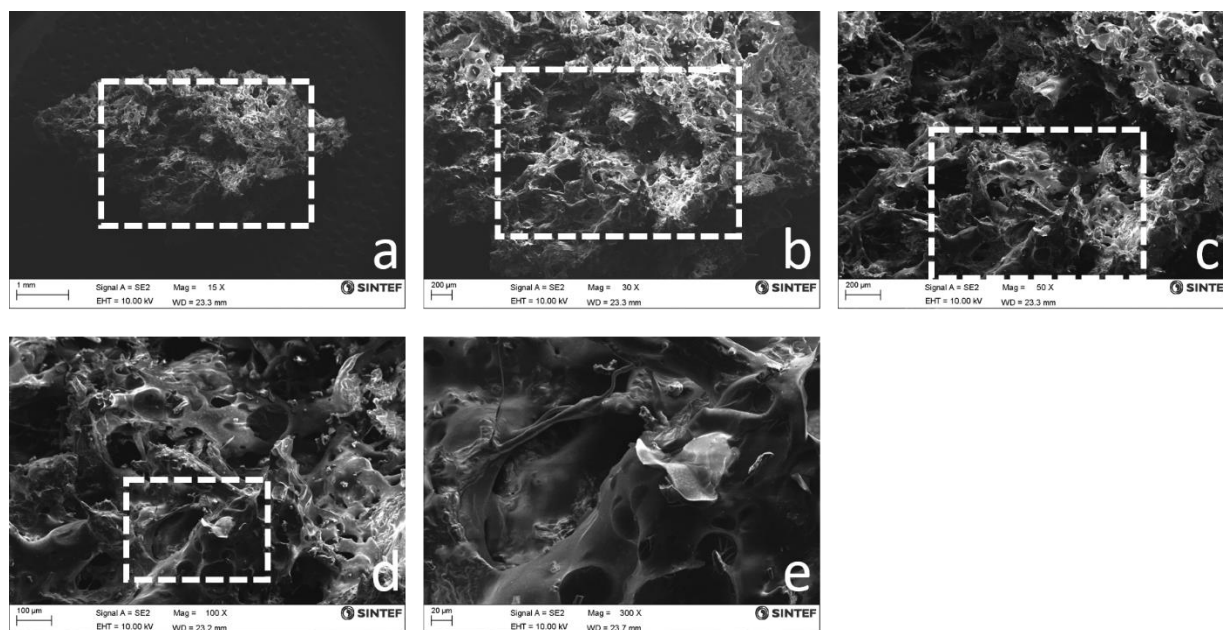


Figure 6.38. (a) Scanning electron microscopy images of charcoal from constant-volume carbonization of birch grains of particle size <0.2 mm at a mass loading of 240 g/L, at a heat treatment temperature of 300°C , an initial nitrogen pressure of 0.1 MPa and a short immersion time of around 30 min, (b), (c) and (d) higher magnification views of selected areas in (a), (b), (c) respectively.

6.8. Effect of Feedstock

The study of the feedstock has not been the main focus of this research. The majority of the WHTB experiments were performed with either birch or spruce feedstocks. Figures 6.39 and 6.40 show the effect of biomass type (spruce or birch) on pyrolysis product yields and char proximate analysis. Table 4.1 showed similar elemental and proximate analysis for both of the raw biomass species. Regarding the cellulose, hemicellulose and lignin contents, spruce appears to have a higher lignin content and less cellulose and hemicellulose than birch.

In view of these structural components, one would be inclined to think that spruce would result in higher char yields. This is the case for the experiments performed at a HTT of 300°C and particle size of <2 mm. Nonetheless, the higher char yield of spruce was due to a higher content of volatiles but not to improved fixed-carbon yields. As the experimental conditions favor the achievement of equilibrium, that is, by reducing particle size from <2 mm to <0.2 mm or by increasing the temperature from 300 to 400°C, product yields and char analysis became similar for both feedstocks.

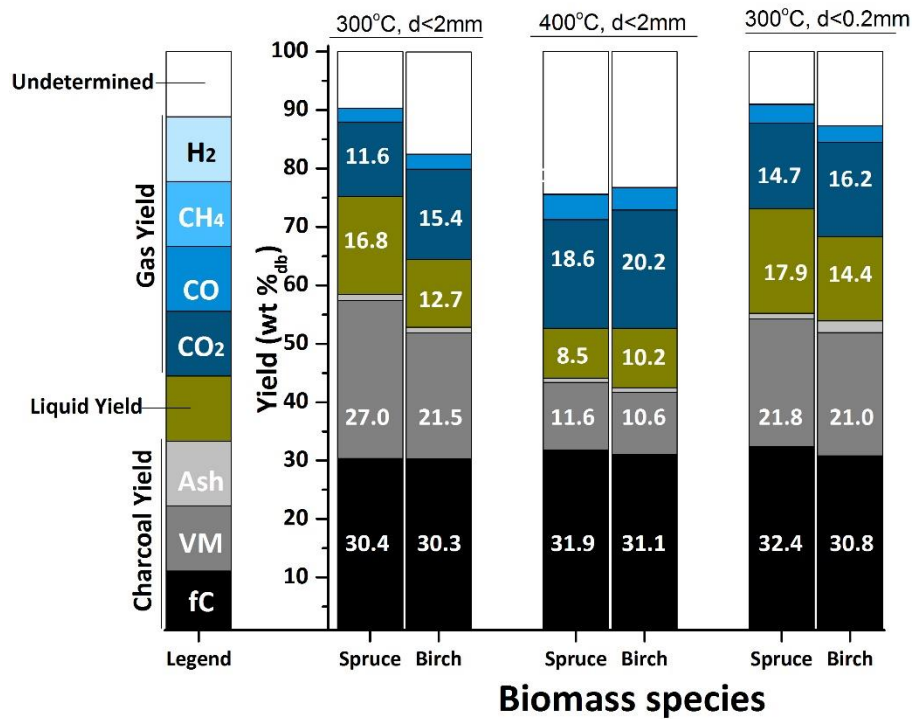


Figure 6.39. Effect of feedstock on the yields of char, condensates and gas from constant-volume carbonization at an initial N₂ pressure of 0.1 MPa, immersion time of 190 minutes and mass loading of 130 g/L.

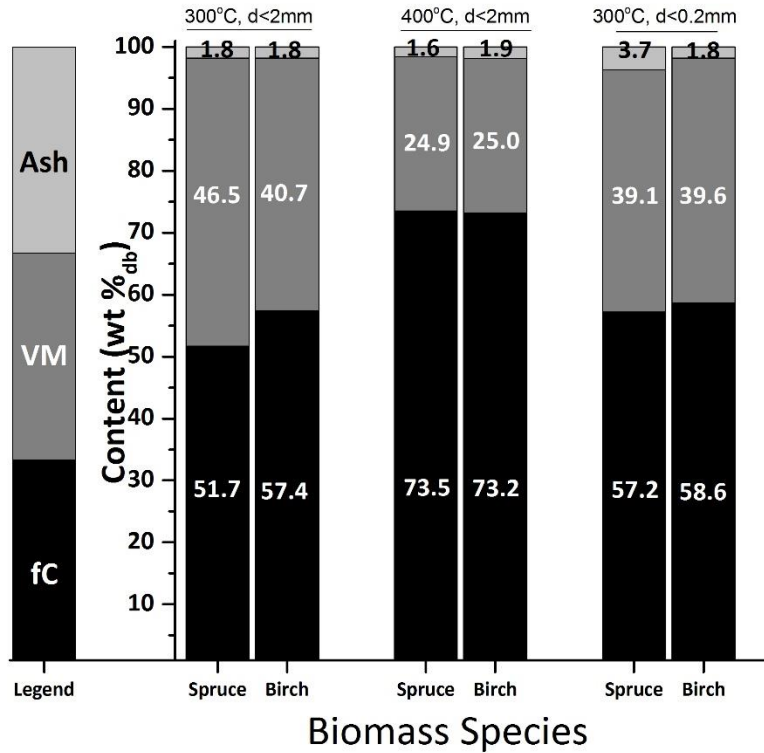


Figure 6.40. Effect of feedstock on the proximate analysis of char from constant-volume carbonization at an initial N₂ pressure of 0.1 MPa, immersion time of 190 minutes and mass loading of 130 g/L.

Exceptionally, three isolated experiments tested the pyrolysis of oak, cellulose and rice husk biomasses under a pre-test pressure of 0.1 MPa a HTT of 300°C. Figures 6.41 and 6.42 show the results of three experiments in addition to two of the experiments with spruce and birch at the same pressure and HTT. Other experimental parameters such as particle size, mass loading or immersion time were not kept constant between experiments and therefore a direct quantitative comparison between experimental results is not possible.

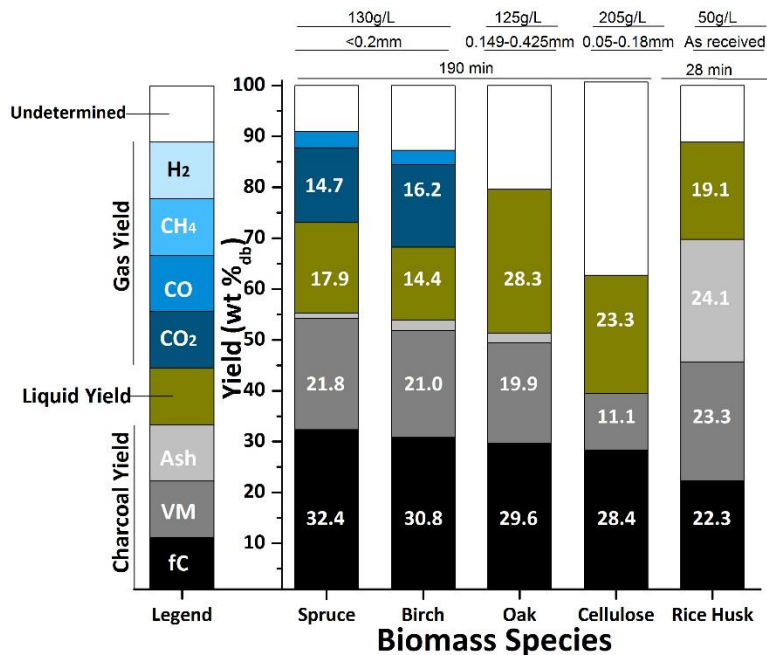


Figure 6.41. Effect of feedstock on the yields of char, condensates and gas from constant-volume carbonization at an initial N₂ pressure of 0.1 MPa and a heat treatment temperature of 300°C.

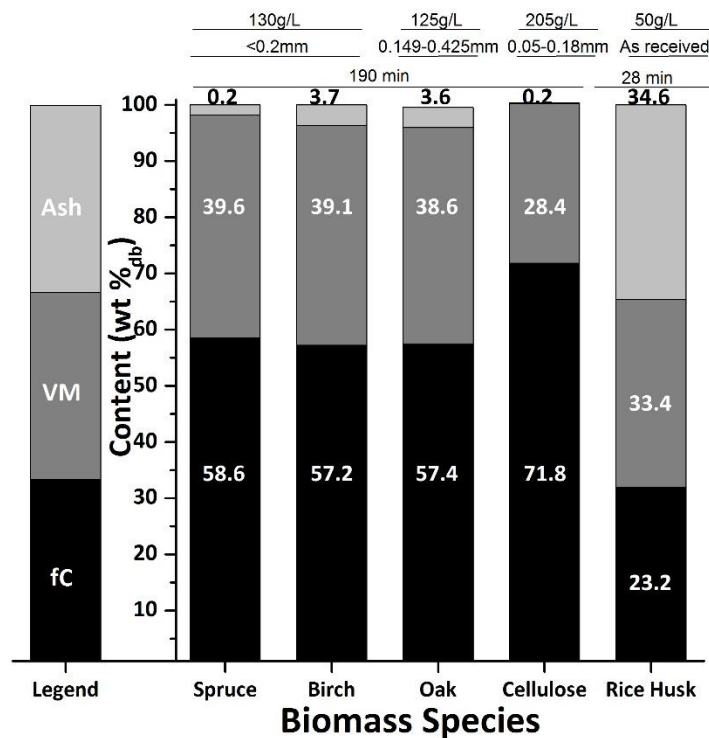
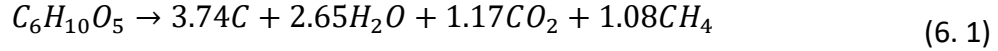


Figure 6.42. Effect of feedstock on the proximate analysis of charcoals from constant-volume carbonization at an initial N₂ pressure of 0.1 MPa and a heat treatment temperature of 300°C.

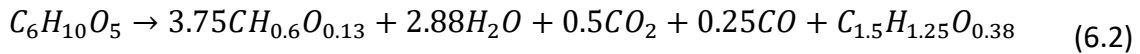
The experimental parameters employed for the oak test were fairly similar to those employed for birch and spruce runs. In addition, elemental and proximate analysis of the original biomasses were also comparable (see Table 4.1). Regarding the structural components, oak shows a lower lignin content and higher cellulose. As a result, one may think that oak would produce lower char yield. Nonetheless, product yields and char proximate analysis from the three tests are relatively similar.

In the case of the pyrolysis of cellulose, lower yields of charcoal than from spruce, birch or oak were obtained, which was expected due to the absence of lignin in the cellulosic feedstock. The charcoal showed a slightly lower fixed-carbon yield but manifested a surprisingly low content of volatiles at the modest temperature of 300°C employed. Therefore, the low yield of charcoal was mainly due to an enhanced release of volatiles and therefore to a considerable improvement of charcoal quality in terms of proximate analysis. Differences in mass loading and particle size parameters for the cellulose experiment in comparison to the other feedstock experiments do not appear to explain the differences observed from the experimental results (see Sections 6.5 and 6.6.).

Antal and Grønli³⁹ reported charcoal yield estimations from cellulose pyrolysis. The following stoichiometric equation was derived from Stanjan theoretical products that followed the attainment of thermochemical equilibrium at 400°C and 1 MPa and predicted a yield of carbon from cellulose of 27.7 wt. %. Stanjan specified only carbon with non-condensable gases as pyrolysis products and did not include volatiles in the calculations.

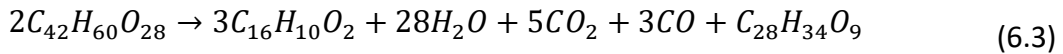


The stoichiometric equation was contrasted with the approximate expression derived by Klason et al.¹⁹⁰ (also replicated by Antal and Grønli)³⁹ from experimental observations of cellulose pyrolysis at 400°C which lead to a charcoal (first product in the equation) yield of 34.0 wt. % and a tar (last product in the equation) yield of 15.6 wt % and a fixed-carbon yield of 27.8 wt %.



Note that H is unbalanced across the reaction but is an accurate reflection of the cited article.

Klason and co-workers¹⁹¹ also reported an approximate equation for the carbonization of “wood” at 400°C that revealed a charcoal (first product in the equation) yield of 34.7 wt. % and a tar (last product in the equation) yield of 25.4 wt. % and a fixed-carbon yield of 28.5 wt. %.



While Klason and co-workers^{190,191} approximate equations for both cellulose and wood pyrolysis showed similar charcoal and fixed-carbon yields. Tar yields differed considerably. Cellulose pyrolysis results in approximately a 10 wt. % lower yield than wood pyrolysis (15.6 wt. % versus 25.4 wt. %). In a sealed reactor like the WHTB, tars are not released but instead remain in the reaction zone resulting in a negligible amount of free-tar. The release of less volatiles from pure cellulose could explain the lower volatile matter of its char as was observed in comparing it to char from wood under identical experimental conditions.

Finally, the experiment with rice husk resulted in low fixed-carbon yields and large amounts of volatiles and ash in the final charcoal. The results can be explained by the large amount of ash in

the original biomass (see Table 4.1) in combination with a shorter experimental time (28 min versus 190 min).

Figure 6.43 shows theoretical fixed-carbon yields of the different feedstocks predicted by FactSage. Note that the FactSage algorithm can serve as reference values for the equilibrium yields. The calculations considers the biomass elemental analysis and processing conditions such as temperature and pressure. But other factors such as the biomass structural components (cellulose, hemicelluloses and lignin) or ash constituents which that have been proved to be of significance during the evolution of the pyrolysis processes are ignored.

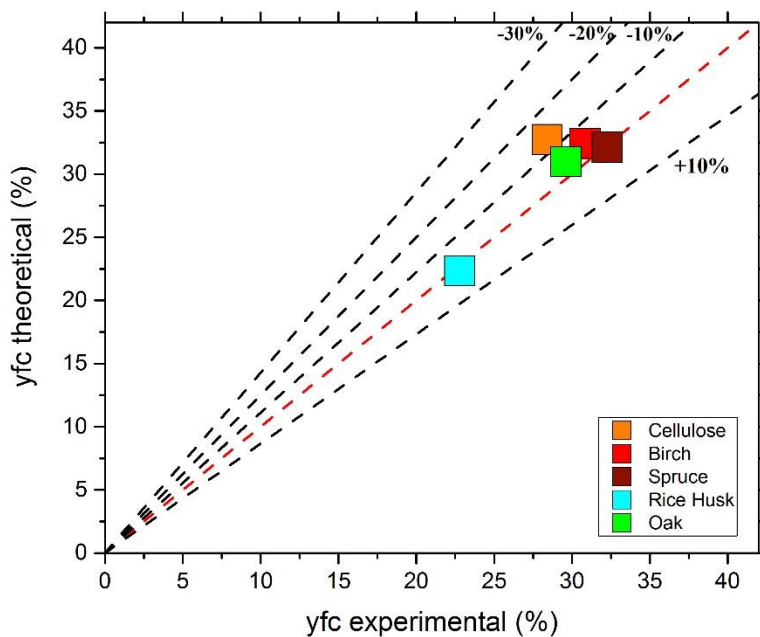


Figure 6.43. Parity plot displaying the experimental fixed carbon yields from CVC vs the theoretical values predicted by FactSage for cellulose, rice husk, oak, birch and spruce at a heat treatment temperature of 300°C and a pretest pressure of 0.1 MPa.

Finally, FactSage results are relatively sensitive to the elemental composition of the biomass introduced as input data. Figure 6.44 shows a 2% difference in the fixed-carbon yield estimated by FactSage for birch pyrolysis with the elemental composition given by two different laboratories: The R3 Laboratory in Hawaii (see Table 4.1) and SINTEF Energy Research in Norway (Analysis published in ⁵²). This indicates that small variations in elemental analysis which could be due to experimental human errors or small variations in the elemental composition within the same sample could result in moderate differences in the predicted-fixed carbon yield limiting values.

In experiments in which equilibrium is almost attained, these differences along with other factors such as the fact that the experimental fixed-carbon yield consists of 95.27% elemental carbon (and not 100% carbon as it is assumed to, see Section 5.3), could result in calculations of experimental fixed-carbon values slightly over the limiting fixed-carbon yield values. In conclusion, FactSage and experimental values are not 100% accurate but provides a reasonably good estimate of the closeness to equilibrium. It can be concluded that the WHTB successfully “attained” the fixed-carbon yields predicted by thermodynamical equilibrium.

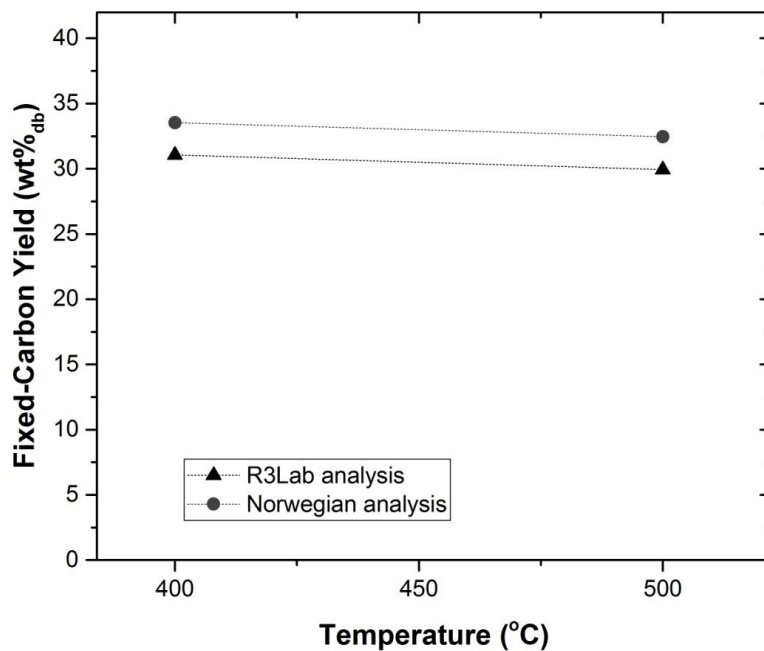


Figure 6.44. Effect of small changes in the birch elemental analysis (provided by two laboratories) on the theoretical product fixed-carbon yield from the constant-volume carbonization of birch at 300°C predicted by FactSage.

CHAPTER 7. MODELING EFFORT

This chapter identifies models relevant to the WHTB and the experimental data that will allow the models to be evaluated for applicability. As pointed out by Di Blasi,¹⁸⁴ a number of issues make quantitative predictions and their comparison with experimental data rather complicated. For example, large uncertainties exist in the physical and chemical properties of the pyrolyzing char and in the kinetic models and rates used in mathematical simulations. Additionally, properties can greatly differ between biomass species and heavily impact product evolution during pyrolysis. For example, the biomass solid density, specific heat, thermal conductivity, porosity, permeability, inorganic matter composition or ratios of cellulose, hemicellulose, and lignin all have an influence on the pyrolytic process and in the resultant product distribution.

Table 3.1 presented a number of kinetic schemes from the literature, some of which accounted solely for primary reactions whereas others also considered secondary interactions. In this section, a two models have been developed in MATLAB to simulate CVC of biomass in the WHTB. Since experimental evidence suggest that secondary reactions are important during CVC, the models evaluate the kinetic schemes that include them and simultaneously solve kinetic expressions together with the conservation equations for mass and energy to finally display product yields. To our knowledge, this is the first time CVC is being simulated. All simulations found in literature pertain to “open” reactor systems. Therefore, this first attempts in CVC modelling have been kept relatively simple and make use of literature kinetic data derived from “open” pyrolysis processes. One needs to remember, nonetheless, that kinetic rates and

pyrolysis properties are likely to considerably change between “open” and sealed (CVC) vessels. Finally, the model is evaluated against experimental CVC data.

The first model presented here (CVC model 1) applies the reaction scheme of Shafizadeh and Chin with secondary reactions¹⁶³ and the second model (CVC model 2) applies the scheme of Koufopoulos et al. with secondary reactions²¹² (see Table 3.1). A third scheme with secondary reactions elaborated by Grønli and Melaaen¹⁸⁸ is also displayed in Table 3.1. This scheme just accounts for secondary gas formation from primary tar but excludes secondary char-forming reactions. Therefore, it is not relevant to CVC and has been discarded.

7.1. CVC model 1 (employing kinetic scheme of Shafizadeh and Chin with secondary reactions)

The chemical process of biomass pyrolysis proposed by Shafizadeh and Chin¹⁶³ is described through a primary and a secondary stage as given in Figure 7.1. The kinetic scheme involves three parallel competitive reactions that consider primary production of gas, tar, and char, and a consecutive reaction that accounts for the secondary cracking of tar into gas and char.

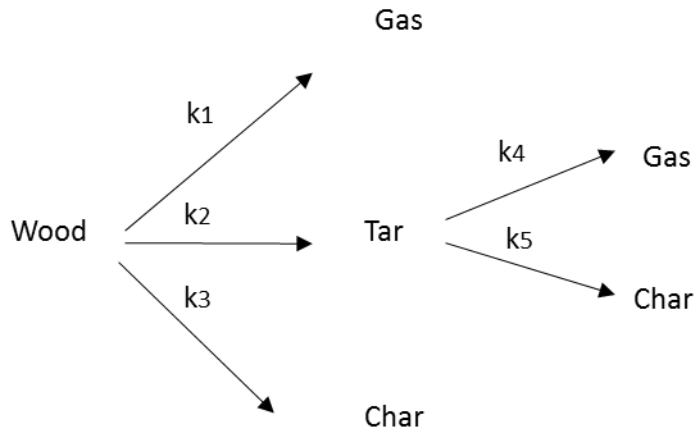


Figure 7.1. Kinetic scheme of Shafizadeh and Chin¹⁶³ with secondary reactions

Mathematical models developed by Di Blasi¹⁷⁹, Hagge and Bryden¹⁸⁰ and Lu et al.¹⁸¹ utilize this reaction scheme coupled with heat and mass transfer phenomena. The models simulate biomass pyrolysis of a single particle as a function of time in an “open” reactor where the volatile products are swept out by an inert gas. The following assumptions are shared by the three models:

- Biomass particles are modeled as one-dimensional.
- Heat transfer is transported by conduction, convection, and radiation.
- Mass transfer is driven by pressure and concentration gradients.
- A constant atmospheric pressure is maintained at the particle surface.
- Gases behave as ideal gases.
- Conservation of momentum by Darcy’s law is included to calculate pressure and gas velocity profiles along the solid particle.
- Kinetic expressions are assumed to follow an Arrhenius type expression of the form

$$k_i = A_i \exp(-E_i/R_o T) \quad (7.1)$$

- Primary reactions are represented as endothermic processes and secondary reactions as exothermic processes.

Very few attempts have been made in the literature to estimate activation energies E_i and preexponential factors A_i of the kinetic data (k_1 - k_5), and heats of reactions (Δh_1 - Δh_5). Table 7.1 displays the references employed in each mathematical model for such data.

In the models, the kinetic constants k_1 - k_5 and heat of reactions Δh_1 - Δh_5 should correspond to the same biomass sample. Nonetheless, given the limited amount of literature available concerning kinetic data, the three models mentioned here needed to make use of kinetic constants and heats of reactions derived from diverse types of woods samples. Flaws may be consequently introduced in their estimations. Di Blasi¹⁸⁴ discusses the effect of secondary reactions through the introduction of variations on the kinetic parameters of both primary and secondary reactions.

Table 7.1. References used in the literature models for kinetic and enthalpy data for kinetic scheme of Shafizadeh and Chin.¹⁶³

Model	k_1, k_2, k_3	k_4	k_5	$\Delta h_1, \Delta h_2, \Delta h_3$	$\Delta h_4, \Delta h_5$
Di Blasi ^{179, a}	Thurner and Mann ²¹³ Chan et al. ¹⁸² Font et al. ²¹⁴	Liden et al. ²¹⁵	Di Blasi ^{216, b}	Chan et al. ^{182, c}	Koufopoulos et al. ^{178, d}
Hagge and Bryden ¹⁸⁰	Thurner and Mann ²¹³	Liden et al. ²¹⁵	Di Blasi ^{216, b}	Di Blasi ^{216, c, e}	Liden et al. ^{215, d}
Lu et al. ¹⁸¹	Font et al. ^{214, f} Wagenaar et al. ²¹⁷	Liden et al. ²¹⁵	Di Blasi ^{216, b}	Chan et al. ^{182, c}	Koufopoulos et al. ^{178, d}

a. Di Blasi performs three simulations. Each one with a different k_1 - k_3 data set taken from ^{182,213,214}. Di Blasi transforms the units of the preexponential factors A_1 - A_3 given by Thurner and Mann ²¹³ from min^{-1} to s^{-1} . The conversion factor introduced in the calculations is erroneous. Di Blasi multiplies by 60 (or 6 in the case of A_1) instead of dividing. The preexponential factor A_4 of Di Blasi reportedly taken from Liden et al.²¹⁵ does not agree with the values displayed by Liden et al.²¹⁵

b. Di Blasi²¹⁶ estimated k_5 using an erroneous k_1 value due to the erroneous conversion factor explained in the previous footnote.

c. The models employ reverse signs for the heat of reactions, endothermic processes were given a negative enthalpy and exothermic processes were given a positive enthalpy.

d. All models display the same heat of reactions values for reactions 4 and 5, (Δh_4 and Δh_5) even though supposedly, the values are specified to be taken from different references: Di Blasi¹⁷⁹ and Lu et al.¹⁸¹ from Koufopoulos et al.^{178, b}, and Hagge and Bryden from Liden et al.²¹⁵ Nonetheless, even though the original articles^{178,181} were requested, I was unable to find the specified values in them.

e. Hagge and Bryden specifies Di Blasi²¹⁶ as the reference for Δh_1 - Δh_3 values but the original article used by Di Blasi²¹⁶ is Chan et al.¹⁸². Chan et al.¹⁸² just give a single value for the overall endothermic heat of reaction and this value is shared for the enthalpies of the three primary reactions in all models. The value is derived from a different kinetic scheme than the one in Figure 7.1 which is employed by all models and may introduce inconsistencies in the models.

f. Lu et al.¹⁸¹ used Font et al.²¹⁴ dataset when modeling the pyrolysis of hardwood particles. The dataset was found to be comparable to that of Nunn et al.²¹⁸, who reported kinetic data for hardwood in the high-temperature range (300–1100°C).

Di Blasi¹⁷⁹ calculated space and history profiles of the main variables and predicted final product yields from the pyrolysis of a large ($\tau = 0.025$ m) anisotropic wooden grain exposed to a specific

external radiative heat flux. She studied the effects of (1) shrinkage level, (2) intensity of the external radiation and (3) orientation of the wood particle with respect to the one-dimensional heat flux. Considerable quantitative discrepancies between predicted and experimental data were found. Nonetheless both sets of data showed good qualitative agreement.

The model from Hagge and Bryden¹⁸⁰ analyzed the effect of shrinkage on the pyrolysis process and described the conditions of pyrolysis or combustion under which shrinkage must be contemplated. The conclusions of this study showed a negligible shrinkage influence on the processing times and final product yields when considering a thermally thin ($Bi < 0.2$) and thermally thick ($0.2 \leq Bi \leq 10$) regimes. Whereas in the thermal wave regime $Bi > 10$, char shrinkage effect increases with both temperature and particle size. Bi refers to the Biot number defined as $Bi = h_{rad}L_c/k$ where h_{rad} is the heat transfer coefficient, L_c is the characteristic length and k is the thermal conductivity.

Finally, the model by Lu et al.¹⁸¹ simulated the rapid pyrolysis of wooden particles of various shapes and sizes without considering shrinkage and compared the predictions with experimental data.

The mathematical models provided by the authors mentioned above served as the basis for the development of CVC model 1, which solves the kinetic expressions derived from Shafizadeh and Chin with secondary reactions simultaneously to heat and mass conservation equations. The model represents the one-dimensional, time-dependent pyrolysis of biomass in a reactor that retains tar and gas products in the pyrolyzing zone. Due to the differences encountered between

CVC and “open” pyrolysis processes, mass and energy balances and boundary conditions were rewritten for the CVC as follows:

- **Mass balance for wood (w), char (c), tar (T) and non-condensable gas (G)**

$$\begin{aligned}
 & \text{Rate of accumulation of mass component in system} \\
 & = \text{Rate of production of mass component} \\
 & + \text{Rate of mass component entering system by inflow} \\
 & - \text{Rate of mass component leaving by outflow}
 \end{aligned} \tag{7.2}$$

In a sealed reactor, input and output terms are null and the rate of accumulation of a mass component corresponds to the rate of production by the chemical reactions as represented by the following equations:

$$\frac{\partial(\rho_w V)}{\partial t} = -(k_1 + k_2 + k_3)\rho_w V \tag{7.3}$$

$$\frac{\partial(\rho_c V)}{\partial t} = k_3\rho_w V + k_5\rho_T V \tag{7.4}$$

$$\frac{\partial(\rho_T V)}{\partial t} = k_2\rho_w V - (k_4 + k_5)\rho_T V \tag{7.5}$$

$$\frac{\partial(\rho_G V)}{\partial t} = k_1\rho_w V + k_4\rho_T V \tag{7.6}$$

Where $\rho_w = \frac{M_w}{V}$, $\rho_c = \frac{M_c}{V}$, $\rho_T = \frac{M_T}{V}$, $\rho_G = \frac{M_G}{V}$ are the wood, charcoal, tar and gas apparent densities. t is time. M_w, M_c, M_T, M_G are the masses of wood, charcoal, tar and gas

k_1, k_2, k_3, k_4, k_5 are the kinetic constants for reactions 1-5. V is the reactor volume.

Mass balances are simplified to:

$$\frac{\partial M_w}{\partial t} = -(k_1 + k_2 + k_3)M_w \quad (7.7)$$

$$\frac{\partial M_c}{\partial t} = k_3M_w + k_5M_T \quad (7.8)$$

$$\frac{\partial M_T}{\partial t} = k_2M_w - (k_4 + k_5)M_T \quad (7.9)$$

$$\frac{\partial M_G}{\partial t} = k_1M_w + k_4M_T \quad (7.10)$$

Note that the models of Di Blasi,¹⁷⁹ Hagge and Bryden,¹⁸⁰ and Lu et al.¹⁸¹ and in consequence the new CVC models developed, use units of mass and not moles as typically employed in kinetic rates.

A close look at the kinetic scheme in Figure 7.1 and at the mass balance Equations 7.7-7.10 revealed that at steady state, the final product is estimated to be composed of just char and gas with no tar or biomass left behind. The kinetic scheme simulates biomass decomposition into primary gas, tar and char. The primary tar becomes a reactant that decomposes into secondary char and gas. Since there are no reverse reactions and tar and biomass are not end products, eventually both biomass and tar are supposed to disappear. A quick numerical calculation using mass balance Equations 7.7-7.10 above shows that at steady state—when mass derivatives of the components are null as in, $\frac{\partial(M_w)}{\partial t} = \frac{\partial(M_c)}{\partial t} = \frac{\partial(M_T)}{\partial t} = \frac{\partial(M_G)}{\partial t} = 0$ —both M_w and M_T become zero.

Model predictions regarding tar formation reflects the negligible free tar recovered in CVC processes. In “open” reactors nonetheless, experiments of slow pyrolysis with ample time to reach equilibrium result in the production of some tar whose yield heavily depends on the experimental conditions such as temperature and pressure. For example, at 300°C and atmospheric pressure, some of the tar compounds have been found to be in volatile and remain as liquid/tar.^{84,90} It is well known that it is not possible to completely volatilize tar after it has been condensed (i.e. it has to be heated to temperatures that crack the molecules by breaking bonds to fully volatilize condensed oils/tars).

- **Energy balance**

$$\begin{aligned}
 & \text{Rate of energy accumulation in system} \\
 & = \text{Rate of heat added to system} \\
 & - \text{Rate of work done on system} \\
 & + \text{Rate of energy entering system by inflow} \\
 & - \text{Rate of energy leaving system by outflow}
 \end{aligned} \tag{7.11}$$

Or in terms of defined variables

$$\frac{dE}{dt} = \dot{Q} - \dot{W}_s + \dot{E}_{mass,in} - \dot{E}_{mass,out} \tag{7.12}$$

In a sealed reactor, the flow streams are null and Equation 7.12 reduces to

$$\frac{dE}{dt} = \dot{Q} - \dot{W} \tag{7.13}$$

The total energy may be considered as the result of the summation of many contributions.

Common energy components include the internal, kinetic and potential energies. In sealed

reactors, the kinetic and potential energy terms are typically neglected and the internal energy U represents the dominant energy contribution. Equation 7.13 can be expressed as

$$\frac{dU}{dt} = \dot{Q} - \dot{W} \quad (7.14)$$

Appealing to the extensive property of internal energy and using enthalpy H terms, the internal energy can therefore be expressed as

$$U = \sum_i M_i u_i = \sum_i M_i (h_i - P v_i) \quad (7.15)$$

Where P is the system pressure, u_i the specific internal energy of component i , h_i its specific enthalpy, v_i its specific volume and M_i its mass.

Equation 7.15 can be developed into

$$U = \sum_i M_i u_i = \sum_i M_i (h_i - P v_i) = \sum_i M_i h_i - P \sum_i M_i v_i = \sum_i M_i h_i - PV \quad (7.16)$$

Introducing Equation 7.16 into 7.14 results in:

$$\frac{\partial(\sum_i M_i h_i - PV)}{\partial t} = \dot{Q} - \dot{W} \quad (7.17)$$

The left side of the equation can be extended to

$$\begin{aligned} \frac{\partial(\sum_i M_i h_i - PV)}{\partial t} &= \frac{\partial(\sum_i M_i h_i)}{\partial t} - \frac{\partial(PV)}{\partial t} \\ &= \sum_i M_i \frac{\partial h_i}{\partial t} + \sum_i h_i \frac{\partial M_i}{\partial t} - P \frac{\partial V}{\partial t} - V \frac{\partial P}{\partial t} \end{aligned} \quad (7.18)$$

Where

$$\sum_i M_i \frac{\partial h_i}{\partial t} = \sum_i M_i c_{p,i} \frac{\partial T}{\partial t} \quad (7.19)$$

And

$$\sum_i h_i \frac{\partial M_i}{\partial t} = V \sum_k \Delta h_k r_k \quad (7.20)$$

See reference ²¹⁹ for derivation of Equation 7.20.

And in a constant-volume reactor as the WHTB

$$P \frac{\partial V}{\partial t} = 0 \quad (7.21)$$

Incorporating Equations 7.19-7.21 in 7.18, the equation becomes

$$\sum_i M_i c_{p,i} \frac{\partial T}{\partial t} + V \sum_k \Delta h_k r_k - V \frac{\partial P}{\partial t} = \dot{Q} - \dot{W} \quad (7.22)$$

Where $c_{p,i}$ is the specific heat capacity of component i , Δh_k the heat of reaction k and r_k the rate of reaction k calculated as

$$r_1 = k_1 \frac{M_w}{V} \quad (7.23)$$

$$r_2 = k_2 \frac{M_w}{V} \quad (7.24)$$

$$r_3 = k_3 \frac{M_w}{V} \quad (7.25)$$

$$r_4 = k_4 \frac{M_T}{V} \quad (7.26)$$

$$r_5 = k_5 \frac{M_T}{V} \quad (7.27)$$

In previous models in “open” reactors, the heat \dot{Q} term accounted for conduction, radiation and convection. In CVC models 1 and 2, \dot{Q} is assumed to be governed by just conduction through the stainless steel wall of the reactor as in Equation 7.28. The convective heat term was neglected since pyrolysis products are not being flushed during CVC.

$$\dot{Q} = \frac{k}{t_w} A(T_s - T) \quad (7.28)$$

k is the thermal conductivity and t_w is the thickness of the stainless steel wall. T_s is the temperature of the outer wall whose value is assumed constant and equal to the sand bath temperature during the whole pyrolysis process. T is the temperature inside the reactor which is assumed to be uniform in all the reaction zones. This assumption does not reflect the experimental temperature profile. In the actual experiment, the inner temperature of the biomass heats up more slowly. The development of a detailed model that includes spatial temperature profile would require the use of finite elements and the estimation of data—such as the biomass void volume and volatile or char thermal conductivities and their evolution with time and space—that are currently largely uncertain. The model was therefore elaborated on the basis of a uniform temperature.

The work \dot{W} term on the right side of Equation 7.22 can be divided into three components: The work performed by the flowing streams; the shaft work performed by stirrers, compressors, etc.

and the work performed by moving system boundaries. All these contributions are null in the WHTB since this system is characterized by being hermetically sealed (i.e., with no flow streams), by being equipped with no stirrers or any other movable equipment and by having a constant-volume with fixed system boundaries. Thus, $\dot{W} = 0$

If the heat term is introduced in Equation 7.22, the energy balance equation becomes

$$\sum_i M_i c_{p,i} \frac{\partial T}{\partial t} + V \sum_k \Delta h_k r_k - V \frac{\partial P}{\partial t} = \frac{k}{t_w} A(T_s - T) \quad (7.29)$$

And reorganizing

$$\sum_i M_i c_{p,i} \frac{\partial T}{\partial t} - V \frac{\partial P}{\partial t} = \frac{k}{t_w} A(T_s - T) + V \sum_k (-\Delta h_k) r_k \quad (7.30)$$

The pressure is assumed to follow the ideal gas law

$$P = \frac{n_g R_o T}{V_g} \quad (7.31)$$

In Di Blasi¹⁷⁹, the moles of total volatiles n_g are calculated as

$$n_g = \frac{M_g}{W_g} \quad (7.32)$$

Where M_g and W_g refers to the mass and molecular weights of the total volatiles. And the mass of total volatiles is given by the summation of the masses of tar M_T and non-condensable gases M_G .

$$M_g = M_G + M_T \quad (7.33)$$

The total moles of volatiles in the model is then calculated as

$$n_g = \frac{M_G + M_T}{W_g} \quad (7.34)$$

In the Di Blasi¹⁷⁹ model, M_G and M_T are assumed to vary with time and the molecular weight of total volatiles W_g is assumed constant during the process. The W_g value is not published in Di Blasi¹⁷⁹ article.

In CVC models 1 and 2, the total moles of species in the gas phase, n_g , is calculated as the sum of moles of tar, n_T , and non-condensable gases, n_G , and both vary with time. The nomenclature g , G and T refer to total volatiles, non-condensable gases and tar, respectively, was taken from Di Blasi¹⁷⁹.

$$n_g = n_G + n_T \quad (7.35)$$

Rewriting in terms of masses, M_i , and molecular weights, W_i , of the components yields

$$n_g = \frac{M_G}{W_G} + \frac{M_T}{W_T} \quad (7.36)$$

Instead of using a constant molecular weight for total volatiles, the CVC model 1 uses a mean molecular weight for non-condensable gas W_G and another for tar W_T .

The reactor volume V is the sum of the volume occupied by volatiles, V_g , (tar plus non-condensable gases) and the solid V_s .

$$V = V_g + V_s \quad (7.37)$$

The solid volume V_s is assumed—as in the model developed by Di Blasi¹⁷⁹—to decrease with time in a way that corresponds to the loss of solid mass as in:

$$\frac{V_s}{V_{s0}} \cong \frac{M_s}{M_{s0}} = \frac{(M_w + M_c)}{M_{w0}} \quad (7.38)$$

Where V_{s0} and M_{s0} are the initial solid volume and mass, respectively. V_s and M_s are the solid volume and mass which depends on time. And $M_s = M_w + M_c$ with M_w and M_c being the wood and char masses, respectively. Initially, the reactor only contains wood, so the solid mass at $t=0$ will be $M_{s0} = M_{w0}$. Note that Equation 7.38 implicitly holds the assumption that the biomass and char densities are similar.

The volume occupied by gas is then

$$V_g = V - V_s = V - V_{s0} \frac{(M_w + M_c)}{M_{w0}} \quad (7.39)$$

Then, introducing the expressions for the gas moles n_g and gas volume V_g from Equations 7.38 and 7.39 in the Ideal Gas Law of Equation 7.31, the pressure of the reactor is calculated as

$$P = \frac{n_g R_o T}{V - V_{wo} \frac{(M_w + M_c)}{M_{wo}}} = \frac{\left(\frac{M_G}{W_G} + \frac{M_T}{W_T}\right) R_o T}{V - V_{wo} \frac{(M_w + M_c)}{M_{wo}}} \quad (7.40)$$

And the pressure derivative with time as

$$\frac{\partial P}{\partial t} = \frac{\partial}{\partial t} \left(\frac{\left(\frac{M_G}{W_G} + \frac{M_T}{W_T}\right) R_o T}{V - V_{wo} \frac{(M_w + M_c)}{M_{wo}}} \right) \quad (7.41)$$

$$\frac{\partial P}{\partial t} = \frac{\frac{\partial \left(\left(\frac{M_G}{W_G} + \frac{M_T}{W_T}\right) R_o T \right)}{\partial t} \left(V - V_{wo} \frac{(M_w + M_c)}{M_{wo}} \right) - \left(\frac{M_G}{W_G} + \frac{M_T}{W_T} \right) R_o T \frac{\partial \left(V - V_{wo} \frac{(M_w + M_c)}{M_{wo}} \right)}{\partial t}}{\left(V - V_{wo} \frac{(M_w + M_c)}{M_{wo}} \right)^2} \quad (7.42)$$

$$\begin{aligned} & \frac{\partial P}{\partial t} \\ &= \frac{R_o T \left(\frac{1}{W_G} \frac{\partial M_G}{\partial t} + \frac{1}{W_T} \frac{\partial M_T}{\partial t} \right) \left(V - V_{wo} \frac{(M_w + M_c)}{M_{wo}} \right) + \left(\frac{M_G}{W_G} + \frac{M_T}{W_T} \right) R_o \frac{\partial T}{\partial t} \left(V - V_{wo} \frac{(M_w + M_c)}{M_{wo}} \right) + \left(\frac{M_G}{W_G} + \frac{M_T}{W_T} \right) R_o T \frac{V_{wo}}{M_{wo}} \left(\frac{\partial M_w}{\partial t} + \frac{\partial M_c}{\partial t} \right)}{\left(V - V_{wo} \frac{(M_w + M_c)}{M_{wo}} \right)^2} \quad (7.43) \end{aligned}$$

$$\begin{aligned} \frac{\partial P}{\partial t} &= \frac{R_o T \left(\frac{1}{W_G} \frac{\partial M_G}{\partial t} + \frac{1}{W_T} \frac{\partial M_T}{\partial t} \right) + \left(\frac{M_G}{W_G} + \frac{M_T}{W_T} \right) R_o \frac{\partial T}{\partial t}}{\left(V - V_{wo} \frac{(M_w + M_c)}{M_{wo}} \right)} \\ &+ \frac{\left(\frac{M_G}{W_G} + \frac{M_T}{W_T} \right) R_o T \frac{V_{wo}}{M_{wo}} \left(\frac{\partial M_w}{\partial t} + \frac{\partial M_c}{\partial t} \right)}{\left(V - V_{wo} \frac{(M_w + M_c)}{M_{wo}} \right)^2} \quad (7.44) \end{aligned}$$

In the CVC model, the pressure is continuously increasing. This behavior contrasts with the pressure profile observed in “open” reactors. “Open” reactors models depict the continuous

purge of volatiles under the assumption of a constant atmospheric pressure at the particle surface.

In a sealed reactor, pressure and its derivative needs to be calculated.

Including the $\frac{\partial P}{\partial t}$ expression in Equation 7.44 in the energy balance of Equation 7.30

$$\begin{aligned}
 \sum_i M_i c_{p,i} \frac{\partial T}{\partial t} - V \left(\frac{R_o T \left(\frac{1}{W_G} \frac{\partial M_G}{\partial t} + \frac{1}{W_T} \frac{\partial M_T}{\partial t} \right) + \left(\frac{M_G}{W_G} + \frac{M_T}{W_T} \right) R_o \frac{\partial T}{\partial t}}{\left(V - V_{wo} \frac{(M_w + M_c)}{M_{wo}} \right)} \right. \\
 \left. + \frac{\left(\frac{M_G}{W_G} + \frac{M_T}{W_T} \right) R_o T \frac{V_{wo}}{M_{wo}} \left(\frac{\partial M_w}{\partial t} + \frac{\partial M_c}{\partial t} \right)}{\left(V - V_{wo} \frac{(M_w + M_c)}{M_{wo}} \right)^2} \right) \\
 = \frac{k}{t_w} A (T_s - T) + V \sum_k (-\Delta h_k) r_k
 \end{aligned} \tag{7.45}$$

Reorganizing

$$\begin{aligned}
 \frac{\partial T}{\partial t} \left(\sum_i M_i c_{p,i} - \frac{\left(\frac{M_G}{W_G} + \frac{M_T}{W_T} \right) R_o V}{\left(V - V_{wo} \frac{(M_w + M_c)}{M_{wo}} \right)} \right) \\
 = \frac{k}{t_w} A (T_s - T) + V \sum_k (-\Delta h_k) r_k \\
 + V R_o T \left[\frac{\left(\frac{1}{W_G} \frac{\partial M_G}{\partial t} + \frac{1}{W_T} \frac{\partial M_T}{\partial t} \right)}{\left(V - V_{wo} \frac{(M_w + M_c)}{M_{wo}} \right)} + \frac{\left(\frac{M_G}{W_G} + \frac{M_T}{W_T} \right) \frac{V_{wo}}{M_{wo}} \left(\frac{\partial M_w}{\partial t} + \frac{\partial M_c}{\partial t} \right)}{\left(V - V_{wo} \frac{(M_w + M_c)}{M_{wo}} \right)^2} \right]
 \end{aligned} \tag{7.46}$$

The final expression for the temperature derivative with time is then

$$\frac{\partial T}{\partial t} = \frac{\frac{k}{t_w} A(T_s - T) + V \sum_k (-\Delta h_k) r_k + V R_o T \left[\frac{\left(\frac{1}{W_G} \frac{\partial M_G}{\partial t} + \frac{1}{W_T} \frac{\partial M_T}{\partial t} \right)}{\left(V - V_{wo} \frac{(M_w + M_c)}{M_{wo}} \right)} + \frac{\left(\frac{M_G}{W_G} + \frac{M_T}{W_T} \right) \frac{V_{wo}}{M_{wo}} \left(\frac{\partial M_w}{\partial t} + \frac{\partial M_c}{\partial t} \right)}{\left(V - V_{wo} \frac{(M_w + M_c)}{M_{wo}} \right)^2} \right]}{\left(\sum_i M_i C_{p,i} - \frac{\left(\frac{M_G}{W_G} + \frac{M_T}{W_T} \right) R_o V}{\left(V - V_{wo} \frac{(M_w + M_c)}{M_{wo}} \right)} \right)} \quad (7.47)$$

CVC model 1 is represented by the system of differential equations composed by the mass and energy balance (Equations 7.7-7.10 and 7.47). The MATLAB code in Appendix O uses the ode45 function, also known as Runge-Kutta method, to solve this set of equations. The code assumes an initial quiescent environment at ambient conditions and uses the kinetic data and property values given in Table 7.2. As in previous models that illustrate “open” reactor performance, a variety of references that use different biomass types needed to be employed with the implication of the introduction of uncertainties.

Table 7.2. Kinetic data and property values applied to constant-volume carbonization (CVC) model 1. Superscripts meanings shown in footnotes at the bottom of the table.

Kinetic data k_1, k_2, k_3 Thurner and Mann ²¹³			
$k_i = A_i \exp(-E_i/R_o T)$			
A_1	1.43×10^4	s^{-1}	
A_2	4.13×10^6	s^{-1}	
A_3	7.38×10^5	s^{-1}	
E_1	88.6	kJ/mol	
E_2	112.7	kJ/mol	
E_3	106.5	kJ/mol	
Kinetic data k_4 Liden et al. ²¹⁵			
A_4	4.28×10^6	s^{-1}	
E_4	107.5	kJ/mol	
Kinetic data k_5 Di Blasi ²¹⁶			
A_5	1×10^5	s^{-1}	
E_5	107.5	kJ/mol	
Heats of reaction data $\Delta h_1, \Delta h_2, \Delta h_3$ Chan et al. ¹⁸²			
$\Delta h_1, \Delta h_2, \Delta h_3$	0.418	kJ/g	
Heats of reaction data $\Delta h_4, \Delta h_5$ Di Blasi ¹⁷⁹			
$\Delta h_4, \Delta h_5$	-0.042	kJ/g	
Property values			
R_o	8.314×10^{-3}	kJ/mol K	Ideal gas constant
W_G^a	44	g/mol	Molecular weight non-condensable gas
W_T^b	200	g/mol	Molecular weight tar
k_{SS}	0.019	kW/m K	Thermal conductivity of stainless steel at 225°C ²²⁰

Table 7.2. Kinetic data and property values applied to constant-volume carbonization (CVC) model 1 (Continued).

t_w	0.0021	m	Wall thickness reactor
Rad	0.0127	m	Outer radius of reactor (1 inch diameter)
L	0.1524	m	Reactor length (6 inch)
$c_{p,w}$	1.5×10^{-3}	kJ/g K	Specific heat capacity of wood taken from ²²¹
$c_{p,c}$	1.5×10^{-3}	kJ/g K	Specific heat capacity of char taken from ²²¹
$c_{p,T}$	1.1×10^{-3}	kJ/g K	Specific heat capacity of tar taken from ^{179.c}
$c_{p,G}$	1.1×10^{-3}	kJ/g K	Specific heat capacity of non-condensable gases taken from ^{179.c}
V	7.72×10^{-5}	m ³	Reactor volume (calculated as $\pi \cdot Rad^2 \cdot L$). ^d
$V_{wo}^{e,f}$	0.2V	m ³	Initial volume occupied by the solid
T_s	573	K	Sand bath temperature
T_o	298	K	Initial reactor temperature
P_o	100	kPa	Initial reactor pressure
M_{wo}	10	g	Initial biomass mass. ^e
<p>a. The molecular weight of the non-condensable gas is estimated to be that of CO₂ since experimental analysis proved that CO₂ is the chief gas component.</p> <p>b. Additional CVC model 1 simulations that tested the effect of the tar molecular weight in a 40-400g/mol range were performed. Results are presented below.</p> <p>c. Di Blasi¹⁷⁹ employed an average cp value (taken from Kansas) for total volatiles (tar plus non-condensable gases). This value was used in the WHTB model as the heat capacity value for both tar and non-condensable gases.</p> <p>d. Additional CVC model 1 simulations that tested the effect of the reactor volume from $V = \pi \cdot Rad^2 \cdot L$ to $V = 2\pi \cdot Rad^2 \cdot L$ and the effect of the initial volume occupied by the solid (V_{wo}) from 0.2V to 0.4V were performed. Results are presented below.</p> <p>e. V_{wo} equal 0.2 V is based in WHTB experiments.</p> <p>f. Additional CVC model 1 simulations that tested the effect of the reactor volume from $V = \pi \cdot Rad^2 \cdot L$ to $V = 2\pi \cdot Rad^2 \cdot L$ and the effect of the initial volume occupied by the solid (V_{wo}) from 0.2V to 0.4V were performed. Results are presented below.</p> <p>g. Additional CVC model 1 simulations that tested the effect of the biomass initial mass in a 10-100g range were performed. Results are presented below.</p>			

Figures 7.2 and 7.3 illustrate product yields, temperature and pressure history profiles predicted by the CVC model 1. Temperature increases almost instantaneously to reach the sand bath temperature, the yield of virgin wood reduces asymptotically with time until it gets consumed whereas the concentrations of char and non-condensable gases, and the system pressure, increase to reach asymptotic steady state values. The tar yield peaks at a maximum value and subsequently recedes to its final depleted value.

The predictions from CVC model 1 contrast with experimental values. WHTB experiments of spruce or birch under a mass loading of 129 g of biomass per liter of reactor, a 300°C HTT and at atmospheric initial pressure resulted in final experimental pressures of around 5 MPa (measured before the WHTB cool down), a temperature history profile similar to the one shown in Figure 5.1, char yields of 50-60%, non-condensable gas yields of 15-20% and liquid yield as the balance (see Table 5.1). In comparison, CVC model 1 predictions regarding the pyrolysis of biomass at similar initial conditions and HTT shows that near-equilibrium conditions are quickly reached. The results show a pressure of 10 MPa approximately (see Figure 7.3), char and gas yields of ~31% and ~69% respectively, no water and negligible tar (see Figure 7.2). As previously explained, tar is not an end product in the kinetic schemes of the WHTB model and therefore is predicted to disappear when steady state is achieved. Water is not present in these kinetic schemes and therefore is not accounted for in the MATLAB model.

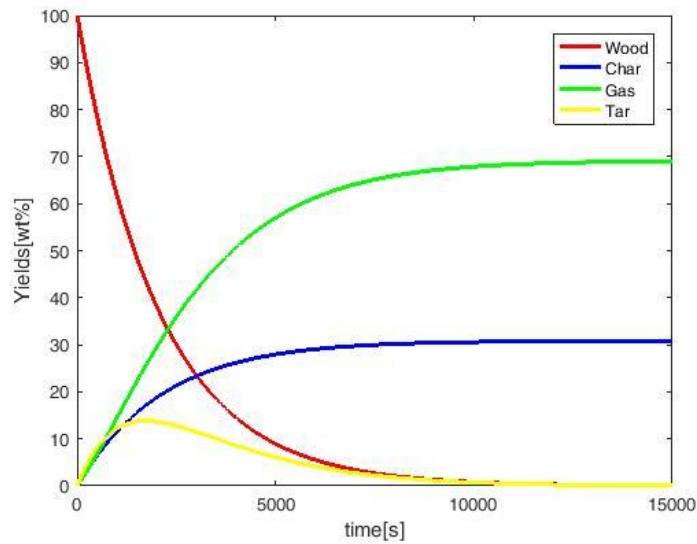


Figure 7.2. History profile of wood, char and volatile yields predicted by CVC model 1 assuming constant-volume carbonization of biomass at a heat treatment temperature of 300°C and an initial pretest pressure of 0.1 MPa.

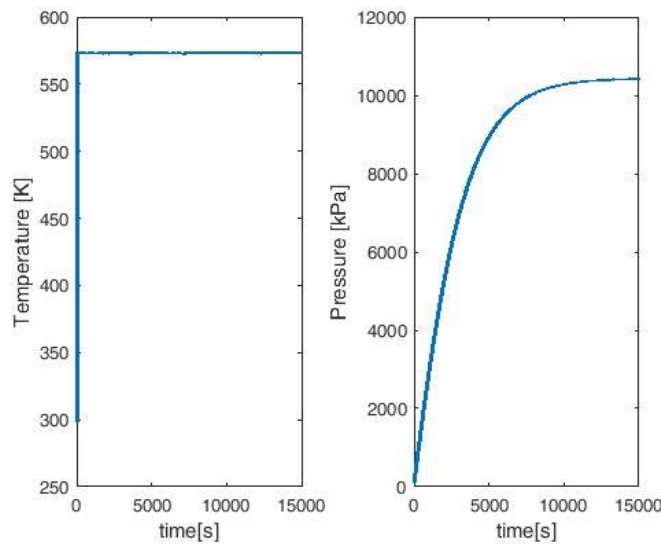


Figure 7.3. History profile of temperature and pressure predicted by CVC model 1 assuming a constant-volume carbonization of biomass at a heat treatment temperature of 300°C and an initial pretest pressure of 0.1 MPa

The large differences between the model predictions and the experimental values can be explained by several factors. For instance, current models do not take into account the biomass composition such as the elemental analysis or cellulose, hemicellulose and lignin ratios, which have been proved to affect pyrolysis processes. These values could have been integrated in the

kinetic data and property values but one needs to remember that the MATLAB model was developed in the basis of data derived from “open” reactor systems that evacuate volatiles from the reaction zone which may considerably differ from CVC data. Also, given the limited published data, the use of values from several authors that employed different biomass sources and pyrolysis processes would be expected to contribute to differences between model and experimental results.

The predicted temperature profile reflects the simplifications inherent in the model. CVC model assumptions include a uniform temperature inside the reactor and consider heat transfer to be governed by conduction through the reactor stainless steel wall, with convection and radiation terms neglected. In the actual WHTB experiments, the internal reactor temperature is not uniform and large spatial heating gradients exist within the bed of solid particles. Temperature spatial profiles have not been considered in the model. Given the number of unknown model parameters, extending the model complexity to gain additional insights was not expected to be productive. For example, little is known regarding thermal conductivities of the reacting medium, or of the pyrolysis gas, or regarding properties of the internal gas convection currents within the WHTB.

In the CVC model 1, the heat transfer (Equation 7.28) is assumed to have an unrealistically high heat coefficient equal to $\frac{k}{t_w} A = 0.11 \text{ kW/K}$ which results in a near step function of temperature with time. To test the effect of slowing down the heat transfer, this coefficient was replaced with a parameterized coefficient. When its value was reduced from 0.11 to 10^{-3} kW/K , initial effects on the profiles of temperature, pressure and product yields were observed. Profiles that assumed

parameterized coefficients of 10^{-3} , 10^{-4} and 10^{-5} kW/ are reported in Appendix P. As the heat transfer slows down, the CVC model 1 predicts the achievement of steady state after longer carbonization times but predicts comparable final pressures, temperatures and product yields.

Regarding pressure calculations, differences are also expected with experimental values. In the MATLAB model, the whole reactor is assumed to be at a uniform temperature of 300°C while experimentally, a large reaction region (the dead volume) is close to room temperature which reduces the overall system pressure during an experiment. During the WHTB experiments, the non-condensable gas (whose pressure and composition are measured at the end of each experiment), tar (which has been found by SEM condensed on the char surface plus a negligible fraction in WHTB walls and tubing) and water (which seems to be a main pyrolytic liquid product found at the end of the experiments mainly as char moisture content) contribute to the total pressure in the system.

In the MATLAB code, the system pressure is calculated as the sum of non-condensable gas and tar partial pressures. Water, even though it is a major experimental pyrolytic product, is not included in the literature kinetic scheme of Figure 7.1 and its vapor pressure is not taken into consideration in pressure calculations. Consequently, at near-equilibrium conditions, the non-condensable gas pressure becomes basically the sole contribution to the total pressure predicted by MATLAB and the calculated pressure becomes basically proportional to the initial amount of biomass.

- **Effect of Temperature**

Figure 7.4 displays theoretical char and gas yield values calculated with CVC model 1 in a 300-500°C temperature range. Even though the predicted char yield value of around 31% is not close to the actual experimental char yields of around 55%, 43% and 40% at 300, 400 and 500°C respectively, the 31% char yield value and the plateau profile surprisingly agrees with experimental fixed-carbon yields.

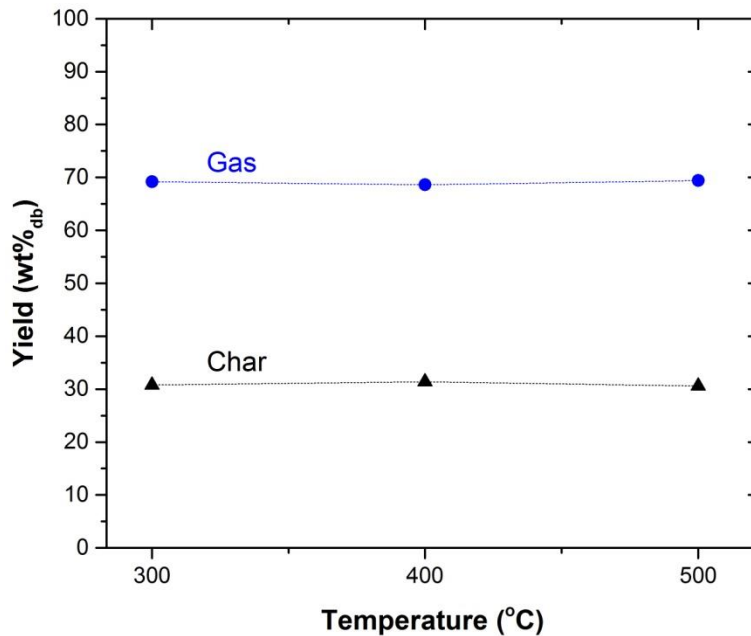


Figure 7.4. Effect of heat treatment temperature on the yields of char and gas predicted by CVC model 1.

- **Effect of biomass loading, biomass volume and reactor volume**

The effects of mass loading on product yields and on pressure and temperature profiles were simulated by modifying the biomass initial mass in a 10-100 g range while keeping the rest of parameter values as the ones in Table 7.2. The effect of biomass volume was tested by changing

the initial solid volume from 0.2V to 0.4V (with V being the reactor volume of 0.0772 L) while keeping the rest of the parameters constant. Finally, the effect of reactor volume was studied with values ranging from 0.0772 to 0.1544 L. A negligible effect on product yields (in wt. percentage) was observed in all cases. As expected, pressure profiles were similar as the one in Figure 7.3 but the near-equilibrium pressure varied almost directly proportional to the increase in the initial biomass loaded, inversely proportional to the increase in reactor volume, and increased with the initial solid volume. The pressure went from 10.4 to 11.1 MPa as the biomass initial volume increased from 0.2V to 0.4V (with V=0.0772 L), i.e. as the gas volume decreased from 0.8 to 0.6V.

- **Effect of volatile molecular weight**

Due to the difficulties of characterizing experimental tar products, little is known about the production of tar, such as its molecular mass range, its structure or whether it is really in the gas phase when pyrolyzing- there is some evidence to suggest that some of the tar is entrained as liquid or ejected violently as liquid during decomposition.

At present, different techniques are employed for sampling and analyzing the tar derived from pyrolysis gases, such as gravimetry, gas chromatography and high-performance liquid chromatography.²²² The two chromatographic methods generally identify tar compounds of sizes up to coronene (i.e. around 7 rings, molecular weight of 300 g/mol)^{223,224} whereas the heavier fraction of tar (compounds larger than 3 rings)²²³ is typically analyzed gravimetrically.^{223,224}

Characterization methods for analyzing these heavy tars, nonetheless, are currently not well-developed,²²⁴ and usually result in underestimations of actual tar molecular weights.

The different types of analysis provide complimentary information of tar properties and can be performed individually but certain information overlaps.²²⁵ For example, Oesch et al.²²⁴ observed that the ~65% of tar compounds obtained by gravimetry could be recognized by a general gas chromatographic method. If the GC analysis was modified to a higher-temperature method, the amount of the gravimetric tar compounds identified increased to ~85%. The upper limit of tar molecular weight identified under the high-temperature chromatography was 302 g/mol. For heavier tars, the GC resolution became insufficient plus heavy model compounds could not be acquired in the commercial market.

During the pyrolysis of wood in a fluidized bed reactor, Thunman et al.²²⁶ reported no final tar condensation inside the reaction zone or filters but observed minor quantities of soot and tar on the outlet tube wall. The elemental composition and heating value of lumped hydrocarbons (no tar) analyzed by GC was estimated as $C_6H_{6.2-8}O_{0.1-1}$ and 37 MJ/kg respectively. From the elemental estimations, a molecular weight range for the lumped hydrocarbons of 79.8-96 g/mol can be calculated.

Richard and Thunman²²⁷ compared tar analysis from different researchers and estimated a final tar elemental composition of $C_{4.5}H_{6.5}O_{2.4}$ —i.e. molecular weight of 98.9 g/mol. They concluded that tar composition is dictated by several factors such as temperature, heating rate or volatile

residence time and stated that the “The best assumption that can be made is to consider the tar composition to be the same as that of wood for low temperature of devolatilisation, and the same as that of lumped hydrocarbons for high temperature of devolatilisation.” The elemental composition of the feedstocks employed in the present work tabulated in Table 4.1 reflects a spruce composition of $(\text{CH}_{0.1334}\text{O}_{0.9866}\text{N}_{0.004261}\text{S}_{0.0002344})_n$ with an unknown value of n and a similar composition for birch. This composition gives a molecular weight of n times 28g/mol. Based on the above information, a tar molecular weight in a 40-400 g/mol range was tested in the CVC model 1. The results show no effect of molecular weight in product yields and in the final predicted near-equilibrium pressure. These results were expected since CVC model 1 predicted no tar yield present when steady state is achieved.

7.2. CVC model 2 (employing kinetic scheme of Koufopoulos et al. with secondary reactions)

Figure 7.5 presents Koufopoulos et al.¹⁷⁸ kinetic scheme for biomass pyrolysis with secondary reactions. The scheme involves two parallel reactions (Reactions 1 and 2) for primary production of volatiles (tar plus non-condensable gases) and char, and a third reaction (Reaction 3) in which the primary products further react to form secondary char and volatiles. To keep consistency throughout this report, the nomenclature used herein has been slightly changed from the one employed by Koufopoulos et al.¹⁷⁸ The term volatiles was employed by Koufopoulos et al.¹⁷⁸ to refer just to the tar fraction whereas this report refers to the sum of tar plus non-condensable gases.

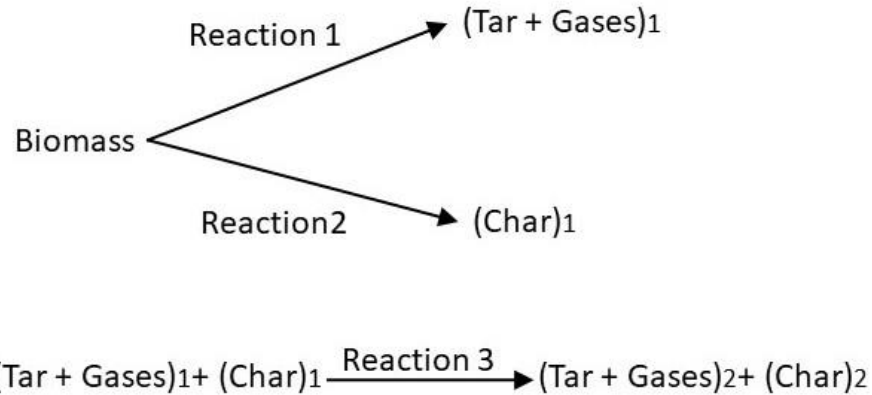


Figure 7.5. Kinetic scheme of Koufopoulos et al.¹⁷⁸ with secondary reactions.

Koufopoulos et al.¹⁷⁸, Babu and Chaurasia¹⁸³ and Sadhukhan et al.²²⁸ applied this kinetic scheme coupled with mass and energy balances in mathematical models that simulated the pyrolysis of single cylindrical biomass particles in “open” reactors. Their results were validated against experimental data. The following assumptions were taken by the models:

- Biomass particles are modeled as one-dimensional
- Heat transfer is transported by conduction, convection, and radiation (just diffusion and convection for Babu and Chaurasia)¹⁸³
- Babu and Chaurasia¹⁸³ accounted for the shrinkage effect while Koufopoulos et al.¹⁷⁸ and Sadhukhan et al.²²⁸ neglected it.
- Kinetic expressions are assumed to follow Arrhenius type expressions of the forms
 - For Koufopoulos et al.¹⁷⁸ and Babu and Chaurasia¹⁸³

$$k_i = A_i \exp\left(\frac{D_i}{T} + \frac{L_i}{T^2}\right) \text{ for } i = 1,2 \quad (7.48)$$

$$k_i = A_i \exp\left(-\frac{E_i}{R_o T}\right) \text{ for } i = 3 \quad (7.49)$$

- For Sadhukhan et al.²²⁸

$$k_i = A_i \exp\left(-\frac{E_i}{R_o T}\right) \text{ for } i = 1,2,3 \quad (7.50)$$

Table 7.3 displays the references employed in each mathematical model for kinetic data A_i , D_i , L_i and E_i , as well as for the process enthalpies. A_i and E_i are the preexponential factor and activation energy of the Arrhenius equation while D_i and L_i are kinetic parameters of the modified Arrhenius Equation 7.48 introduced by Koufopoulos et al.¹⁷⁸ to fit data predicted by the model to experimental data.

Table 7.3. References used in the literature models for kinetic and enthalpy data for kinetic scheme of Koufopoulos et al.¹⁷⁸ with secondary reactions.

Model	k_1, k_2, k_3	Δh
Koufopoulos et al. ¹⁷⁸	Koufopoulos et al. ¹⁷⁸ .	Koufopoulos et al. ¹⁷⁸ .
Babu and Chaurasia ¹⁸³	Koufopoulos et al. ¹⁷⁸	Koufopoulos et al. ¹⁷⁸ .
Sadhukhan et al. ²²⁸	Sadhukhan et al. ²²⁸	Sadhukhan et al. ²²⁸

Koufopoulos et al.¹⁷⁸ and Sadhukhan et al.²²⁸ determined kinetic parameters and heats of reaction for the pyrolysis of biomass by fitting model predictions to experimental results, Koufopoulos et al.¹⁷⁸ estimated two heats of reaction for the pyrolysis process: a modest endothermic heat which dominates at low conversions (below 5 % of biomass weight loss) and is associated to reactions of bond breakage or release of chemically bonded moisture, and an exothermic heat which dominates at high conversions and is likely to relate to reactions

involving oxygen. Simulations over a broad range of pyrolysis parameters and processing conditions showed an increase on the impact of heat transfer and secondary reactions as the HTT and the particle size increased.

Sadhukhan et al.²²⁸ also estimated their own kinetic data and overall heat of reaction by matching their mathematical model with experimental data, and subsequently predicted the effects of temperature and particle size on pyrolysis time and product distribution. They estimated a decline in char yields and an increase in total volatiles as the HTT was raised but no significant effect on final product yields with biomass particle size.

Babu and Chaurasia¹⁸³ used kinetic and heat of reaction data derived by Koufopoulos et al.¹⁷⁸ and applied it to a new model that included the particle shrinkage effect. They concluded that shrinkage barely influences pyrolysis time or product yields in a thermally thin regime but becomes important in a thermally thick regime.

The CVC model 2 was developed using the Koufopoulos et al.¹⁷⁸ model as the basis.

Mathematical equations for this CVC process were rewritten as follows:

- **Mass balance for wood (w), char (c1 and c2), and volatiles (G1 and G2)**

Equations 7.51-7.55 describe the rates of accumulation of each mass component in the sealed reactor

$$\frac{\partial(\rho_w V)}{\partial t} = -(k_1 + k_2)\rho_w V \quad (7.51)$$

$$\frac{\partial(\rho_{c_1}V)}{\partial t} = k_2\rho_wV - k_3\rho_{c_1}V \quad (7.52)$$

$$\frac{\partial(\rho_{G_1}V)}{\partial t} = k_1\rho_wV - k_3\rho_{c_1}V \quad (7.53)$$

$$\frac{\partial(\rho_{c_2}V)}{\partial t} = \delta k_3\rho_{c_1}V \quad (7.54)$$

$$\frac{\partial(\rho_{G_2}V)}{\partial t} = (1 - (\delta - 1))k_3\rho_{c_1}V \quad (7.55)$$

Where $\rho_w = \frac{M_w}{V}$, $\rho_{c_1} = \frac{M_{c_1}}{V}$, $\rho_{c_2} = \frac{M_{c_2}}{V}$, $\rho_{G_1} = \frac{M_{G_1}}{V}$, $\rho_{G_2} = \frac{M_{G_2}}{V}$ are the wood, primary charcoal, secondary charcoal, primary gas and secondary gas apparent densities; G_1 and G_2 represent the total volatiles (tar plus non-condensable gas) from primary and secondary reactions; t is time; $M_w, M_{c_1}, M_{c_2}, M_{G_1}$ and M_{G_2} are the masses of wood, primary charcoal, secondary charcoal, primary volatiles and secondary volatiles; k_1, k_2 and k_3 are the kinetic constants; V is the reactor volume; and δ – term introduced by Koufopoulos et al.¹⁷⁸ – is the coefficient of deposition, which represents the amount of total volatiles deposited on the char sites because of secondary interactions (reaction 3) and is related to the volatile residence time. The coefficient varies in a 1-2 range depending on the extent of deposition.

Mass balance equations 7.51-7.55 for CVC model 2 are simplified to:

$$\frac{\partial M_w}{\partial t} = -(k_1 + k_2)M_w \quad (7.56)$$

$$\frac{\partial M_{G_1}}{\partial t} = k_1M_w - k_3M_{c_1} \quad (7.57)$$

$$\frac{\partial M_{c_1}}{\partial t} = k_2M_w - k_3M_{c_1} \quad (7.58)$$

$$\frac{\partial M_{C_2}}{\partial t} = \delta k_3 M_{C_1} \quad (7.59)$$

$$\frac{\partial M_{G_2}}{\partial t} = (2 - \delta) k_3 M_{C_1} \quad (7.60)$$

Equations 7.56, 7.58 and 7.59 for charcoal and biomass accumulation rates replicate the ones displayed by Koufopoulos et al.¹⁷⁸ CVC model 2 also includes accumulation rates of primary and secondary gas (Equations 7.57 and 7.60). Koufopoulos et al.¹⁷⁸ did not focus on volatile yields and their accumulation rates were not specified or calculated. Notice that Equation 7.59 for the production of secondary char excludes the volatiles concentration in the kinetic expression. The volatiles effect on the secondary reactions is included in the coefficient of deposition δ .

The kinetic scheme makes a distinction between the primary and secondary formation of charcoal (C_1 and C_2) and volatiles (G_1 and G_2). The volatiles combine tar plus non-condensable gas. Notice that all reactions are assumed to have order 1. Koufopoulos et al.¹⁷⁸ and Sadhukhan et al.²²⁸ followed this assumption for simplicity. In a previous publication²²⁹, Koufopoulos justified the utilization of the same order for reactions 1 and 2.

- **Energy balance**

To calculate the energy balance, the same line of thinking as in the previous model (CVC model 1) was followed but with certain adaptations that incorporated the new char and volatile terms. The expressions for pressure, its first derivative with time and the temperature derivative with time became:

$$P = \frac{n_g RT}{V - V_{wo} \frac{(M_w + M_c)}{M_{wo}}} = \frac{\left(\frac{M_g}{W_g}\right) RT}{V - V_{wo} \frac{(M_w + M_{c1} + M_{c2})}{M_{wo}}} \quad (7.61)$$

$$\frac{\partial P}{\partial t} = \frac{RT \left(\frac{1}{W_g} \frac{\partial M_g}{\partial t}\right) + \left(\frac{M_g}{W_g}\right) R \frac{\partial T}{\partial t}}{\left(V - V_{wo} \frac{M_w + M_{c1} + M_{c2}}{M_{wo}}\right)} + \frac{\left(\frac{M_g}{W_g}\right) RT \frac{V_{wo}}{M_{wo}} \left(\frac{\partial M_w}{\partial t} + \frac{\partial M_{c1}}{\partial t} + \frac{\partial M_{c2}}{\partial t}\right)}{\left(V - V_{wo} \frac{M_w + M_{c1} + M_{c2}}{M_{wo}}\right)^2} \quad (7.62)$$

$$\frac{\partial T}{\partial t} = \frac{\frac{k}{t_w} A(T_s - T) + V \sum_k (-\Delta h_k) r_k + VRT \left[\frac{\left(\frac{1}{W_g} \frac{\partial M_g}{\partial t}\right)}{\left(V - V_{wo} \frac{M_w + M_{c1} + M_{c2}}{M_{wo}}\right)} + \frac{\left(\frac{M_g}{W_g}\right) \frac{V_{wo}}{M_{wo}} \left(\frac{\partial M_w}{\partial t} + \frac{\partial M_{c1}}{\partial t} + \frac{\partial M_{c2}}{\partial t}\right)}{\left(V - V_{wo} \frac{M_w + M_{c1} + M_{c2}}{M_{wo}}\right)^2} \right]}{\left(\sum_i M_i c_{p,i} - \frac{\left(\frac{M_g}{W_g}\right) RV}{\left(V - V_{wo} \frac{M_w + M_{c1} + M_{c2}}{M_{wo}}\right)}\right)} \quad (7.63)$$

With

$$r_1 = k_1 \frac{M_w}{V} \quad (7.64)$$

$$r_2 = k_2 \frac{M_w}{V} \quad (7.65)$$

$$r_3 = k_3 \frac{M_{c1}}{V} \quad (7.66)$$

$$M_g = M_{G1} + M_{G2} \quad (7.67)$$

Regarding differences between literature models, Sadhukhan et al.²²⁸ model also uses analogous kinetic expressions as the ones of Koufopoulos et al.¹⁷⁸ for biomass and secondary char mass balances (Equations 7.56 and 7.59) but the equation for the primary char mass balance is different. Their equation expressed as $\frac{\partial(\rho_{c1}V)}{\partial t} = k_2 \rho_w^n V$ only accounts for primary char

formation through reaction 2 and neglects its consumption through secondary reaction 3. Babu and Chaurasia¹⁸³ model uses considerably different kinetic expressions from those of Sadhukhan et al.²²⁸ and Koufopoulos et al.¹⁷⁸ but employs kinetic and heat of reaction data extracted from the latter one which implies that direct application of their data may introduce some inconsistencies in the model.

Energy balances in literature models that employ Koufopoulos et al.¹⁷⁸ kinetic scheme only consider a single heat of reaction for the whole process and use specific heat capacities of char and wood while ignoring the volatile contribution. In contrast, literature models that employed Shafizadeh and Chin kinetic scheme (studied in the previous section) and both CVC models 1 and 2 apply a heat value to each reaction and use specific heat capacities of char, wood and volatiles.

The MATLAB code representing CVC model 2 is given in Appendix Q. The code assumes an initial quiescent environment at ambient conditions and takes kinetic data, property values from Table 7.4.

Table 7.4. Kinetic data and property values applied to constant-volume carbonization (CVC) model 2. Superscripts meanings shown in footnotes at the bottom of the table.

Kinetic data k_1, k_2, k_3 Koufopoulos et al. ¹⁷⁸ $k_i = A_i \exp(D_i/T + L_i/T^2)$ for $i=1,2$ $k_i = A_i \exp(-E_i/R_0T)$ for $i=3$			
A_1	9.973×10^{-5}	s^{-1}	
D_1	17254.4	K	
L_1	-9061227	K^2	
A_2	1.068×10^{-3}	s^{-1}	
D_2	10224.4	K	
L_2	-6123081	K^2	
A_3	5.7×10^5	s^{-1}	
E_3	81	kJ/mol	
Heats of reaction data $\Delta h_1, \Delta h_2$ Chan et al. ¹⁸²			
Δh_1^a	0.418	kJ/g	
Δh_2^a	0.418	kJ/g	
Heat of reaction data Δh_3 Di Blasi ²¹⁶			
Δh_3^a	-0.042	kJ/g	
Property values			
R_o	8.314×10^{-3}	kJ/mol K	Ideal gas constant
W_g^b	200	g/mol	Molecular weight of total volatiles
k_{SS}	0.019	kW/m K	Thermal conductivity of stainless steel at $225^\circ C$ ²²⁰
t_w	0.0021	m	Wall thickness reactor
Rad	0.0127	m	Outer radius reactor (1 inch diameter)
L	0.1524	m	Reactor length (6 inch)
$c_{p,w}^a$	1.5×10^{-3}	kJ/g K	Specific heat capacity of wood taken from ²²¹
$c_{p,c1}$ and $c_{p,c2}^a$	1.5×10^{-3}	kJ/g K	Specific heat capacity of char taken from ²²¹

Table 7.4. Kinetic data and property values applied to constant-volume carbonization (CVC) model 2 (Continued).

$c_{p,G1}$ and $c_{p,G2}$ ^a	1.1×10^{-3}	kJ/g K	Specific heat capacity of tar taken from 179.
V	7.72×10^{-5}	m ³	Reactor volume (calculated as $\pi \cdot Rad^2 \cdot L$).
V_{wo}	0.2V	m ³	Initial volume occupied by the solid
T_s	573	K	Sand bath temperature
T_o	298	K	Initial reactor temperature
P_o	100	kPa	Initial reactor pressure
M_{wo}	10	g	Initial biomass mass
<p>a. Additional CVC model 2 simulations that applied heats of reactions and specific heat capacity values from Koufopoulos et al.¹⁷⁸ Results are presented below.</p> <p>b. Additional CVC model 2 simulations that tested the effect of the volatile molecular weight in a 44-400g/mol range. Results are presented below.</p>			

Figures 7.6 and 7.7 illustrate predictions from the CVC model 2 regarding evolution of product yields, temperature and pressure with time under the assumptions of a HTT of 300°C and a mass loading of ~130 g/L. Analogous to Figures 7.2 and 7.3 derived from CVC model 1, the temperature rise to the sand bath temperature appears to be immediate, while pressure and yields of char and volatiles increase with time to asymptotic values of 2.2 MPa (versus experimental pressure of 5 MPa), ~40% (versus experimental char yields of 50-60%) and ~60% (versus experimental gas yields of 40-60%) (See Figures 7.6 and 7.7). Figure 7.8 splits char and volatile yields information from Figure 7.6 into yields of primary and secondary products. The graph indicates that the kinetics of primary char conversion to secondary char occurs rapidly with little accumulation of primary char.

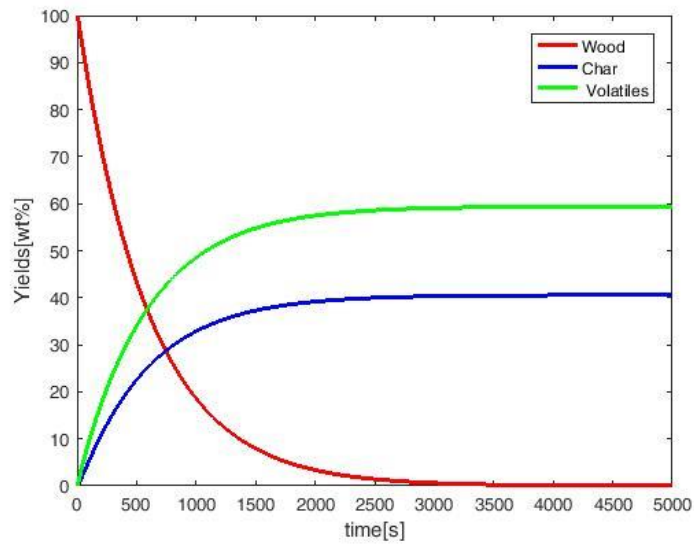


Figure 7.6. History profile of wood, char and volatile yields predicted by CVC model 2 assuming constant-volume carbonization of biomass at a heat treatment temperature of 300°C and an initial pretest pressure of 0.1 MPa.

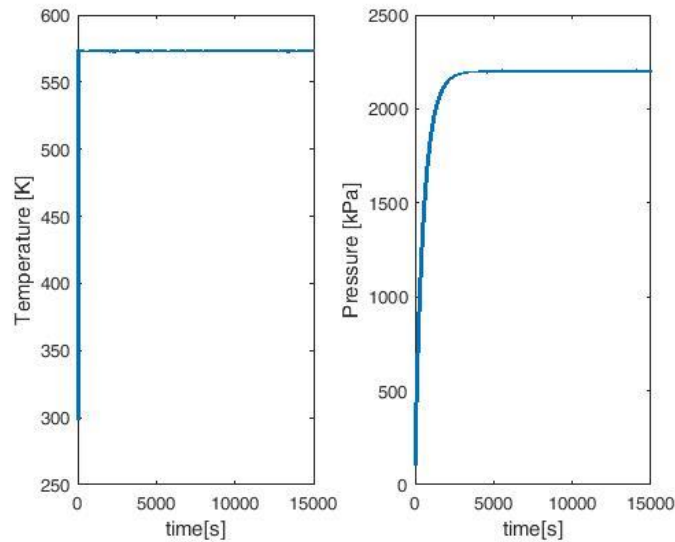


Figure 7.7. History profile of temperature and pressure predicted by CVC model 2 assuming a constant-volume carbonization of biomass at a heat treatment temperature of 300°C and an initial pretest pressure of 0.1 MPa.

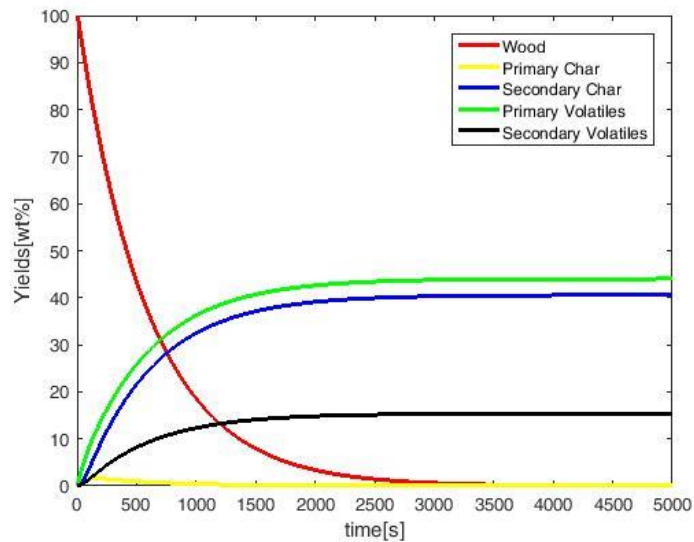


Figure 7.8. History profile of wood, char and volatile yields predicted by CVC model 2 assuming constant-volume carbonization at a heat treatment temperature of 300°C and an initial pretest pressure of 0.1 MPa. The primary and secondary fractions of char and volatile yields are shown.

Discrepancies between experimental and theoretical data in this model can also be justified by the same reasons described in CVC model 1. Furthermore, the large differences observed for the calculated pressures are explained by the high sensitivity of pressure with the volatile molecular weight. Varying the weight from 200 g/mol (a reasonable weight for tar and probably an overestimation of the weight of total volatiles) to 44 g/mol (weight for CO₂ and probably an underestimation of the weight of total volatiles) raise the predicted pressure in the model from around 2 to almost 10 MPa. A 10 MPa value is similar to the pressure predicted in CVC model 1 which estimated a final volatile product only composed of non-condensable gases with a molecular weight similar to that of CO₂.

Similarly to the temperature profile from CVC model 1, the heat transfer coefficient employed in CVC model 2 (equal to $\frac{k}{t_w} A = 0.11 \text{ kW/K}$) only accounted for heat conduction through the thin

reactor stainless steel. The coefficient was therefore unrealistically high and led to a prediction of an immediate temperature rise. Similar to the steps followed in CVC model 1, slower parameterized heat transfer coefficients were tested in order to determine the heat transfer impacts on product distribution predicted by CVC model 2. Appendix R displays temperature, pressure and product yield history profiles at fictitious heat transfer coefficients of 10^{-3} , 10^{-4} and 10^{-5} kW/K. At a parameterized heat transfer coefficient of 10^{-3} kW/K, similar profiles as the ones obtained at a coefficient of 0.11 kW/K were obtained (Figures 7.6 and 7.7). As the parameterized heat transfer coefficient was reduced to 10^{-4} and 10^{-5} kW/K and the heat transfer slowed down, the CVC model 2 predicted the achievement of steady state after longer carbonization times, the production of higher charcoal yields (60 wt.% and 80 wt.% at respective heat transfer coefficients of 10^{-4} and 10^{-5} kW/K) and lower volatile yields, and in consequence, the attainment of lower final pressures (1.6 and 1 MPa at respective parameterized heat transfer coefficients of 10^{-4} and 10^{-5} kW/K).

- **Effect of Temperature**

Experimentally, the pyrolysis of biomass under a mass loading of ~130g/L and HTT's of 300, 400 and 500°C resulted in char yields of around 55, 43 and 40% respectively. Quantitatively, most of the predicted char yields (see Figure 7.9) show considerable discrepancies with experimental values whereas qualitatively, there is agreement regarding product yield behavior with temperature. Char yield is shown to decline and volatiles to increase as the temperature is raised.

The yields in the model were originally calculated using the same deposition factor as the one used by Koufopoulos et al.¹⁷⁸ ($\delta=1.45$). This factor corresponds to a pyrolysis process in an “open” reactor, therefore a process characterized by a lower extent of secondary reactions and, in consequence, by a smaller deposition factor in comparison to CVC processes. Figure 7.9 shows that an increase in the deposition factor from 1.45 to 2 implies a 15% increase on the predicted char yield. At 300°C, the predicted yield at a deposition factor of 2 agrees with the experimental value but higher temperature calculations lead to underestimations of the experimental values.

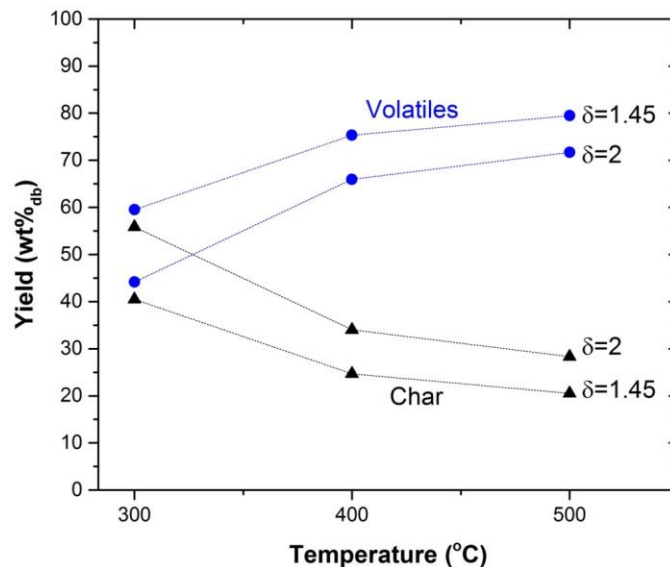


Figure 7.9. Effect of heat treatment temperature on the yields of char and volatiles predicted by the CVC model 2 using deposition factors of 1.45 and 2.

- **Effect of biomass loading and biomass volume**

The effect of biomass loading was investigated by varying the initial biomass amount in a 10-100 g range while keeping the reactor volume and the solid volume constant at 0.0772L (calculated as $V = \pi \cdot \text{Rad}^2 \cdot L$) and at 0.01544 L (0.2V) respectively . On the other hand, the

effect of solid volume was simulated by increasing the initial solid volume from 0.2V to 0.4V (i.e. decreasing the initial gas volume from 0.8V to 0.6V) while keeping the biomass constant at 10 g.

In all cases, a negligible effect on product yields (in wt. percentage) was observed. As expected, the near-equilibrium pressure showed an almost direct proportional relation to the initial biomass loaded and increased with higher initial solid volumes, i.e. lower gas volumes. Increasing the solid volume from 0.2V to 0.4V (the rest of parameters are defined in Table 7.4) raised the pressure from 2.2 to 2.6 MPa.

- **Effect of volatile molecular weight**

As in the literature mathematical models, the volatile molecular weight is assumed constant throughout the pyrolysis process even though in reality, it is continuously changing as the process evolves. Changing the volatile molecular weight parameter within a 44-400 g/mol range while maintaining the rest of parameter values as specified in Table 7.4 presented no impact on the predicted product yield distribution (see yields in Figure 7.8) and as expected, higher volatile molecular weights reduced the pressure calculated at near-equilibrium conditions. Pressure declined from 9.6 to 1.2 MPa when the volatile weight was raised from 44 to 400 g/mol.

- **Effect of property values: specific heat capacities and enthalpies**

In the original simulations of CVC model 2, specific heat capacities and reaction enthalpies replicated the values from the CVC model 1. The idea was to maintain consistent property values in both CVC models in order to test differences from just the two kinetic schemes. Additional CVC model 2 simulations applied specific heat capacity values and heats of reactions provided by Koufopoulos et al.¹⁷⁸

First, wood and char specific heat capacities ($c_{p,w}$ and $c_{p,c}$) were changed from the values given in Table 7.4 to the following values given by Koufopoulos et al.¹⁷⁸ which are dependent on the process temperature.

$$c_{p,w} = \frac{1112.0 + 4.85(T - 273)}{10^6} \quad (5.68)$$

$$c_{p,c1} = c_{p,c2} = \frac{1003.2 + 2.09(T - 273)}{10^6} \quad (5.69)$$

Volatile specific heat capacities were not provided by Koufopoulos et al.¹⁷⁸ and therefore their values, as well as the rest of the parameters, were maintained as in Table 7.4.

A second set of changes were made. Reaction enthalpies were modified from the ones in Table 7.4 (analogous to the ones in CVC model 1) to radically different enthalpies estimated by

Koufopoulos et al.¹⁷⁸ while keeping the rest of the values as defined in Table 7.4. The new simulations used the endothermic value given by Koufopoulos et al.¹⁷⁸ for primary reactions ($\Delta h_1 = \Delta h_2 = 0.020$ kJ/g) and the exothermic one for secondary interactions ($\Delta h_3 = -0.255$ kJ/g); even though strictly speaking Koufopoulos et al.¹⁷⁸ did not determine heats for single reaction processes but distinguished two overall heats of reaction. One low endothermic dominant at low biomass conversion processes and one exothermic at higher conversions.

Simulations with both the new property specific heat capacities and enthalpy values resulted in barely any changes to the product distribution and the near-equilibrium pressure predicted. Changing the specific heat capacities results in char yield, volatile yield and pressure estimations of 40.47%, 59.53% and 2.6 MPa respectively, whereas the new enthalpies tested lead to char yield, volatile yield and pressure of 40.49 % and 59.52% and 2.5 MPa respectively. All values are similar to the ones displayed in Figures 7.6 and 7.7.

7.3. Conclusions from the CVC models

Two simple models (CVC model 1 and CVC model 2) that estimated product yields, temperature and pressure profiles from CVC were developed. The CVC models made use of kinetic data and property values from literature models that were derived from “open” reactor systems. Typically, kinetic constants or heats of reaction derived in the literature were obtained by fitting the results from mathematical models to experimental results from specific processes. Good agreement is then observed between predictions and their experimental results but the agreement fails when

different systems or process conditions are employed. For example, Di Blasi¹⁷⁹ showed great differences between predictions obtained from three different kinetic data sets. In the same manner, kinetic data and properties of the pyrolyzing medium are likely to change considerably between “open” and sealed (CVC) vessels. In most cases, both CVC models presented herein displayed considerable differences between predictions and experimental results.

The development of the CVC models and the detailed study of literature models pertaining to pyrolysis in “open” reactors revealed reasons that the applicability of the models is largely limited. For example, there are many unknown kinetic data and property values, the pyrolysis processes is inherently complex, and the models data that have been developed have been derived from a diversity of biomass samples or processes. Consequently, simplifying assumptions are introduced in to the models; e.g. property values—such as c_p or molecular weights of char, tar and gas—that are continuously changing throughout the pyrolysis process, are usually assumed constant. In addition, properties that have been proved to be of significant importance to the pyrolysis process—such as the lignin, cellulose, hemicellulose and ash contents—are typically ignored. For simplicity, spatial profiles and char shrinkage phenomena were also ignored in the CVC models but could be included in future versions of the models when additional experimental data become available.

In conclusion, a number of challenges remain to be resolved before a broad pyrolysis model is realized that accurately and robustly predicts outcomes for different carbonization systems, process conditions, and biomass types.

CHAPTER 8. CONCLUSIONS

In conclusion, the results presented herein demonstrate that by using the CVC process and selecting appropriate processing conditions, charcoals can be produced with properties tailored for their end use. For example, low value charcoals can be produced at moderate temperature (300°C) and short reaction time (<60 min) in greater yield (50-60%) than any other known process; these charcoals are suited to combustion applications. At the other end of the spectrum, high value biocarbons / biocokes with low volatiles and high fixed carbon content (>85%) can be produced by using higher temperature (500-550°C) and longer reaction times (~3 hours). This opens up the opportunity for the production of metallurgical grade chars in a single step process which is of great interest to industry.

In addition, the morphological characteristics of charcoals can also be tuned. Higher HTT, pretest pressures, heating rates and possibly smaller particle sizes resulted in a change from a particulate charcoal that retained the structure of the virgin feedstock to a solidified single piece of coke-like material that had undergone a TPP transition and formed to the shape of the reactor vessel.

The following list highlights the research main findings:

1. A new reactor design for biomass carbonization was presented. The reactor— referred to as the Wall Heated Tubing Bomb (WHTB)— has an internal volume of ~0.22 L, which permits loadings of ~30 g and ~50 g of spruce and birch sawdust (particle size <2mm)

respectively, and enabled constant-volume pyrolysis to be performed at elevated temperatures and pressures in a safe and controlled manner.

2. Solid and gas yields, and proximate analysis results exhibited good repeatability of $\pm 2\%$, absolute. Liquid yields showed greater variation. This was expected due to the difficulty of recovering liquids condensed in the tubing system of the WHTB and/or WDV.
3. In comparison to carbonization processes in “open” reactors such as conventional or flash carbonization, the retention of volatiles under pressure in CVC led to improved mass and energy balances and to greater solid yields mainly due to enhanced secondary reactions. The resultant products are charcoals with higher fixed-carbon yields, non-condensable gases mainly composed of CO₂ and negligible free tars which minimizes disposal issues and environmental impacts.
4. In comparison to hydrothermal carbonization, the higher temperatures employed in CVC processes (which would result in radically higher pressures if used in HTC processes) enables a more profound charcoal devolatilization and in consequence, charcoals with higher fixed-carbon and energy contents are produced.
5. Constant-volume carbonization of spruce and birch produced a charcoal with a fixed-carbon yield that approached the limiting value predicted by thermodynamics for the process conditions.
6. In comparison to CVC, slightly opening the reactor to permit a constant atmospheric-pressure resulted in the formation of a notable fraction of free tar (versus negligible free tar formed in a sealed reactor) and a char with more volatile and less fixed-carbon contents and a lower fixed-carbon yield. The results indicate a lower extent of secondary charring reactions when an open reactor is used.

7. Trends reported in literature regarding the effect of temperature on carbonization in “open” reactors showed that the improvement of char properties (higher fixed-carbon and lower volatile contents) associated with higher heat treatment temperatures was generally accompanied by a significant loss of the fixed-carbon yield. In comparison, raising the HTT in a 300 -550°C range during CVC under an initial nitrogen pressure of 0.1 MPa improved char properties while preserving the valuable fixed-carbon yield near-theoretical limiting values. At a temperature of 500°C, charcoal derived from birch was a highly devolatilized solid product rich in fixed-carbon content (>85 wt. %), fixed-carbon yield (34 wt. %) and with an improved higher heating value (~34MJ/kg).
8. A beneficial effect of pressure on the final char properties and yields has been reported for “open” reactor systems. In CVC, the pretest pressure (from 0.1 to 2.17 MPa) did not show an influence on product yields or char proximate analysis. Nonetheless, it had an effect on the char morphology, enhancing plastic transformations. The findings confirmed that it is the volatile pressure and/or their residence time—rather than the total system pressure which typically has a notable influence on these properties in “open” reactors— that are the dominant factors influencing the final pyrolytic yields and proximate analysis values. As the CVC pretest pressure had no discernable effect on the final char yield or fixed-carbon or volatile contents, the use of an external gas to pressurize the system could be eliminated, thereby simplifying the process and reducing costs.
9. Heating rate plays a significant role in carbonization processes in “open” reactors. As the rate is reduced, the product composition shifts towards less tar and more char until an apparent asymptotic value is reached. Experiments in “open” reactors cover a broad

range of heating rates. Fast pyrolysis or gasification favour the production of volatiles by employing high rates (as high as $\sim 1000^{\circ}\text{C/s}$ or greater) and by minimizing restrictions to heat and mass transfer phenomena, i.e. by using small particles and short vapour residence times. While slow pyrolysis or carbonization processes employ low heating rates ($0.1\text{-}1^{\circ}\text{C/s}$) and attempt to limit mass transfer phenomena while promoting secondary char formation. In the same way, CVC heating rates are compromised by the use of deep-packed beds of particles which impose mass and heat transfer barriers. Altering the heating rate (from ~ 0.09 to 0.5°C/s at HTT of 300°C ; or from ~ 0.03 to 0.09°C/s at HTT of 500°C) used to reach the carbonization temperature did not affect product yield or char proximate analysis as long as the WHTB reactor soaking time at carbonization temperature was maintained for a specific period of time (120 minutes at HTT of 500°C , or 180 minutes at HTT of 300°C). In summary, the use of higher heating rates in “open” reactor configurations appears to limit secondary charring reactions but the heating rate does not appear to affect product yields and char proximate analysis for CVC.

10. Regarding the particle size effect, larger particles benefit secondary char-forming reactions in “open” reactors. In sealed vessels, smaller particle sizes seem to favor these secondary reactions. The quicker release of volatiles into the gas phase due to the use of smaller grain sizes ($<0.2\text{ mm}$) combined with the volatile retention in the constant-volume reactor accelerates the carbonization process, induces higher pressures and more pronounced exotherms, and prevents the carbon losses that are observed from “open” reactors. The resultant CVC chars derived from smaller grain sizes maintain or improve fixed-carbon contents without sacrificing fixed-carbon yields.

11. Increasing the feedstock loading per liter of reactor volume raises the volatiles partial pressure in CVC. Previous work at HNEI that used small sealed crucibles showed an increase in char yields with higher mass loadings. Nonetheless, the most recent pyrolysis tests of spruce and birch in the WHTB appear to indicate that there is a limit to the mass loading effect in sealed vessels. Short experiments with birch and spruce showed a minor increase on the fixed-carbon yields with the mass loading and a minor increase, if any, on the fixed-carbon contents. Long experiments with birch (long experiments with spruce were not performed) presented no significant changes to the fixed-carbon yields or contents at the loadings tested.
12. Prolonging immersion times in the current WHTB from 30 to 190 minutes led to higher gas yields and charcoals with less volatile matter and similar or improved fixed-carbon yields.
13. An increase in temperature, heating rate and pretest pressure; and possibly a decrease in biomass particle size transformed the final biochar product from particulate into a solidified single piece resembling coke, which implies it has undergone a transient plastic phase (TPP) transition. The modification of the char structure can become an opportunity for briquetting charcoals derived from small biomass grains previously impractical for carbonization or for improving char porosities for applications such as adsorption or soil amending. The TPP formation is a new observed phenomena for slow pyrolysis processes. In previous studies, its formation was reported only from fast pyrolysis under heating rates 2-3 orders of magnitude higher than those used in the current study and temperatures of at least 600°C versus ~400°C in CVC (note that this temperature in CVC

is not the sole factor in TPP formation but depends on other experimental conditions as well).

14. The high intraparticle volatile concentration and intraparticle volatile time in CVC contributed to the shift of char plasticization to modest temperatures and heating rates in comparison to the conditions necessary to produce the same effect in “open” reactors.
15. Two simple mathematical models that predicted product yields, pressure and temperature in CVC were developed on the basis of kinetic schemes and property values derived from “open” configurations. Considerable quantitative differences observed between experimental and predicted results are explained by the fact that kinetics between closed and “open” reactors are likely to be different and by several inconsistencies found in the literature models. For example, given the limited available literature data and the large unknowns in property values of char, tar and gas materials during the pyrolysis process, literature mathematical models often make use of property values and kinetic and heat of reaction data from different authors that employed distinct feedstocks. Furthermore, kinetic data sets greatly vary between authors, properties that continuously change during the carbonization process such as the molecular weight and heat capacities of gases, tar and char are typically considered constant, or properties known to have a strong influence on the pyrolysis process—such as the lignin, cellulose hemicellulose and mineral matter contents—are usually not included in the pyrolytic models.

CHAPTER 9. FUTURE WORK

Stepping back and looking at the PhD rough and bumpy journey, the results have been pleasantly surprising. The PhD origins go back to Dr. Antal and his vision of a new carbonization process: the CVC. The R3Lab team launched it and the final results presented herein showed a surprisingly promising potential. In the future, work could focus on its scale-up. Now, the main issue faced by a possible industrial CVC reactor is the need of costly high pressure equipment. The reported pressures considerably exceeded those measured in other high-pressure carbonization vessels such as the flash carbonization reactor. Fortunately, there is hope and large room for improvement. Adding a dead volume in the WHTB proved to be able to produce chars with comparable qualities (i.e. char proximate analysis, yields and calorific values) and drastically reduce the pressure needs of the reactor vessel allowing the reduction of capital costs. The idea that lays behind this WHTB reactor design with a hot reaction zone and an incremented cold dead region on top is the following: Non-condensable and lighter gas products will have a tendency to occupy the upper parts of the cold dead volume. Increasing the dead volume would reduce the reactor pressure mainly due to the non-condensable gas influence. The heavy tarry vapors will more likely condense in the long vertical tubing as they try to ascend to the top of the cold dead volume. The condensed tars will keep recirculating into the reaction zone offering additional opportunities of secondary char formation.

Future research work could determine the maximum additional dead volume, and consequently the minimum possible reactor pressure, that could be employed while maintaining char yields

and proximate analysis. Improved ways of tar recirculation could also be explored. Tar recirculation could be enhanced by lengthening the vertical dead volume tubing and/or by cooling the dead volume down. Both of these factors would also reduce reactor pressure needs.

Future work should also focus on ways of efficiently heating the biomass either externally or internally, and on analyzing possible hot local spots and heterogeneity within the pyrolyzing char during carbonization at the larger scale.

APPENDIX A. PRESSURE TERMS

A.1. Design Pressure

“ . . .the piping system must either be designed to safely contain the maximum possible pressure, considering such factors as failure of control devices and dynamic events such as surge[what the author refers to as the design pressure], or be provided with overpressure protection, such as safety relief valve.”²³⁰

“ . . . If the event being considered complies with the Code requirements of 302.2.4, the allowable stress and/or component pressure rating may be exceeded for a short time, as discussed below in section 3.3. Although this is often considered to be an allowable variation above the design condition, the variation limitations are related to the maximum allowable working pressure of the piping, not the design conditions, which could be lower than the maximum allowable pressure at temperature.”²³⁰

Defining a design pressure value for the WHTB is not trivial. One could think that the highest pressure ever observed from all WHTB CVC experiments could serve as a value for the design pressure. Alternatively, the design pressure could take into consideration all of the worst case experimental scenarios. Since the peak pressure during an experiment is influenced by the CVC experimental conditions—such as the pretest nitrogen pressure, the mass loading and the HTT—the worst case scenarios must consider:

- the highest possible mass loading: ~240 g/L with birch – or higher if cellulose powder or another biomass types with higher packing density were used;
- the highest possible pretest nitrogen pressure: ~16.5 MPa (achieved if the pressure in a full nitrogen cylinder was released into the WHTB reactor and achieved equilibrium);
- the highest possible HTT: ~550°C (note that even though 600°C is specified as the maximum sand bath temperature by the manufacturer, 550°C was the maximum achieved in practice at full power).

In the first case, i.e. when only the peak experimental pressure is considered, the design pressure would be 17.9 MPa. This corresponds to the peak pressure observed during the carbonization of birch at a HTT of 550°C, a pretest nitrogen pressure of 0.1 MPa and a standard mass loading of around 130 g/L. Note that an experiment that carbonized birch at a HTT of 400°C, a pretest nitrogen pressure of 2.17 MPa and a standard mass loading of around 130 g/L also resulted in a large pressure rise with a recorded peak pressure of 17.5 MPa.

In the second case, i.e. when all possible worst case scenarios are taken into account, the design pressure would be over 40 MPa. The inert gas contribution at 550 °C would be around 23 MPa $\left(16.5 \text{ MPa} \frac{(550+273)K}{(298+273)K}, \text{ not considering volume changes}\right)$, and the product gas contribution would be over 17.9MPa (pressure observed under a standard mass loading with atmospheric initial pressure; a higher loading would result in higher pressures).

In constant-volume carbonization experiments, it is critical that the experimenter is aware of the risk of overpressurization and ensure that the system is safe. Since constructing and utilizing a

practical system that can withstand this worst-case and highly unlikely pressure of ~40MPa would be costly, the WHTB system was designed to include overpressure protection, i.e. burst diaphragm.

A.2. Allowable Working Pressure or Maximum Allowable Working Pressure (MAWP)

The concept of maximum allowable working pressure (or allowable working pressure)—even though not used in the ASME B31.3 code²³⁰—is useful since piping systems are assemblies of standardized parts with allowable working pressures specified by the manufacturer. The WHTB reactor is built from Swagelok components. Table A.1 taken from Swagelok and published on the web²³¹ shows allowable working pressures for fractional stainless steel seamless piping at 37°C as a function of the outside diameter and wall thickness. This tubing is the weakest part of the WHTB reactor, i.e. the reactor body, and therefore defines the allowable working pressure for the whole WHTB system. The other parts of the WHTB reactor are stronger, being made of tubing of smaller diameter and not being exposed to the most severe conditions in terms of temperature and pressure.

To determine allowable working pressures at elevated temperatures, the allowable working pressure from Table A.1 needs to be multiplied by the temperature factors shown in Table A.2. For example, the WHTB reactor body made from type 316 stainless steel, 1in. OD x 0.083 in. wall has an allowable working pressure of 3100 psig at -20 to 100°F (-28 to 37°C) (Table A.2). At 1000°F (537°C), the allowable working pressure is reduced to 2356 psig (3100psig x 0.76),

calculated as the multiplication of 3100 psig and the elevated temperature factor at 1000°F of 0.76 (Table A.3). Figure A.1 illustrates the allowable working pressures of the WHTB at temperatures ranging from room temperature to 537°C. Notice that the WHTB can experience temperatures of 550°C, which lays above the maximum temperature tabulated by Swagelok. At temperatures from 537 to 566°C, the derating temperature factor is 0.755. Therefore a WHTB allowable working pressure of 2,341 psig has been estimated (see Appendix A.2.2 *How does Swagelok calculate the Derating Temperature Factors?* for details).

Allowable variations above the maximum allowable working pressure are also permitted in the system for short periods of times as long as several conditions are satisfied, one of which is that this maximum allowable working pressure is not exceeded by more than some percentage.²³⁰ See Appendix A.4. *Allowances for Pressure* for a detailed description of permissible pressure variations.

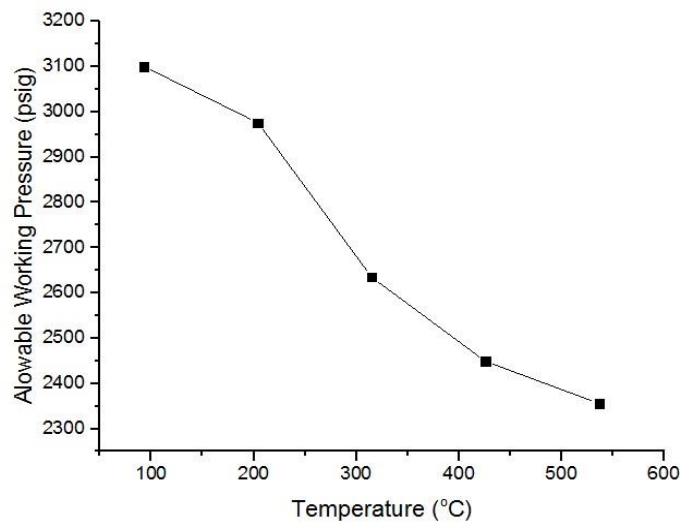


Figure A.1. Allowable working pressure with temperature for a 1” outer diameter Swagelok tube with a wall thickness of 0.21 cm (0.083”)

Table A.1. Fractional Stainless Steel Seamless tubing. Allowable working pressures are calculated from an S value of 20 000 psi (137.8 MPa) for ASTM A269 tubing at -20 to 100°F (-28 to 37°C), as listed in ASME B31.3, except as noted. For welded and drawn tubing, a derating factor must be applied for weld integrity:

- for double-welded tubing, multiply working pressure by 0.85.
- for single-welded tubing, multiply working pressure by 0.80.

Tube OD in.	Tube wall thickness, in.																Swagelok Fitting Series
	0.010	0.012	0.014	0.016	0.020	0.028	0.035	0.049	0.065	0.083	0.095	0.109	0.120	0.134	0.156	0.188	
	Working Pressure, psig Note: For gas service, select a tube wall thickness outside of the shaded area. See Gas Service																
1/16	5600	6800	8100	9400	12000												100
1/8						8500	10900										200
3/16						5400	7000	10200									300
1/4						4000	5100	7500	10200								400
5/16							4000	5800	8000								500
3/8							3300	4800	6500	7500							600
1/2							2600	3700	5100	6700							810
5/8								2900	4000	5200	6000						1010
3/4								2400	3300	4200	4900	5800					1210
7/8								2000	2800	3600	4200	4800					1410
1									2400	3100	3600	4200	4700				1610
1 1/4										2400	2800	3300	3600	4100	4900		2000
1 1/2											2300	2700	3000	3400	4000	4900	2400
2												2000	2200	2500	2900	3600	3200

Table A.2. Derating temperature factors.

Temperature		Tubing Materials							
°F	°C	Aluminum	Copper	Carbon Steel	304, 304/304L	316, 316/316L	317, 317/317L	321	347
200	93	1.00	0.80	0.95	1.00	1.00	1.00	1.00	1.00
400	204	0.40	0.50	0.87	0.93	0.96	0.96	0.96	0.96
600	315				0.82	0.85	0.85	0.85	0.85
800	426				0.76	0.79	0.79	0.79	0.79
1000	537				0.69	0.76	0.76	0.76	0.76

A.2.1. How does Swagelok calculate the Allowable Working Pressure?

As stated in one of the multiple emails exchanged with Swagelok, to calculate the allowable working pressure “We use the 75,000 tensile and a 20,000 stress factor at room temperature as a base [taken from ASME B31.3 Table A-1 (see Appendix B)]. We then apply the factor from the chart of factors for the given size [Table A.3 (duplicated from²³²)], and then the allowable working pressure is calculated”. In conclusion, the tabulated factors in Table A.3, dependent on the tube dimensions, relate allowable working pressure with allowable stress.

The equations that derive in the factors displayed in Table A.3 was requested from Swagelok but no response was received. In the past, several authors have formulated equations that relate pressure and stress. For example, Duffill, Lamé and Barlow developed Equations A.1, A.2 and A.3 respectively, which relate both parameters by respective factors of $2 \frac{K-1}{K+1}$, $\frac{2t(D-t)}{D^2-2Dt+2t^2}$ and $\frac{2t}{D}$. Tables A.4, A.5 and A.6 show the chart of factors obtained from the use of Duffill, Lamé and Barlow for the same tubing dimensions specified by Swagelok. A comparison between the various charts of factors shows that Swagelok’s is the most conservative, followed closely by the chart of factors calculated from Barlow’s equation, then Lamé’s and finally Duffill’s.

• Duffill equation:

$$P = 2S \frac{K - 1}{K + 1} \quad (\text{A.1})$$

Where P is pressure, S is the tensile strength, D the outer diameter, d the inner diameter and K is the ratio between outer and inner diameters, $K = D/d$.

• Lamé equation:

$$P = \frac{2St(D - t)}{D^2 - 2Dt + 2t^2} \quad (\text{A.2})$$

Or equivalently

$$P = \frac{S(D^2 - d^2)}{(D^2 + d^2)} \quad (\text{A.3})$$

where S is the tensile strength, D the outer diameter, t the wall thickness and d the inner diameter.

• Barlow equation:

$$P = \frac{2St}{D} \quad (\text{A.4})$$

where S is the tensile strength, D the outer diameter, and t the wall thickness. Barlow equation is a very common equation but less precise.

Table A.3. Swagelok Chart of factors for use in calculating allowable working pressures of tubing. Allowable working pressure=Factor x Allowable stress value in psi. Based on ANSI B31.3-1993.

Tube OD (in.)	Tube Wall Thickness(in.)																		Swagelok Tube Fitting Series
	0.010	0.012	0.014	0.016	0.020	0.028	0.035	0.049	0.065	0.083	0.095	0.109	0.120	0.134	0.148	0.156	0.180	0.188	
1/16	0.280	0.343	0.409	0.474	0.604														100
1/8						0.426	0.545												200
3/16						0.274	0.352	0.513											300
1/4						0.201	0.257	0.375	0.513										400
5/16							0.202	0.293	0.403										500
3/8							0.167	0.240	0.329										600
1/2							0.123	0.176	0.239	0.314									810
5/8							0.104	0.148	0.200	0.261	0.304								1010
3/4								0.122	0.165	0.241	0.249	0.290							1210
7/8								0.104	0.140	0.182	0.210	0.244							1410
1								0.090	0.122	0.158	0.182	0.211	0.235						1610
1 1/4									0.096	0.124	0.144	0.166	0.184	0.208	0.231	0.245	0.287		2000
1 1/2										0.103	0.118	0.137	0.151	0.170	0.189	0.200	0.234	0.246	2400
2											0.088	0.101	0.112	0.126	0.139	0.147	0.172	0.180	3200

Note: All pressure ratings are based on minimum wall thicknesses of ASTM A269. Various tubing specifications within the code have varying wall thickness tolerances. All charts and tables are for reference only and are based on information contained in the 1993 edition of the code. No implication is made that these figures can be used for design work. Applicable codes and practices in industry should be considered. Swagelok Company is not responsible for the accuracy of information presented in these tables. ANSI Codes are the successor to and replacement of ASA Piping Codes.

Table A.4. Chart of factors calculated with Duffill equation (see Equation A.1).

Tube OD (in.)	Tube Wall Thickness(in.)																		
	0.010	0.012	0.014	0.016	0.020	0.028	0.035	0.049	0.065	0.083	0.095	0.109	0.120	0.134	0.148	0.156	0.180	0.188	
1/16	0.320	0.384	0.448	0.512	0.640														
1/8						0.448	0.560												
3/16						0.299	0.373	0.523											
1/4						0.224	0.280	0.392	0.520										
5/16							0.224	0.314	0.416										
3/8							0.187	0.261	0.347										
1/2							0.140	0.196	0.260	0.332									
5/8							0.112	0.157	0.208	0.266	0.304								
3/4								0.131	0.173	0.221	0.253	0.291							
7/8								0.112	0.149	0.190	0.217	0.249							
1								0.098	0.130	0.166	0.190	0.218	0.240						
1 1/4									0.104	0.133	0.152	0.174	0.192	0.214	0.237	0.250	0.288		
1 1/2										0.111	0.127	0.145	0.160	0.179	0.197	0.208	0.240	0.251	
2											0.095	0.109	0.120	0.134	0.148	0.156	0.180	0.188	

Table A.5. Chart of factors calculated with Lamé equation (see Equation A.2)

Tube OD (in.)	Tube Wall Thickness(in.)																		
	0.010	0.012	0.014	0.016	0.020	0.028	0.035	0.049	0.065	0.083	0.095	0.109	0.120	0.134	0.148	0.156	0.180	0.188	
1/16	0.381	0.475	0.577	0.688	0.941														
1/8						0.577	0.778												
3/16						0.351	0.459	0.708											
1/4						0.252	0.326	0.488	0.703										
5/16							0.252	0.372	0.525										
3/8							0.206	0.301	0.419										
1/2							0.151	0.217	0.299	0.398									
5/8							0.119	0.170	0.232	0.306	0.358								
3/4								0.140	0.190	0.249	0.290	0.340							
7/8								0.119	0.160	0.210	0.244	0.285							
1								0.103	0.139	0.181	0.210	0.245	0.273						
1 1/4									0.110	0.142	0.165	0.191	0.212	0.240	0.269	0.285	0.336		
1 1/2										0.117	0.135	0.157	0.174	0.196	0.219	0.232	0.273	0.287	
2											0.100	0.115	0.128	0.144	0.160	0.169	0.198	0.208	

Table A.6. Chart of factors calculated with Barlow equation (see Equation A.4)

Tube OD (in.)	Tube Wall Thickness(in.)																		
	0.010	0.012	0.014	0.016	0.020	0.028	0.035	0.049	0.065	0.083	0.095	0.109	0.120	0.134	0.148	0.156	0.180	0.188	
1/16	0.368	0.450	0.533	0.615	0.771														
1/8						0.533	0.676												
3/16						0.341	0.436	0.629											
1/4						0.248	0.317	0.460	0.625										
5/16							0.248	0.359	0.491										
3/8							0.204	0.294	0.402										
1/2							0.150	0.215	0.292	0.383									
5/8							0.118	0.169	0.229	0.299	0.347								
3/4								0.139	0.188	0.245	0.284	0.331							
7/8								0.118	0.159	0.207	0.240	0.279							
1								0.103	0.138	0.180	0.208	0.241	0.268						
1 1/4									0.109	0.142	0.163	0.189	0.210	0.237	0.264	0.280	0.327		
1 1/2										0.117	0.135	0.156	0.173	0.194	0.216	0.229	0.268	0.281	
2											0.099	0.115	0.127	0.143	0.159	0.168	0.196	0.205	

A.2.2. How does Swagelok calculate the Derating Temperature Factors?

To calculate Swagelok allowable stress data, allowable working pressure data or ultimate tensile stress (UTS) data at elevated temperatures, one needs to multiply the data at room temperature by Swagelok's derating temperature factors given in Table A.3 and published on the web.²³¹ The derating temperature factors are calculated with Equation A.5. This equation was obtained from a personal email with Mark C. Bossart—Swagelok's Technical Service Representative and uses allowable stress data from ASME B31.3 Table A-1 (see Appendix B).

$$\text{Derating factor} = \frac{\text{Stress value at high temperature}}{\text{Stress factor at Min.Temp.}} \quad (\text{A.5})$$

$$(\text{example: } 800F, \text{ Derating factor} = \frac{15.9}{20} = .795 \text{ \% derate})$$

For example, at 1000°F (537°C), the WHTB derating temperature factor will be 0.76 (15.3ksi/20ksi). At 1050°F (566°C), the WHTB derating temperature factor will be 0.755 (15.1ksi/20ksi).

A.3. Catastrophic Failure Pressure and Safety Factor

The catastrophic failure pressure (also referred as the burst pressure) is defined as the pressure at which the vessel will rupture. A large safety factor, defined as the ratio between the catastrophic failure pressure and the allowable working pressure (see equation A.6), is usually implemented in order to avoid serious accidents and ensure safe working conditions.

$$\text{Safety Factor} = \frac{\text{Catastrophic Failure Pressure}}{\text{Allowable Working Pressure}} \quad (\text{A.6})$$

Swagelok components have a safety factor of 3.75 at all working temperatures. A segment from emails exchanged with Byron Gregory, Swagelok’s Senior Account Manager, are presented below (in italics) to show how Swagelok calculates the safety factor.

$$\begin{aligned} & \text{Safety Factor} \\ & = \frac{\text{UTS at Room Temp (Table A – 1) (75000 psi)}}{\text{Allowable Stress at Room Temp (Table A – 1) (20000 psi)}} \quad (\text{A.7}) \\ & = 3.75 \end{aligned}$$

Burst pressure = Safety factor x Allowable Working Pressure of a given size of tubing less any derate. Example: For a 1/2” Outer Diameter and 0.049” thick SS tube, the Allowable Working Pressure is 3700 PSI at 100°F and the Burst Pressure is 3.75 X 3700 = 13,875 PSI. At 800°F: Burst Pressure=3.75 X 2941 =11,030 PSI.

Table A.7 tabulates WHTB catastrophic failure pressures from room temperature to 537°C. The values are calculated as the product of Swagelok safety factor (3.75) and the allowable working pressures of the most vulnerable WHTB component, i.e. the reactor body, at temperature.

Table A.7. WHTB catastrophic failure pressure in ksi calculated with data from Swagelok. The unit kilopound per square inch (ksi) is a scaled unit derived from psi, equivalent to a thousand psi.

T°F	T°C	Swagelok (ksi)
Room T-200	Room T-93	11.63
400	204	11.16
600	315	9.88
800	426	9.18
1000	537	8.84

A.4. Allowances for Pressure

“ . . . Increases in pressure and temperature above the design conditions are permitted for short term events, as long as several conditions are satisfied, one of which is that this maximum allowable working pressure is not exceeded by more than some percentage. . . The following conditions are requirements for use of the variations: ” ²³⁰

- *“The piping system shall not have pressure-containing components of cast iron or other nonductile material.”* [Condition satisfied for the WHTB system].
- *“The nominal pressure stress (hoop stress for straight pipe or, for rated components, the pressure divided by the allowable pressure plus two-thirds the yield strength) must be less than the yield strength of the material.”* [As shown in equation A.8]

$$\begin{aligned} \text{Nominal Pressure Stress} &= \frac{\text{Reactor Pressure}}{\text{Allowable Pressure}} + \frac{2}{3} \text{Yield Strength} & \text{(A.8)} \\ &< \text{Yield Strength} \end{aligned}$$

These conditions are satisfied for the WHTB system. The nominal pressure is calculated using the maximum permissible pressure in the WHTB, which is defined by the burst diaphragm set pressure of 3075 psig (see Section 4.1), and the allowable working pressure and yield strength at the most aggressive experimental conditions reached in the WHTB, i.e. at 550°C. Allowable working pressure and yield strength at elevated temperatures are calculated by multiplying the values at room temperatures (displayed in Table A.2 and in ASME B31.3 Table A-1, (See Appendix B) respectively) by the derating temperature factor at 566°C (550°C is not tabulated by Swagelok, therefore the derating temperature factor was calculated manually). Thus,

allowable working pressure and yield strength at 550°C are 2341 psig (0.755 x 3100 psig) and 22.7 ksi (0.755x 30 ksi) and the nominal pressure stress is 16.5 ksi (Nominal Pressure Stress = 3075/ 2341 + 2/3x22.7 ksi = 16.4 ksi) which is lower than the yield strength of 22.7 ksi. Thus, ASME condition (Nominal pressure <Yield Strength) is satisfied.

- *“The longitudinal stresses must be within the normally permitted limits.”* [ASME condition is satisfied.]

When a capped thin-walled tube or cylinder is subjected to internal pressure, a hoop and longitudinal stress are produced in the wall. The longitudinal stress is a normal stress parallel to the axis of the cylinder and can be expressed as:

$$\sigma_z = \frac{Pd}{4t} \quad (\text{A.9})$$

where P , d and t are the pressure, tube diameter and tube wall thickness, respectively.

The radial stress, σ_r , is stress in a direction coplanar with but perpendicular to the cylinder and can be expressed as:

$$\sigma_r = P \quad (\text{A.10})$$

where P is the pressure.

Assuming the WHTB is a capped cylinder (1 inch diameter and 0.083 inches wall thickness) exposed to the maximum permissible pressure set by the burst diaphragm (3075 psig), the longitudinal and hoop stresses are

$$\sigma_z = \frac{Pd}{4t} = \frac{3075 \text{psig } 1 \text{in}}{4 \cdot 0.083 \text{in}} = 9262.05 \text{psig}$$

$$\sigma_r = P = 3075 \text{psig}$$

The ASME Code presents equations for determining the stress levels in a piping system and provides stress limits for comparison. These theories are maximum principal stress failure theory and maximum shear stress failure theory. The maximum principal stress failure theory states that when one of the mutually perpendicular principal stresses exceeds the yield strength of the material at temperature, failure will occur. The WHTB yield strength at the most severe temperature of 550°C was calculated, as previously stated, by multiplying the value at room temperature by the derating temperature factor at 566°C (0.755). The result of the yield strength is 22700 psi (0.755 x 30 ksi). Thus, the ASME code (principal stresses < material yield strength) is satisfied.

The maximum shear failure theory states that when the maximum shear stress (arithmetic average of largest and smallest principal stresses) exceeds one-half the yield strength of the material at temperature, failure will occur. As the WHTB shear stress (Shear stress = $\frac{7033.13\text{psig}+2335\text{psig}}{2} = 4684.1 \text{ psig}$) does not exceed one-half the yield strength (22.8 ksi/2=11.4 ksi), the ASME condition is satisfied.]

- *“The total number of pressure-temperature variations above the design conditions must be less than 100 over the life of the system (note that this is the number anticipated in the design of the system, not some count taken during operation of the system; the ASME B31.3 Code is for design of new piping systems).”* [ASME condition satisfied for the WHTB. Each reactor is used a maximum of 3 times.]
- *“The maximum pressure must be less than the test pressure; this can be a limitation if*

pneumatic or alternative leak testing was used.” [ASME condition satisfied for the WHTB.

Every new reactor is hydrostatically tested at ~3500 psig (see Section A.6), which is over the maximum permissible pressure of 3075 psig defined by the burst diaphragm rupture pressure.]

“ . . . If the above conditions are satisfied [as in the case of the WHTB], and if the owner approves, the pressure rating or allowable stress (essentially the maximum allowable working pressure) may be exceeded by 33% for events that are not more than 10 hours at any one time nor more than 100 hours per year, and by 20% for events that are not more than 50 hours at any one time nor more than 500 hours per year.”

In conclusion, the WHTB allowable working pressure in the worst case scenario, i.e. at the highest experimental temperature of 550°C, could reach a maximum pressure of 3158 psig (2375 psig x 1.33) for events that are not more than 10 hours at any one time nor more than 100 hours per year.

A.5. Burst Diaphragm Rupture Pressure

“ . . . the Piping Code allows the set pressure to be any value, as long as the maximum pressure during the relieving event, including consideration of potential accumulation (additional pressure buildup beyond the pressure at which the valve opens), does not exceed one of the following two alternatives: a) the maximum relieving pressure permitted by BPVC section VIII, Division 1, or b) the maximum pressure permitted in the allowances for variations provisions of ASME B31.3. However, the owners approval is required for the set pressure to exceed the design pressure.”²³⁰

In conclusion, the WHTB can have a rated burst diaphragm pressure greater than the allowable working pressure as long as the burst pressure does not exceed the maximum pressure plus allowances (3158 psig for events that are not more than 10 hours at any one time nor more than 100 hours per year). A burst diaphragm rated at 3075 psig at 22°C was selected.

The maximum relieving pressure permitted by BPVC section VIII, Division 1 mentioned above does not apply to the WHTB. BPVC section VIII, Division 1 does not cover, among others, *“vessels having an inside diameter, width, height or cross section diagonal not exceeding 6 in., with no limitation on length of vessel or pressure.”*

A.6. Hydrostatic Testing Pressure

According to the 2010 ASME Boiler & Pressure Vessel Code, *“new power boilers or boilers that have been out of service for an extended period of time should be subjected to a hydrostatic test of 1.5 times the design pressure.”*[Since the latter term is not used in the piping system, design pressure is replaced with maximum allowable working pressure (MAWP) for the WHTB system.] *“. . . For new field erected units this is normally conducted by the boiler manufacturer as soon as the pressure parts are assembled.”*²³⁰cBased on a defined allowable working pressure of 2341 psig, every new reactor needs to be tested at a hydrostatic pressure of around 3512 psig (1.5 x 2341psig). Due to the burst diaphragm pressure limitation of 3075 psig, the burst diaphragm needs to be removed and capped during the hydrostatic test.

A.7. Leak Testing Pressure

Finally, periodic leak tests protect against leaks during experiments and ensure the reliability of the experimental pressure data collection. The leak testing pressure is performed under nitrogen the day prior to an experiment and is set at the maximum expected operating pressure for a particular experiment. The procedure is based on ASTM E2930-13²³³ which describes a method for determining the leakage rate of a vessel subject to a positive pressure difference.

Leak testing pressures of experiments with predicted maximum expected operating pressures greater than the maximum pressure of a full nitrogen cylinder (around 2300 psig) are limited to this value.

APPENDIX B. ASME ALLOWABLE STRESS

Table B.1. ASME basic allowable stresses in tension for metals

2017
 CHS
 S-FILES
 REVISION
 (10)

ASME B31.3-2010

Table A-1 Basic Allowable Stresses in Tension for Metals¹ (Cont'd)
 Numbers in Parentheses Refer to Notes for Appendix A Tables; Specifications Are ASTM Unless Otherwise Indicated

Material	Spec. No.	P-No. or S-No. (5)	Grade	UNS No.	Notes	Min. Temp., °F (6)	Specified Min. Strength, ksi		Min. Temp.															
							Tensile	Yield	to 100	200	300	400	500	600										
Stainless Steel (3)(4a) (Cont'd)																								
Pipes and Tubes (2) (Cont'd)																								
18Cr-10Ni-Cb pipe	A 312	8	TP347	S34700	...	-425	75	30	20.0	20.0	20.0	20.0	20.0	19.3										
Type 347 A 240	A 358	8	347	S34700	(30)(36)	-425	75	30	20.0	20.0	20.0	20.0	20.0	19.3										
18Cr-10Ni-Cb pipe	A 376	8	TP347	S34700	(30)(36)	-425	75	30	20.0	20.0	20.0	20.0	20.0	19.3										
18Cr-10Ni-Cb pipe	A 409	8	TP347	S34700	(30)(36)	-425	75	30	20.0	20.0	20.0	20.0	20.0	19.3										
18Cr-10Ni-Cb pipe	A 512	8	TP348	S34800	...	-325	75	30	20.0	20.0	20.0	20.0	20.0	19.3										
Type 348 A 240	A 358	8	348	S34800	(30)(36)	-325	75	30	20.0	20.0	20.0	20.0	20.0	19.3										
18Cr-10Ni-Cb pipe	A 376	8	TP348	S34800	(30)(36)	-325	75	30	20.0	20.0	20.0	20.0	20.0	19.3										
18Cr-10Ni-Cb pipe	A 409	8	TP348	S34800	(30)(36)	-325	75	30	20.0	20.0	20.0	20.0	20.0	19.3										
23Cr-12Ni	A 451	8	CPH10 or CPH10	IP3402	(12)(14)(28)(35)(39)	-325	70	30	20.0	20.0	19.9	19.4	18.9	18.3										
25Cr-20Ni pipe	A 312	8	TP310	...	(28)(29)(35)(39)	-325	75	30	20.0	20.0	20.0	20.0	20.0	18.3										
Type 310S A 240	A 358	8	310S	S31008	(28)(29)(31)(35)(36)	-325	75	30	20.0	20.0	20.0	20.0	20.0	18.3										
18Cr-10Ni-Cb	A 451	8	CP8C	IP2710	(28)	-325	70	30	20.0	20.0	20.0	18.6	17.5	16.6										
18Cr-10Ni-Ti pipe	A 312	8	TP321	S32100	(28)(30)	-425	75	30	20.0	20.0	20.0	20.0	20.0	19.3										
smls < 3/4 in. thk; wid																								
Type 321 A 240	A 358	8	321	S32100	(28)(30)(36)	-425	75	30	20.0	20.0	20.0	20.0	20.0	19.3										
18Cr-10Ni-Ti pipe	A 376	8	TP321	S32100	(28)(30)(36)	-425	75	30	20.0	20.0	20.0	20.0	20.0	19.3										
< 3/8 in. thk																								
18Cr-10Ni-Ti pipe	A 409	8	TP321	S32100	(28)(30)(36)	-425	75	30	20.0	20.0	20.0	20.0	20.0	19.3										
18Cr-10Ni-Ti pipe	A 376	8	TP321H	S32109	(30)(36)	-325	75	30	20.0	20.0	20.0	20.0	20.0	19.3										
< 3/8 in. thk																								
18Cr-10Ni-Ti pipe	A 312	8	TP321H	S32109	...	-325	75	30	20.0	20.0	20.0	20.0	20.0	19.3										
smls < 3/4 in. thk; wid																								
16Cr-12Ni-Mo tube	A 269	8	TP316	S31600	(14)(26)(28)(31)(36)	-425	75	30	20.0	20.0	20.0	19.3	18.0	17.0										
16Cr-12Ni-2Mo pipe	A 312	8	TP316	S31609	(26)(28)	-425	75	30	20.0	20.0	20.0	19.3	18.0	17.0										
Type 316 A 240	A 358	8	316	S31600	(26)(28)(31)(36)	-425	75	30	20.0	20.0	20.0	19.3	18.0	17.0										
16Cr-12Ni-2Mo pipe	A 376	8	TP316	S31600	(26)(28)(31)(36)	-425	75	30	20.0	20.0	20.0	19.3	18.0	17.0										
16Cr-12Ni-2Mo pipe	A 409	8	TP316	S31600	(26)(28)(31)(36)	-425	75	30	20.0	20.0	20.0	19.3	18.0	17.0										
18Cr-3Ni-3Mo pipe	A 312	8	TP317	S31700	(26)(28)	-325	75	30	20.0	20.0	20.0	19.3	18.0	17.0										
18Cr-3Ni-3Mo pipe	A 409	8	TP317	S31700	(26)(28)(31)(36)	-325	75	30	20.0	20.0	20.0	19.3	18.0	17.0										
16Cr-12Ni-2Mo pipe	A 376	8	TP316H	S31609	(26)(31)(36)	-325	75	30	20.0	20.0	20.0	19.3	18.0	17.0										
16Cr-12Ni-2Mo pipe	A 312	8	TP316H	S31609	(26)	-325	75	30	20.0	20.0	20.0	19.3	18.0	17.0										
18Cr-10Ni-Cb pipe	A 376	8	TP347H	S34709	(30)(36)	-325	75	30	20.0	20.0	20.0	20.0	20.0	19.3										
18Cr-10Ni-Cb pipe	A 312	8	TP347	S34700	(28)	-425	75	30	20.0	20.0	20.0	20.0	20.0	19.3										
Type 347 A 240	A 358	8	347	S34700	(28)(30)(36)	-425	75	30	20.0	20.0	20.0	20.0	20.0	19.3										
18Cr-10Ni-Cb pipe	A 376	8	TP347	S34700	(28)(30)(36)	-425	75	30	20.0	20.0	20.0	20.0	20.0	19.3										
18Cr-10Ni-Cb pipe	A 409	8	TP347	S34700	(28)(30)(36)	-425	75	30	20.0	20.0	20.0	20.0	20.0	19.3										
18Cr-10Ni-Cb pipe	A 312	8	TP348	S34800	(28)	-325	75	30	20.0	20.0	20.0	20.0	20.0	19.3										
Type 348 A 240	A 358	8	348	S34800	(28)(30)(36)	-325	75	30	20.0	20.0	20.0	20.0	20.0	19.3										
18Cr-10Ni-Cb pipe	A 376	8	TP348	S34800	(28)(30)(36)	-325	75	30	20.0	20.0	20.0	20.0	20.0	19.3										
18Cr-10Ni-Cb pipe	A 409	8	TP348	S34800	(28)(30)(36)	-325	75	30	20.0	20.0	20.0	20.0	20.0	19.3										
18Cr-10Ni-Cb pipe	A 312	8	TP347H	S34709	...	-325	75	30	20.0	20.0	20.0	20.0	20.0	19.3										
18Cr-10Ni-Cb pipe	A 312	8	TP348H	S34809	...	-325	75	30	20.0	20.0	20.0	20.0	20.0	19.3										

Table B.1. ASME basic allowable stresses in tension for metals (Continued)

ASME B31.3-2010

Table A-1 Basic Allowable Stresses in Tension for Metals¹ (Cont'd)
 Numbers in Parentheses Refer to Notes for Appendix A Tables; Specifications Are ASTM Unless Otherwise Indicated (10)

Basic Allowable Stress, S , ksi (1), at Metal Temperature, T

650	700	750	800	850	900	950	1000	1050	1100	1150	1200	1250	1300	1350	1400	1450	1500	Grade	Spec. No.
Stainless Steel (3)(4a) (Cont'd)																			
Pipes and Tubes (2) (Cont'd)																			
19.0	18.7	18.5	18.3	18.2	18.1	18.1	16.0	12.1	9.1	6.1	4.4	3.3	2.2	1.5	1.2	0.9	0.8	TP347	A 312
19.0	18.7	18.5	18.3	18.2	18.1	18.2	16.0	12.1	9.1	6.1	4.4	3.3	2.2	1.5	1.2	0.9	0.8	347	A 358
19.0	18.7	18.5	18.3	18.2	18.1	18.2	16.0	12.1	9.1	6.1	4.4	3.3	2.2	1.5	1.2	0.9	0.8	TP347	A 376
19.0	18.7	18.5	18.3	18.2	18.1	18.1	16.0	12.1	9.1	6.1	4.4	3.3	2.2	1.5	1.2	0.9	0.8	TP347	A 469
19.0	18.7	18.5	18.3	18.2	18.1	18.1	16.0	12.1	9.1	6.1	4.4	3.3	2.2	1.5	1.2	0.9	0.8	TP348	A 312
19.0	18.7	18.5	18.3	18.2	18.1	18.2	16.0	12.1	9.1	6.1	4.4	3.3	2.2	1.5	1.2	0.9	0.8	348	A 358
19.0	18.7	18.5	18.3	18.2	18.1	18.1	16.0	12.1	9.1	6.1	4.4	3.3	2.2	1.5	1.2	0.9	0.8	TP348	A 376
19.0	18.7	18.5	18.3	18.2	18.1	18.1	16.0	12.1	9.1	6.1	4.4	3.3	2.2	1.5	1.2	0.9	0.8	TP348	A 469
17.9	17.5	17.0	16.5	16.0	15.4	14.9	11.1	8.5	6.5	5.0	3.8	2.9	2.3	1.8	1.3	0.9	0.8	CPH10 or CPH20	A 451
18.2	17.9	17.7	17.4	17.2	16.9	16.7	13.8	10.3	7.6	5.5	4.0	3.0	2.2	1.7	1.3	1.0	0.8	TP310	A 312
18.2	17.9	17.7	17.4	17.2	16.9	16.7	13.8	10.3	7.6	5.5	4.0	3.0	2.2	1.7	1.3	1.0	0.8	310S	A 358
16.2	15.8	15.5	15.2	14.9	14.6	14.3	14.0	12.7	9.7	6.1	4.4	3.3	2.2	1.5	1.2	0.9	0.8	CPH8C	A 451
17.9	17.5	17.2	16.9	16.7	16.5	16.4	16.2	12.3	9.1	6.9	5.4	4.1	3.2	2.5	1.9	1.5	1.1	TP321	A 312
17.9	17.5	17.2	16.9	16.7	16.5	16.4	16.2	12.3	9.1	6.9	5.4	4.1	3.2	2.5	1.9	1.5	1.1	321	A 358
17.9	17.5	17.2	16.9	16.7	16.5	16.4	16.2	12.3	9.1	6.9	5.4	4.1	3.2	2.5	1.9	1.5	1.1	TP321	A 376
17.9	17.5	17.2	16.9	16.7	16.5	16.4	16.2	12.3	9.1	6.9	5.4	4.1	3.2	2.5	1.9	1.5	1.1	TP321H	A 409
17.9	17.5	17.2	16.9	16.7	16.5	16.4	16.2	12.3	9.1	6.9	5.4	4.1	3.2	2.5	1.9	1.5	1.1	TP321H	A 376
17.9	17.5	17.2	16.9	16.7	16.5	16.4	16.2	12.3	9.1	6.9	5.4	4.1	3.2	2.5	1.9	1.5	1.1	TP321H	A 312
16.6	16.3	16.1	15.9	15.7	15.6	15.4	15.3	15.1	12.4	9.8	7.4	5.5	4.1	3.1	2.3	1.7	1.3	TP316	A 269
16.6	16.3	16.1	15.9	15.7	15.6	15.4	15.3	15.1	12.4	9.8	7.4	5.5	4.1	3.1	2.3	1.7	1.3	TP316	A 312
16.6	16.3	16.1	15.9	15.7	15.6	15.4	15.3	15.1	12.4	9.8	7.4	5.5	4.1	3.1	2.3	1.7	1.3	316	A 358
16.6	16.3	16.1	15.9	15.7	15.6	15.4	15.3	15.1	12.4	9.8	7.4	5.5	4.1	3.1	2.3	1.7	1.3	TP316	A 376
16.6	16.3	16.1	15.9	15.7	15.6	15.4	15.3	15.1	12.4	9.8	7.4	5.5	4.1	3.1	2.3	1.7	1.3	TP316	A 469
16.6	16.3	16.1	15.9	15.7	15.6	15.4	15.3	15.1	12.4	9.8	7.4	5.5	4.1	3.1	2.3	1.7	1.3	TP317	A 312
16.6	16.3	16.1	15.9	15.7	15.6	15.4	15.3	15.1	12.4	9.8	7.4	5.5	4.1	3.1	2.3	1.7	1.3	TP317	A 409
16.6	16.3	16.1	15.9	15.7	15.6	15.4	15.3	15.1	12.4	9.8	7.4	5.5	4.1	3.1	2.3	1.7	1.3	TP316H	A 376
16.6	16.3	16.1	15.9	15.7	15.6	15.4	15.3	15.1	12.4	9.8	7.4	5.5	4.1	3.1	2.3	1.7	1.3	TP316H	A 312
19.0	18.7	18.5	18.3	18.2	18.1	18.1	18.1	17.4	14.1	10.5	7.9	5.9	4.4	3.2	2.5	1.8	1.3	TP347H	A 376
19.0	18.7	18.5	18.3	18.2	18.1	18.1	18.1	17.4	14.1	10.5	7.9	5.9	4.4	3.2	2.5	1.8	1.3	TP347H	A 312
19.0	18.7	18.5	18.3	18.2	18.1	18.1	18.1	17.4	14.1	10.5	7.9	5.9	4.4	3.2	2.5	1.8	1.3	347H	A 358
19.0	18.7	18.5	18.3	18.2	18.1	18.1	18.1	17.4	14.1	10.5	7.9	5.9	4.4	3.2	2.5	1.8	1.3	TP347H	A 376
19.0	18.7	18.5	18.3	18.2	18.1	18.1	18.1	17.4	14.1	10.5	7.9	5.9	4.4	3.2	2.5	1.8	1.3	TP347H	A 469
19.0	18.7	18.5	18.3	18.2	18.1	18.1	18.1	17.4	14.1	10.5	7.9	5.9	4.4	3.2	2.5	1.8	1.3	348H	A 312
19.0	18.7	18.5	18.3	18.2	18.1	18.1	18.1	17.4	14.1	10.5	7.9	5.9	4.4	3.2	2.5	1.8	1.3	TP348H	A 376
19.0	18.7	18.5	18.3	18.2	18.1	18.1	18.1	17.4	14.1	10.5	7.9	5.9	4.4	3.2	2.5	1.8	1.3	TP348H	A 409
19.0	18.7	18.5	18.3	18.2	18.1	18.1	18.1	17.4	14.1	10.5	7.9	5.9	4.4	3.2	2.5	1.8	1.3	TP347H	A 312
19.0	18.7	18.5	18.3	18.2	18.1	18.1	18.1	17.4	14.1	10.5	7.9	5.9	4.4	3.2	2.5	1.8	1.3	TP348H	A 312

PRODUCT INFO SHEET

Nanmac Corporation

Quality • Performance • Solutions

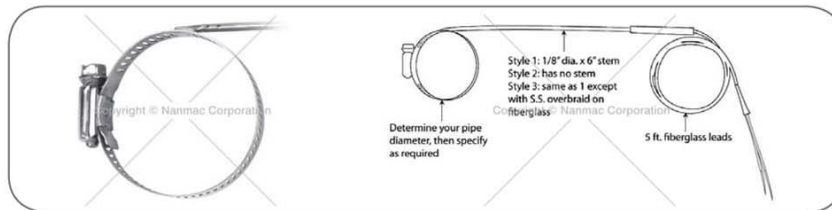
Hose Clamp Thermocouples D6 Series

Our line of hose clamp thermocouples consists of three basic styles.

Style 1: Has an 1/8 inch OD by six inches long stainless steel sheath. The thermocouple wires inside the sheath are insulated with a high temperature mineral oxide insulation. Standard units have a grounded junction which is brazed to the stainless steel pipe clamp. Two (2) versions of the attachment are available: i.e. tangential and perpendicular. Unless otherwise specified, we will furnish the tangential style. The perpendicular style is available upon request at no additional cost. The style 1 units have five feet of fiberglass insulated extension wire connected to the stainless steel sheath.

Style 2: Is the same as style 1, except the stainless steel sheath is deleted. The fiberglass insulated thermocouple wires are welded directly to the stainless steel pipe clamp.

Style 3: Is the same as style 2, except the fiberglass insulated thermocouple wires have a stainless steel overbraid which reduces stray, unwanted electromagnetic pickup and increases lead wire durability.



NOTES:

- All units come with five feet of 20 gage fiberglass insulated extension leads, other materials are available.
- All thermocouples are mounted in a tangential style as shown above, unless a perpendicular style is specified.
- All thermocouples are grounded to hose clamp for fast response.
- All units are available in thermocouple calibration types E, J, K, N & T.
- Various terminations are available, contact us.
- When ordering, specify part number and thermocouple type.
Example: D6-5-J
- To specify (U - ungrounded) junction add the suffix "U" to the part number.
- To specify (P - perpendicular) style versus tangential add suffix "P" to the part number.

Specifications

Pipe OD (in.)	Style 1	Style 2	Style 3
	Part No.	Part No.	Part No.
7/32 → 5/8	D6-5	D6-522	D6-53
3/8 → 1/2	D6-6	D6-62	D6-63
3/8 → 5/8	D6-8	D6-82	D6-83
1/2 → 5/8	D6-10	D6-102	D6-103
5/8 → 3/4	D6-12	D6-122	D6-123
3/4 → 1	D6-16	D6-162	D6-163
1 → 1-1/4	D6-20	D6-202	D6-203
1-1/4 → 1-1/2	D6-24	D6-242	D6-243
1-1/4 → 1-3/4	D6-28	D6-282	D6-283
1-1/2 → 2	D6-32	D6-322	D6-323
1-3/4 → 2-1/4	D6-36	D6-362	D6-363
2-1/16 → 3	D6-40	D6-402	D6-403
2-5/16 → 3-1/4	D6-44	D6-442	D6-443
3 → 3-1/4	D6-52	D6-522	D6-523
3-1/4 → 3-1/2	D6-60	D6-602	D6-603
4 → 4-1/2	D6-68	D6-682	D6-683
4-1/16 → 5	D6-72	D6-722	D6-723
4-5/8 → 5-1/2	D6-80	D6-802	D6-803
5-1/8 → 6	D6-88	D6-882	D6-883
5-7/8 → 6-3/4	D6-104	D6-1042	D6-1043

PO Box 6640
1657 Washington St., Bldg. 3
Holliston MA 01746
www.Nanmac.com
engineering@nanmac.com

Foremost in Temperature Measurement™
NANMAC

US & Canada: 1.800.786.4669
International: 1.508.872.4811
Fax: 1.508.879.5450
info@nanmac.com

Figure C.2. Hose Clamp Thermocouple D6-16-U for Reactor Walls and D6-6-U for Reactor Arms

**APPENDIX D. SOP and JSA 1: Milling Biomass Material into
Finely Divided Particles with a Fritsch Universal Cutting Mill
“Pulverisette 19”**

**Laboratory
Standard Operating Procedures
University of Hawaii at Manoa**

Please fill out and place in your Chemical Hygiene Plan

Milling Biomass Material into Finely Divided Particles with a Fritsch Universal Cutting Mill “Pulverisette 19”

Date: 04/20/2018

Principal Investigator: Scott Q. Turn

Produced By: Maidier Legarra Arizaleta, Trevor Morgan and Scott Turn

Room and Building: AEI 122 (Work Shop)

Phone Number: PI Scott Turn: 808-956-2346

UH Emergency: 808-956-6911 (on campus 66911)/ Emergency: 911

Section 1 Process:

(Check One) Process

Hazardous Chemical

Hazard Class

Summary: This SOP is for the use of the FRITSCH Universal Cutting Mill “Pulverisette 19”. The cutting mill can be used for rapid comminution of soft to medium-hard and fibrous materials. This SOP covers cutting biomass materials into smaller particles.

The main hazards related to the use of the cutting mill are the exposure and handling of small particles of biomass material, the presence of a rotating cutting blade in the mill, and electricity.

A detailed 'Operating Method' that describes how to operate the cutting mill is provided in FRITSCH's manual.
Read the operating instructions carefully before use!

Section 2: Describe Process Hazards, Hazardous Chemical or Hazard Class.

Table 2.1. NFPA Hazard Classification:

Chemical	Health	Fire	Reactivity	Specific
Biomass Material	NA ^a	NA ^a	NA ^a	NA ^a
^a Not Available				

Small particles of biomass material: Follow normal clean up procedures. Inhalation: Can irritate the nose and throat. Skin Contact: May cause mild irritation. Eye Contact: May cause mild irritation. Ingestion: Can irritate the mouth, throat and stomach.

When oxidizable materials such as metals, organic materials, wood, coal, plastic, etc. are ground or sieved, the risk of spontaneous ignition (dust explosion) exists whenever the fine particles exceed concentrations in air of ~30 g/m³, a concentration that would appear like a dense fog (<http://www.dustexplosion.info/dust%20explosions%20-%20the%20basics.htm>).

Hot surfaces: Some surfaces can become hot while operating the mill

Mains Electricity: Standard electrical connections to the cutting mill are provided by the equipment suppliers (see Table 2.2).

Table 2.2. Nominal Voltage, Power Consumption, Power Output, Current Input of Universal cutting mill p-19

Universal cutting mill p-19			
Nominal Voltage	Power Consumption	Power Output	Current Input
115V/1 ~	1700W	1100W	15A

Rotary Cutting Blades: The mill has 'safety interlocks' which prevent the operator from opening the mill to expose the cutting blades while it is in normal operation. A switch on the back of the mill has to set to the correct position to open the mill and access the cutting blades, when the blades are exposed it is NOT possible to start the mill.

Section 3: Personal Protective Equipment.

Safety goggles, nitrile gloves, covered shoes, dust mask, long pants. Wear hearing protection, i.e. ear muffs, while operating the mill. Beware of the sharp edges of the rotor! Wear protective leather work gloves while cleaning the cutting chamber or changing the rotor. If the surface is hot, use heat resistant gloves.

Section 4: Engineering Controls.

Finely divided biomass material: Use local exhaust or general ventilation to minimize exposure to dust. Provide eyewash in work area, if contact or splash hazard exists. Good housekeeping practice is required; e.g., frequent vacuuming of dust during operation to eliminate accumulation.

Mill: Use the instrument indoors only. Do not operate in a confined space. The air must not contain any electrical conductive dust. When applicable, ventilation must be provided or the instrument must be operated under an exhaust hood. Ensure that the machine is fastened securely and the wheels are chocked, as considerable transverse forces do occur. Ensure that there is good access to the cutting mill. Ensure that to the right of the mill there is sufficient space for the upper housing section including the funnel to be opened. Do not block the ventilation louver at the rear. There is a danger of overheating if the louver is blocked. The ambient temperature must be between 0 and 40 °C and the maximum relative humidity of 80% for temperatures up to 31 °C, linearly decreasing down to 50% relative humidity at 40 °C. A maximum of 20 starts per hour are permitted for the mill. The minimum switching cycle is 10 seconds. Jog mode is prohibited, as this may cause damage to the device.

Hot surfaces: If the mill gets too hot it could damage the mill (due to expansion), in addition, it is not good practice to mill biomass at elevated temps as changes in composition may result. If the mill gets too hot to touch then the mill is not being used correctly. When it gets hot, the breaker switch or the motor thermal protection will trip. Wait for it to cool down before restarting. Mill the material in small batches with regular breaks to let it cool down. Cycle and

break times are related to the material being milled, i.e. harder materials will create more heat. The operator needs to regularly check the temp and work accordingly.

Electricity: Inspect electrical cords, plugs, and receptacles prior to each use.

Section 5: Special Handling and Storage Requirements.

Biomass material:

Handling: Only use where there is adequate ventilation. Avoid ignition sources.

Storage: Store in an area that is cool, ventilated.

Mill:

No one other than authorized persons should operate the instrument and it must be serviced and repaired by trained specialists.

Protective equipment must be used as intended and must not be disabled or dismantled.

All protective devices should be regularly checked for completeness and to ensure that they are functioning correctly.

The cutting mill is equipped with a safety interlock for personal protection, which locks the front closure hatch during operation.

The safety switch prevents operation of the cutting mill when the grinding chamber is not closed or when no collecting basin is inserted.

Do not operate the machine without a feed funnel. The feed funnels are mechanical protective devices which permit safe feeding.

When changing the funnel, disconnect the machine from the mains supply and fit the new funnel immediately.

Section 6: Spill and Accident Procedures.

Biomass material: Stop or reduce leak if safe to do so. Collect using shovel/scoop or approved HEPA vacuum and place in a suitable container for disposal. Biomass can be disposed of in a standard trash receptacle.

Small Fire: Fire extinguisher, appropriately trained personnel only. Locate nearest fire extinguishers in AEI 122 (Work Shop) prior to using Fritsch cutting mill.

Large Fire: Leave the room and call (x6-6911 or 911).

Section 7: Waste Disposal Procedures.

Sawdust: Follow normal clean up procedures.

Section 8: Special Precautions Animal Use.

Not Applicable

Section 9: Required Approvals:

EHSO Lab Safety Training, approval from PI. Read and understand all the methods, QRA's, JSA's and SOP's developed for using the mill, the operating manual and the operating instructions of FRITSCH Universal Cutting Mill "Pulverisette 19"

Section 10: Decontamination.

All work surfaces shall be cleaned with paper towel at the end of the mill use and at the end of the day.

Section 11: Designated Areas.

AEI 122 (Work Shop) in location approved by Ryan Kurasaki.

Section 12: Method

Note: Schematic instructions are given in this section. A detailed 'Operating Method' that describes how to operate the cutting mill is provided in FRITSCH's manual. **Read the operating instructions carefully before use!**

To Remove/ Clean Cutting Rotor & Chamber

1. Plug in power and turn switch on back to **HAND** position.
2. Open door hatch with red handle. As you open door, lift top hatch up and to right so that it rests on rubber stop.
3. Pull out rotor, being careful of sharp cutting edges.
4. Reverse procedure for reinstallation. Make sure inside of rotor fully engages drive in on motor shaft.

To Remove/ Replace Outlet Bin

1. Face front of chopper and pull black levers on each side of bin top toward you: Slide it in.
2. To replace, slide bin in and push levers in. Chopper will not run if bin is not pushed all the way in.

To Operate

1. Plug in power cord and turn switch on back to **AUTO** position. Light in green **START** pushbutton will come on. Light indicates only that power is on. It does not indicate that chopper is ready to run, e.g., bin in place.
2. Make sure cutting chamber door is closed and latched, and bin is in place.
3. Push **START** pushbutton. Feed material slowly- do not overload.
4. Push **STOP** button to turn off.
5. Turn switch on back to **OFF** position and unplug power cord when finished.

Problems

- Chopper does not start: consult attachments and/or seek assistance
- Chopper stops while running and light in **STOP** pushbutton comes on: motor was overloaded. Wait for light to turn off then restart.

JOB SAFETY ANALYSIS

Safety Information for the University of Hawaii at Manoa

NAME OF DEPARTMENT: HAWAII NATURAL ENERGY INSTITUTE

Title of Job or Task: Milling Biomass Materials into Finely Divided Particles with Fritsch Universal Cutting Mill “Pulverisette 19”

TASK	HAZARDS	CONTROLS
<p>1. Mill biomass materials into finely divided particles with the FRITSCH Universal Cutting Mill “Pulverisette 19”</p>	<p>Biomass materials can irritate eyes, the nose and throat. If ingested, can irritate mouth, throat and stomach.</p> <p>Biomass materials can burn easily if ignited.</p> <p>Sharp cutting blade in the mill</p> <p>Some surfaces can become hot while operating the mill</p> <p>120 V AC from mains to mill.</p>	<p>PPE</p> <p>Safety glasses or goggles</p> <p>Nitrile Gloves</p> <p>Dust mask fitted to the worker CHECK</p> <p>Long pants</p> <p>Wear protective leather work gloves while cleaning the cutting chamber or changing the rotor. If the surface is hot, use heat resistant gloves.</p> <p>Wear hearing protection (ear muffs) while operating the mill</p> <p>Engineered controls</p> <p>Only handle where there is adequate ventilation. Use local exhaust or general ventilation to minimize exposure to dust.</p> <p>Provide eyewash in work area, if contact or splash hazard exists.</p> <p>Avoid ignition sources</p> <p>Mill: Use the instrument only indoors. Do not operate in a confined space. The air must not contain any electrically conductive dust. When applicable, ventilation must be provided or the instrument must be operated under an exhaust hood. . Ensure that the machine is fastened securely and the wheels are blocked with chocks, as considerable transverse forces do occur. Ensure that there is good</p>

			<p>access to the cutting mill. Do not block the ventilation louver at the rear. There is a danger of overheating if the louver is blocked. The ambient temperature must be between 0 and 40 °C and the maximum relative humidity of 80% for temperatures up to 31 °C, linearly decreasing down to 50% relative humidity at 40 °C. A maximum of 20 starts per hour are permitted for the mill. The minimum switching cycle is 10 seconds. Jog mode is prohibited, as this may cause damage to the device.</p> <p>Beware of hot surfaces! If the mill gets too hot it could damage the mill (due to expansion), in addition, it's not good practice to mill biomass at elevated temps as you can change its composition. If the mill gets too hot to touch then the mill is not being used correctly. When it gets hot, the breaker switch or the motor trips, you need to wait for it to cool down before you can restart it. Mill the material in small batches with regular breaks to let it cool down. Cycle and break times are related to the material being milled, i.e. harder materials will create more heat. The operator needs to regularly check the temp and work accordingly.</p> <p>Inspect electrical cords, plugs, and receptacles prior to each use.</p>
	<p>Required Training: EHSO Lab Safety Training, Read UH Chemical hygiene plan, Specific lab activity training by PI or lab supervisor. Read and understand all the methods, QRA's, JSA's and SOP's developed for using the mill, the operating manual and the operating instructions of FRITSCH Universal Cutting Mill "Pulverisette 19"</p>	<p>Required Personal Protective Equipment (PPE)</p> <p>Safety glasses or goggles</p> <p>Nitrile Gloves</p> <p>Flame resistant lab coat</p> <p>Dust mask</p> <p>Long pants</p> <p>Wear protective gloves while cleaning the cutting chamber or changing the rotor in the mill. Wear ear protection while operating the mill</p>	

Other Information: See Scott Turn, Trevor Morgan and Maider Legarra-Arizaleta for more information on Job Hazard Analysis

JSA Completed By: Maider Legarra-Arizaleta, Scott Turn and Trevor Morgan

Date Created: 04/20/2018

OSHA Reference: _____

For more information about this JSA, contact the *University of Hawaii Environmental Health and Safety Office* <http://www.hawaii.edu/ehso/industrial/> or by phone at 956-3204

APPENDIX E. SOP and JSA 2: Assembly, Loading and Leak

Testing of the Wall Heated Tubing Bomb

Laboratory

Standard Operating Procedures

University of Hawaii at Manoa

Please fill out and place in your Chemical Hygiene Plan

Assembly, Loading and Leak Testing of the Wall Heated Tubing Bomb

Date: 04/20/2018

Principal Investigator: Scott Q. Turn

Produced By: Maidier Legarra Arizaleta, Trevor Morgan, Scott Turn, Lloyd Paredes and Pablo J. Arauzo Gimeno

Room and Building: POST 11/12

Phone Number: PI Scott Turn: 808-956-2346/ POST 11: 808-956-9903/POST 12: 808-956-3790/ UH Emergency: 808-956-6911 (on campus 66911)/ Emergency: 911

Section 1 Process:

(Check One) Process

Hazardous Chemical

Hazard Class

Summary: This SOP covers the loading, assembly and leak testing the Wall Heated Tubing Bomb (WHTB). The main hazards related to the loading, assembly and leak testing the WHTB are potential exposure and handling of chemicals (sawdust and compressed nitrogen (N₂)), exposure to elevated pressures (<3100 psig) and electricity (120 V, 20 Amps).

A detailed 'Operation Method' is provided in section 12. The method refers to additional SOP's provided in separate documents: (1) an SOP for the moisture content analysis of the feed, (2) an SOP for Gas Chromatograph (GC) operation, (3) an SOP for Water Displacement Vessel (WDV) operation and (4) an SOP for volume evaluation.

Useful definitions:

Design Pressure: . . . *the piping system must either be designed to safely contain the maximum possible pressure, considering such factors as failure of control devices and dynamic events such as surge* [what the author refers to as the design pressure], *or be provided with overpressure protection, such as safety relief valve.* (Becht, 2002)

Defining a design pressure value for the WHTB is tricky. One could think that the highest pressure ever observed from all WHTB constant-volume carbonization experiments could serve as a value for the design pressure. Another could think that the design pressure needs to consider all the worst cases scenarios. Since the pressure evolved during the experiments is influenced by the constant-volume carbonization experimental conditions—such as the

pretest nitrogen pressure, the mass loading and the heat treatment temperature. The worst case scenarios would consider the highest possible mass loading—that would be ~240 g/L with birch powder of <0.2mm but higher if we use cellulose powder of 0.05-0.18mm or other fine powder with high packing density; the highest possible pretest nitrogen pressure which would be around 16.5 MPa (achieved if a tank of nitrogen completely full fills the WHTB reactor until equilibrium is achieved); and the highest possible heat treatment temperature—that would be 550°C (note that even though 600°C is specified as the maximum sand bath temperature by the manufacturer, 550°C was the maximum achieved in real life under full power).

In the first case, i.e. when just the peak experimental pressures are considered, the design pressure would be 17.9 MPa (2596 psi). This corresponds to the peak pressure observed during the carbonization of birch at a heat treatment temperature of 550°C, a pretest nitrogen pressure of 0.1 MPa and a standard mass loading of around 130g/L. Note that an experiment that carbonized birch at a heat treatment temperature of 400°C, a pretest nitrogen pressure of 2.17 MPa and a standard mass loading of around 130 g/L also resulted in a great pressure rise with a recorded peak pressure of 17.5 MPa.

In the second case, i.e. when all possible worst case scenarios are taken into account, the design pressure would be magnified to over 40 MPa. The inert gas contribution at 550 °C would be around 23 MPa ($16,5 \text{ MPa} \frac{(550+273)K}{(298+273)K}$, not considering volume changes) and the reaction gases contribution would be over 17.9 MPa (pressure observed under a standard mass loading with atmospheric initial pressure, a higher loading would release higher pressures).

In constant-volume carbonization experiments, it is critical that the experimenter is aware of the risk of overpressurization and ensure that the system is safe. Since installing a system that can hold the hypothetical and highly unlikely pressure of over 40MPa under high temperatures is impractical and costly, overpressure protection was implemented in the form of a burst diaphragm.

Allowable Working Pressure or Maximum Allowable Working Pressure (MAWP):

The concept of maximum allowable working pressure (or allowable working pressure)—even though not used in the ASME B31.3 code—is useful since piping systems are assemblies of standardized parts with allowable working pressures specified by the manufacturer. The WHTB reactor is built from Swagelok components. Swagelok published on the web allowable working pressures for Fractional Stainless Steel Seamless piping at 37°C as a function of the outside diameter and wall thickness (https://www.swagelok.com/downloads/webcatalogs/EN/MS_01-107.PDF, n.d.). This tubing is the one employed in the weakest part of the WHTB reactor, which is the reactor body, and therefore defines the allowable working pressure for the whole WHTB system. The rest of the WHTB parts are stronger due to them being made of tubing of smaller diameter and not being exposed to the severe conditions in terms of temperature and pressure the reactor body is exposed to. To determine allowable working pressure at elevated temperatures, the allowable working pressure at 37°C needs to be multiplied by temperature derating factors also published on the web. Figure 1.1 illustrates the allowable working pressures of the WHTB at temperatures ranging from room temperature to 537°C. Allowable variations above the maximum allowable working pressure are also permitted in the system for some periods of times as long as long as several conditions are satisfied, one of which is that this maximum allowable working pressure is not exceeded by more than some percentage. See section Allowances for Pressure below for a detailed description of permissible pressure variations.

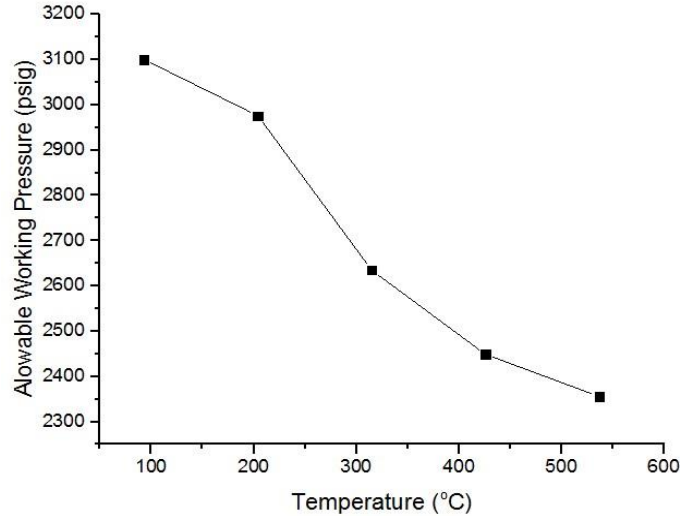


Figure 1.1. Allowable working pressure with temperature for a 1” outer diameter Swagelok tube with a wall thickness of 0.21 cm (0.083”)

Catastrophic Failure Pressure and Safety Factor: The catastrophic failure pressure (also referred as the burst pressure) is defined as the pressure at which the vessel will rupture. Large safety factors between the catastrophic failure pressure and the allowable working pressure are usually implemented in order to avoid serious accidents and ensure safe working conditions

Swagelok components have a safety factor of 3.75 at all working temperatures. Below, fractions from emails exchanged with Byron Gregory, Swagelok’s Senior Account Manager, are presented to show Swagelok’s calculation of this safety factor value and the equation of the catastrophic failure pressure at elevated temperatures

$$\begin{aligned}
 \text{Safety Factor} &= \frac{\text{UTS at Room Temperature (Table A – 1) (75000 psi)}}{\text{Allowable Stress at Room Temperature (Table A – 1) (20000 psi)}} & (1.70) \\
 &= 3.75
 \end{aligned}$$

Burst pressure = Safety factor x Allowable Working Pressure of a given size of tubing less any derate. Example: For a 1/2” Outer Diameter and 0.049” thick SS tube, the Allowable Working Pressure is 3700 PSI at 100°F and the Burst Pressure is 3.75 X 3700 = 13,875. At 800°F: Burst Pressure=3.75 X 2941 =11,030 PSI.

Table 1.1 tabulates WHTB catastrophic failure pressures from room temperature to 537°C. The values are calculated as the product of Swagelok safety factor (3.75) and the allowable working pressures of the most vulnerable WHTB component, i.e. the reactor body, at temperature.

Table 1.1. WHTB catastrophic failure pressure in ksi calculated with data from Swagelok. The unit kilopound per square inch (ksi) is a scaled unit derived from psi, equivalent to a thousand psi.

T°F	T°C	Swagelok (ksi)
Room T-200	Room T-93	11.63
400	204	11.16
600	315	9.88
800	426	9.18
1000	537	8.84

Notice that the WHTB can experience temperatures of 550°C, which lays above the maximum temperature tabulated by Swagelok in Table 1.1. A derating factor of 0.755 has been estimated for temperatures between 537 and 566°C (see Section How Swagelok calculates the Derating Temperature Factors in Maider’s PhD manuscript for details).

Allowances for Pressure:

... *If the above conditions are satisfied [as in the case of the WHTB, see Appendix A1 for conditions], and if the owner approves, the pressure rating or allowable stress (essentially the maximum allowable working pressure) may be exceeded by 33% for events that are not more than 10 hours at any one time nor more than 100 hours per year, and by 20% for events that are not more than 50 hours at any one time nor more than 500 hours per year.*

In conclusion, the WHTB allowable working pressure in the worst case scenario, i.e. at the highest experimental temperature of 550°C, could reach a maximum pressure of 3158 psig (0.755 x 3100psig x 1.33) for events that are not more than 10 hours at any one time nor more than 100 hours per year.

Burst Diaphragm Rupture pressure: ... *the Piping Code allows the set pressure to be any value, as long as the maximum pressure during the relieving event, including consideration of potential accumulation (additional pressure buildup beyond the pressure at which the valve opens), does not exceed one of the following two alternatives a) the maximum relieving pressure permitted by BPVC section VIII, Division 1, or b) the maximum pressure permitted in the allowances for variations provisions of ASME B31.3. However, the owner's approval is required for the set pressure to exceed the design pressure.* (Becht, 2002)

In conclusion, the WHTB can have a burst diaphragm set over the allowable working pressure as long as the pressure does not exceed the maximum pressure plus allowances (3158 psig for events that are not more than 10 hours at any one time nor more than 100 hours per year). A burst diaphragm rated at 3075 psig at 22°C was selected.

The maximum relieving pressure permitted by BPVC section VIII, Division 1 mentioned above does not apply to the WHTB. BPVC section VIII, Division 1 does not cover, among others, "vessels having an inside diameter, width, height or cross section diagonal not exceeding 6 in., with no limitation on length of vessel or pressure."

Hydrostatic Testing Pressure: According to the 2010 ASME Boiler & Pressure Vessel Code, *new power boilers or boilers that have been out of service for an extended period of time should be subjected to a hydrostatic test of 1.5 times the design pressure.* [Since the latter term is not used in the piping system, design pressure is substituted for maximum allowable working pressure (MAWP) for the WHTB system.] *For new field erected units this is normally conducted by the boiler manufacturer as soon as the pressure parts are assembled.* (Becht, 2002) Based on a defined allowable working pressure of 2341 psig (3100psig x 1.33), every new reactor needs to be tested at a hydrostatic pressure of around 3512 psig (1.5 x 2341psig). Due to the burst diaphragm pressure limitation of 3075 psig, the burst diaphragm needs to be removed and capped during the hydrostatic test.

Leak Testing Pressure: Finally, periodic leak tests ensure the absence of leaks during experiments and the reliability of the experimental pressure data collection. The leak testing pressure is performed under nitrogen the day prior to an experiment and is set at the maximum expected operating pressure for a particular experiment. The procedure is based on ASTM E2930-13 which describes a method for determining the leakage rate of a vessel subject to a positive pressure difference. Leak testing pressures of experiments that predict pressures beyond the maximum pressure of full nitrogen tanks (around 2300 psig) are compromised by the tank capacity.

Section 2: Describe Process Hazards, Hazardous Chemical or Hazard Class.

Table 2.1. NFPA Hazard Classification^a Simple Asphyxiant, ^b Not Available:

Chemical	Health	Fire	Reactivity	Specific
Compressed Nitrogen	0	0	0	SA ^a
Sawdust	NA ^b	NA ^b	NA ^b	NA ^b

Sawdust: Inhalation: Can irritate the nose and throat. Skin Contact: May cause mild irritation. Eye Contact: May cause mild irritation. Ingestion: Can irritate the mouth, throat and stomach.

Compressed Nitrogen: Inhalation: No known significant effects or critical hazards. Skin contact: Contact with rapidly expanding gas may cause burns or frostbite. Eye contact: Contact with rapidly expanding gas may cause burns or frostbite. In addition to any other important health or physical hazards, this product may displace oxygen and cause rapid suffocation (when concentrations are sufficient to reduce oxygen levels below 19.5%).

Mains Electricity: All the electrical connections and cables related to the mass balance, laptop, pressure sensors and National instrument (NI) data acquisition equipment are standard 120 V (20 amps) components as provided by the equipment suppliers.

Section 3: Personal Protective Equipment.

Safety glasses or goggles, flame resistant lab coat, nitrile gloves, covered shoes.

Sawdust: NIOSH-approved particulate mask. It is good practice to avoid breathing product; avoid skin and eye contact and wash hands after handling.

Section 4: Engineering Controls.

Compressed Nitrogen: General laboratory ventilation is sufficient to control worker exposure to airborne contaminants in the present location (POST 11). Install a 'flow restrictor' valve in the line from the nitrogen cylinder to the WHTB to prevent excessive release of nitrogen into the environment.

Use appropriate tools to open and close valves in order to avoid direct contact of the experimenter with the pressurized reactor and lines. Ensure pressure does not exceed the burst disk pressure.

Activate LabVIEW alarms to indicate when the reactor pressure is 100 psig over the test pressure or 200 psig below the burst disk pressure.

Perform experiment inside the welded steel-Polycarbonate structure shown in Figure 4.1. Stay behind the protective polycarbonate panel in Figure 4.2 during experiments. The wall heated tubing bomb (WHTB) reactor is housed in a structure made of a welded steel frame with *Hygard CG375 containment grade sheet—2 -ply polycarbonate laminate 3/8" thick that meets ASTM F 1915 and HP White TP 0500*—covering each side of the structure, see Figure 4.1.



Figure 4.1. Welded steel-polycarbonate structure for enclosing WHTB during an experiment

During the safety review (Sept 2016) one of the reviewers asked whether the polycarbonate (PC) sheet provides sufficient protection for the reaction conditions being used in the WHTB experiments. In particular the reviewer asked that we compare the impact resistance of the PC with the stored energy in the WHTB reactor at the most extreme test conditions, and improve the shielding if necessary.

The stored energy in the WHTB reactor was determined for the most extreme test conditions envisioned for the experimental campaign (max. pressure ~17.9 MPa (2596 psi) @ 550°C). The stored energy was determined according to the method outlined by the Lawrence Livermore National Laboratory (LBL), using the equation provided in Appendix E of the following link: http://www2.lbl.gov/ehs/pub3000/CH7.html#_Appendix_C:_Safety. The stored energy (U) is derived using equation 4.1:

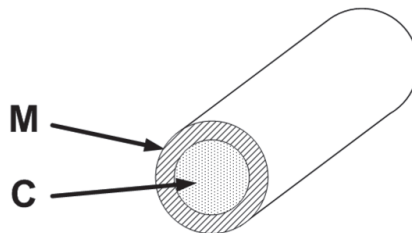
$$U = \frac{P_h V_h}{\gamma - 1} \left[1 - \left(\frac{P_l}{P_h} \right)^{\frac{\gamma - 1}{\gamma}} \right] \quad (4.1)$$

Where: V_h = The volume of the vessel (0.2184L for the WHTB); P_h = The absolute high pressure contained in the vessel; P_l = The absolute low pressure surrounding the vessel. Generally this would be one atmosphere; γ = The adiabatic exponent or ratio of specific heats, C_p/C_v . The value is 1.666 for monatomic gases such as argon and helium; 1.4 for diatomic gases such as nitrogen, oxygen, hydrogen, and air; and variable for polyatomic gases such as methane, water, and carbon dioxide, but generally very nearly 1.3.

Using equation 4.1, the stored energy in the WHTB reactor is 1887 psi ft.lbs, which is equivalent to ~0.5 g of TNT. According to LBL stored energies in excess of 73750 ft.lbs (100 kJ) are considered high hazard.

An attempt was made to relate the stored energy in the WHTB reactor with the impact resistance of the PC sheet. Peer-reviewed articles on the design of blast shields and methods for calculating the force of impacts from explosions were referred to as a basis for the comparison (Moore) (Lozano & Petr, 2015). To determine the force of an impact it is necessary to know the mass of the projectile and its velocity. The Gurney equation (4.2) can be used to derive the initial velocity of fragments generated by detonation of an explosive device.

$$\frac{V_0}{\sqrt{2E}} = \left(\frac{M}{C} + \frac{1}{2} \right)^{-\frac{1}{2}} \quad (2)$$



(4.71)

Where,

$V_0 \equiv$ Initial Fragment Velocity (m/s).

$\sqrt{2E} \equiv$ Gurney Constant for a given explosive (m/s).

$M \equiv$ Mass of the accelerated shell or sheet of material (kg).

$C \equiv$ Explosive charge mass (kg).

Upon studying the literature it became apparent that there is no way to make a direct comparison between the stored energy in the WHTB reactor (as it is currently designed) with the force of an impact due to an uncontrolled release of the stored energy. To make this comparison a number of assumptions are required, specifically it is necessary to define the mass of a projectile which isn't readily apparent for our situation. In addition, the Gurney equation is for an explosion which is not the same phenomenon as would be experienced by rupture of the WHTB reactor vessel. In the case of the WHTB reactor a significant amount of the stored energy would be consumed by the rupturing of the vessel (the amount of energy is unknown and would be significantly different depending how the vessel ruptured). In addition, it is extremely unlikely that the entire vessel would fragment as in the case of an explosive device.

Furthermore, it should not be possible for the WHTB reactor to rupture or fragment under the conditions being used, i.e. the maximum pressure expected during an experiment is ~2596 psi. The maximum allowable working pressure is 3100 psig at 37°C and 2356 psig at 537°C, and the catastrophic failure pressure is 11625 psig at 37°C and 8835 psig at 537°C. Therefore the primary engineered controls to prevent rupture of the vessel are (1) the selection of appropriately sized tubing, and (2) sensors to monitor temperature and pressure to prevent the system being over-pressurized and audible alarms to notify personnel when reactor conditions are approaching levels beyond those prescribed for the experiment.

The secondary engineered control is in the form of an appropriately rated burst disk (currently set at 3075 psi at 22°C) with the outlet directed into a ~5.4L volume of water to act as a shock absorber that will cool and disperse the energy of the escaping gases. The only way the WHTB reactor could rupture in an uncontrolled manner is if the burst disk failed to rupture (which is virtually impossible in this case) and if the temperature and pressure of the system ran out of control (this is also highly unlikely considering the design of the system and the control measures). The only other possibility of uncontrolled release of the stored energy is that a part of the WHTB reactor is seriously fatigued, and this is also highly unlikely due to regular inspection of the system, the type of materials used, regular replacement of the reactor after three uses, and a leak test before each experiment at the maximum pressure that would be achieved during the test.

Therefore the PC sheeting on the structure housing the WHTB reactor is unlikely to be needed for protection against projectiles coming off the reactor due to rupture or fragmentation, it is instead a tertiary level of protection from splashes of heated sand bath solids or hot pyrolysis gases, liquid and solids that may leak from the reactor in the event of the vessel rupturing, however improbable.

Nonetheless, to provide additional protection against a catastrophic failure of the primary and secondary engineered controls it was decided that a PC screen would be installed in the structure housing the WHTB reactor. Hygard CG375 containment grade sheet (3/8" thick), 2-ply polycarbonate laminate that meets ASTM F 1915 was installed for this purpose. A description of the Hygard CG375 sheet obtained from the supplier is provided below:

"Makrolon Hygard stands for transparent, multilayer laminated polycarbonate sheets. They meet all security requirements with regard to protection against forced entry and ballistic impact. The CG (containment glazing) grades are particularly suitable for protection against forced entry with heavy tools such as sledge hammers and axes. Containment grade Hygard CG375 containment grade sheet is a 3/8", 2-ply polycarbonate laminate that meets ASTM F 1915 and HP White TP 0500. Unlike glass-clad products, this all-polycarbonate laminate resists spalling and white-out after repeated high force impacts, an advantage in maintaining visibility of a threat during an attack. Hygard CG375 sheet has a seven (7) year Limited Product Warranty against coating failure, yellowing, and hazing."

As a final level of protection for the operator of the WHTB reactor an additional shielding screen was constructed using a wooden frame with 1/4" Makrolon GP sheet, this screen is located between the reactor housing structure and the computer used to monitor the reaction conditions, see Figure 4.2. This screen was already in use before the upgrade described in this document. The 1/4" PC sheet is the Makrolon GP (general purpose) type purchased locally from Min Plastics and Supply but also marketed by Covestro of Sheffield, MA, USA. According to data sheet provided by Covestro, the impact resistance of a 1/8" thick sheet of Makrolon GP is >47 ft.lbs based on ASTM D3763 where a 1" diameter steel dart is used. Covestro was contacted to obtain information for the 1/4" thick sheet. The impact resistance of the 1/4" PC sheet is >96 ft.lbs. For context, the impact from 0.22 caliber bullet fired from a pistol (handgun) is ~117 ft.lbs (Wikipedia) and when fired from a long rifle ~135 ft.lbs (shooterscalculator.com). These values confirm the information from the PC sheet supplier who informed us that a 0.22 caliber bullet would pass through the 1/4" Makrolon GP sheet.



Figure 4.2. Polycarbonate screen shield

Sawdust: Use a local exhaust ventilation and enclosure, if necessary, to control amount in the air. Provide eyewash in work area, if contact or splash hazard exists.

Electricity: Inspect electrical cords, plugs, and receptacles prior to each use.

Section 5: Special Handling and Storage Requirements.

Sawdust:

Handling: Avoid generating dusts. Only use where there is adequate ventilation. Avoid ignition sources. Use heat resistant gloves when using the oven.

Storage: Store in an area that is cool, ventilated.

Compressed Nitrogen:

Storage: Store in accordance with local regulations. Store in a segregated and approved area. Store away from direct sunlight in a dry, cool and well-ventilated area. Keep container tightly closed and sealed until ready for use.

Cylinders should be stored upright, with valve protection cap in place, and firmly secured to prevent falling or being knocked over. Cylinder temperatures should not exceed 52 °C (125 °F).

Handling: Put on appropriate personal protective equipment. Contains gas under pressure. Avoid contact with eyes, skin and clothing. Avoid breathing gas. Empty containers retain product residue and can be hazardous. Do not puncture or incinerate container. Use equipment rated for cylinder pressure. Close valve after each use and when empty. Protect cylinders from physical damage; do not drag, roll, slide, or drop. Use a suitable hand truck for cylinder movement.

Section 6: Spill and Accident Procedures.

Sawdust: Stop or reduce leak if safe to do so. Avoid generating dust. Collect using shovel/scoop or approved HEPA vacuum and place in a suitable container for disposal.

Compressed Nitrogen:

No action shall be taken involving any personal risk or without suitable training. Evacuate surrounding areas. Keep unnecessary and unprotected personnel from entering. Avoid breathing gas. Provide adequate ventilation. Wear appropriate respirator (Self-Contained Breathing Apparatus SCBA) when ventilation is inadequate.

Small spill: Shutoff source of gas. Stop leak if without risk. Contact emergency personnel (see Phone number information above) if necessary.

Large spill: Immediately contact emergency personnel (see Phone number information above). Stop leak if without risk. Note: Call supplier for emergency contact information (AirGas 24-hour phone 1-866-734-3438).

Small Fire: Fire extinguisher, appropriately trained personnel only. There are fire extinguishers in POST 11 and POST 12 indicated as FE on the floor map below.

Large Fire: Leave the room and call (956-6911).

Section 7: Waste Disposal Procedures.

Sawdust: Follow normal clean up procedures.

Compressed Nitrogen:

Unused product/ empty container: Return cylinder and unused product to supplier. Do not attempt to dispose of residual or unused quantities.

Disposal: For emergency disposal, secure the cylinder and slowly discharge gas to the atmosphere in a well ventilated area or outdoors.

Section 8: Special Precautions Animal Use.

Not Applicable

Section 9: Required Approvals:

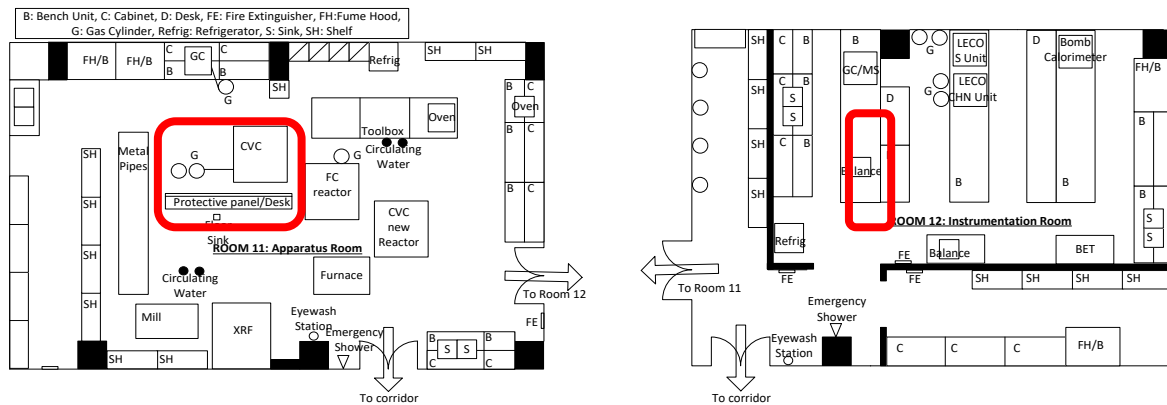
EHSO Lab Safety Training, approval and training from PI or lab supervisor. Read and understand all methods, QRA's, JSA's and SOP's developed for the operation of the Assembly, Loading and Leak Testing of the Wall Heated Tubing Bomb.

Section 10: Decontamination.

All work surfaces will be cleaned with paper towel at the end of the test and at the end of the day.

Section 11: Designated Areas.

The R³ Lab Room 11 and Room 12 framed sections in the maps below are designated, respectively, for leak testing and reactor loading.



Section 12. Method:

1. Load the WHTB: An example of a Loading Form is given in Figure 13.1. The Loading Form is divided into five tables: Table 1 with data from the *Proposal Conditions*, Table 2 with data from the *Reactant Moisture Content Analysis*, Table 3 with data from the *Solid Reactant Feed Bomb Load* and finally, Table 4 with data of the *Reactant Moist Mass* and Table 5 with the *Volume Evaluation*.

Fill Table 3 in the Loading Form following the instructions in section 13.

2. See SOP for moisture content analysis of the feed (ASTM E871-82): To analyze the feed moisture content, fill in Table 2 in the Loading Form following the moisture content SOP.
3. See SOP for Gas Chromatograph (GC) operation: Prepare GC, condition GC, check air leaks and fix them if necessary by following the corresponding SOP.
4. See SOP for Water Displacement Vessel (WDV) operation: Follow the WDV SOP to fill the WDV with water in order to displace the gases inside.
5. See SOP for WHTB Volume Evaluation: Determine the WHTB volume by following the corresponding SOP.
6. Leak testing. Figure 12.1 shows a complete WHTB diagram

- 6.1 Ensure that the WHTB is mounted in the welded steel-polycarbonate structure. Connect the WHTB Assembly to the Nitrogen Charging System at QD1. Do NOT immerse the reactor in the sandbath. Confirm the valve positions throughout the system match those in Table 12.1. Every time a valve or regulator position is modified a new Table will be presented.

Table 12.1.

V0	V1	V2	V3	V4	V5	Reg1 Inlet	Reg1 Outlet
Closed	Closed	Closed	Closed	Closed	Closed	0 psig	0 psig

- 6.2 Open V₀. The pressure at the inlet of regulator 1 will increase

Table 12.2.

V0	V1	V2	V3	V4	V5	Reg1 Inlet	Reg1 Outlet
Open	Closed	Closed	Closed	Closed	Closed	N ₂ Supply Cylinder Pressure	0 psig

- 6.2.1 Compare the pressure shown on the Reg1 inlet with the experiment pressure requirements.

- 6.2.1.1 If the pressure shown on the Reg1 inlet is not sufficient to reach the experiment pressure requirements (Leak Testing Experimental Pressure), the N₂ supply cylinder must be replaced; (see SOP for gas cylinder replacement). After cylinder replacement, return to Step 6.1.

- 6.2.1.2 If sufficient pressure exists in the N₂ supply cylinder, turn the Reg1 knob clockwise until the pressure on the outlet of Reg1 equals the experiment pressure requirements

Table 12.3.

V0	V1	V2	V3	V4	V5	Reg1 Inlet	Reg1 Outlet
Open	Closed	Closed	Closed	Closed	Closed	N ₂ Supply Cylinder Pressure	Leak Testing Experimental Pressure

- 6.3 Apply Snoop to valves and reactor junctions.

6.4 Fully open V1 and V2 and slowly open V4 until the reactor pressure reaches 100 psig

Table 12.4.

V0	V1	V2	V3	V4	V5	Reg1 Inlet	Reg1 Outlet
Open	Open	Open	Closed	Open	Closed	N ₂ Supply Cylinder Pressure	Leak Testing Experimental Pressure

6.5 Close V4 and inspect system for leaks

Table 12.5.

V0	V1	V2	V3	V4	V5	Reg1 Inlet	Reg1 Outlet
Open	Open	Open	Closed	Closed	Closed	N ₂ Supply Cylinder Pressure	Leak Testing Experimental Pressure

6.5.1 If no snoop bubbles appear, continue to 6.6

6.5.2 If bubbles appear, the reactor is leaking. Before attempting to fix any leaks, depressurize the reactor and lines by turning knob of regulator counterclockwise until completely disengaged and by slowly opening V3 and V5.

Table 12.6.

V0	V1	V2	V3	V4	V5	Reg1 Inlet	Reg1 Outlet
Open	Open	Open	Open	Closed	Open	N ₂ Supply Cylinder Pressure	>Leak Testing Experimental Pressure

With a depressurized reactor, fix leaks by tightening the corresponding junction (or if necessary untightening, disconnecting, cleaning and retightening). Restart from 6.5. If leaks are not fixed after two attempts, replace the leaking connection (you may need to reload a new reactor and start over again from 6.1).

6.6 Slowly open V4 until the reactor pressure reaches the leak testing pressure while inspecting system for leaks

Table 12.7.

V0	V1	V2	V3	V4	V5	Reg1 Inlet	Reg1 Outlet
Open	Open	Open	Closed	Open	Closed	N ₂ Supply Cylinder Pressure	Leak Testing Experimental Pressure

6.6.1 If bubbles appear, the reactor is leaking. Go back to 6.5.2

6.6.2 If no snoop bubbles appear at the leak test pressure, close V4 and wait 1h. The reactor is successfully leak tested if no bubbles appear and the reactor can hold the leak test pressure during the 1h.

Table 12.8.

V0	V1	V2	V3	V4	V5	Reg1 Inlet	Reg1 Outlet
Open	Open	Open	Closed	Closed	Closed	N ₂ Supply Cylinder Pressure	Leak Testing Experimental Pressure

6.6.3 Finalize the leak test by closing V0, slowly opening V3 and V5 to avoid gas hammering while depressurizing the reactor and turning regulator 1 knob counterclockwise.

Table 12.9.

V0	V1	V2	V3	V4	V5	Reg1 Inlet	Reg1 Outlet
Closed	Open	Open	Open	Closed	Open	0 psig	0 psig

6.7 Close V1, V2, V3 and V5 once depressurized.

Table 12.8.

V0	V1	V2	V3	V4	V5	Reg1 Inlet	Reg1 Outlet
Closed	Closed	Closed	Closed	Closed	Closed	0 psig	0 psig

7. Perform volume evaluation (see SOP 6: Volume Evaluation of the Wall Heated Tubing Bomb)
8. Install three clamp thermocouples (TC7, TC8 and TC11). TC7 and TC8 in the middle of the WHTB bodies (see Fig 12.1) and TC11 in the tubing arms.
9. Connect all thermocouple plugs (From TC1 to TC11) to the extension wires connected to LabVIEW.
10. Pressurize WHTB ~ 100 psig over the desired initial nitrogen experimental pressure to keep the biomass under an inert atmosphere and be ready for experiments.
 - o Ensure that the WHTB is mounted in the welded steel-polycarbonate structure. Connect the WHTB Assembly to the Nitrogen Charging System at QD1. Do NOT immerse the reactor in the sandbath. Confirm the valve positions throughout the system match those in Table 12.9.

Table 12.9

V0	V1	V2	V3	V4	V5	Reg1 Inlet	Reg1 Outlet
Closed	Closed	Closed	Closed	Closed	Closed	0 psig	0 psig

- Open V₀. The pressure at the inlet of regulator 1 will increase

Table 12.10

V0	V1	V2	V3	V4	V5	Reg1 Inlet	Reg1 Outlet
Open	Closed	Closed	Closed	Closed	Closed	N ₂ Supply Cylinder Pressure	0 psig

- Turn the Reg1 knob clockwise until the pressure on the outlet of Reg1 reaches ~ 100 psig

Table 12.11.

V0	V1	V2	V3	V4	V5	Reg1 Inlet	Reg1 Outlet
Open	Closed	Closed	Closed	Closed	Closed	N ₂ Supply Cylinder Pressure	~ 100 psig

- Fully open V₁ and V₂ and slowly open V₄ until the reactor pressure reaches 100 psig

Table 12.12.

V0	V1	V2	V3	V4	V5	Reg1 Inlet	Reg1 Outlet
Open	Open	Open	Closed	Open	Closed	N ₂ Supply Cylinder Pressure	~ 100 psig

- Close V₄

Table 12.13.

V0	V1	V2	V3	V4	V5	Reg1 Inlet	Reg1 Outlet
Open	Open	Open	Closed	Closed	Closed	N ₂ Supply Cylinder Pressure	Leak Testing Experimental Pressure

- Finalize the leak test by closing V₀, slowly opening V₃ and V₅ to avoid gas hammering while depressurizing the reactor and turning regulator 1 knob counterclockwise.

Table 12.14.

V0	V1	V2	V3	V4	V5	Reg1 Inlet	Reg1 Outlet
Closed	Open	Open	Open	Closed	Open	0 psig	0 psig

- Close V₁, V₂, V₃ and V₅ once depressurized.

Table 12.15.

V0	V1	V2	V3	V4	V5	Reg1 Inlet	Reg1 Outlet
Closed	Closed	Closed	Closed	Closed	Closed	0 psig	0 psig

Ensure pressure transducer PT2 reads zero and disconnect Quick Disconnect QD1. The WHTB is ready for the experiment.

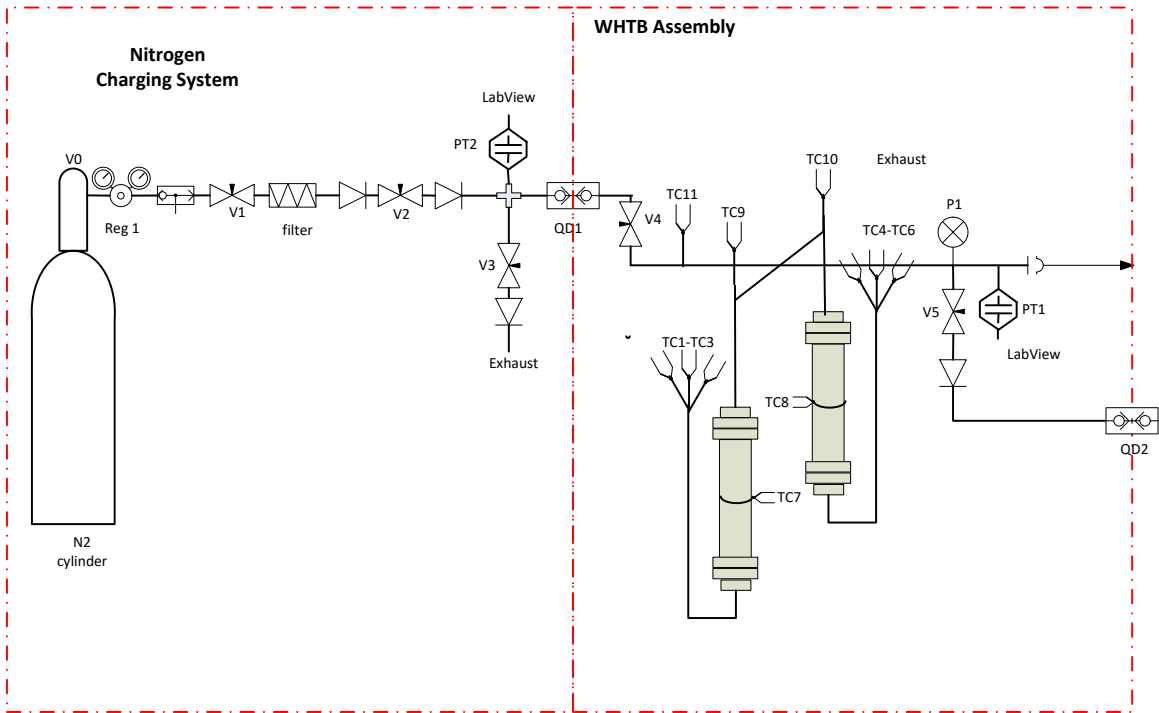
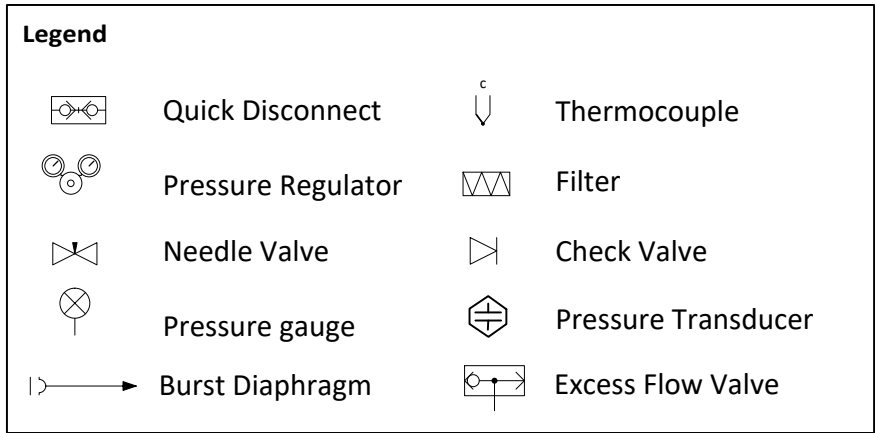


Figure 12.1. WHTB diagram

Section 13. Loading Form

WHTB Pyrolysis Setup

Table 1. Proposal Conditions

Date:	Pyrolysis Feed:	Packing:
Pressurizing Gas:	Manufacturer:	Nominal Bomb Pressure [psig]:
Experimenters:	Lot Number:	Nominal Sand Bath Temperature [°C]:

Table 2. Reactant Moisture Content Analysis

Tare mass [g]:	Tare and sample mass [g]:	Moisture Content [%]: #DIV/0!
Final mass 1 [g]:	Valid final mass [g]: 0.000	
Final mass 2 [g]:		
Final mass 3 [g]:		
Final mass 4 [g]:		
Final mass 5 [g]:		
Final mass 6 [g]:		
Final mass 7 [g]:		

Table 3. Solid Reactant Feed Bomb Load

	Cork	Reactor Body New	TC Bottom New	Reactor Top No Cap	Filter Paper	Maximum Reactants	Sample Reactants	Remaining Reactants	SS Screen	Stem	Antiseize	mass [g]
1	X											
2	X	X										
3	X		X									
4	X							X				
5	X			X								
6	X	X	X									
7	X	X	X					X				
8	X	X	X	X				X				
9	X				X							
10	X				X	X						
11	X				X		X					
12	X			X				X				
13	X			X				X		X		
14	X	X	X	X		X		X				
15	X								X			

Table 4. Reactant Moist Mass [g]

by filter paper difference	10-11	0.00
by reactor, SS screen, TC bottom and reactor top difference	14-8	0.00
Experimental Mass		0.00

Table 5. Void Volume Evaluation

Iteration	VOLUME EVALUATION	Initial Cart Pressure Pcart1 [psig]	Initial Reactor Pressure Preact1[psig]	Room T [degC]	Room Pressure [mmHg]	Final Cart Pressure Pcart1 [psig]	Final Reactor Pressure Preact1 [psig]	LEAK TEST	DOM start m3	DOM End m3	BACKFILL FROM SEQUESTERED VOLUME	Sequestered Volume Pressure [psig]	Emptied Reactor Pressure [psig]	Backfilled reactor and Sequestered Pressure [psig]
1														
2														
3														
4														
5														

Last Modified 3/18/2017

Figure 13.1. Loading Form

Instructions for Table 3 in Loading Form

The components mentioned in the instructions are shown and labeled in Figure 13.2.

1. Weigh cork. The cork is NOT part of the assembled reactor. It serves as a weight reference and holds the reactor and filter paper upright.
2. Weigh cork plus reactor body
3. Weigh cork plus thermocouple
4. Weigh cork plus stainless steel (SS) screen
5. Weigh cork plus reactor top
6. Weigh cork, reactor body and TC
7. Weigh cork, reactor body, TC and SS screen
8. Weigh cork, reactor body, TC, SS screen and reactor top
9. Weigh cork plus filter paper. The filter is NOT part of the assembled reactor. It will hold the biomass in excess.
10. Weigh cork plus the filter paper with around 20-30 grams of sawdust biomass taken from the batch (named *maximum reactants* in Table 3 of the Loading Form)
11. Away from the balance, with the reactor body and TC assembled; carefully pour biomass from the filter paper into the reactor body until 0.5 inches from its top. Using a funnel to pour biomass will prevent losing sample and tapping the reactor will compact the biomass and will allow more sample mass to be loaded. When the loading step is finished (with an approximate weight of 14g of sawdust in the reactor body in a standard experiment), weigh cork plus the filter paper with the remaining reactants
12. Weigh the cork, reactor top and the SS screen with the SS screen inserted in the reactor top.
13. Spread an anti-seize paste on the threads of the reactor top in an attempt to reduce wear and increase the number of times the reactor can be reused. Weigh the cork, reactor top with the anti-seize paste, and SS screen
14. Hand tighten reactor top and reactor body. Weigh cork with the assembled reactor, i.e. with the TC in the reactor body, the SS screen on top, the biomass loaded and the reactor top hand tightened. Finalize the process by tightening the reactor top with a torque wrench. The reactor is now ready to be leak tested.
15. Weigh the stem

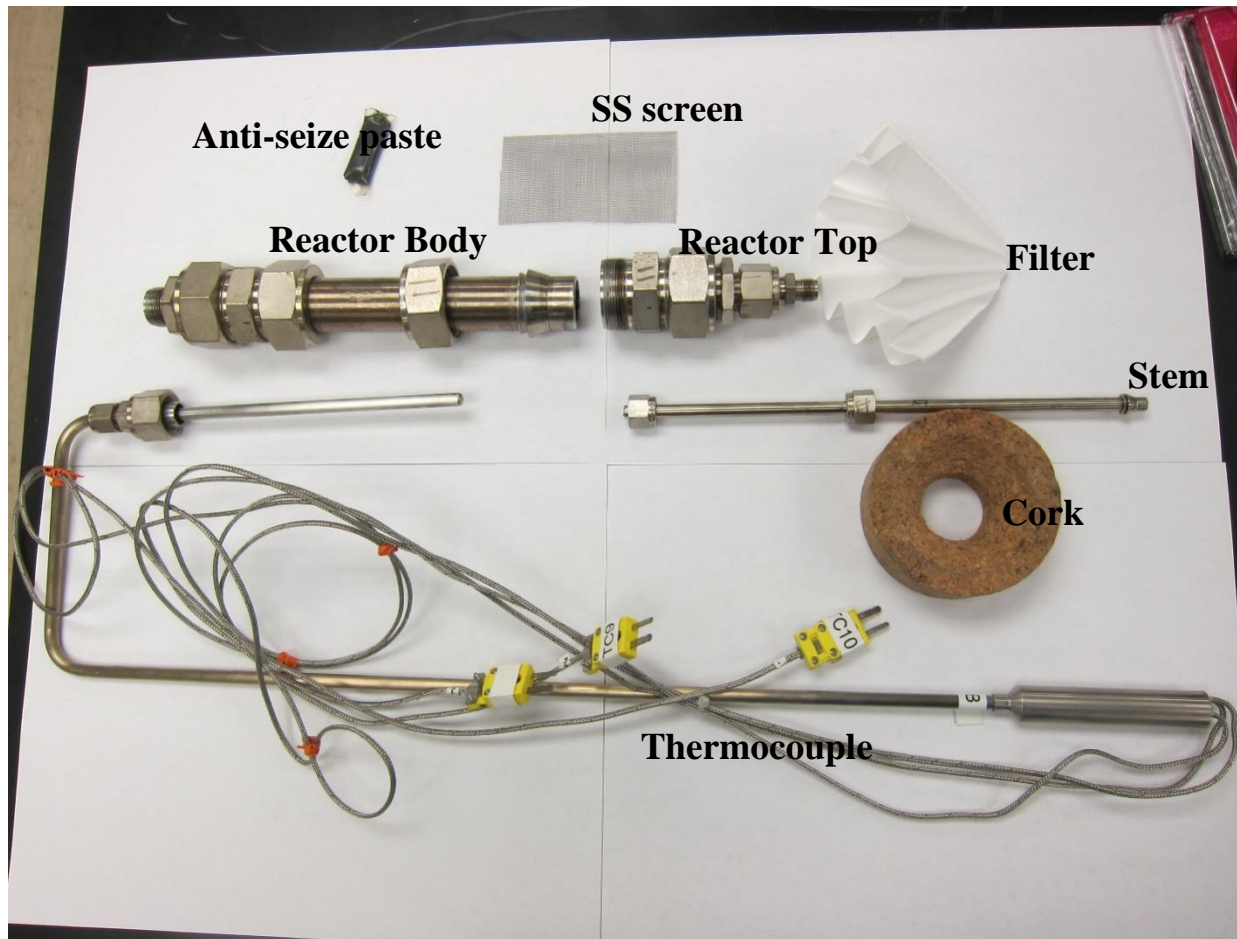


Figure 13.2 The Wall Heated Tubing Bomb (WHTB) components.

APPENDIX 1. Allowances for Pressure requirements:

The following conditions are requirements for use of the variations according to the ASME (Becht, 2002):

- The piping system shall not have pressure-containing components of cast iron or other nonductile material.
- The nominal pressure stress (hoop stress for straight pipe or, for rated components, the pressure divided by the allowable pressure plus two-thirds the yield strength) must be less than the yield strength of the material.
- The longitudinal stresses must be within the normally permitted limits.
- The total number of pressure-temperature variations above the design conditions must be less than 100 over the life of the system (note that this is the number anticipated in the design of the system, not some count taken during operation of the system; the ASME B31.3 Code is for design of new piping systems).
- The maximum pressure must be less than the test pressure; this can be a limitation if pneumatic or alternative leak testing was used.

Before continuing with the requirements, let's examine the mentioned conditions in our WHTB

- The WHTB does not contain nonductile material components.
- The nominal pressure stress in our WHTB (the pressure divided by the allowable pressure plus two-thirds the yield strength) must be less than the yield strength of the material, i.e.,

$$\text{Nominal Pressure Stress} = \frac{\text{Reactor Pressure}}{\text{Allowable Pressure}} + \frac{2}{3} \text{Yield Strength} < \text{Yield Strength} \quad \text{A. 3}$$

The nominal pressure is calculated using a reactor pressure equal to the maximum permissible pressure in the WHTB, which is defined by the burst diaphragm set pressure of 2900 psig, and using the allowable working pressure and yield strength at the most aggressive experimental conditions reached in the WHTB, i.e. at 400°C.

Allowable working pressure and yield strength at elevated temperatures are calculated by multiplying the values at room temperatures from ASME B31.3 Table A-1 (See Appendix A.3) by the Swagelok derating temperature factor at 426°C (closest value to 400°C (https://www.swagelok.com/downloads/webcatalogs/EN/MS_01-107.PDF.) Thus, allowable working pressure and yield strength at 426 °C are 2449 psig (0.76 x 3100 psig, see also Figure 1) and 22.8 ksi (0.76 x 30ksi) and the nominal pressure stress is 16.38 ksi (Nominal Pressure Stress = 2900/2449 + 2/3x22.8ksi = 16.38ksi). Thus, ASME condition (Nominal pressure < Yield Strength) is satisfied.

- The longitudinal stresses are within the normally permitted limits.

When a capped thin-walled tube or cylinder is subjected to internal pressure, a hoop and longitudinal stress are produced in the wall.

The longitudinal stress is a normal stress parallel to the axis of the cylinder and can be expressed as:

$$\sigma_z = \frac{Pd}{4t} \quad A.4$$

where P, d and t are the pressure, tube diameter and tube thickness respectively.

The radial stress is a stress in direction coplanar with but perpendicular to the cylinder and can be expressed as:

$$\sigma_r = P \quad A.5$$

where P is the pressure.

Assuming our WHTB is a capped cylinder with the reactor body dimensions (1 inch diameter and 0.083 inches wall thickness) that is exposed to the maximum permissible pressure set by the burst diaphragm equal to 2900 psig, the longitudinal and hoop stresses are

$$\sigma_z = \frac{Pd}{4t} = \frac{2900\text{psig} \cdot 1\text{in}}{4 \cdot 0.083\text{in}} = 8734.94 \text{ psig}$$

$$\sigma_r = 2900\text{psig}$$

The ASME Code presents equations for determining the stress levels in a piping system and provides stress limits for comparison. These theories are maximum principal stress failure theory and maximum shear stress failure theory. The maximum principal stress failure theory states that when anyone of the mutually perpendicular principal stresses exceed the yield strength of the material at temperature, failure will occur. The WHTB yield strength at the most severe temperature of 400°C is calculated, as previously stated, by multiplying the value at room temperature by the derating temperature factor at 426°C (closest value to 400°C tabulated). The result of the yield strength is 22.8 ksi (0.76 x 30ksi). Thus, ASME condition (principal stresses < material yield strength) is satisfied.

The maximum shear failure theory states that when the maximum shear stress (arithmetic average of largest minus smallest principal stresses) exceeds one-half the yield strength of the material at temperature, failure will occur. As the WHTB shear stress (Shear stress = (8734.94psig+2900psig)/2 = 5817.47psig) does not exceed one-half the yield strength (22.8 ksi/2=11.4ksi), ASME condition is satisfied.

- The total number of pressure-temperature variations above the design conditions are less than 100 over the life of the system. Each reactor is used less than 10 times.
- The maximum pressure is less than the test pressure. Every new reactor is hydrostatically tested at ~3200 psig, which is over the maximum permissible pressure of 2900 psig defined by the burst diaphragm rupture pressure.

Once all the conditions are tested and satisfied, let's continue with ASME requirements (Becht, 2002):“If the above conditions are satisfied, and if the owner approves, the pressure rating or allowable stress (essentially the maximum allowable working pressure) may be exceeded by 33% for events that are not more than 10 hours at any one time nor more than 100 hours per year, and by 20% for events that are not more than 50hours at any one time nor more than 500 hours per year. It is clear how a variation in pressure is handled. There is sometimes confusion relative to variations in temperature. The variation in temperature decreases the allowable stress or pressure rating. Thus, the stress or pressure may exceed the allowable value during a variation in temperature, without a change in pressure. If the above variations are used, the designer must determine that the piping system, including the effects of the variations, is safe over the service life of the piping, using methods that are acceptable to the owner.”

In conclusion, the WHTB allowable working pressure in the worst case scenario, i.e. at the highest experimental temperature of 400°C, could reach a maximum pressure of 3257 psig (2449psig x 1.33) for events that are not more than 10 hours at any one time nor more than 100 hours per year. And of 2939 psig for events that are not more than 50 hours at any one time nor more than 500 hours per year.

Bibliography

Becht, C. (2002). *PROCESS PIPING. The complete guide to ASME B31.3.*

https://www.swagelok.com/downloads/webcatalogs/EN/MS_01-107.PDF. (n.d.).

Lozano, E., & Petr, V. (2015). Design and testing of blast shields for different blasting application. In *Blasting and Fragmentation* (Vol. 9). Colorado, USA: AXPRO Group, Colorado School of Mines.

Moore, H. W. (n.d.). *Effectiveness of Transparent Shields in Protecting Explosive*. Naval Surface Warfare Center, Indian Head Division, Silver Spring, MD 20903-5640.

JOB SAFETY ANALYSIS

Safety Information for the University of Hawaii at Manoa

NAME OF DEPARTMENT: HAWAII NATURAL ENERGY INSTITUTE

Title of Job or Task: Assembly, Loading and Leak Testing of the Wall Heated Tubing Bomb

TASK	HAZARDS	CONTROLS
1. Load Reactor	<p>Sawdust can irritate eyes, the nose and throat. If ingested, can irritate mouth, throat and stomach.</p> <p>Sawdust can burn easily if ignited.</p> <p>120 V AC from mains to mass balance.</p>	<p>PPE</p> <p>Safety glasses or goggles</p> <p>Nitrile Gloves</p> <p>Flame resistant lab coat</p> <p>NIOSH-approved particulate mask</p> <p>Covered shoes</p> <p>Engineered controls</p> <p>Only handle where there is adequate ventilation. Use a local exhaust ventilation and enclosure, if necessary, to control amount in the air.</p> <p>Provide eyewash in work area, if contact or splash hazard exists.</p> <p>Avoid generating dusts. Avoid ignition sources.</p> <p>Inspect electrical cords, plugs, and receptacles prior to each use.</p>
2. Check and fix leaks in the reactor	<p>Compressed nitrogen</p> <p>H280 – Contains gas under pressure; may explode if heated.</p> <p>OSHA-H01 – May displace oxygen and cause rapid suffocation.</p> <p>Overpressurization of the reactor</p> <p>120 V AC from mains to electrical equipment (NI data acquisition system, laptop and pressure sensors).</p>	<p>PPE</p> <p>Safety glasses or goggles</p> <p>Flame resistant lab coat</p> <p>Covered shoes</p> <p>Engineered controls</p> <p>Implement pressure alarms in LabVIEW for experimental pressure objective and for warning of impending burst disk rupture.</p> <p>Good general ventilation should be sufficient to control worker exposure to airborne contaminants.</p>

			<p>Perform leak testing inside the Unistrut-Polycarbonate structure</p> <p>Direct tube from burst diaphragm to a bucket full of water</p> <p>Use appropriate tool to open and close valves in order to avoid direct contact of the experimenter with the pressurized reactor and lines.</p> <p>Inspect electrical cords, plugs, and receptacles prior to each use.</p>
	<p>Required Training: EHSO Lab Safety Training, Read UH Chemical hygiene plan, Specific lab activity training by PI or lab supervisor, read and understand all methods, QRA's, JSA's and SOP's developed for the operation of the Assembly, Loading and Leak Testing of the Wall Heated Tubing Bomb.</p>	<p>Required Personal Protective Equipment (PPE)</p> <p>Safety glasses or goggles</p> <p>Nitrile Gloves</p> <p>Flame resistant lab coat</p> <p>NIOSH-approved particulate mask</p> <p>Covered shoes</p>	
<p>Other Information:</p> <p>JSA Completed By:</p> <p>Date Created:</p> <p>OSHA Reference:</p>	<p>See Scott Turn, Trevor Morgan, Lloyd Paredes, Pablo J. Arauzo-Gimeno and Maider Legarra-Arizaleta for more information on Job Hazard Analysis</p> <p>Maider Legarra-Arizaleta, Scott Turn, Trevor Morgan, Lloyd Paredes and Pablo J. Arauzo-Gimeno</p> <p>April 20, 2018</p> <p>_____</p> <p>For more information about this JSA, contact the <i>University of Hawaii Environmental Health and Safety Office</i> http://www.hawaii.edu/ehso/industrial/ or by phone at 956-3204</p>		

APPENDIX F. SOP and JSA 3: Analysis of Feed Moisture Content

Laboratory Standard Operating Procedures University of Hawaii at Manoa

Please fill out and place in your Chemical Hygiene Plan

Analysis of Feed Moisture Content

Date: 04/20/2018

Principal Investigator: Scott Q. Turn

Produced By: Maidier Legarra Arizaleta, Trevor Morgan and Scott Turn

Room and Building: POST 11/12

Phone Number: PI Scott Turn: 808-956-2346/ POST 11: 808-956-9903/POST 12: 808-956-3790/

UH Emergency: 808-956-6911 (on campus 66911)/ Emergency: 911

Section 1 Process:

(Check One) Process

Hazardous Chemical

Hazard Class

Summary: This SOP covers the analysis of the feed moisture content. The main hazards related to this SOP are potential exposure and handling of biomass feedstock, elevated temperatures (<105 °C) and electricity (220 V, 20 Amps). A detailed 'Operation Method' that describes how to determine the feed moisture content is provided in section 12.

Section 2: Describe Process Hazards, Hazardous Chemical or Hazard Class.

Table 2.1. NFPA Hazard Classification ^aNot Available:

Chemical	Health	Fire	Reactivity	Specific
Sawdust	NA ^a	NA ^a	NA ^a	NA ^a

Sawdust: Inhalation: Can irritate the nose and throat. Skin Contact: May cause mild irritation. Eye Contact: May cause mild irritation. Ingestion: Can irritate the mouth, throat and stomach.

Mains Electricity: All the electrical connections and cables related to the drying oven and mass balance are standard 120 V (20 amps) components as provided by the equipment suppliers.

Elevated Temperature: Internal oven surfaces, sample holder, and sample are ~105°C.

Section 3: Personal Protective Equipment.

Safety glasses or goggles, flame resistant lab coat, heat resistant gloves, covered shoes, long pants

Sawdust: NIOSH-approved particulate mask. It is good practice to avoid breathing product; avoid skin and eye contact and wash hands after handling.

Section 4: Engineering Controls.

Sawdust: Use a local exhaust ventilation and enclosure, if necessary, to control amount in the air. Provide eyewash in work area, if contact or splash hazard exists.

Electricity: Inspect electrical cords, plugs, and receptacles prior to each use.

Section 5: Special Handling and Storage Requirements.

Sawdust

Handling: Avoid generating dusts. Only use where there is adequate ventilation. Avoid ignition sources. Use heat resistant gloves when using the oven. Promptly remove and properly dispose of accumulations.

Storage: Store in an area that is cool, ventilated.

Section 6: Spill and Accident Procedures.

Sawdust: Stop or reduce leak if safe to do so. Avoid generating dust. Collect using shovel/scoop or approved HEPA vacuum and place in a suitable container for disposal.

Small Fire: Fire extinguisher, appropriately trained personnel only. There are fire extinguishers in POST 11 and POST 12 indicated as FE on the floor map below.

Large Fire: Leave the room and call (956-6911).

Section 7: Waste Disposal Procedures.

Sawdust: Follow normal clean up procedures.

Section 8: Special Precautions Animal Use.

Not Applicable

Section 9: Required Approvals:

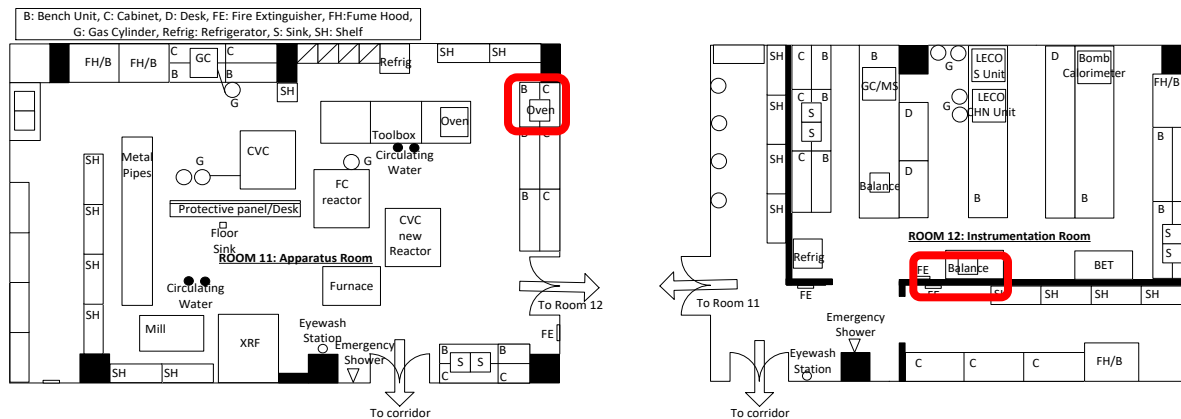
EHSO Lab Safety Training, approval and training from PI or lab supervisor. Read and understand all methods, QRA's, JSA's and SOP's developed for the determination of the feed moisture content.

Section 10: Decontamination.

All work surfaces will be cleaned with paper towel at the end of the test and at the end of the day.

Section 11: Designated Areas.

The R³Lab Room 11 and Room 12 framed sections in the maps below are designated for the feed moisture content analysis.



Section 12. Method:

This test method follows the Standard Test Method ASTM E871-82, which covers the determination of total weight basis moisture in the analysis sample of particulate wood fuel. For practical purposes, several modifications are implemented and described in the corresponding steps.

1. Sampling

- *Place of Sampling:* Take the sample where the wood is being loaded into or unloaded from means of transportation or when discharged from storage bins or conveyors.

NOTE 1—Samples collected from the surface of piles are, in general, unreliable because of the exposure to the environment. If necessary, collect nine increments from a foot or more below the surface at nine points covering the pile.

- *Collection of Gross Sample:*

- Collect increments regularly, systematically, and with such frequency that the entire quantity of wood sampled will be represented proportionally in the gross sample.
- The quantity of the sample shall be large enough to be representative but not less than 10 kg (22 lb.).
- Place the samples in an airtight container immediately after collection. Maintain the samples in the airtight container whenever possible to prevent gains or losses in moisture from the atmosphere.

- Sample reduction may be done by two methods, a coning and dividing process, or by using a riffle. The operations of mixing, coning, and quartering are described in Practice D346.

- Accomplish coning and dividing reduction by placing the gross sample on a sheet of rubber or oil cloth. Thoroughly mix it by raising first one corner of the cloth and then the other. After mixing cone and quarter sample, continue the operations until the sample is reduced sufficiently so that one quarter weighs about 50 g (0.11 lb.). This shall constitute a laboratory sample.
- Accomplish riffle reduction using a standard coal riffle. Riffle the gross sample repeatedly until one half of the riffle sample equals about 50 g (0.11 lb.), which will constitute a laboratory sample. Riffles and procedures are described in Practice D2013.

- 2. Fill Table 2 in the Loading Form following the instructions in section 13. Figure 13.1 shows an example of a Loading Form, which is divided into four tables: Table 1 with data from the *Proposal Conditions*, Table 2

with data from the *Reactant Moisture Content Analysis*, Table 3 with data from the *Solid Reactant Feed Bomb Load* and finally, Table 4 with data of the *Reactant Moist Mass* and Table 5 with the *Volume Evaluation*.

Section 13. Loading Form

WHTB Pyrolysis Setup

Table 1. Proposal Conditions

Date: _____ Pyrolysis Feed: _____ Packing: _____
 Pressurizing Gas: _____ Manufacturer: _____ Nominal Bomb Pressure [psig]: _____
 Experimenters: _____ Lot Number: _____ Nominal Sand Bath Temperature [°C]: _____

Table 2. Reactant Moisture Content Analysis

Tare mass [g]: _____ Tare and sample mass [g]: _____ Moisture Content [%]: #DIV/0!
 Final mass 1 [g]: _____ Valid final mass [g]: 0.000
 Final mass 2 [g]: _____
 Final mass 3 [g]: _____
 Final mass 4 [g]: _____
 Final mass 5 [g]: _____
 Final mass 6 [g]: _____
 Final mass 7 [g]: _____

Table 3. Solid Reactant Feed Bomb Load

	Co/K	Reactor Body New	TC Bottom New	Reactor Top No Cap	Filter Paper	Maximum Reactants	Sample Reactants	Remaining Reactants	SS Screen	Stem	Antisize	mass [g]
1	X											
2	X	X										
3	X		X									
4	X							X				
5	X			X								
6	X	X	X									
7	X	X	X					X				
8	X	X	X	X				X				
9	X				X							
10	X			X	X							
11	X			X		X						
12	X		X				X					
13	X		X				X		X			
14	X	X	X	X		X	X					
15	X							X				

Table 4. Reactant Moist Mass [g]

by filter paper difference	10-11	0.00
by reactor, SS screen, TC bottom and reactor top difference	14-8	0.00
Experimental Mass		0.00

Table 5. Void Volume Evaluation

Iteration 1	VOLUME EVALUATION					LEAK TEST					BACKFILL FROM SEQUESTERED VOLUME				
	Initial Cart Pressure Pcart.1 [psig]	Initial Reactor Pressure Preact.1 [psig]	Room T [degC]	Room Pressure [mmHg]	Final Cart Pressure Pcart.1 [psig]	Final Reactor Pressure Preact.1 [psig]	DCM start m3	DCM End m3	Sequestered Volume Pressure [psig]	Empty Reactor Pressure [psig]	Backfilled Reactor and Sequestered Pressure [psig]				
1															
2															
3															
4															
5															

Last Modified: 3/18/2017

Figure 13.1. Loading Form

Instructions for Table 2 in Loading Form

16. Dry sample container (see Figure 13.2) for 30 min at $103 \pm 1^\circ\text{C}$ in the oven, then cool in desiccator to room temperature. Weigh to the nearest 0.0001 g and record as *Tare Mass[g]*. The high precision of 0.0001 g specified here is in accordance with the balance precision even though in this case ASTM E871 just requires a precision of 0.02 g.
17. Place around 5 g of sample in the container, weigh the sample and container to the nearest 0.0001 g and record as *Tare and Sample Mass[g]*.
This step introduced the following modifications from the ASTM E871 method: a minimum of 50 g of sample is required by ASTM E871 instead of the 5 g specified here. However, the sample weight was greatly reduced in order not to run out of sample. Again, the high precision of 0.0001 g is in accordance with the balance precision. In this case ASTM E871 requires a precision of 0.01 g.
18. Place the sample and container in the oven for 16 h at $103 \pm 1^\circ\text{C}$.
Remove the sample and the container from the oven and cool in the desiccator to room temperature. Remove the sample and container from the desiccator, weigh immediately to the nearest 0.0001g and record the weight as *Final Mass 1 [g]*. In this case ASTM E871 requires a precision of 0.01 g.
19. Return the sample and container to the oven at $103 \pm 1^\circ\text{C}$ for 2 h. Remove the sample and the container from the oven and cool in the desiccator to room temperature. Remove the sample and container from the desiccator, weigh immediately to the nearest 0.0001 g.
20. Repeat 4 recording each weight in *Final Mass 2 [g]*, *Final Mass 3 [g]*...
21. Continue 4 until the total weight change between weightings varies less than 0.0005 g or the weight increases. The minimum weight recorded will be automatically selected by the Excel spreadsheet as the *Valid final mass [g]*. ASTM E871 specifies variation between weightings of 0.2 %. The modification introduced here imposes a more severe restriction.
22. The spreadsheet displays the mass percent moisture content in the analysis sample as *Moisture Content [%]*. The moisture content is calculated as:

$$\text{Mass percent moisture content } [\%] = \frac{\text{Tare and Sample Mass}[g] - \text{Valid final mass } [g]}{\text{Tare and Sample Mass}[g] - \text{Tare Mass}[g]} \times 100$$



Figure 13.2 Glass Feed Moisture Content Container

JOB SAFETY ANALYSIS

Safety Information for the University of Hawaii at Manoa

NAME OF DEPARTMENT: HAWAII NATURAL ENERGY INSTITUTE

Title of Job or Task: Analysis of the Feed Moisture Content

TASK	HAZARDS	CONTROLS
1.Feed Moisture Content Analysis	<p>Sawdust can irritate eyes, the nose and throat. If ingested, can irritate mouth, throat and stomach.</p> <p>Sawdust can burn easily if ignited.</p> <p>Hot sawdust and oven surfaces when removing samples from the oven</p> <p>120 V AC from mains to drying oven and mass balance.</p>	<p>PPE</p> <p>Safety glasses or goggles</p> <p>Nitrile Gloves</p> <p>Flame resistant lab coat</p> <p>Heat resistant gloves when taking sample of the oven</p> <p>NIOSH approved particulate mask.</p> <p>Engineered controls</p> <p>Only handle where there is adequate ventilation. Use a local exhaust ventilation and enclosure, if necessary, to control amount in the air.</p> <p>Provide eyewash in work area, if contact or splash hazard exists.</p> <p>Avoid generating dusts. Avoid ignition sources.</p> <p>Inspect electrical cords, plugs, and receptacles prior to each use.</p>
<p>Required Training: EHSO Lab Safety Training, Read UH Chemical hygiene plan, Specific lab activity training by PI or lab supervisor,</p>	<p>Required Personal Protective Equipment (PPE)</p> <p>Safety glasses or goggles</p> <p>Heat resistant gloves</p> <p>Nitrile Gloves</p> <p>Flame resistant lab coat</p> <p>NIOSH approved particulate mask.</p>	

	<p>Read and understand ASTM E871-82, all methods, QRA's, JSA's and SOP's developed for the determination of the feed moisture content.</p>	
<p>Other Information: JSA Completed By: Date Created: OSHA Reference:</p>	<p>See Scott Turn, Trevor Morgan, Lloyd Paredes, Pablo J. Arauzo-Gimeno and Maider Legarra-Arizaleta for more information on Job Hazard Analysis</p> <p>Maider Legarra-Arizaleta, Scott Turn, and Trevor Morgan</p> <p>April 20, 2018</p> <p>_____</p> <p>For more information about this JSA, contact the <i>University of Hawaii Environmental Health and Safety Office</i> http://www.hawaii.edu/ehso/industrial/ or by phone at 956-3204</p>	

APPENDIX G. SOP and JSA 4: Gas Chromatograph Operation

Laboratory Standard Operating Procedures

University of Hawaii at Manoa

Please fill out and place in your Chemical Hygiene Plan

Gas Chromatograph Operation

Date: 04/20/2018

Principal Investigator: Scott Q. Turn

Produced By: Maidier Legarra-Arizaleta, Trevor Morgan, Scott Turn, Lloyd Paredes and Pablo J. Arauzo-Gimeno and

Room and Building: POST 11/12

Phone Number: PI Scott Turn: 808-956-2346/ POST 11: 808-956-9903 /POST 12: 808-956-3790/

UH Emergency: 808-956-6911 (on campus 66911)/ Emergency: 911

Section 1 Process:

(Check One) Process

Hazardous Chemical

Hazard Class

Summary: This SOP is for the use of a Micro Gas Chromatograph (MicroGC) instrument. This SOP covers the use of the MicroGC instrument for the analysis of gas samples, as well as the transfer of calibration gases from cylinders to gas bags. The main hazards related to the use of the MicroGC are potential exposure to chemicals (Matheson Calibration Gas Mix E and Matheson Calibration Gas Mix G, experimental gases, vacuum oil, and helium gas), the presence of pressurized gas cylinders and electricity (120 V, 20 Amps).

The main steps for using the MicroGC that are relevant to the SOP are listed in section 12. A detailed 'Operation Method' that is PC based, i.e. changing settings to control the MicroGC, and therefore do not pose a hazard to the operator, is provided in a separate document.

Section 2: Describe Process Hazards, Hazardous Chemical or Hazard Class.

Table 2.1. NFPA Hazard Classification (Health, Fire, reactivity and Specific) and Exposure limit.

Chemical	Health	Fire	Reactivity	Specific	Exposure limit
Compressed Helium	0	0	0	SA ^a	
Calibration Gas Mix G (Matheson):	2	0	0		
Carbon dioxide 15%				SA ^a	ACGIH ^b TWA ^c 5000 ppm
Carbon monoxide 7%				SA ^a	ACGIH ^b TWA ^c 25 ppm
Oxygen 5%					
Methane 4.5 %				SA ^a	
Nitrogen Balance				SA ^a	

Calibration Gas Mix E [#]	2	4	0		
(Matheson):					
Nitrogen <91%				SA ^a	
Oxygen ≤23.5%					
Carbon dioxide <20%				SA ^a	ACGIH ^b TWA ^c 5000 ppm
Carbon monoxide 3-100%				SA ^a	ACGIH ^b TWA ^c 25 ppm
Hydrogen 3-100%				SA ^a	
Methane 3-100%				SA ^a	
Pyrolysis Gases:					
Nitrogen	0	0	0	SA ^a	
Carbon monoxide	2	4	0	SA ^a	ACGIH ^b TWA ^c 25 ppm
Carbon dioxide	1	0	0	SA ^a	ACGIH ^b TWA ^c 5000 ppm
Methane	1	4	0	SA ^a	
Hydrogen	0	4	0	SA ^a	

^a Simple Asphyxiant

^b ACGIH: American Conference of Governmental Industrial Hygienist

^c TWA: Time Weighted Average

[#]: Matheson SDS library does NOT contain an SDS for our specific calibration gas identified as Mix E (1% CO₂, 1% CO, 1% O₂, 1% CH₄, 1% H₂, Nitrogen balance). Matheson recommended the use of a SDS for a Matheson gas mixture closest to our calibration gas and based on ranges of concentrations, i.e. nitrogen <91%, oxygen ≤23.5%, carbon dioxide 1-20%, carbon monoxide 3-100%, hydrogen 3-100%, methane 3-100%.

This generic SDS covers various calibration gases with the same gas components as Mix E but different concentration ranges as shown by Table 2.1. Oxygen and carbon dioxide concentrations in Mix E falls within the generic SDS concentration ranges. However, concentrations of CO, H₂ and CH₄ falls below their respective generic SDS concentration ranges and N₂ concentration exceeds the generic SDS N₂ range. Thus, the concentration ranges covered by the generic SDS represent potentially more hazardous mixtures than Mix E.

Calibration gas Mix G: Contains gas under pressure; may explode if heated. May damage fertility or the unborn child. May cause damage to organs through prolonged or repeated exposure. May displace oxygen and cause rapid suffocation. Rapid release of compressed gas may cause frostbite.

Calibration gas Mix E: Extremely flammable gas. Contains gas under pressure; may explode if heated. Harmful if inhaled. May damage fertility or the unborn child. May cause damage to organs through prolonged or repeated exposure. May displace oxygen and cause rapid suffocation. Rapid release of compressed gas may cause frostbite.

Compressed Helium: Contains gas under pressure; may explode if heated. May displace oxygen and cause rapid suffocation (when concentrations are sufficient to reduce oxygen levels below 19.5%).

Pyrolysis gases: The final experimental gases, consisting of a maximum of ~10 grams of the pyrolysis products (CO, CO₂, CH₄ and H₂) and the N₂ originally fed into the reactor, are transferred at the end of an experiment from the Wall Heated Tubing Bomb (WHTB) to the Water Displacement Vessel (WDV) and finally released into a lab snorkel exhaust. The calculation below shows that a release of the pyrolysis gases into the lab is too small to present a hazard to lab personnel. Therefore, good ventilation is sufficient to prevent the exposure of the lab personnel to high local concentrations, nonetheless, all pyrolysis gases must be vented into a lab snorkel exhaust.

POST 12 has an approximate volume of 129.80 m³ (V_{POST 12, approx}=5.18m x 9.75m x 2.57m). The room filled with air at 1 am and ~20 °C equates to a mass of air of 156.5 kg as shown by the following equation:

$$m_{Air} = \frac{1 \text{ atm } 129800L}{0.082 \frac{\text{atmL}}{\text{mol K}} 293K} \frac{28.966 \text{ g}}{1 \text{ mol}} = 156488.3g \approx 156.5 \text{ kg}$$

The release of the final pyrolysis gases into POST 12 will change the composition and concentration of gas in the room. The 10 g of pyrolysis products that are released consist of a mixture of mainly CO₂ (more than half), then CO with traces of CH₄ and H₂. The nitrogen released into the Lab is equal to the nitrogen originally fed into the reactor volume which is around 0.22 L. The mass of nitrogen fed in the reactor varies from an approximate value of 0.14 g to around 5.5 g depending on the initial nitrogen reactor pressure, from 0 psig to 300psig respectively, as shown by the following equations:

$$m_{N_2 \text{ at } 0 \text{ psig}} = \frac{1 \text{ atm} \cdot 0.22 \text{ L}}{0.082 \frac{\text{atm} \cdot \text{L}}{\text{mol} \cdot \text{K}} \cdot 293 \text{ K}} \frac{28 \text{ g}}{1 \text{ mol}} = 0.26 \text{ g}$$

$$m_{N_2 \text{ at } 300 \text{ psig}} = \frac{21.41 \text{ atm} \cdot 0.22 \text{ L}}{0.082 \frac{\text{atm} \cdot \text{L}}{\text{mol} \cdot \text{K}} \cdot 293 \text{ K}} \frac{28 \text{ g}}{1 \text{ mol}} = 5.5 \text{ g}$$

The release of 10 g of pyrolysis gas and 5.5 g of nitrogen (maximum nitrogen mass fed into the reactor) do not coexist as it will exceed the maximum reactor pressure ratings. Releasing 10 g of pyrolysis gas into the POST 12 environment corresponds with mass concentrations of pyrolysis gases of 63.9ppm_w (10 g pyrolysis gases / 156488 g air) and 5.5 g of nitrogen concentration correspond to 35.14ppm_w (5.5g N₂/156488 g air). Thus, unintended release of the final experimental pyrolysis gases into the lab environment does not pose a hazard for the experimenter. Notice that these calculations are somewhat simplistic; this assumes instantaneous and complete mixing of the leaked contaminant and the entirety of the room's air. An exhaust snorkel directed to the reactor could eliminate localized high concentrations.

Prior to measuring their volume in the WDV, gases contained in the WHTB are at elevated pressure (420 to 2000 psig at experimental test temperature). The total volume of these contained gases at standard pressure and temperature are <8 L.

Mains Electricity: All electrical connections to the laptop, MicroGC and vacuum pump are standard 120 V (20 amps) lines as provided by the equipment suppliers.

Section 3: Personal Protective Equipment.

Safety glasses or goggles, flame resistant lab coat, covered shoes, long pants.

Calibration Gas Mix G and Calibration Gas Mix E: Under conditions of frequent use or heavy exposure, respiratory protection may be needed. Respiratory protection is ranked in order from minimum to maximum. Consider warning properties before use. Any supplied-air respirator with a full face piece that is operated in a pressure-demand or other positive-pressure mode in combination with an auxiliary self-contained breathing apparatus operated in pressure-demand or other positive-pressure mode. Any self-contained breathing apparatus that has a full face piece and is operated in a pressure-demand or other positive-pressure mode. Protective gloves are not required, but recommended.

Section 4: Engineering Controls.

Compressed Helium: Good general ventilation should be sufficient to control worker exposure to airborne contaminants. Monitor oxygen level to ensure the experimenter is not exposed to oxygen concentrations below the hazardous level of 19.5%. Install a 'flow restrictor' valve in the line from the helium cylinder to the MicroGC to prevent excessive release of helium into the environment.

Calibration Gas Mix G and Calibration Gas Mix E: Lab snorkel or fume hood. Ensure lab snorkel or fume hood are working properly.

Pyrolysis gases: A standard laboratory air exchange ventilation rate is sufficient to prevent worker exposure to hazardous concentrations of airborne contaminants, nonetheless, pyrolysis gases should be released into the lab snorkel exhaust or fume hood.

Electricity: Inspect electrical cords, plugs, and receptacles prior to each use.

Section 5: Special Handling and Storage Requirements.

Compressed Helium:

Handling: During normal operation, the gas cylinder is NEVER to be closed or the flow to the MicroGC stopped; the MicroGC requires a constant flow of helium to prevent damage to the column. Before handling a cylinder put on appropriate personal protective equipment. The cylinder contains gas under pressure. Avoid contact with eyes, skin and clothing. Avoid breathing gas. Empty containers retain product residue and can be hazardous. Do not puncture or incinerate container. Use equipment rated for cylinder pressure. Protect cylinders from physical damage; do not drag, roll, slide, or drop. Use a suitable hand truck for cylinder movement.

Storage: Store in accordance with local regulations. Store in a segregated and approved area. Store away from direct sunlight in a dry, cool and well-ventilated area. Keep container tightly closed and sealed until ready for use. Cylinders should be stored upright, with valve protection cap in place, and firmly secured to prevent falling or being knocked over. Cylinder temperatures should not exceed 52 °C (125 °F).

Calibration gas Mix G:

Handling: Use only outdoors or in a well-ventilated area. Do not breathe gas. Wash hands thoroughly after handling. Avoid ignition sources.

Calibration gas Mix E:

Handling: Use only outdoors or in a well-ventilated area. Do not breathe gas. Wash hands thoroughly after handling. Avoid ignition sources. All equipment used when handling the product must be grounded.

Calibration gas Mix G and Calibration gas Mix E:

Storage: Store locked up. Protect from sunlight. Store in a well-ventilated place. Store and handle in accordance with all current regulations and standards. Subject to storage and handling regulations: U.S. OSHA 29 CFR 1910.101. Keep separated from incompatible substances, i.e. oxidizing materials, metals, combustible materials, halo carbons, bases, reducing agents, amines, metal salts, metal carbide, halogens, lithium, and metal oxides.

Pyrolysis gases:

Use only outdoors or in a well-ventilated area. Do not breathe gas. Wash hands thoroughly after handling. Avoid ignition sources.

Section 6: Spill and Accident Procedures.

Calibration gas Mix G: Stop leak if possible without personal risk. Keep unnecessary people away, isolate hazard area and deny entry. Remove sources of ignition. Stay upwind and keep out of low areas. Do not direct water at spill

or source of leak. Ventilate closed spaces before entering. Avoid release to the environment. Call emergency phone (see above) for large releases.

Calibration gas Mix E: Stop leak if possible without personal risk. Keep unnecessary people away, isolate hazard area and deny entry. Remove sources of ignition. All equipment used when handling the product must be grounded. Stay upwind and keep out of low areas. Do not direct water at spill or source of leak. Ventilate closed spaces before entering. Avoid release to the environment. Call emergency phone (see above) for large releases.

Compressed Helium: No action shall be taken involving any personal risk or without suitable training. Evacuate surrounding areas. Keep unnecessary and unprotected personnel from entering. Avoid breathing gas. Provide adequate ventilation. Wear appropriate respirator (Self-Contained Breathing Apparatus SCBA) when ventilation is inadequate.

Small spill: Shutoff source of gas. Stop leak if without risk. Contact emergency personnel (see Phone number information above) if necessary.

Large spill: Immediately contact emergency personnel (see Phone number information above). Stop leak if without risk. Note: Call supplier for emergency contact information (AirGas 24-hour phone 1-866-734-3438).

Pyrolysis gases: Stop or reduce leak if safe to do so. Provide adequate ventilation. According to the above mentioned calculations, exposure to mixed pyrolysis gases at the concentrations generated under the test conditions is not hazardous.

Small Fire: Fire extinguisher, appropriately trained personnel only. There are fire extinguishers in POST 11 and POST 12 indicated as FE on the floor map below.

Large Fire: Leave the room and call emergency phone (see above).

Section 7: Waste Disposal Procedures.

Calibration gases Mix G and Mix E: Return cylinder and unused product to supplier. (MATHESON TRI-GAS, INC. General Information: 1-800-416-2505)

Compressed Helium: Disposal or return of cylinders is only to be performed by appropriately trained personnel.

Unused product/ empty container: Return cylinder and unused product to supplier (AirGas 24-hour phone 1-866-734-3438). Do not attempt to dispose of residual or unused quantities.

Disposal: For emergency disposal, secure the cylinder and slowly discharge gas to the atmosphere in a well ventilated area or outdoors.

Pyrolysis gases: For emergency disposal, slowly discharge gas to the lab snorkel exhaust or fume hood. Ensure lab snorkel or fume hood are working properly.

Section 8: Special Precautions Animal Use.

Not Applicable

Section 9: Required Approvals:

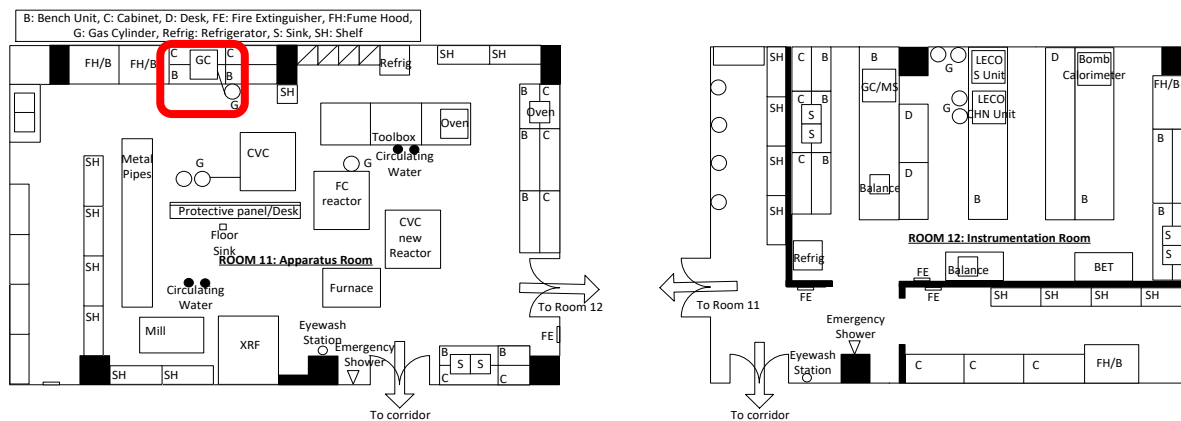
EHSO Lab Safety Training, approval and training from PI or lab supervisor. Read and understand all methods, QRA's, JSA's and SOP's developed for the operation of the MicroGC instrument.

Section 10: Decontamination.

All work surfaces will be cleaned with paper towel at the end of the test and at the end of the day.

Section 11: Designated Areas.

The R3Lab Room 11 framed sections in the maps below is designated for GC operation



12. Method:

Notes:

The filter inside the gastight syringe, consisting of Drierite desiccant (Drierite from MIDLAND SCIENTIFIC, INC. Stock# 23005, 8 mesh, $\geq 98\%$ CaSO_4 , $< 2\%$ CoCl_2) between two glass wool pieces, adsorbs small drops of liquid and prevent them from entering the micro GC. The change in color of desiccant from blue to pink (see Figure 12.1) corresponds with a change from a dry to a moist desiccant, and therefore it indicates the need of filter replacement.



Figure 12.1. Gastight syringe with blue dry drierite desiccant (left) and with moist drierite desiccant (Right)

Every time the filter is replaced and joints disassembled, use DOW CORNING high vacuum grease while assembling before tightening it for a better seal.

When analyzing gases, set the needle at a 90° angle from its injection port (see Figure 12.2) in order to prevent air leaks

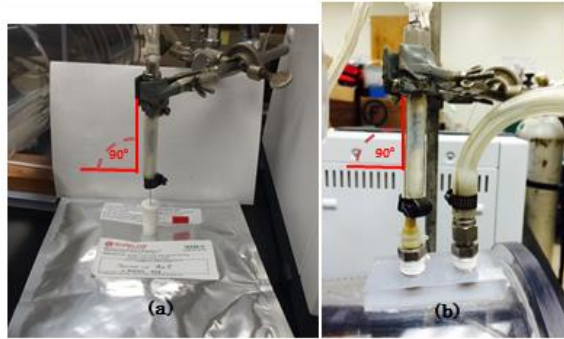


Figure 12.2 Correct position of the needle during injection from the gas bag (Left) and from the Water Displacement Vessel (Right)

Method 1. Micro Gas Chromatograph (MicroGC) Leak Test, Analysis of gases and Conditioning

1. Figures 12.3 and 12.4 show a complete diagram of the MicroGC assembly connected to the gas bag and to the Water Displacement Vessel assembly respectively.

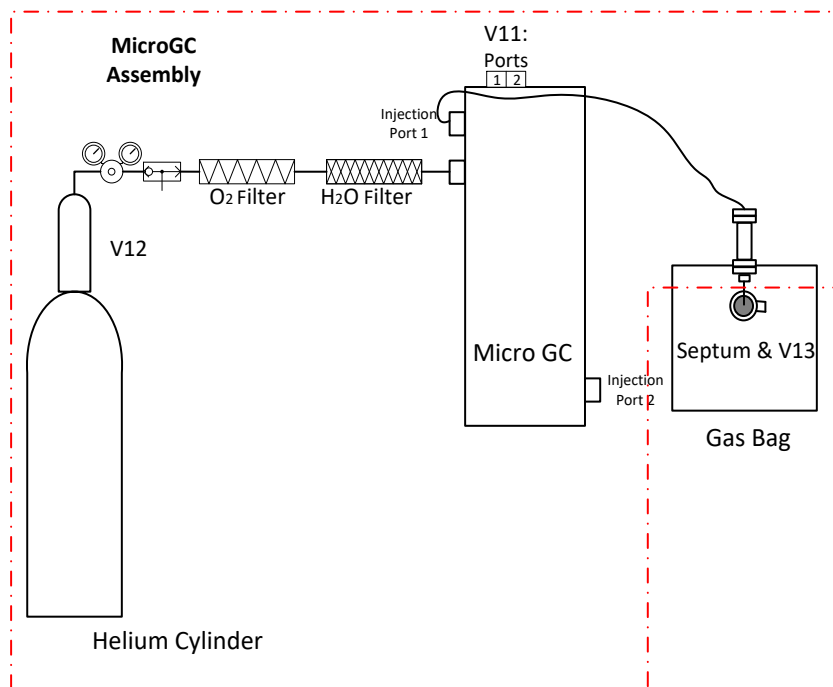


Figure 12.3 MicroGC Assembly connected to Gas Bag

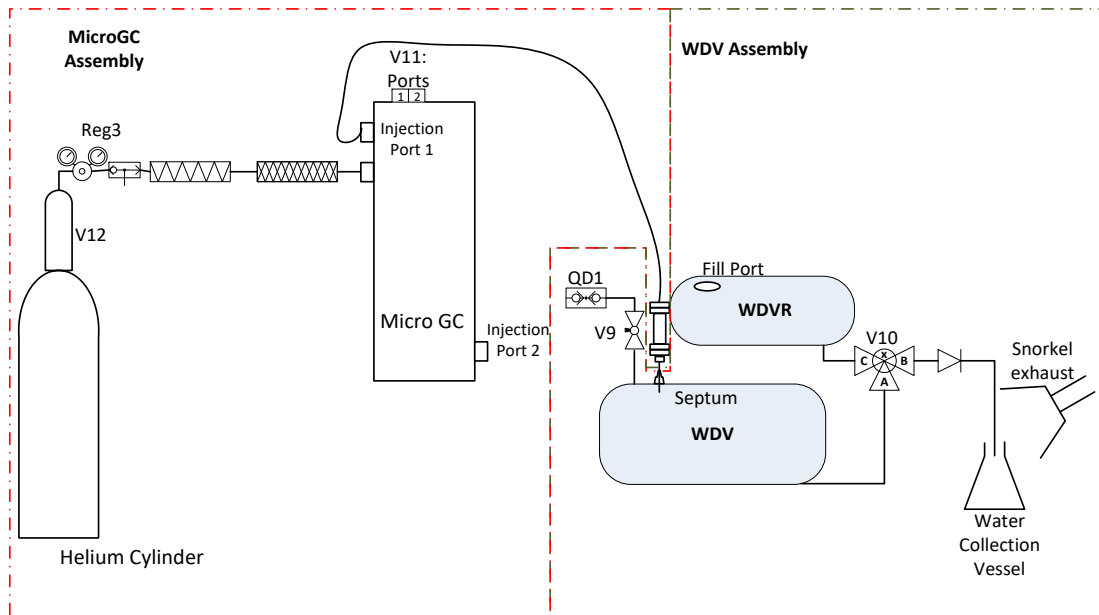
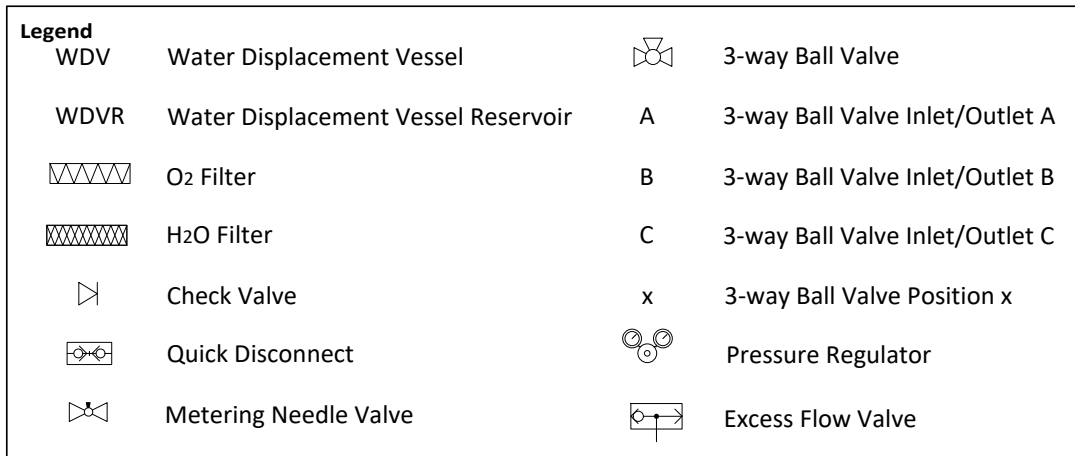


Figure 12.4 MicroGC Assembly connected to Water Displacement Vessel (WDV) Assembly

2. Fill Gas Bag with Calibration Gas Mix G (See Instructions in Method 2 below)
3. Perform leak test to the MicroGC assembly
 - 3.1 Ensure that the MicroGC assembly is NOT connected either to the gas bag or to the WDV assembly as in Figures 12.3 and 12.4 respectively.
 - 3.2 Assess the status of the Helium cylinder by reading the inlet and outlet pressures on regulator Reg3 and confirm the valve positions match those of Table 12.1. Every time a valve or regulator position is modified a new Table will be presented.

Table 12.1.

V11	V12	V13	Reg3 Inlet	Reg3 Outlet
Port 1	Open	Closed	>500 psig	80-90 psig

3.1 Determine the helium pressure requirements.

If the pressure shown on the Reg3 inlet is over 500 psig, proceed to Step 4. If not, the helium supply cylinder must be replaced (see SOP for gas cylinder replacement). After cylinder replacement, return to Step 3.

3.2 Follow instructions in the GC operation manual, section *MicroGC Assembly Leak Test*. The instructions specify, step by step, the computer commands to perform a leak test and the moment the MicroGC assembly connects to the Gas Bag as in Figure 12.3.

4. If leaks are detected, identify and fix them

Based on years of experience with the GC; the gas bag, the MicroGC syringe, and joints in the tubing are potential leak spots ranked from more to less frequent. To fix leaks, these elements are revised and fixed in the same order.

4.1 Change gas bag.

4.1.1 Keep the used gas bag, labelled it as *used*.

Note: Usually a gas bag leaks due to too many punctures in the septum. Once we collected enough *used* gas bags, all the septa will be replaced at once by following the manual instructions and the gas bags will be retested with leak tests to the MicroGC assembly (See instructions in the GC operation manual, section *MicroGC Assembly Leak Test*). Relabel and reuse gas bags that do not leak and dispose of the ones that leak.

4.1.2 Refill a new gas bag with Calibration Gas Mix G (See Method 2).

4.1.3 Perform leak test to the MicroGC assembly (See GC operation manual, section *MicroGC Assembly Leak Test*). If no leaks are detected, proceed to step 5. If leaks are detected, proceed to 4.2.

4.2 Check syringe.

4.2.1 Untighten, disassemble, clean joints, assemble and retighten the syringe.

4.2.2 Perform leak test to the MicroGC assembly (See GC operation manual, section *MicroGC Assembly Leak Test*). If no leaks are detected, proceed to step 5. If leaks are detected, proceed to 4.2.3.

4.2.3 Replace the used syringe for a new one and perform leak test to the MicroGC assembly (See GC operation manual, section *MicroGC Assembly Leak Test*). If no leaks are detected, proceed to step 5. If leaks are detected, proceed to 4.3.

4.3 Tubing leaks.

4.3.1 Check the equipment employed to transfer calibration gases from the gas cylinders to the gas bags (see Figure 12.5). Apply Snoop to valves and junctions. Pressurize the tubing and check for snoop bubbles.

4.3.1.1 If bubbles do not appear, proceed to 4.3.2

4.3.1.2 If bubbles appear, the tubing is leaking. Before attempting to fix any leaks, depressurize the tubing. To fix leaks: untighten, disassemble, clean joints, assemble and retighten the leaking joints. Repeat 4.3.1 one more time.

If bubbles do not appear after the repetition, tubing leaks are fixed. Perform leak test to the MicroGC assembly (See GC operation manual, section *MicroGC Assembly Leak Test*). If no leaks are detected, proceed to step 5. If leaks are detected, proceed to 4.3.2.

If bubbles appear after the repetition, change the tubing. Bubbles should disappear.

Perform leak test to the MicroGC assembly (See GC operation manual, section *MicroGC Assembly Leak Test*). If no leaks are detected, proceed to step 5. If leaks are detected, proceed to 4.3.2.

4.3.2 Check the GC tubing connecting syringe and GC. Untighten and disassemble the tubing from the GC. Apply Snoop to valves and junctions. Pressurize the tubing and check for snoop bubbles.

4.3.2.1 If bubbles do not appear, call MicroGC technician in Oahu: Dorian Taylor 808-542-8326.

4.3.2.2 If bubbles appear, the tubing is leaking. Before attempting to fix any leaks, depressurize the tubing. To fix leaks, untighten, disassemble, clean joints, assemble and retighten the leaking joints. Repeat 4.3.2 one more time.

If bubbles do not appear after the repetition, tubing leaks are fixed. Perform leak test to the MicroGC assembly (See GC operation manual, section *MicroGC Assembly Leak Test*). If no leaks are detected, proceed to step 5. If leaks are detected, call MicroGC technician in Oahu: Dorian Taylor 808-542-8326.

- 4 Ensure the MicroGC assembly is disconnected from the Gas Bag or from the WDV Assembly
- 5 Analysis of Calibration and Experimental Gases: Fill Gas Bag with Calibration Gas Mix E (See Instructions in Method 2 below). Wait until the experimental day to analyze calibration and experimental gases. Follow instructions in the GC operation manual, section *Analysis of Calibration and Experimental Gases*. The instructions specify, step by step, the computer commands to perform analysis to calibration and experimental gases and the moments the MicroGC needs to be connected to the Gas Bag or to the WDV Assembly. The MicroGC is connected to a Gas Bag as in Figure 12.3 when analyzing calibration gases and to the WDV assembly as in Figure 12.4 when analyzing experimental gases.
- 6 When the analysis is complete, ensure the MicroGC assembly is disconnected from the Gas Bag or from the WDV Assembly
- 7 Condition the column for at least one day. Follow instructions in the GC operation manual, section *Conditioning*.

Method 2: Transfer Calibration Gases from Cylinder to Gas Bag

1. Perform tasks under a lab snorkel that is working correctly. Connect the vacuum pump, gas bag and calibration gas cylinder as shown in Figure 12.5. Confirm the valve positions throughout the system match those in Table 12.2. Every time a valve position is modified a new Table will be presented.

Table 12.2.

V13	V14	V15
Closed	Closed	Closed

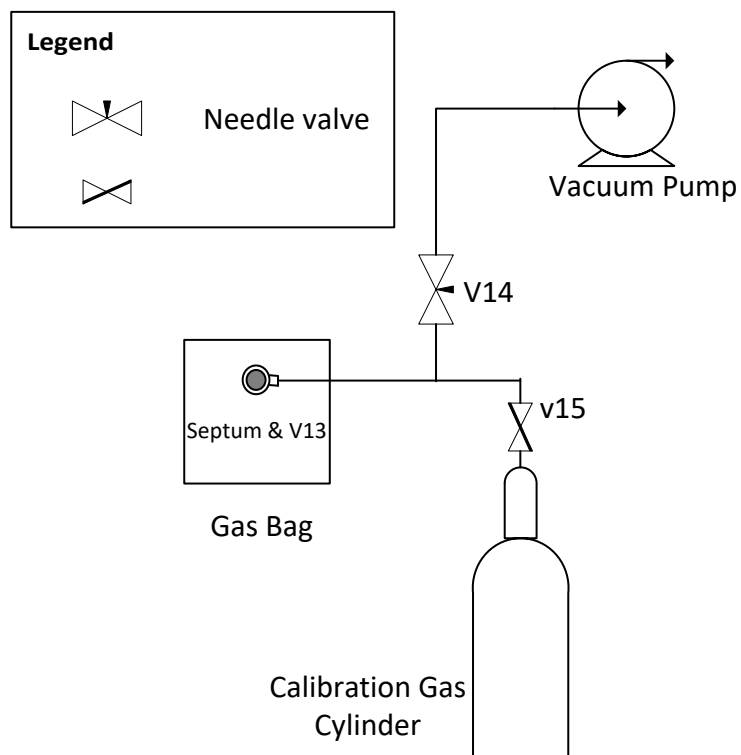


Figure 12.5. Gas bag filling diagram.

- Purge lines and empty gas bag. Plug in the vacuum pump and open valves V13 and V14 for ~1 minute (DO NOT OPEN V15!! while purging otherwise the calibration gas in the cylinder will be vacuumed by the pump).

Table 12.3.

V13	V14	V15
Open	Open	Closed

- Stop purging by closing V14 and unplugging the pump. As the system is vacuumed at this point, the air will enter the system if any joint is not sealed.

Table 12.4.

V13	V14	V15
Open	Closed	Closed

- Fill the gas bag by opening V15.

Table 12.5.

V13	V14	V15
Open	Closed	Open

5. Close all valves when gas bag is full

Table 12.6.

V13	V14	V15
Closed	Closed	Closed

6. Disconnect the pump, air bag and cylinder. Clean and put everything in place.

JOB SAFETY ANALYSIS

Safety Information for the University of Hawaii at Manoa

NAME OF DEPARTMENT: HAWAII NATURAL ENERGY INSTITUTE

Title of Job or Task: GC Operation

TASK	HAZARDS	CONTROLS
1. GC leak test	<p>Calibration gas Mix G Gases Under Pressure - Compressed gas Reproductive Toxicity (1A) Specific Target Organ Toxicity - Repeated Exposure (1) (Central nervous system) Simple Asphyxiant Helium Contains gas under pressure; may explode if heated. May displace oxygen and cause rapid suffocation.</p> <p>120 V AC from mains to MicroGC and laptop.</p>	<p>PPE Safety glasses or goggles Flame resistant lab coat Covered shoes Under conditions of frequent use or heavy exposure, respiratory protection may be needed.</p> <p>Engineered controls Use Lab snorkel to collect gases from GC exhaust Good general ventilation should be sufficient to control worker exposure to airborne contaminants. Inspect electrical cords, plugs, and receptacles prior to each use.</p>
2. Identify and Fix Leaks	<p>Calibration gas Mix G Gases Under Pressure - Compressed gas Reproductive Toxicity (1A) Specific Target Organ Toxicity - Repeated Exposure (1) (Central nervous system) Simple Asphyxiant Helium Contains gas under pressure; may explode if heated. May displace oxygen and cause rapid suffocation. 120 V AC from mains to MicroGC and laptop.</p>	<p>PPE Safety glasses or goggles Flame resistant lab coat Covered shoes Under conditions of frequent use or heavy exposure of calibration gases, respiratory protection may be needed.</p> <p>Engineered controls Use Lab snorkel to collect gases from GC exhaust Good general ventilation should be sufficient to control worker exposure to airborne contaminants.</p>

	<p>3. Analysis of Calibration and Experimental Gases</p>	<p>Calibration gas Mix G Gases Under Pressure - Compressed gas Reproductive Toxicity (1A) Specific Target Organ Toxicity - Repeated Exposure (1) (Central nervous system) Simple Asphyxiant</p> <p>Calibration gas Mix X (attributed to Mix E) Flammable Gases (1) Gases Under Pressure - Compressed gas Acute Toxicity - Inhalation - Gas (4) Reproductive Toxicity (1) Specific Target Organ Toxicity - Single Exposure (1) (circulatory system, nervous system, Hematopoietic System) Specific Target Organ Toxicity - Repeated Exposure (1) (blood, Cardiovascular system, respiratory system) Specific Target Organ Toxicity - Repeated Exposure (2) (heart) Simple Asphyxiant</p> <p>Helium Contains gas under pressure; may explode if heated. May displace oxygen and cause rapid suffocation.</p> <p>Pyrolysis gases Unintended release of the final experimental pyrolysis gases into the lab environment does not pose a hazard for the experimenter (See SOP).</p> <p>120 V AC from mains to MicroGC and laptop.</p>	<p>Inspect electrical cords, plugs, and receptacles prior to each use.</p> <p>PPE Safety glasses or goggles Flame resistant lab coat Covered shoes Under conditions of frequent use or heavy exposure, respiratory protection may be needed.</p> <p>Engineered controls Use Lab snorkel to collect gases from GC exhaust Good general ventilation should be sufficient to control worker exposure to airborne contaminants. Inspect electrical cords, plugs, and receptacles prior to each use.</p>
--	--	---	--

	4. Conditioning	<p>Helium Contains gas under pressure; may explode if heated. May displace oxygen and cause rapid suffocation 120 V AC from mains to MicroGC and laptop.</p>	<p>PPE Safety glasses or goggles Flame resistant lab coat Covered shoes</p> <p>Engineered controls Use Lab snorkel to collect gases from GC exhaust Good general ventilation should be sufficient to control worker exposure to airborne contaminants. Inspect electrical cords, plugs, and receptacles prior to each use.</p>
	5. Transfer Calibration Gases from Cylinder to Gas Bag	<p>Calibration gas Mix G Gases Under Pressure - Compressed gas Reproductive Toxicity (1A) Specific Target Organ Toxicity - Repeated Exposure (1) (Central nervous system) Simple Asphyxiant</p> <p>Calibration gas Mix X (attributed to Mix E) Flammable Gases (1) Gases Under Pressure - Compressed gas Acute Toxicity - Inhalation - Gas (4) Reproductive Toxicity (1) Specific Target Organ Toxicity - Single Exposure (1) (circulatory system, nervous system, Hematopoietic System) Specific Target Organ Toxicity - Repeated Exposure (1) (blood, Cardiovascular system, respiratory system) Specific Target Organ Toxicity - Repeated Exposure (2) (heart) Simple Asphyxiant 120 V AC from mains to vacuum pump.</p>	<p>PPE Safety glasses or goggles Flame resistant lab coat Covered shoes Under conditions of frequent use or heavy exposure, respiratory protection may be needed.</p> <p>Engineered controls Use Lab snorkel to collect gases from GC exhaust Good general ventilation should be sufficient to control worker exposure to airborne contaminants. Inspect electrical cords, plugs, and receptacles prior to each use.</p>

	<p>Required Training: EHSO Lab Safety Training, Read UH Chemical hygiene plan, Specific lab activity training by PI or lab supervisor, read and understand all methods, QRA's, JSA's and SOP's developed for the operation of the MicroGC instrument.</p>	<p>Required Personal Protective Equipment (PPE)</p> <p>Safety glasses or goggles</p> <p>Flame resistant lab coat</p> <p>Covered shoes</p> <p>Under conditions of frequent use or heavy exposure of calibration gases Mix E and Mix G, respiratory protection may be needed.</p>
<p>Other Information:</p> <p>JSA Completed By:</p> <p>Date Created:</p> <p>OSHA Reference:</p>	<p>See Trevor Morgan, Lloyd Paredes, Scott Turn, Pablo J. Arauzo-Gimeno and Maider Legarra-Arizaleta for more information on Job Hazard Analysis</p> <p>Maider Legarra-Arizaleta, Trevor Morgan, Scott Turn, Lloyd Paredes and Pablo J. Arauzo-Gimeno and</p> <p>April 20, 2018</p> <p>_____</p> <p>For more information about this JSA, contact the <i>University of Hawaii Environmental Health and Safety Office</i> http://www.hawaii.edu/ehso/industrial/ or by phone at 956-3204</p>	

APPENDIX H. SOP and JSA 5: Water Displacement Vessel

Operation

Laboratory Standard Operating Procedures

University of Hawaii at Manoa

Please fill out and place in your Chemical Hygiene Plan

Water Displacement Vessel Operation

Date: 04/20/2018

Principal Investigator: Scott Q. Turn

Produced By: Maidar Legarra Arizaleta

Room and Building: POST 11/12

Phone Number: PI Scott Turn: 808-956-2346/ POST 11: 808-956-9903 /POST 12: 808-956-3790/

UH Emergency: 808-956-6911 (on campus 66911)/ Emergency: 911

Section 1 Process:

(Check One) Process

Hazardous Chemical

Hazard Class

Summary:

This covers the operation of the Water Displacement Vessel (WDV). The main hazards related to the WDV operation are potential exposure and handling of chemicals (pyrolysis gases) and exposure to elevated pressures (<3200 psig).

This SOP includes two methods in section 12. Method 1 prepares the WDV for the experimental day by replacing all the gas inside the WDV with water. Method 2, performed on the experimental day, transfers the final experimental gases to water-filled WDV and prepares the WDV for next experiment.

Section 2: Describe Process Hazards, Hazardous Chemical or Hazard Class.

Table 2.1. NFPA Hazard Classification and Exposure limit. ^aSimple Asphyxiant, ^bACGIH: American Conference of Governmental Industrial Hygienist, ^cTWA: Time Weighted Average

Chemical	Health	Fire	Reactivity	Specific	Exposure limit
Pyrolysis gas products:					
Nitrogen	0	0	0	SA ^a	
Carbon monoxide	2	4	0	SA ^a	ACGIH ^b TWA ^c 25 ppm
Carbon dioxide	1	0	0	SA ^a	ACGIH ^b TWA ^c 5000 ppm
Methane	1	4	0	SA ^a	
Hydrogen	0	4	0	SA ^a	

Pyrolysis gases: The final experimental gases, consisting of a maximum of ~10 grams of the pyrolysis products (CO, CO₂, CH₄ and H₂) and the N₂ originally fed into the reactor, are transferred at the end of an experiment from the Wall Heated Tubing Bomb (WHTB) to the Water Displacement Vessel (WDV) and finally released into a lab snorkel exhaust. The calculation below shows that a release of the pyrolysis gases into the lab is too small to present a hazard to lab personnel. Therefore, good ventilation is sufficient to prevent the exposure of the lab personnel to high local concentrations, nonetheless, all pyrolysis gases must be vented into a lab snorkel exhaust.

POST 12 has an approximate volume of 129.80 m³ (V_{POST 11, approx}=5.18m x 9.75m x 2.57m). The room filled with air at 1 atm and ~20 °C equates to a mass of air of 156.5 kg as shown by the following equation:

$$m_{Air} = \frac{1 \text{ atm } 129800L}{0.082 \frac{\text{atmL}}{\text{mol K}}} \frac{28.966 \text{ g}}{1 \text{ mol}} = 156488.3g \approx 156.5 \text{ kg}$$

The release of the final pyrolysis gases into POST 12 will change the composition and concentration of gas in the room. The 10 g of pyrolysis products that are released consist of a mixture of mainly CO₂ (more than half), then CO with traces of CH₄ and H₂. The nitrogen released into the Lab is equal to the nitrogen originally fed into the reactor volume which is around 0.22 L. The mass of nitrogen fed in the reactor varies from an approximate value of 0.14 g to around 5.5 g depending on the initial nitrogen reactor pressure, from 0 psig to 300 psig respectively, as shown by the following equations:

$$m_{N_2 \text{ at } 0 \text{ psig}} = \frac{1 \text{ atm} 0.22L}{0.082 \frac{\text{atmL}}{\text{mol K}}} \frac{28 \text{ g}}{1 \text{ mol}} = 0.26g$$

$$m_{N_2 \text{ at } 300 \text{ psig}} = \frac{21.41 \text{ atm} 0.22L}{0.082 \frac{\text{atmL}}{\text{mol K}}} \frac{28 \text{ g}}{1 \text{ mol}} = 5.5g$$

The release of 10 g of pyrolysis gas and 5.5 g of nitrogen (maximum nitrogen mass fed into the reactor) do not coexist as it will exceed the maximum reactor pressure ratings. Releasing 10 g of pyrolysis gas into the POST 12

environment corresponds with mass concentrations of pyrolysis gases of 63.9ppm_w (10 g pyrolysis gases / 156488 g air) and 5.5 g of nitrogen concentration correspond to 35.14ppm_w (5.5g N₂/156488 g air). Thus, unintended release of the final experimental pyrolysis gases into the lab environment does not pose a hazard for the experimenter. Notice that these calculations are somewhat simplistic; this assumes instantaneous and complete mixing of the leaked contaminant and the entirety of the room's air. A snorkel directed to the reactor could eliminate localized high concentrations.

Prior to measuring their volume in the WDV, gases contained in the WHTB are at elevated pressure (420 to 2000 psig at experimental test temperature). The total volume of these contained gases at standard pressure and temperature are <8 L.

Section 3: Personal Protective Equipment.

Safety glasses or goggles, flame resistant lab coat, long pants, covered shoes.

Section 4: Engineering Controls.

Pyrolysis gases: A standard laboratory air exchange ventilation rate is sufficient to prevent worker exposure to hazardous concentrations of airborne contaminants, nonetheless, pyrolysis gases should be released into the lab snorkel exhaust.

Electricity: Inspect electrical cords, plugs, and receptacles prior to each use.

Section 5: Special Handling and Storage Requirements.

Pyrolysis gases

Handling: Avoid contact with eyes, skin and clothing. Avoid breathing gas. Only use where there is adequate ventilation. Avoid ignition sources. Use the custom-made WHTB holder (shown in Figure 5.1) for WHTB reactor relocation.

Storage: Store the WDV in an area that is cool, ventilated.



Figure 5.1. Custom-made WHTB -holder for reactor relocation.

Section 6: Spill and Accident Procedures.

Stop or reduce leak if safe to do so. Provide adequate ventilation. According to the above mentioned calculations, exposure to mixed pyrolysis gases at the concentrations generated under the test conditions is not hazardous.

Small Fire: Fire extinguisher, appropriately trained personnel only. There are fire extinguishers in POST 11 and POST 12 indicated as FE on the floor map below.

Large Fire: Leave the room and call (956-6911).

Section 7: Waste Disposal Procedures.

Pyrolysis gases: For emergency disposal, slowly discharge gas to the lab snorkel exhaust or fume hood. Make sure hood is working, e.g. with a Kim wipe.

Section 8: Special Precautions Animal Use.

Not Applicable

Section 9: Required Approvals:

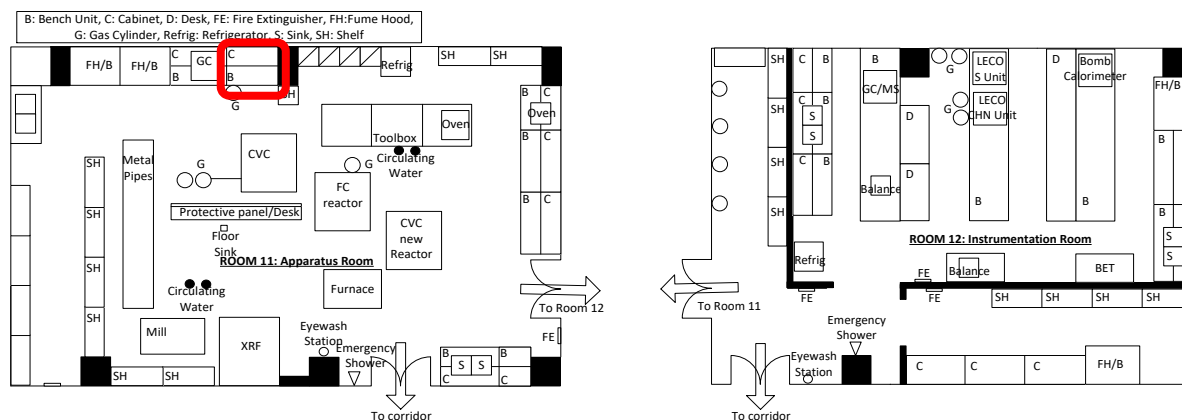
EHSO Lab Safety Training, approval and training from PI or lab supervisor. Read and understand all methods, QRA's, JSA's and SOP's developed for the operation of the WDV.

Section 10: Decontamination.

All work surfaces will be cleaned with paper towel at the end of the test and at the end of the day in keeping with good laboratory practice.

Section 11: Designated Areas.

The R³Lab Room 11 framed section in the map below is designated for WDV preparation and loading.



Section 12.

Method1: Fill Water Displacement Vessel (WDV)

Figure 12.1 and Figure 12.2 show, respectively, a schematic diagram of the WDV and a photograph of the WDV with its parts labelled. The schematic diagram in Figure 12.1 labels the inlet/outlets of the 3-way valve (V10) as A, B and C, as well as an extra position X in between B and C. The X position is not a real position, i.e. it is half way (90 degree) between B and C as shown on the diagram and effectively serves to shut off all flow. The valve can be positioned as A-X, i.e. Closed; A-B, connecting WDV with *Water Collection Vessel*; and A-C, connecting WDV with *Water Displacement Vessel Reservoir (WDVR)*. Figure 12.3 shows a photograph of the 3-way valve with the actual labels as *Valve Closed*, *Fill WDV* and *Empty WDV*. These labels respectively correspond to positions A-X, A-B and A-C.

1. Check the initial valve positions match those in Table 12.1. Every time valve positions are modified, a new table will be shown.

Table 12.1.

V9	V10
Closed	A-X

2. Position V10 in *Fill WDV* mode (or A-B)

Table 12.2.

V9	V10
Closed	A-B

3. Open V9. Water will start flowing from WDVR to WDV displacing the gas inside into the snorkel exhaust. Add water to the WDVR when the vessel becomes half empty.

Table 12.3.





V9	V10
Open	A-B

4. Eliminate any gas pocket inside the WDV with the help of a pipette at QD1. In order to unseal QD1, an auxiliary connection is attached in this step in order to open it.

5. When WDV is completely filled with water (i.e. all gas has been purged), close V9 and V10

Table 12.4.

V9	V10
Closed	A-X

Legend			
WDV	Water Displacement Vessel		3-way Ball Valve
WDVR	Water Displacement Vessel Reservoir	A	3-way Ball Valve Inlet/Outlet A
	Metering Needle Valve	B	3-way Ball Valve Inlet/Outlet B
	Quick Disconnect	C	3-way Ball Valve Inlet/Outlet C
	Check Valve	x	3-way Ball Valve Position x

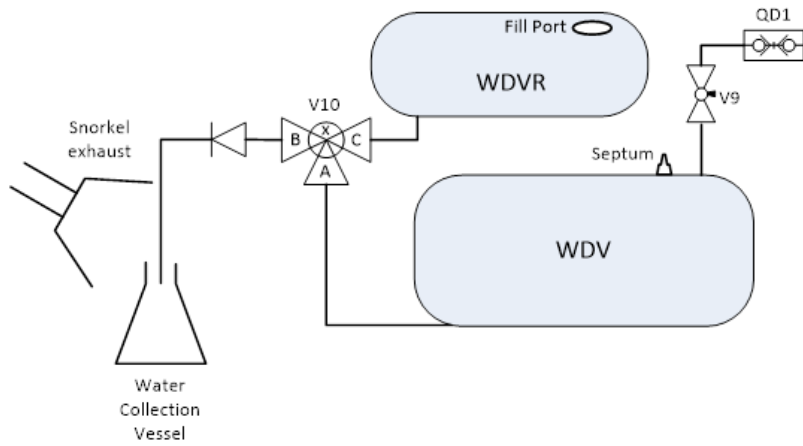


Figure 12.1. Water Displacement Vessel

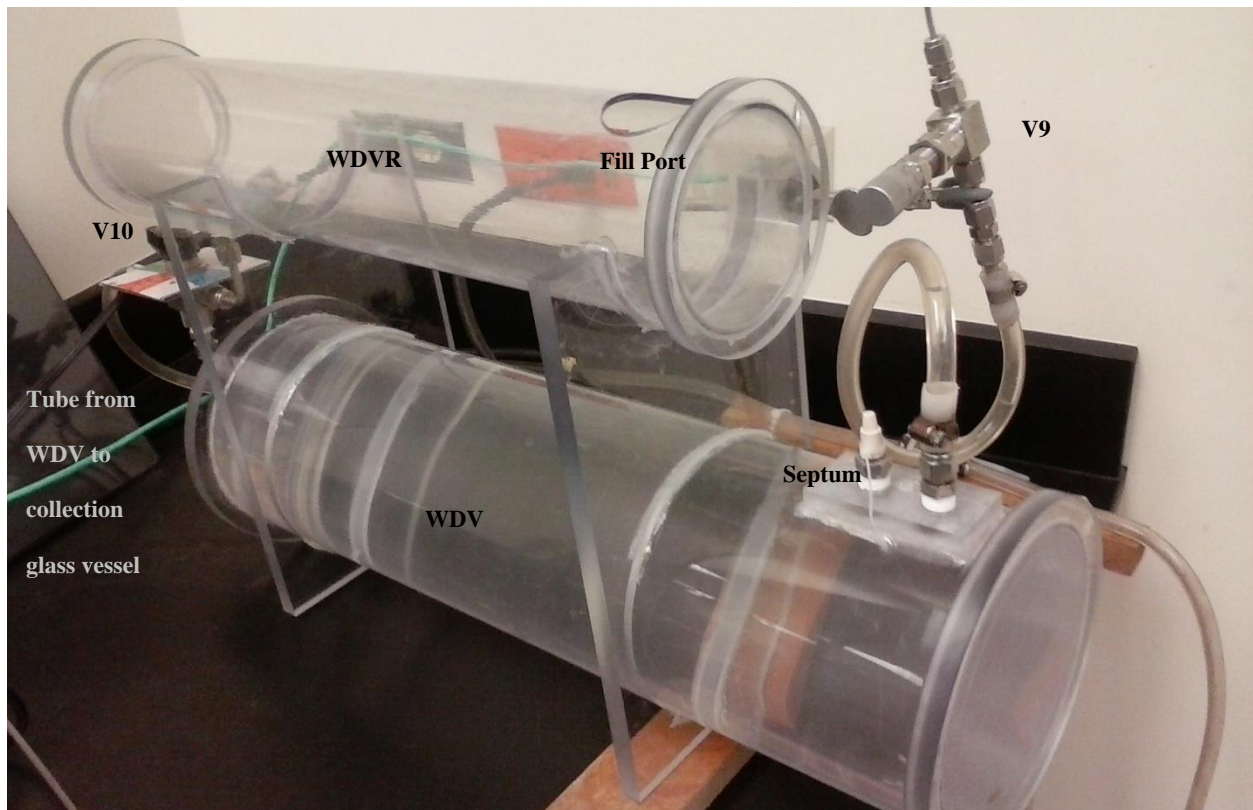


Figure 12.2. Water Displacement Vessel Photograph

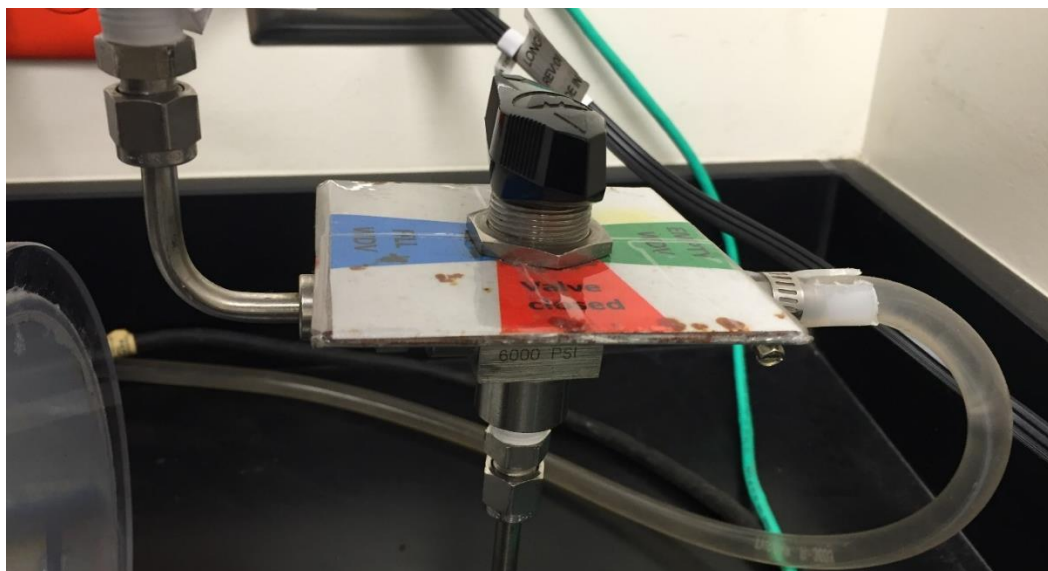


Figure 12.3. 3-way Valve (V10) Photograph

Method 2: Loading experimental gases from the WHTB to the Water Displacement Vessel (WDV)

1. Read the output from thermocouple TC1 and verify that the Wall Heated Tubing Bomb (WHTB) is at ambient temperature.
2. Secure the WHTB to the custom-made hand truck shown in Figure 5.1 and safely transport the WHTB from its position next to the sand bath to the WDV.
3. Connect the WHTB to the WDV with Quick Disconnect QD1. Figure 12.4 shows a diagram of the WHTB setup. A weighed conical glass flask is placed by the outlet from V10 to collect the displaced water.

The schematic diagram in Figure 12.4 labels the inlet/outlets of the 3-way valve (V10) as A, B and C, as well as an extra position X in between B and C. The X position is not a real position, i.e. it is half way (90 degree) between B and C as shown on the diagram and effectively serves to shut off all flow. The valve can be positioned as A-X, i.e. Closed; A-B, connecting WDV with *Water Collection Vessel*; and A-C, connecting WDV with Water Displacement Vessel Reservoir WDVR. Figure 12.3 shows a photograph of the 3-way valve with the actual labels as *Valve Closed*, *Fill WDV* and *Empty WDV*. These labels respectively correspond to positions A-X, A-B and A-C.

4. Check the initial valve positions match those in Table 12.5. Every time valve positions are modified, a new table will be shown.

Table 12.5.

V4	V5	V9	V10
Closed	Closed	Closed	A-X

5. **Position V10 in Empty WDV (or A-C).** This will prevent the pressure from building up in the WDV as the WDV cannot withstand elevated pressures.

Table 12.6.

V4	V5	V9	V10

Closed	Closed	Closed	A-C
--------	--------	--------	-----

6. Open V4

Table 12.7.

V4	V5	V9	V10
Open	Closed	Closed	A-C

7. Slowly open V9 until gas starts flowing from the WHTB to the WDV displacing the water inside the WDV. The displaced water is collected by the water collection vessel.

Table 12.8.

V4	V5	V9	V10
Open	Closed	Open	A-C

8. When water stops flowing, close V4 and V9.

Table 12.9.

V4	V5	V9	V10
Closed	Closed	Closed	A-C

9. Weigh the filled water collector and record its weight on the Excel file

10. Disconnect WHTB from WDV with the quick disconnect valve QD1

11. Position V10 in *Fill WDV* mode (or A-B). It will add small amounts of water into the WDV to maintain it at atmospheric pressure

Table 12.10.

V4	V5	V9	V10
Closed	Closed	Closed	A-B

12. The GC analysis can be started

13. After the GC analysis is complete, vent the pyrolysis gases from the system. Check the initial valve positions match those of Table 12.11.

Table 12.11.

V9	V10
Closed	A-X

14. Position V10 in *Fill WDV* mode (or A-B)

Table 12.12.

V9	V10
Closed	A-B

15. Open V9. Water will start flowing from WDVR to WDV displacing the gas inside into the lab snorkel exhaust. Keep adding water to the Water Displacement Vessel Reservoir. Maintain water level of WDVR above half its volume

Table 12.13.

V9	V10
Open	A-B

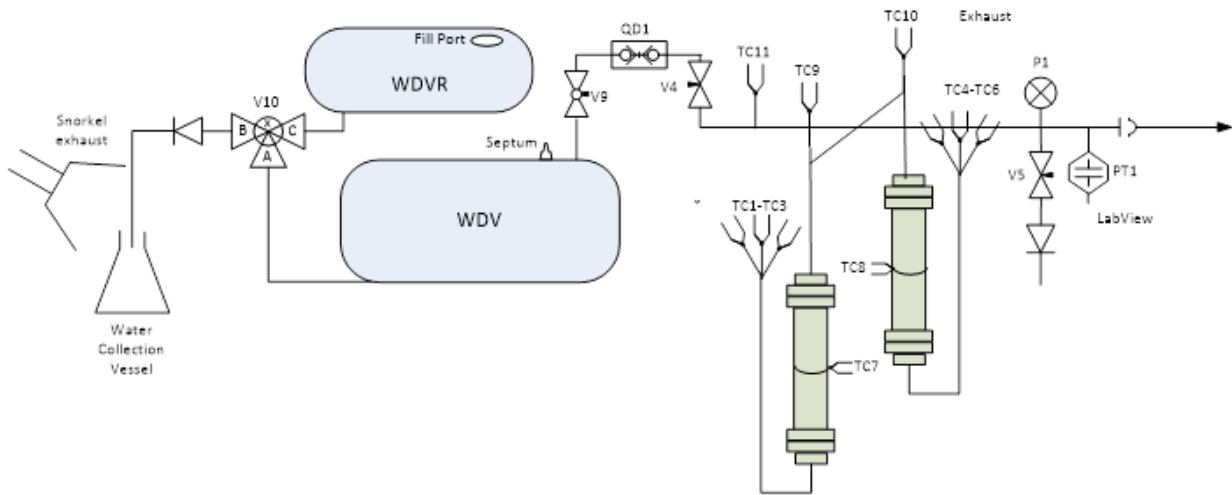
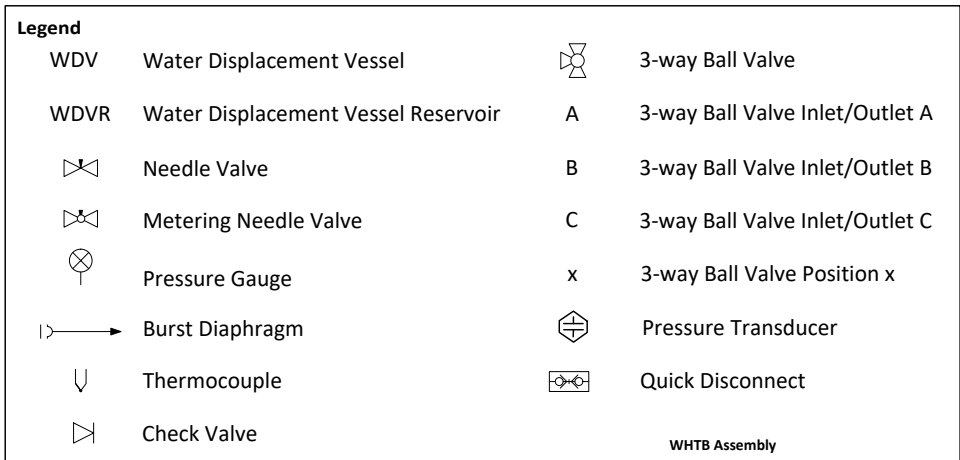


Figure 12.4. WHTB connected to WDV diagram

JOB SAFETY ANALYSIS

Safety Information for the University of Hawaii at Manoa

NAME OF DEPARTMENT: HAWAII NATURAL ENERGY INSTITUTE

Title of Job or Task: Water Displacement Vessel Operation

TASK	HAZARDS	CONTROLS
1. Prepare Water Displacement Vessel (WDV)	Pyrolysis gas product in the WDV	<p>PPE</p> <p>Safety glasses or goggles Nitrile Gloves Flame resistant lab coat Long pants</p> <p>Engineered controls</p> <p>Good general ventilation should be sufficient to control worker exposure to airborne contaminants. Use lab exhaust snorkel to avoid accumulation of high concentrations of gas. Avoid ignition sources.</p>
2. Loading experimental gases from the reactor to the WDV	<p>Pyrolysis gas product</p> <p>Transportation of a pressurized WHTB</p> <p>Overpressurization of the WDV</p>	<p>PPE</p> <p>Safety glasses or goggles Nitrile Gloves Flame resistant lab coat Long pants</p> <p>Engineered controls</p> <p>Good general ventilation should be sufficient to control worker exposure to airborne contaminants. Use lab exhaust snorkel to avoid accumulation of high concentrations of gas. Avoid ignition sources. Use the custom-made hand truck for WHTB reactor transportation</p>

<p>Other Information:</p> <p>JSA Completed By:</p> <p>Date Created:</p> <p>OSHA Reference:</p>			<p>Ensure the WDV 3-way valve is positioned in <i>empty</i> mode while transferring gases from the reactor to the WDV to avoid overpressurization in the WDV</p>
	<p>Required Training: EHSO Lab Safety Training, Read UH Chemical hygiene plan, Specific lab activity training by PI or lab supervisor, Read and understand all methods, QRA's, JSA's and SOP's developed for the operation of the WDV</p>	<p>Required Personal Protective Equipment (PPE)</p> <p>Safety glasses or goggles</p> <p>Nitrile Gloves</p> <p>Flame resistant lab coat</p> <p>Long pants</p>	
	<p>See Scott Turn, Trevor Morgan, Lloyd Paredes, Pablo J. Arauzo-Gimeno and Maider Legarra-Arizaleta for more information on Job Hazard Analysis</p> <p>Maider Legarra-Arizaleta, Trevor Morgan, Scott Turn, Lloyd Paredes and Pablo J. Arauzo-Gimeno</p> <p>April 20, 2018</p> <p>_____</p> <p>For more information about this JSA, contact the <i>University of Hawaii Environmental Health and Safety Office</i> http://www.hawaii.edu/ehso/industrial/ or by phone at 956-3204</p>		

APPENDIX I. SOP and JSA 6: Volume Evaluation of the Wall

Heated Tubing Bomb

Laboratory Standard Operating Procedures

University of Hawaii at Manoa

Please fill out and place in your Chemical Hygiene Plan

Volume Evaluation of the Wall Heated Tubing Bomb

Date: 04/20/2018

Principal Investigator: Scott Q. Turn

Produced By: Maider Legarra-Arizaleta, Trevor Morgan, Scott Turn, Lloyd Paredes and Pablo J. Arauzo-Gimeno

Room and Building: POST 11/12

Phone Number: PI Scott Turn: 808-956-2346/ POST 11: 808-956-9903/POST 12: 808-956-3790/

UH Emergency: 808-956-6911 (on campus 66911)/ Emergency: 911

Section 1 Process:

(Check One) Process

Hazardous Chemical

Hazard Class

Summary: This SOP is for evaluating the volume of the Wall Heated Tubing Bomb (WHTB). The main hazards related to the volume evaluation of the Wall Heated Tubing Bomb (WHTB) are potential exposure to chemicals (compressed N₂ gas), the exposure to elevated pressures (<3000 psig) and electricity (220 V, 20Amps). A detailed 'Operation Method' is provided in section 12.

Section 2: Describe Process Hazards, Hazardous Chemical or Hazard Class.

Table 2.1. NFPA Hazard Classification and Exposure limit. ^aSimple Asphyxiant, ^bACGIH: American Conference of Governmental Industrial Hygienist, ^cTWA: Time Weighted Average

Chemical	Health	Fire	Reactivity	Specific	Exposure limit
Nitrogen	0	0	0	SA ^a	
Alundum	NA	NA	NA	NA	10mg/m ³ 8-hour TWA ^c inhalable dust
Charcoal	1	2	1		ACGIH ^b TWA ^c 2mg/m ³

Compressed Nitrogen: Inhalation: No known significant effects or critical hazards. Skin contact: Contact with rapidly expanding gas may cause burns or frostbite. Eye contact: Contact with rapidly expanding gas may cause burns or frostbite. In addition to any other important health or physical hazards, this product may displace oxygen and cause rapid suffocation (when concentrations are sufficient to reduce oxygen levels below 19.5%).

Mains Electricity: All the electrical connections and cables related to the laptop, pressure sensors, and National instrument (NI) data acquisition equipment are standard 120 V (20 amps) components as provided by the equipment suppliers.

Section 3: Personal Protective Equipment.

Safety glasses or goggles, heat resistant gloves, flame resistant lab coat, covered shoes, long pants.

Section 4: Engineering Controls.

Compressed Nitrogen: General laboratory ventilation is sufficient to control worker exposure to airborne contaminants in the present location (POST 11). Install an excess 'flow restrictor' valve in the line from the Nitrogen cylinder to the WHTB to prevent excessive release of nitrogen into the environment.

Perform experiment inside the Unistrut- polycarbonate structure in Figure 4.1. Polycarbonate sheets are 2-ply polycarbonate laminate 3/8'' thick each (Hygard CG375). The Hygard sheet meets all security requirements with regard to protection against forced entry and ballistic impact.

Use appropriate tools to open and close valves in order to avoid direct contact of the experimenter with the pressurized reactor and lines. Ensure pressure does not exceed the burst disk pressure.

Activate LabVIEW alarms to indicate when the reactor pressure is 100 psig over the test pressure or 200 psig below the burst disk pressure.



Figure 4.1. Welded steel-polycarbonate structure for enclosing WHTB during an experiment

Electricity: Inspect electrical cords, plugs, and receptacles prior to each use.

Section 5: Special Handling and Storage Requirements.

Compressed Nitrogen:

Storage: Store in accordance with local regulations. Store in a segregated and approved area. Store away from direct sunlight in a dry, cool and well-ventilated area. Keep container tightly closed and sealed until ready for use.

Cylinders should be stored upright, with valve protection cap in place, and firmly secured to prevent falling or being knocked over. Cylinder temperatures should not exceed 52 °C (125 °F).

Handling: Put on appropriate personal protective equipment. Contains gas under pressure. Avoid contact with eyes, skin and clothing. Avoid breathing gas. Empty containers retain product residue and can be hazardous. Do not puncture or incinerate container. Use equipment rated for cylinder pressure. Close valve after each use and when empty. Protect cylinders from physical damage; do not drag, roll, slide, or drop. Use a suitable hand truck for cylinder movement.

Section 6: Spill and Accident Procedures.

Compressed Nitrogen:

No action shall be taken involving any personal risk or without suitable training. Evacuate surrounding areas. Keep unnecessary and unprotected personnel from entering. Avoid breathing gas. Provide adequate ventilation. Wear appropriate respirator (Self-Contained Breathing Apparatus SCBA) when ventilation is inadequate.

Small spill: Shutoff source of gas. Stop leak if without risk. Contact emergency personnel (see Phone number information above) if necessary.

Large spill: Immediately contact emergency personnel (see Phone number information above). Stop leak if without risk. Note: Call supplier for emergency contact information (AirGas 24-hour phone 1-866-734-3438).

Small Fire: Fire extinguisher, appropriately trained personnel only. There are fire extinguishers in POST 11 and POST 12 indicated as FE on the floor map below.

Large Fire: Leave the room and call (956-6911).

Section 7: Waste Disposal Procedures.

Compressed Nitrogen:

Unused product/ empty container: Return cylinder and unused product to supplier. Do not attempt to dispose of residual or unused quantities.

Disposal: For emergency disposal, secure the cylinder and slowly discharge gas to the atmosphere in a well ventilated area or outdoors.

Section 8: Special Precautions Animal Use.

Not Applicable

Section 9: Required Approvals:

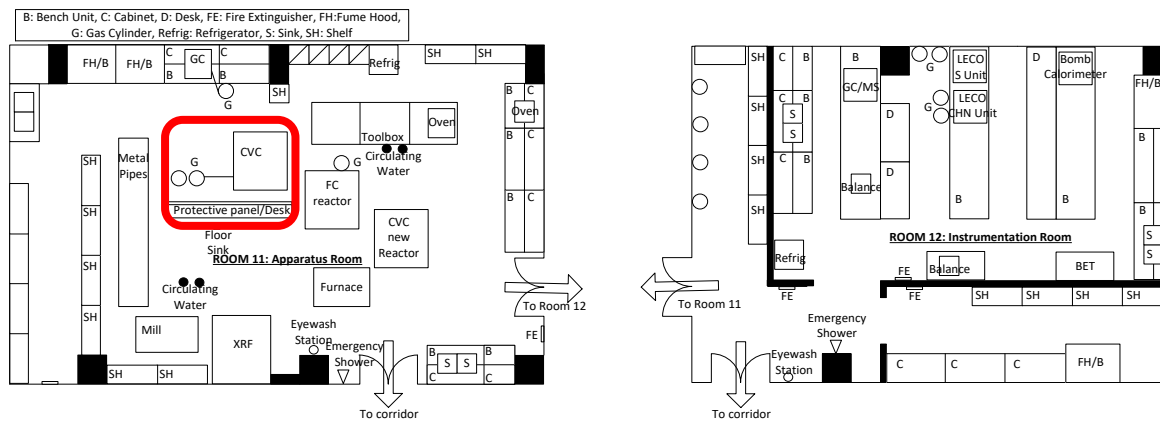
EHSO Lab Safety Training, Hazardous Waste Generator Safety Training, approval and training from PI or lab supervisor. Read and understand all methods, QRA's, JSA's and SOP's developed for evaluating the volume of the WHTB.

Section 10: Decontamination.

EHSO Lab Safety Training, Hazardous Waste Generator Safety Training, approval and training from PI or lab supervisor. Read and understand all methods, JSA's and SOP's developed for evaluating the volume of the WHTB.

Section 11: Designated Areas.

The R³Lab Room 11 framed section in the maps below is designated for volume evaluation.



Section 12. Method:

- Figure 12.1 shows a complete diagram of the WHTB assembly connected to the nitrogen charging system. The equipment is divided into sections in order to provide a clear volume nomenclature. Ensure that the reactor is disconnected from the WHTB assembly at QD1.

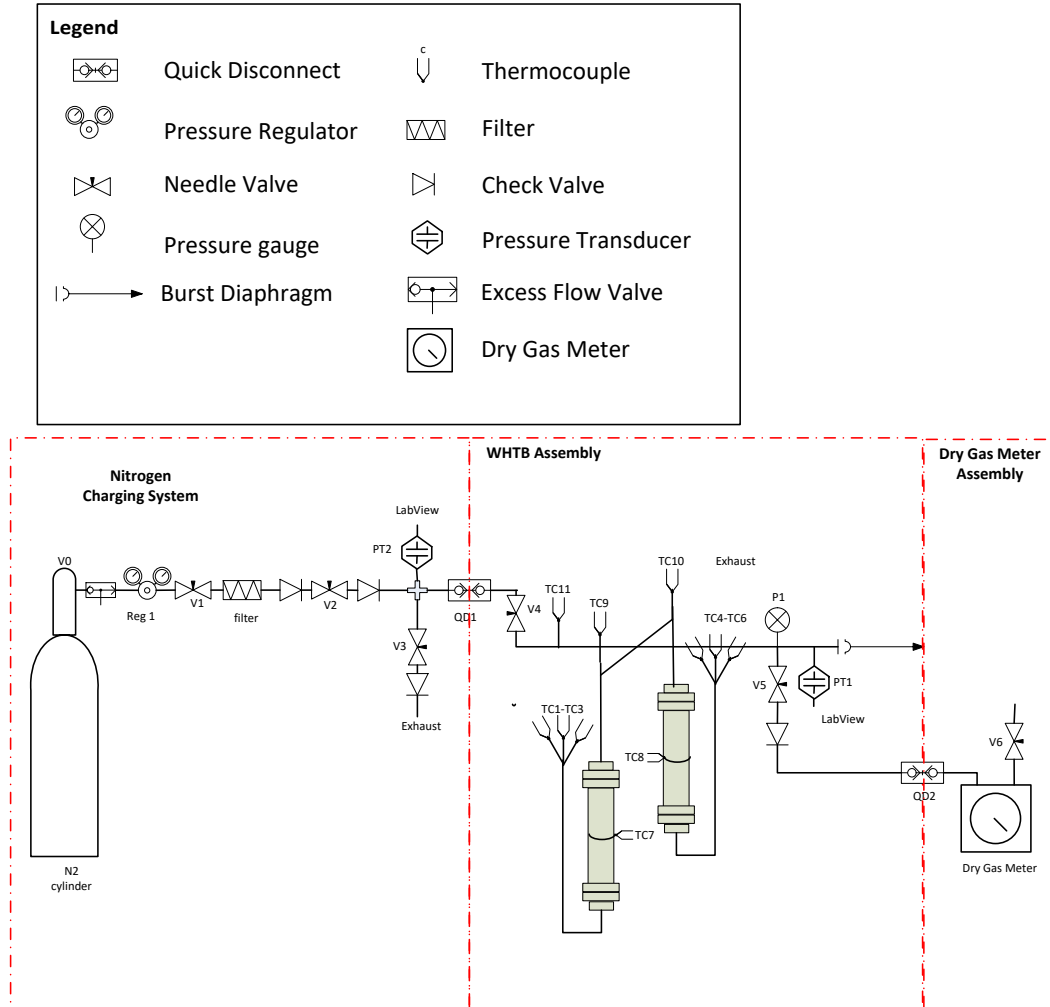


Figure 12.1. WHTB Diagram with Volume Nomenclature

2. Confirm the valves positions match those of Table 12.1. Every time a valve or regulator position is modified a new Table will be presented.

Table 12.1.

V0	V1	V2	V3	V4	V5	V6	Reg1 Inlet	Reg1 Outlet
Closed	Closed	Closed	Closed	Closed	Closed	Open	0 psig	0 psig

3. Open V0. The pressure at the inlet of regulator 1 will increase

Table 12.2.

V0	V1	V2	V3	V4	V5	V6	Reg1 Inlet	Reg1 Outlet

Open	Closed	Closed	Closed	Closed	Closed	Open	N ₂ Supply Cylinder Pressure	0 psig
------	--------	--------	--------	--------	--------	------	---	--------

4. Assess the status of the nitrogen charging system by reading the pressures on the Reg1 inlet
 - 4.1. If the pressure shown on the Reg1 inlet is not sufficient to reach the volume evaluation pressure requirements (>300 psig), the N₂ supply cylinder must be replaced; (see SOP for gas cylinder replacement). After cylinder replacement, return to Step 2.
 - 4.2. If sufficient pressure exists in the N₂ supply cylinder, turn the Reg1 knob clockwise until the pressure on the outlet of Reg1 equals the volume evaluation pressure requirements

Table 12.3.

V0	V1	V2	V3	V4	V5	V6	Reg1 Inlet	Reg1 Outlet
Open	Closed	Closed	Closed	Closed	Closed	Open	N ₂ Supply Cylinder Pressure	300psig

5. Place the loaded reactor (refer to reactor loading SOP) inside the welded steel-polycarbonate structure, mount it on the square tube. Do not immerse the reactor in the sandbath.
6. Connect the reactor to the nitrogen charging system and to the Dry Gas Meter assembly using the quick disconnects QD1 and QD2.
7. An example of a Loading Form is given in Figure 12.2. The Loading Form is divided into five tables: Table 1 with data from the *Proposal Conditions*, Table 2 logs data from the *Reactant Moisture Content Analysis*, Table 3 data from the *Solid Reactant Feed Bomb Load*, Table 4 with Reactant Moisture Content data and finally, Table 5 with data from the *Void Volume Evaluation*. In Table 5 of the Loading Form, write down the *Room Temperature* from the lab mercury thermometer and the *Room Pressure* from the lab mercury barometer.
8. Write down the *Initial Reactor Pressure* from pressure transducer PT1 (atmospheric pressure), and write down the reading on the dry gas meter.
9. Open V1 and V2

Table 12.4.

V0	V1	V2	V3	V4	V5	V6	Reg1 Inlet	Reg1 Outlet
Open	Open	Open	Closed	Closed	Closed	Open	N ₂ Supply Cylinder Pressure	300psig

10. Slowly open V4.

Table 12.5.

V0	V1	V2	V3	V4	V5	V6	Reg1 Inlet	Reg1 Outlet
Open	Open	Open	Closed	Open	Closed	Open	N ₂ Supply Cylinder Pressure	300psig

11. When PT1 reaches ~50 psig, close V4 rapidly

Table 12.6.

V0	V1	V2	V3	V4	V5	V6	Reg1 Inlet	Reg1 Outlet
Open	Open	Open	Closed	Closed	Closed	Open	N ₂ Supply Cylinder Pressure	300psig

12. After stabilization, write down the *Initial Reactor Pressure* from Pressure gauge PT1 and the *Initial Dry Gas Meter* volume in Table 5 of the Loading Form.

13. Slowly open V5 to avoid gas hammering while depressurizing the reactor. Once depressurized, write down the *Final Reactor Pressure* and *Final Dry Gas Meter* volume in Table 5 of the Loading Form.

Table 12.7.

V0	V1	V2	V3	V4	V5	V6	Reg1 Inlet	Reg1 Outlet
Open	Open	Open	Closed	Closed	Open	Open	N ₂ Supply Cylinder Pressure	300psig

14. Close valve V5

Table 12.8.

V0	V1	V2	V3	V4	V5	V6	Reg1 Inlet	Reg1 Outlet
Open	Open	Open	Closed	Closed	Closed	Open	N ₂ Supply Cylinder Pressure	300psig

15. Repeat steps 8 to 14 four times and with each repetition, change PT1 pressure in step 11 to approximately 100, 150, 200 and 250 psig, respectively.

The loaded V_{Bomb} can finally be calculated with equation 12.1.

$$V_{Bomb} = (V_{DGM,f} - V_{DGM,i}) \frac{P_{Lab}}{P_{reactor,i} - P_{reactor,f}} \quad 12.1$$

In order to minimize errors and increase reliability in the calculation of the test volume, the described process is repeated at several test pressures, and the test volume is determined from the slope of the regression equation of $(V_{DGM,f} - V_{DGM,i})P_{Lab}$ versus $(P_{reactor,i} - P_{reactor,f})$ (see equation 12.2)

$$(V_{DGM,f} - V_{DGM,i})P_{Lab} = V_{Bomb}(P_{reactor,i} - P_{reactor,f}) \quad 12.2$$

The Excel file will automatically plot $(V_{DGM,f} - V_{DGM,i})P_{Lab}$ versus $(P_{reactor,i} - P_{reactor,f})$ and display the test volume V_{Bomb} .

WHTB Pyrolysis Setup

Table 1. Proposal Conditions

Date: _____	Pyrolysis Feed: _____	Packing: _____
Pressurizing Gas: _____	Manufacturer: _____	Nominal Bomb Pressure [psig]: _____
Experimenters: _____	Lot Number: _____	Nominal Sand Bath Temperature [°C]: _____

Table 2. Reactant Moisture Content Analysis

Tare mass [g]: _____	Tare and sample mass [g]: _____	Moisture Content [%]: <u>#DIV/0!</u>
Final mass 1 [g]: _____	Valid final mass [g]: <u>0.003</u>	
Final mass 2 [g]: _____		
Final mass 3 [g]: _____		
Final mass 4 [g]: _____		
Final mass 5 [g]: _____		
Final mass 6 [g]: _____		
Final mass 7 [g]: _____		

Table 3. Solid Reactant Feed Bomb Load

	Cork	Reactor Body New	TC Bottom New	Reactor Top No Cap	Filter Paper	Maximum Reactants	Sample Reactants	Remaining Reactants	SS Screen	Stem	Antiseize	mass [g]
1	X											
2	X	X										
3	X		X									
4	X						X					
5	X			X								
6	X	X	X									
7	X	X	X				X					
8	X	X	X	X			X					
9	X				X							
10	X				X	X						
11	X				X		X					
12	X			X			X					
13	X			X			X			X		
14	X	X	X	X		X	X					
15	X									X		

Table 4. Reactant Moist Mass [g]

by filter paper difference	10-11	0.00
by reactor, SS screen, TC bottom and reactor top difference	14-8	0.00
Experimental Mass		0.00

Table 5. Void Volume Evaluation

Iteration 1	VOLUME EVALUATION				LEAN TEST				BACKFILL FROM REQUESTED VOLUME			
	Initial Cart Pressure Part 1 [psig]	Initial Reactor Pressure Press1 [psig]	Room T [degC]	Room Pressure [mmHg]	Final Cart Pressure Part 1 [psig]	Final Reactor Pressure Press 1 [psig]	DGM start m3	DGM End m3	Requested Volume Pressure [psig]	Empty Reactor Pressure [psig]	Backfilled Reactor and Semestered Pressure [psig]	
1												
2												
3												
4												
5												

Last Modified 3/18/2017

Figure 12.2. Loading Form

JOB SAFETY ANALYSIS

Safety Information for the University of Hawaii at Manoa

NAME OF DEPARTMENT: HAWAII NATURAL ENERGY INSTITUTE

Title of Job or Task: Wall Heated Tubing Bomb Volume Evaluation

TASK	HAZARDS	CONTROLS
<p>1. Volume Evaluation</p>	<p>Compressed nitrogen H280 – Contains gas under pressure; may explode if heated. OSHA-H01 – May displace oxygen and cause rapid suffocation.</p> <p>Overpressurization of the reactor</p> <p>120V AC from mains to pressure sensors, laptop and NI data acquisition system.</p>	<p>PPE Safety glasses or goggles Flame resistant lab coat Covered shoes Long pants</p> <p>Engineered controls Implement pressure alarms in LabVIEW for experimental pressure objective and for warning of impending burst disk rupture. Good general ventilation should be sufficient to control worker exposure to airborne contaminants. Perform WHTB volume evaluation inside the Unistrut-polycarbonate structure</p> <p>Direct tube from burst diaphragm to a bucket full of water</p> <p>Use appropriate tool to open and close valves in order to avoid direct contact of the experimenter with the pressurized reactor and lines.</p> <p>Install excess flow restrictors on all gas cylinders actively used in the experiment.</p> <p>Inspect electrical cords, plugs, and receptacles prior to each use.</p>

	<p>Required Training: EHSO Lab Safety Training, Read UH Chemical hygiene plan, Specific lab activity training by PI or lab supervisor, Read and understand all methods, QRA's, JSA's and SOP's developed for evaluating the volume of the WHTB.</p>	<p>Required Personal Protective Equipment (PPE)</p> <ul style="list-style-type: none"> Safety glasses or goggles Flame resistant lab coat Covered shoes Long pants
<p>Other Information: JSA Completed By: Date Created: OSHA Reference:</p>	<p>See Scott Turn, Trevor Morgan, Lloyd Paredes and Maider Legarra-Arizaleta for more information on Job Hazard Analysis</p> <p>Maider Legarra-Arizaleta, Trevor Morgan, Scott Turn, Lloyd Paredes and Pablo J. Arauzo-Gimeno</p> <p>April 20, 2018</p> <p>_____</p> <p>For more information about this JSA, contact the <i>University of Hawaii Environmental Health and Safety Office</i> http://www.hawaii.edu/ehso/industrial/ or by phone at 956-3204</p>	

APPENDIX J. SOP and JSA 7: Performing an Experiment, Unloading and Disassembly of the Wall Heated Tubing Bomb

Laboratory Standard Operating Procedures

University of Hawaii at Manoa

Please fill out and place in your Chemical Hygiene Plan

Performing an Experiment, Unloading and Disassembly of the Wall Heated Tubing Bomb

Date: 04/20/2018

Principal Investigator: Scott Q. Turn

Produced By: Maider Legarra-Arizaleta, Trevor Morgan, Scott Turn, Lloyd Paredes and Pablo J. Arauzo-Gimeno

Room and Building: POST 11/12

Phone Number: PI Scott Turn: 808-956-2346/ POST 11: 808-956-9903 /POST 12: 808-956-3790/

UH Emergency: 808-956-6911 (on campus 66911)/ Emergency: 911

Section 1 Process:

(Check One) Process

Hazardous Chemical

Hazard Class

Summary: This SOP is for performing an experiment and unloading and disassembly of the Wall Heated Tubing Bomb (WHTB) after an experiment.

The main hazards related to an experiment, unloading and disassembly of the Wall Heated Tubing Bomb (WHTB) are potential exposure to chemicals (compressed N₂ gas, alundum, charcoal and cleaning solvent), the exposure to elevated pressures (<3000 psig), elevated temperatures (<550 °C, note that even though 600°C is specified as the maximum sand bath temperature by the manufacturer, 550°C was the maximum achieved in real life under full power), and electricity (120 V, 20 Amps for the mass balance, laptop, pressure sensors, fan, and National Instrument (NI) data acquisition equipment and 240 V 50/60 Hz for the sand bath).

A detailed 'Operation Method' is provided in section 12. The method refers to additional SOP's provided in separate documents: (1) an SOP for purging air from the reactor with nitrogen, (2) an SOP for Gas Chromatograph (GC) operation, (3) an SOP for Water Displacement Vessel (WDV) operation, (4) an SOP for determining the charcoal moisture content and (5) an SOP for changing gas cylinders.

Section 2: Describe Process Hazards, Hazardous Chemical or Hazard Class.

Table 2.1. NFPA Hazard Classification and Exposure limit. ^aSimple Asphyxiant, ^bACGIH: American Conference of Governmental Industrial Hygienist, ^cTWA: Time Weighted Average, ^dWEEL: Workplace Environmental Exposure Levels, ^ePEL: California permissible exposure limits for chemical contaminants (Title 8, Article 107)

Chemical	Health	Fire	Reactivity	Specific	Exposure limit
Nitrogen	0	0	0	SA ^a	
Alundum	NA	NA	NA	NA	10mg/m ³ 8-hour TWA ^c inhalable dust
Charcoal	1	2	1		ACGIH ^b TWA ^c 2mg/m ³
N-Methyl-2-pyrrolidone (NMP) cleaning solvent	2	2	0		WEEL ^d TWA ^c 10ppm PEL ^e 1 ppm, 4 mg/m ³
Pyrolysis Gases:					
Nitrogen	0	0	0	SA ^a	ACGIH ^b TWA ^c 25 ppm ACGIH ^b TWA ^c 5000 ppm
Carbon monoxide	2	4	0	SA ^a	
Carbon dioxide	1	0	0	SA ^a	
Methane	1	4	0	SA ^a	
Hydrogen	0	4	0	SA ^a	

Compressed Nitrogen: Inhalation: No known significant effects or critical hazards. Skin contact: Contact with rapidly expanding gas may cause burns or frostbite. Eye contact: Contact with rapidly expanding gas may cause burns or frostbite. In addition to any other important health or physical hazards, this product may displace oxygen and cause rapid suffocation (when concentrations are sufficient to reduce oxygen levels below 19.5%).

Alundum: Components: Aluminum Oxide 92 - 99% Non-Hazardous, Titanium Dioxide 1.0 - 4.0%, Silicon Dioxide 0.2 – 1.7% Amorphous, Iron Oxide 0.1 – 1.5%.

Abrasives are not dangerous substances or their preparation or handling according to directive 1999/45/EC. No toxicological effects if inhaled or swallowed or with eye or skin contact are known.

Charcoal: Charcoal powder and dust may cause eye and skin irritation. Inhalation and ingestion of charcoal dust may cause nose, throat, and gastrointestinal irritation.

Carbon monoxide hazard: Burning charcoal inside without adequate ventilation can kill you. Odorless carbon monoxide is given off upon combustion. NEVER burn charcoal inside homes, vehicles or tents.

Char dust is not found on the IARC, OSHA, or NTP carcinogen list. Char dust is produced by charcoal breakage. Thus, the concentration of charcoal dust will vary based on the amount of the breakage.

Caution: Wet charcoal may remove oxygen from air causing a potential hazard to workers in a confined space.

Reactivity data: Stable under normal temperatures and pressures. May react vigorously or violently when mixed with strong oxidizing agents, especially when heated. Oxidation rate increases with temperature and oxygen availability. Charcoal fines may heat spontaneously in air. This process is accelerated at increased temperatures and through the addition of water.

NMP: 1-Methyl-2-pyrrolidinone 99.5%

GHS Classification: Flammable liquids (Category 4), Skin Corrosion/Irritation, Category 2; Serious Eye Damage/Eye Irritation, Category 2A; Reproductive toxicity (Category 1B), May damage fertility or the unborn child, Specific Target Organ Toxicity (single exposure), Category 3, May cause respiratory irritation.

Pyrolysis gases: The final experimental gases, consisting of a maximum of ~10 grams of the pyrolysis products (CO, CO₂, CH₄ and H₂) and the N₂ originally fed into the reactor, are transferred at the end of an experiment from the Wall Heated Tubing Bomb (WHTB) to the Water Displacement Vessel (WDV) and finally released into a lab snorkel exhaust. The calculation below shows that a release of the pyrolysis gases into the lab is too small to present

a hazard to lab personnel. Therefore, good ventilation is sufficient to prevent the exposure of the lab personnel to high local concentrations, nonetheless, all pyrolysis gases must be vented into a lab snorkel exhaust.

POST 12 has an approximate volume of 129.80 m³ (V_{POST 12, approx}=5.18m x 9.75m x 2.57m). The room filled with air at 1 atm and ~20 °C equates to a mass of air of 156.5 kg as shown by the following equation:

$$m_{Air} = \frac{1 \text{ atm } 129800L}{0.082 \frac{\text{atmL}}{\text{mol K}}} \frac{28.966 \text{ g}}{1 \text{ mol}} = 156488.3g \approx 156.5 \text{ kg}$$

The release of the final pyrolysis gases into POST 12 will change the composition and concentration of gas in the room. The 10 g of pyrolysis products that are released consist of a mixture of mainly CO₂ (more than half), then CO with traces of CH₄ and H₂. The nitrogen released into the Lab is equal to the nitrogen originally fed into the reactor volume which is around 0.22 L. The mass of nitrogen fed in the reactor varies from an approximate value of 0.14 g to around 5.5 g depending on the initial nitrogen reactor pressure, from 0 psig to 300 psig respectively, as shown by the following equations:

$$m_{N_2 \text{ at } 0 \text{ psig}} = \frac{1 \text{ atm} 0.22L}{0.082 \frac{\text{atmL}}{\text{mol K}}} \frac{28 \text{ g}}{1 \text{ mol}} = 0.26g$$

$$m_{N_2 \text{ at } 680 \text{ psig}} = \frac{21.41 \text{ atm} 0.22L}{0.082 \frac{\text{atmL}}{\text{mol K}}} \frac{28 \text{ g}}{1 \text{ mol}} = 5.5g$$

The release of 10 g of pyrolysis gas and 5.5 g of nitrogen (maximum nitrogen mass fed into the reactor) do not coexist as it will exceed the maximum reactor pressure ratings. Releasing 10 g of pyrolysis gas into the POST 12 environment corresponds with mass concentrations of pyrolysis gases of 63.9 ppm_w (10 g pyrolysis gases / 156488 g air) and 5.5 g of nitrogen concentration correspond to 35.14 ppm_w (5.5g N₂/156488 g air). Thus, unintended release of the final experimental pyrolysis gases into the lab environment does not pose a hazard for the experimenter. Notice that these calculations are somewhat simplistic; this assumes instantaneous and complete mixing of the leaked contaminant and the entirety of the room's air. A snorkel directed to the reactor could eliminate localized high concentrations.

Prior to measuring their volume in the WDV, gases contained in the WHTB are at elevated pressure (420 to 2000 psig at experimental test temperature). The total volume of these contained gases at standard pressure and temperature are <8 L.

High Temperature: The sandbath used to heat the alundum bed material and reactor system is operated at a maximum temperature of 550°C. The sandbath is fluidized with compressed air that is heated by resistance heaters and discharged into the room after fluidizing the alundum bed.

Mains Electricity: All the electrical connections and cables related to the mass balance, laptop, pressure sensors, fan, and National Instrument (NI) data acquisition equipment are standard 120 V (20 amps) components as provided by the equipment suppliers. The sand bath is connected to an electrical supply of 240 V 50/60 Hz as specified by the supplier.

Section 3: Personal Protective Equipment.

Safety glasses or goggles, heat resistant gloves, flame resistant lab coat, covered shoes, long pants, NIOSH approved dust mask.

Alundum: NIOSH-approved particulate mask with category P1 filter must be used if fine dust limits are exceeded.

Charcoal: Use a NIOSH-approved particulate mask under conditions where TLV limits may be exceeded.

NMP: Use fume hood to keep airborne levels below their exposure limits. Ensure fume hood is working properly. If fume hood is not used, you must use a properly fitted and maintained NIOSH approved respirator for organic vapors. A dust mask does not provide protection against vapors. Contact lenses should not be worn while working with chemicals.

Section 4: Engineering Controls.

Compressed Nitrogen: General laboratory ventilation is sufficient to control worker exposure to airborne contaminants in the present location (POST 11). Install an excess 'flow restrictor' valve in the line from the nitrogen cylinder to the WHTB to prevent excessive release of nitrogen into the environment.

Perform experiment inside the welded steel-polycarbonate structure in Figure 4.1. Stay behind the protective polycarbonate panel in Figure 4.2 during experiments. Polycarbonate sheets of Figure 4.1 are 2-ply polycarbonate laminate 3/8" thick each (Makrolon Hygard CG375) and polycarbonate sheet of Figure 4.2 is 1/4 inch Makrolon GP (General Purpose). Makrolon Hygard sheets meet all security requirements with regard to protection against forced entry and ballistic impact. Makrolon GP is virtually unbreakable with 250 times the impact strength of float glass and 30 times that of acrylic.

Use appropriate tools to open and close valves in order to avoid direct contact of the experimenter with the pressurized reactor and lines. Ensure pressure does not exceed the burst disk pressure.

Activate LabVIEW alarms that will signal when the reactor pressure is 100 psig over the test pressure and when the pressure is 200 psig below the burst disk pressure.



Figure 4.1. Welded steel-polycarbonate structure for enclosing WHTB during an experiment



Figure 4.2. Polycarbonate panel to protect experimenters from equipment

Alundum: Use process enclosures to keep airborne levels below recommended exposure limits. Do not use in unventilated spaces.

Charcoal: Use local exhaust or general ventilation to minimize exposure to dust.

NMP: Use ONLY in a fume hood to control airborne levels below recommended exposure limits. Use only with adequate ventilation to prevent buildup of vapors. . Ensure fume hood is working properly. Do not use in areas where vapors can accumulate and concentrate, such as basements, bathrooms or small enclosed areas without a fume hood. Whenever possible, use outdoors in an open air area. If using indoors open all windows and doors and maintain a cross ventilation of moving fresh air across the work area. If strong odor is noticed or you experience slight dizziness, headache, nausea or eye-watering -- STOP -- ventilation is inadequate. Leave area immediately and move to fresh air.

Electricity: Inspect electrical cords, plugs, and receptacles prior to each use.

Section 5: Special Handling and Storage Requirements.

Compressed Nitrogen: Storage: Store in accordance with local regulations. Store in a segregated and approved area. Store away from direct sunlight in a dry, cool and well-ventilated area. Keep container tightly closed and sealed until ready for use. Cylinders should be stored upright, with valve protection cap in place, and firmly secured to prevent falling or being knocked over. Cylinder temperatures should not exceed 52 °C (125 °F). Handling: Put on appropriate personal protective equipment. Contains gas under pressure. Avoid contact with eyes, skin and clothing. Avoid breathing gas. Empty containers retain product residue and can be hazardous. Do not puncture or incinerate container. Use equipment rated for cylinder pressure. Close valve after each use and when empty. Protect cylinders from physical damage; do not drag, roll, slide, or drop. Use a suitable hand truck for cylinder movement.

Alundum: Handling: Avoid dust formation. No danger of fire or dust explosion. Storage: No special precautionary measures

Charcoal: Handling: Wash hands thoroughly after direct contact. Use with adequate ventilation. Minimize dust generation and accumulation. Avoid contact with eyes, skin, and clothing. Keep away from heat, sparks and open flames.

Storage: Keep away from heat, sparks, and open flames. Store in a tightly closed container away from oxidizing materials. Keep in a well-ventilated cool dry area.

NMP: Keep away from sources of ignition - No smoking. Take measures to prevent the build-up of electrostatic charge. For precautions see material safety data sheet. Keep container tightly closed in a dry and well-ventilated place. Containers which are opened must be carefully resealed and kept upright to prevent leakage. Store under inert gas. Moisture sensitive

Pyrolysis gases: Use only outdoors or in a well-ventilated area. Do not breathe gas. Wash hands thoroughly after handling. Avoid ignition sources.

Section 6: Spill and Accident Procedures.

Compressed Nitrogen: No action shall be taken involving any personal risk or without suitable training. Evacuate surrounding areas. Keep unnecessary and unprotected personnel from entering. Avoid breathing gas. Provide adequate ventilation. Wear appropriate respirator (Self-Contained Breathing Apparatus SCBA) when ventilation is inadequate.

Small spill: Shutoff source of gas. Stop leak if without risk. Contact emergency personnel (see Phone number information above) if necessary.

Large spill: Immediately contact emergency personnel (see Phone number information above). Stop leak if without risk. Note: Call supplier for emergency contact information (AirGas 24-hour phone 1-866-734-3438).

Alundum: Take up mechanically and dispose of in the trash.

Charcoal: Remove all sources of ignition. To avoid generating dusty conditions, use a vacuum cleaner to collect the material or carefully pick up the material and place it into a clean dry container and cover for disposal. Wash residual to on-site treatment area, where appropriate. Notice that charcoal may react vigorously or violently when mixed with strong oxidizing agents, especially when heated. Oxidation rate increases with temperature and oxygen availability. Charcoal fines may heat spontaneously in air. This process is accelerated at increased temperatures and through the addition of water.

NMP: *Small spills (<1L):* Do not attempt cleanup if you feel unsure of your ability to do so or if you perceive the risk to be greater than normal laboratory operations. Remove all sources of ignition. Use appropriate personal protective equipment and clean-up the spilled chemical. Avoid breathing vapors, mist or gas. Ensure adequate

ventilation. Prevent further leakage or spillage if safe to do so. Do not let product enter drains. A vapor suppressing foam may be used to reduce vapors. Absorb or cover with dry earth, sand, or other non-combustible material and transfer to compatible containers.

Large spills (>1L): Notify others in area of spill. Remove all sources of ignition. Avoid breathing vapors, mist or gas. Ensure adequate ventilation. Prevent further leakage or spillage if safe to do so. Do not let product enter drains if safe to do so. Dike ahead of the spill. Evacuate area and post entrance ways to spill area. Call the EHSO (808-956-3918) or after hours (956-6911) for spill response. Restrict persons from area of spill or leak until cleanup is complete.

Pyrolysis gases: Stop or reduce leak if safe to do so. Provide adequate ventilation. According to the above mentioned calculations, exposure to mixed pyrolysis gases at the concentrations generated under the test conditions is not hazardous.

Small Fire: Fire extinguisher, appropriately trained personnel only. There are fire extinguishers in POST 11 and POST 12 indicated as FE on the floor map below.

Large Fire: Leave the room and call emergency phone (see above).

Section 7: Waste Disposal Procedures.

Compressed Nitrogen: *Unused product/ empty container:* Return cylinder and unused product to supplier. Do not attempt to dispose of residual or unused quantities. *Disposal:* For emergency disposal, secure the cylinder and slowly discharge gas to the atmosphere in a well ventilated area or outdoors.

Alundum: Dispose of alundum in the trash.

Charcoal: Reclaim if possible; dispose in small quantities (<1 kg) in a closed bag.

NMP: Dispose of as hazardous waste. Do not reuse container

Pyrolysis gases: For emergency disposal, slowly discharge gas to the lab snorkel exhaust or fume hood. Ensure lab snorkel or fume hood are working properly.

Section 8: Special Precautions Animal Use.

Not Applicable

Section 9: Required Approvals

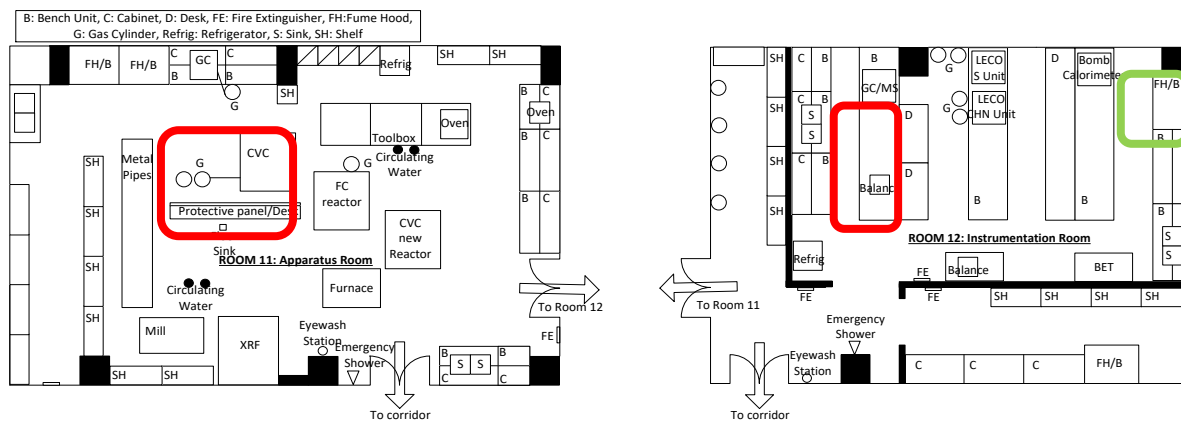
EHSO Lab Safety Training, Hazardous Waste Generator Training, approval and training from PI or lab supervisor. Read and understand all methods, QRA's, JSA's and SOP's developed for performing the experiment.

Section 10: Decontamination.

All work surfaces will be cleaned with paper towel at the end of the test and at the end of the day.

Section 11: Designated Areas.

The R3Lab Room 11 and Room 12 framed sections in red in the maps below are designated, respectively, for experiment performance and reactor unloading. The R3Lab Room 11 framed section in green in the map below is designated for cleaning the WHTB with NMP solvent.



Section 12. Method:

1. Make sure the WHTB has already been assembled, loaded and leak tested (see WHTB Assembly, Loading and Leak Testing SOP)
2. Heat up the alundum in the Technne fluidized sand bath (model SBL-2D). Figure 12.1 shows the sand bath equipment with all its components labelled.
 - 2.1. Turn on the sand bath air
 - 2.2. Turn on the four heating elements using the appropriate Switches
 - 2.3. Turn the 'power control knob 'clockwise to Maximum power.
 - 2.4. Turn on the digital temperature controller and input a set-point temperature 20°C above the experimental heat treatment temperature.
 - 2.5. Measure and record the current (amps) flowing to the sand bath heating elements.
 - 2.6. Compare the measured current flow with historical current flow. If comparable, continue on. If there is a significant difference, cancel the experiment, report situation to lab manager and PI.



Figure 12.1. Techne fluidized sand bath (Model SBL-2D)

3. See SOP for Gas Chromatograph (GC) operation: Analyze calibration gases by following the corresponding SOP.

While the sand bath is coming up to temperature and the GC is analyzing calibration gases, the following tasks are performed.

4. Immediately after energizing the sandbath, turn on the NI Data Acquisition devices and the computer, and launch the LabVIEW program. To record pressure and temperature experimental data every second, change *Input Sample* in LabVIEW from 0 to 1.
5. In order to reach and maintain the desired temperature, ensure sand is well fluidized by breaking the sand with a bamboo rod. Moisture can agglomerate sand at the bottom of the sand bath resulting in a poor fluidization and consequent failure of the heating elements!
6. Start cooling air delivery fan mounted to the side of the canopy hood. It will prevent the WHTB from heating before it is inserted into the sand bath and it will protect the pressure gauge, pressure transducer and WHTB arms from overheating.
7. Check that the battery for the hand drill has sufficient charge to allow it to run the worm gear winch used to lower the reactor into the sand bath. Charge as needed.
8. Wait for the Alundum sand bath temperature to stabilize at the desired set point temperature with the WHTB suspended over the sand bath.
9. Ensure that the WHTB is mounted on the Unistrut support frame within the welded steel-polycarbonate structure. Confirm the valve positions throughout the system match those in Table 12.1. Every time a valve or regulator position is modified a new Table will be presented.

Table 12.1.

V0	V1	V2	V3	V4	V5	Reg1 Inlet	Reg1 Outlet	PT1	PT2
Closed	Closed	Closed	Closed	Closed	Closed	0 psig	0 psig	100 psig above planned initial test pressure	0 psig

10. Figure 12.2 shows a schematic diagram of the WHTB. Ensure pressure transducer PT2 reads zero and that Quick Disconnect QD1 is disconnected.

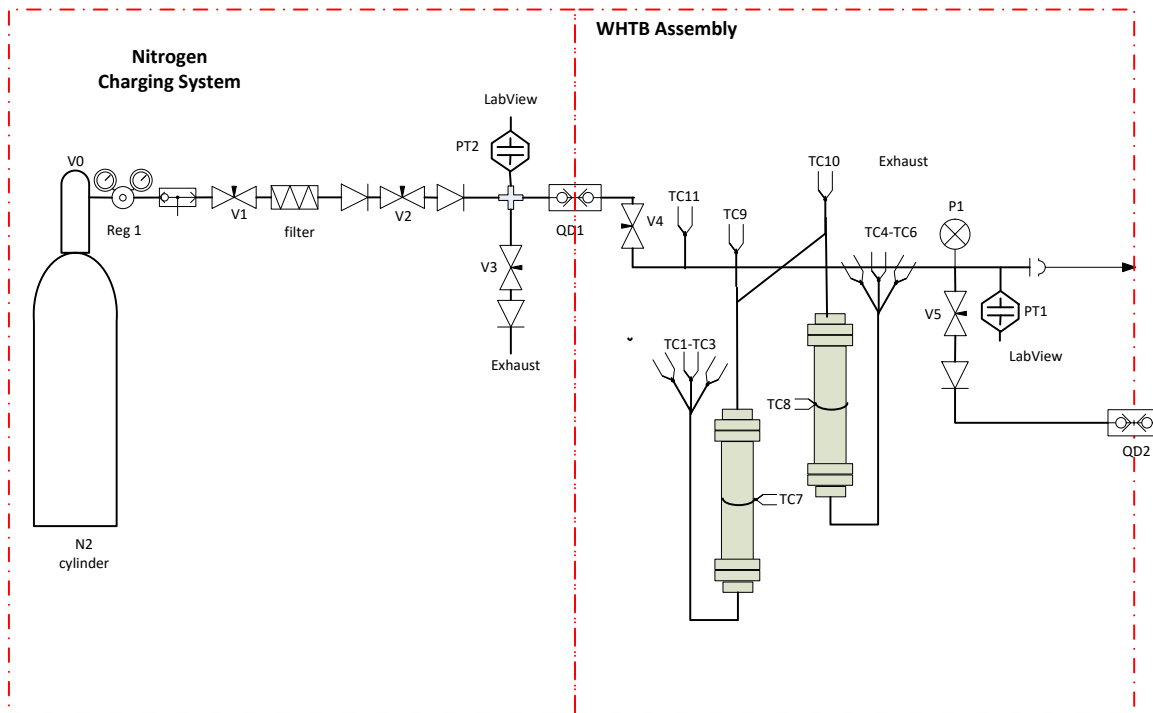
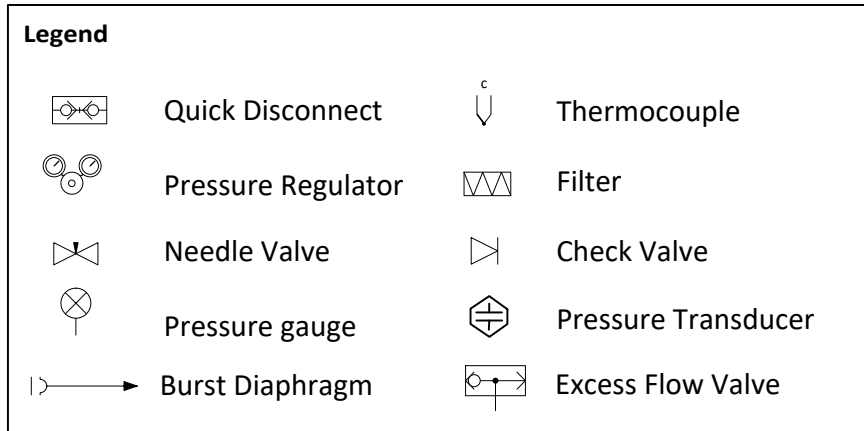


Figure 12.2. WHTB Diagram

11. Depressurize WHTB to experimental pressure.

10.1 Slowly open V5 and monitor output from PT1 on the data acquisition system.

Table 12.2.

V0	V1	V2	V3	V4	V5	Reg1 Inlet	Reg1 Outlet	PT1	PT2
Closed	Closed	Closed	Closed	Closed	Closed	0 psig	0 psig	100 psig above planned initial test pressure	0 psig

10.2 Close V5 when pressure gage P1 and transducer PT1 (LabVIEW) readings indicate the desired initial nitrogen experimental pressure.

Table 12.3.

V0	V1	V2	V3	V4	V5	Reg1 Inlet	Reg1 Outlet	PT1	PT2
Closed	Closed	Closed	Closed	Closed	Closed	0 psig	0 psig	planned initial test pressure	0 psig

- 11 With the Alundum sandbath at the desired initial experimental temperature and the WHTB at the desired initial nitrogen experimental pressure, restart LabVIEW and immediately immerse the WHTB into the sand bath using the motorized pulley. Monitor the movement of the Unistrut frame supporting the reactor to ensure free descent of the reactor into the fluidized alundum bed material.
- 12 Wait behind the protective polycarbonate sheet until the end of the experiment.
 - 12.1 The endpoint of long experiments is defined as 190 minutes after immersion of the WHTB reactor pressure in the sandbath.
 - 12.2 The endpoint of short experiments is defined as 10 minutes after the peak of exotherm is observed.
- 13 After arriving at the endpoint of the experiment, lift the WHTB out of the sand bath with the motorized pulley and position it in front of the fan to accelerate the cooling down stage.
- 14 Wait until the WHTB has cooled down to ~Room Temperature before stopping LabVIEW and disconnecting the thermocouples
- 15 See SOP for Water Displacement Vessel (WDV) operation: Transfer experimental gases from the WHTB to the WDV
- 16 See SOP for GC operation: Analyze experimental gases by following the corresponding SOP.
- 17 Verify that the reactor is depressurized by reading the pressure on gage P1. Loosen and remove the 7/16" Swagelok connections at the reactor top and replace it with a 7/16" Swagelok cap nut.
- 18 Unload the reactor: An example of the Unloading Form is given in Figure 13.1. The Unloading Form is divided into four tables: Table 1 logs data from the *Test Conditions*, Table 2 data from the *Solid Product Bomb Loading*, Table 3 with data from the *Product Moist Mass* and Table 4 with data from the *Moisture Content Charcoal*. Fill Table 2 in the Unloading Form following the instructions in section 13.
- 19 In a fume hood, fill the empty WHTB reactor bodies with NMP cleaning solvent and immerse reactor tops in a bucket with NMP cleaning solvent.
- 20 See SOP for moisture content analysis of the charcoal (ASTM 1756-08): To analyze the charcoal moisture content, fill in Table 3 in the Unloading Form following the moisture content SOP.
- 21 See SOP for proximate analysis of the charcoal (ASTM 1762-84)
- 22 Turn off computer and Data Acquisition devices.

Section 13. Unloading Form

Axially Heated Tubing Bomb Pyrolysis Experiment

Table 1. Test Conditions

Initial Conditions		Final Conditions		Target Pressure [psig] _____
Room Temperature [°C] _____	_____	Room Temperature [°C] _____	_____	Target HTT [°C] _____
Room Pressure [mmHg] _____	_____	Room Pressure [mmHg] _____	_____	
Reactor Pressure [psig] _____	_____	Reactor Pressure [psig] _____	_____	
		After First Sample [psig] _____	_____	

Final Sand Bath Parameters

Low _____

Medium _____

High _____

Boost _____

Energy Regulator Setting _____

Approximate Air Turn Angle [deg] _____

Table 2. Solid Product Bomb Load

	Cook	Reactor	Bottom TC	Reactor Top + Cap	Solid Products	Remaining Products	Pipoc bag	SS Screen	Spilled Sample	Aluminum Dish for charcoal MC	Charcoal	Stem	Aluminum dish for SS	Aluminum Tray for charcoal	Cap	mass (g)
1	X															
2	X												X			
3	X	X	X	X	X		X									
4	X	X	X		X											
5	X				X								X			
6	X								X							
7	X								X	X						
8	X			X			X									
9	X						X						X			
10	X												X			
11	X			X												
12	X	X	X			X										
13	X	X	X	X		X										
14	X	X				X										
15	X		X													
16	X			X												
17	X													X		
18	X										X					

Table 3. Product Moist Mass [g]

5-2	0.00
(3-13)-(8-11)	0.00
4-12	0.00
Mass of solid product	0.00
Mass of solid product based o initial weights	0.00

SHADED GREY: WORK FAST & CAREFUL

ASTM procedure E871-82 _____

Table 4. Moisture content charcoal [%, wb]

Aluminum container (15-1)	0.00
Aluminum container + charcoal (16-1)	0.00
16h vacuum oven + 1h cooldown	
2h vacuum oven + 1h cooldown	
2h vacuum oven + 1h cooldown	
2h vacuum oven + 1h cooldown	
2h vacuum oven + 1h cooldown	
Moisture content charcoal [%, wb]	#DIV/0!
Water SS [g]	#DIV/0!

Table 4. Moisture content SS[% , wb]

Aluminum container (5-1)	0.00
Aluminum container + SS (6-1)	0.00
16h vacuum oven + 1h cooldown	
1h vacuum oven + 1h cooldown	
1h vacuum oven + 1h cooldown	
1h vacuum oven + 1h cooldown	
1h vacuum oven + 1h cooldown	
Moisture content charcoal [%, wb]	#DIV/0!
Water SS [g]	#DIV/0!

Last Modified 3/18/2017

Figure 13.1. Unloading Form

Instructions for Table 2 in Unloading Form

The components mentioned in the instructions are shown and labelled in Figure 13.2.

23. Weigh cork. The cork is NOT part of the assembled WHTB. It serves as a weight reference and holds the reactor upright.
24. Weigh cork plus Aluminum Tray for charcoal or a Ziploc bag. The bag is NOT part of the assembled WHTB. It serves to store the unloaded charcoal.
25. Weigh cork with the reactor, i.e. with a capped reactor top and the reactor body with TC, SS screen and solid products (charcoal and volatiles) inside.
26. Loosen and disassemble the reactor top, weigh cork with the partly disassembled reactor, i.e. with TC, SS screen and charcoal in the reactor body.
27. Disassemble TC, unload solid products into the Ziploc bag. Weigh cork and Ziploc bag with solid products.
28. Weigh cork plus an aluminum disk. The disk is NOT part of the assembled WHTB. It serves to hold the unloaded products during the Moisture Content Analysis.
29. Transfer the entire sample of solid products from Ziploc bag into the aluminum disk. Weigh cork and aluminum disk with solid products.
30. Weigh cork, reactor top and the SS screen.
31. Weigh cork plus an aluminum disk. The disk is NOT part of the assembled WHTB. It serves to hold the SS screen during the Moisture Content Analysis.
32. Disassemble SS screen, weigh cork and the SS screen.
33. Weigh cork and reactor top.
34. Weigh cork with reactor body with remaining products in the reactor body, plus TC.
35. Weigh cork with reactor body with remaining products in the reactor body, plus TC and reactor top.
36. Weigh cork and the reactor body with remaining products.
37. Weigh cork and TC.
38. Weigh cork and reactor top capped
39. Weigh cap
40. Weigh stem

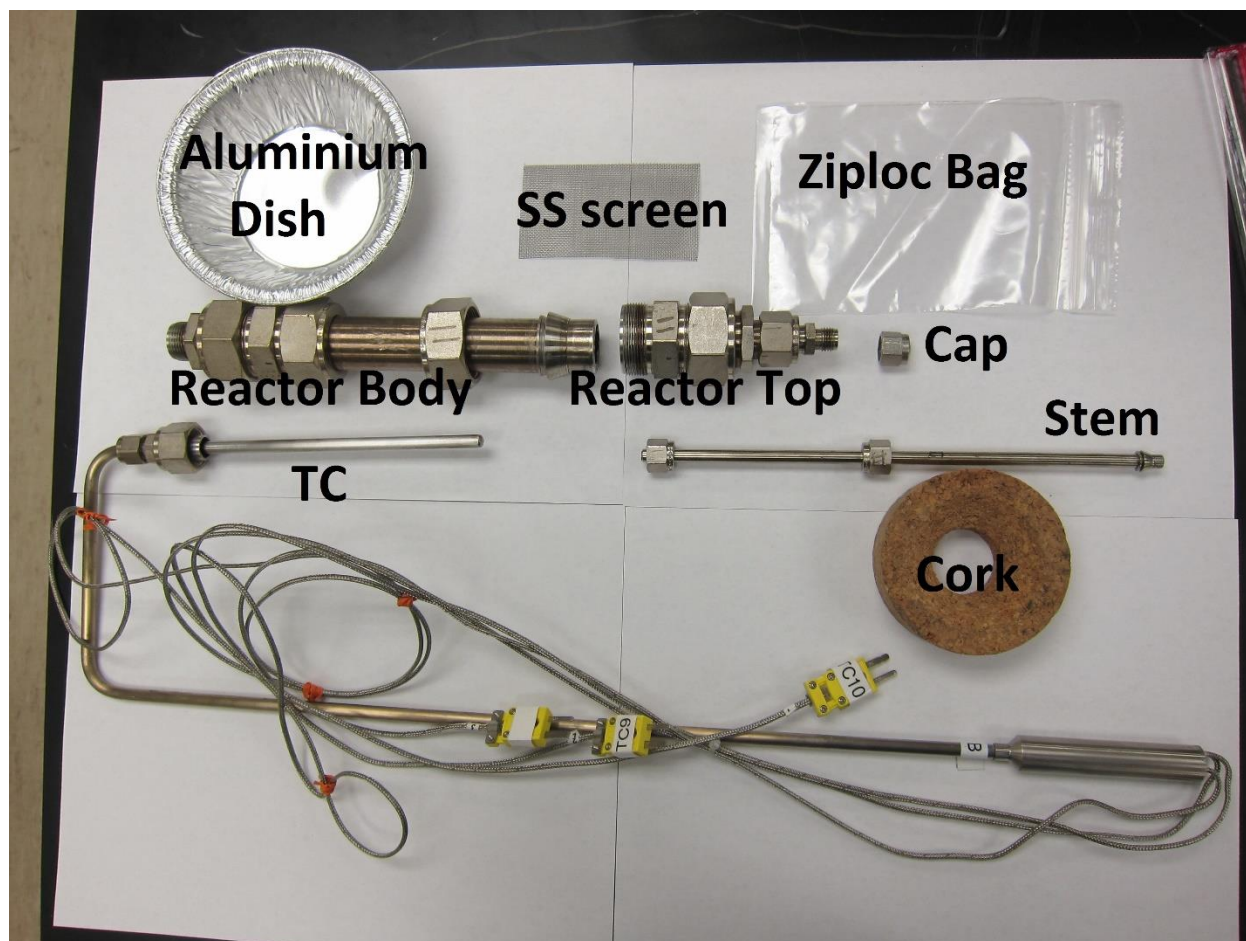


Figure 13.2 The Wall Heated Tubing Bomb (WHTB) components.

JOB SAFETY ANALYSIS

Safety Information for the University of Hawaii at Manoa

NAME OF DEPARTMENT: HAWAII NATURAL ENERGY INSTITUTE

Title of Job or Task: Experiment Performance and Unloading and Disassembly of the Wall Heated Tubing Bomb

TASK	HAZARDS	CONTROLS
1. Heat up the alundum in the Techne fluidized sand bath (model SBL-2D).	Alundum: Abrasives are not dangerous substances or their preparation according to directive 1999/45/EC. Alundum at elevated temperatures. 240V AC from mains to sand bath.	PPE Safety goggles. Flame resistant lab coat. NIOSH approved particulate mask. Covered shoes. Long pants. Engineered controls Use process enclosures to keep airborne levels below recommended exposure limits. Do not use in unventilated spaces. Inspect electrical cord and plug prior to each use.
2. Pressurized WHTB <400 psig	Compressed nitrogen H280 – Contains gas under pressure; may explode if heated. OSHA-H01 – May displace oxygen and cause rapid suffocation. Overpressurization of the reactor 120V AC from mains to pressure sensors, laptop, fan, NI data acquisition system.	PPE Safety glasses or goggles. Flame resistant lab coat. Covered shoes. Long pants. Engineered controls Implement pressure alarms in LabVIEW to warn of over pressurization of the WHTB reactor and impending burst disk rupture.

			<p>Perform WHTB pressurization inside the welded steel-polycarbonate structure.</p> <p>Place welded steel-polycarbonate structure directly beneath the canopy hood in POST 11.</p> <p>Good general ventilation.</p> <p>Direct tube from burst diaphragm to the water reservoir in the corner of the welded steel-polycarbonate structure.</p> <p>Use appropriate tool to open and close valves in order to avoid direct contact of the experimenter with the pressurized reactor and lines.</p> <p>Install excess flow restrictors on all gas cylinders actively used in the experiment.</p> <p>Inspect electrical cord and plug prior to each use.</p>
	<p>3. Immerse WHTB into the sand bath with the motorized pulley.</p>	<p>Alundum at elevated temperatures. Elevated Nitrogen Pressure in the WHTB. Alundum: Abrasives are not dangerous substances or their preparation according to directive 1999/45/EC. Compressed nitrogen H280 – Contains gas under pressure; may explode if heated. OSHA-H01 – May displace oxygen and cause rapid suffocation. 240V AC from mains to sand bath. 120V AC from mains to pressure sensors, laptop, fan, NI data acquisition system and motorized pulley.</p>	<p>PPE Safety glasses or goggles. Flame resistant lab coat. Heat resistant gloves. NIOSH approved particulate mask. Covered shoes. Long pants. Engineered controls Implement pressure alarms in LabVIEW to warn of over pressurization of the WHTB reactor and impending burst disk rupture.</p> <p>Perform WHTB pressurization inside the welded steel-polycarbonate structure.</p> <p>Place welded steel-polycarbonate structure directly beneath the canopy hood in POST 11.</p> <p>Good general ventilation.</p>

			<p>Direct tube from burst diaphragm to the water reservoir in the corner of the welded steel-polycarbonate structure.</p> <p>Perform immersion of the WHTB into the sandbath while standing outside of the welded steel-polycarbonate structure.</p> <p>Install excess flow restrictors on all gas cylinders actively used in the experiment. No action is required in regard to electricity.</p>
	<p>4. Run experiment</p>	<p>Alundum at elevated temperatures Alundum: Abrasives are not dangerous substances or preparations according to directive 1999/45/EC.</p> <p>Elevated Pressure and Temperature in the WHTB</p> <p>240V AC from mains to sand bath. 120V AC from mains to pressure sensors, laptop, fan, NI data acquisition system.</p>	<p>PPE</p> <p>Safety glasses or goggles. Nitrile Gloves. Flame resistant lab coat. Heat resistant gloves. NIOSH approved particulate mask. Covered shoes. Long pants.</p> <p>Engineered controls</p> <p>Implement pressure alarms in LabVIEW to warn of over pressurization of the WHTB reactor and impending burst disk rupture.</p> <p>Perform WHTB pressurization inside the welded steel-polycarbonate structure.</p> <p>Place welded steel-polycarbonate structure directly beneath the canopy hood in POST 11.</p> <p>Good general ventilation.</p> <p>Direct tube from burst diaphragm to the water reservoir in the corner of the welded steel-polycarbonate structure.</p> <p>Perform immersion of the WHTB into the sandbath while standing behind the Unistrut-polycarbonate panel.</p>

			<p>Install excess flow restrictors on all gas cylinders actively used in the experiment.</p> <p>Stand behind the polycarbonate protective panel during the experiment.</p> <p>No action is required in regard to electricity.</p>
	<p>6. Lift the WHTB out of the sand bath with the motorized pulley and place it in front of the fan</p>	<p>Alundum at elevated temperatures</p> <p>Elevated Pressure and Temperature in the WHTB</p> <p>Alundum: Abrasives are not dangerous substances or preparations according to directive 1999/45/EC.</p> <p>240V AC from mains to sand bath.</p> <p>120V AC from mains to pressure sensors, laptop, NI data acquisition system, fan and motorized pulley.</p>	<p>PPE</p> <p>Safety glasses or goggles.</p> <p>Flame resistant lab coat.</p> <p>Heat resistant gloves.</p> <p>NIOSH approved particulate mask.</p> <p>Covered shoes.</p> <p>Long pants.</p> <p>Engineered controls</p> <p>Implement pressure alarms in LabVIEW to warn of over pressurization of the WHTB reactor and impending burst disk rupture.</p> <p>Good general ventilation should be sufficient to control worker exposure to airborne contaminants.</p> <p>Perform removal of the WHTB from the sandbath while standing outside the Unistrut-polycarbonate panel.</p> <p>Direct tube from burst diaphragm to a bucket full of water.</p> <p>Install excess flow restrictors on all gas cylinders actively used in the experiment.</p> <p>Stand behind the polycarbonate protective panel.</p> <p>No action is required in regard to electricity.</p>

<p>7. Unload the reactor</p>	<p>Charcoal GHS Classification: None NFPA Health 1, Fire 2, Reactivity 1, No specific 120V AC from mains to mass balance.</p>	<p>PPE Safety glasses or goggles. Nitrile Gloves. Flame resistant lab coat. NIOSH approved particulate mask. Covered shoes. Long pants. Engineered controls Good general ventilation should be sufficient to control worker exposure to airborne contaminants.</p> <p>Minimize dust generation and accumulation. Avoid contact with eyes, skin, and clothing. Keep away from heat, sparks and open flames.</p>
<p>8. Soak WHTB into a bucket with diluted cleaning solvent (NMP)</p>	<p>Cleaning solvent (NMP): May cause burn to eyes, skin irritant GHS Classification: Skin Corrosion/Irritation, Category 2 Serious Eye Damage/Eye Irritation, Category 2A Reproductive toxicity, Category 1B Specific Target Organ Toxicity (single exposure), Category 3 H227: Combustible liquid. H315: Causes skin irritation. H319: Causes serious eye irritation. H335: May cause respiratory irritation. H360: May damage fertility or the unborn child.</p>	<p>PPE Safety glasses or goggles Nitrile Gloves Flame resistant lab coat Covered shoes Long pants</p> <p>Engineered controls Use fume hood to control airborne levels below recommended exposure limits. Ensure fume hood is working properly.</p>
<p>Required Training: EHSO Lab Safety</p>	<p>Required Personal Protective Equipment (PPE) Safety glasses or goggles Flame resistant lab coat</p>	

	<p>Training, Read UH Chemical hygiene plan, Specific lab activity training by PI or lab supervisor, Read and understand all methods, QRA's, JSA's and SOP's developed for performing the experiment</p>	<p>Heat resistant gloves NIOSH approved particulate mask Covered shoes Long pants</p>
<p>Other Information: JSA Completed By: Date Created: OSHA Reference:</p>	<p>See Scott Turn, Trevor Morgan, Lloyd Paredes and Maider Legarra-Arizaleta for more information on Job Hazard Analysis Maider Legarra-Arizaleta, Trevor Morgan, Scott Turn, Lloyd Paredes and Pablo J. Arauzo-Gimeno April 20, 2018 _____ For more information about this JSA, contact the <i>University of Hawaii Environmental Health and Safety Office</i> http://www.hawaii.edu/ehso/industrial/ or by phone at 956-3204</p>	

APPENDIX K. SOP and JSA 8: Analysis of the Charcoal Moisture

Content

Laboratory Standard Operating Procedures University of Hawaii at Manoa

Please fill out and place in your Chemical Hygiene Plan

Analysis of the Charcoal Moisture Content

Date: 04/20/2018

Principal Investigator: Scott Q. Turn

Produced By: Maider Legarra Arizaleta, Trevor Morgan and Scott Turn

Room and Building: POST 11/12

Phone Number: PI Scott Turn: 808-956-2346/ POST 11: 808-956-9903 /POST 12: 808-956-3790/

UH Emergency: 808-956-6911 (on campus 66911)/ Emergency: 911

Section 1 Process:

(Check One) Process Hazardous Chemical Hazard Class

Summary: This SOP covers the analysis of the charcoal moisture content by Standard Test Method for Determination of Total Solids in Biomass ASTM 1756-08. The main steps for determining the charcoal moisture content that are relevant to the SOP are listed in section 12.

Section 2: Describe Process Hazards, Hazardous Chemical or Hazard Class.

Table 2.1. NFPA Hazard Classification and Exposure limit. ^aACGIH: American Conference of Governmental Industrial Hygienist. ^b TLV-TWA: Threshold Limit Value-Time Weighted Average (TLV-TWA)

Chemical	Health	Fire	Reactivity	Specific	Exposure limit
Charcoal	1	2	1		ACGIH ^a TLV-TWA ^b 2mg/m ³

Charcoal: Charcoal powder and dust may cause eye and skin irritation. Inhalation and ingestion of charcoal dust may cause nose, throat, and gastrointestinal irritation.

Carbon monoxide hazard: Burning charcoal inside without adequate ventilation can kill you. Odorless carbon monoxide is given off upon combustion. NEVER burn charcoal inside homes, vehicles or tents. Char dust is not found on the IARC, OSHA, or NTP carcinogen list. Char dust is produced by charcoal breakage. Thus, the concentration of charcoal dust will vary based on the amount of the breakage. Caution: Wet charcoal may remove oxygen from air causing a potential hazard to workers in a confined space. Reactivity data: Stable under normal temperatures and pressures. May react vigorously or violently when mixed with strong oxidizing agents, especially when heated. Oxidation rate increases with temperature and oxygen availability. Charcoal fines may heat spontaneously in air. This process is accelerated at increased temperatures and through the addition of water.

Elevated Temperature: Internal oven surfaces are ~105°C.

Vacuum System: All the vacuum fittings and tubing are rated appropriately for the size of the vacuum pump.

Mains Electricity: All the electrical connections and cables related to the mass balance, vacuum oven and vacuum pump are standard 120 V (20 amps) components as provided by the equipment suppliers.

Section 3: Personal Protective Equipment.

Safety glasses or goggles, nitrile gloves, heat resistant gloves, flame resistant lab coat, covered shoes, NIOSH approved particulate mask, long pants.

Charcoal: Use a NIOSH-approved respirator under conditions where TLV-TWA may be exceeded.

Section 4: Engineering Controls.

Charcoal: Use local exhaust or general ventilation to minimize exposure to dust.

Vacuum Oven: Appropriately sized vacuum pump, tubing and connections.

Electricity: Inspect electrical cords, plugs, and receptacles prior to each use.

Section 5: Special Handling and Storage Requirements.

Charcoal:

Handling: Wash hands thoroughly after direct contact. Use with adequate ventilation. Minimize dust generation and accumulation. Avoid inhalation and contact with eyes, skin, and clothing. Keep away from heat, sparks and open flames.

Storage: Keep away from heat, sparks, and open flames. Store in a tightly closed container away from oxidizing materials. Keep in a well-ventilated cool dry area.

Section 6: Spill and Accident Procedures.

Charcoal: Remove all sources of ignition. To avoid generating dusty conditions, use a vacuum cleaner to collect the material. Or carefully pick up the material and place it into a clean dry container and cover for disposal. Wash residual to on-site treatment area, where appropriate.

Notice that charcoal may react vigorously or violently when mixed with strong oxidizing agents, especially when heated. Oxidation rate increases with temperature and oxygen availability. Charcoal fines may heat spontaneously in air. This process is accelerated at increased temperatures and through the addition of water.

Small Fire: Fire extinguisher, appropriately trained personnel only. There are fire extinguishers in POST 11 and POST 12 indicated as FE on the floor map below.

Large Fire: Leave the room and call 956-6911 or 911.

Section 7: Waste Disposal Procedures.

Reclaim if possible; otherwise dispose of in accordance with all applicable federal, state and local regulations.

Section 8: Special Precautions Animal Use.

Not Applicable

Section 9: Required Approvals:

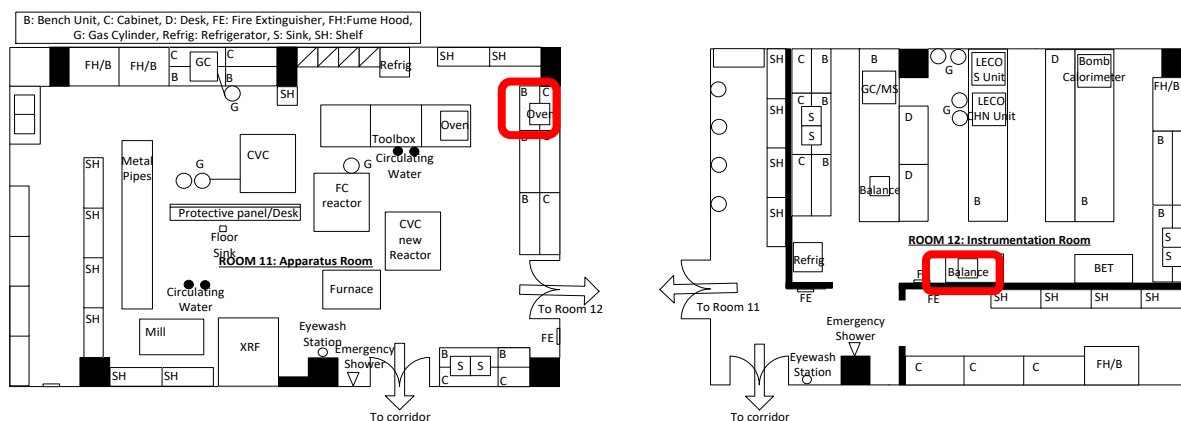
EHSO Lab Safety Training, approval from PI, read and understand all methods, QRA's, JSA's and SOP's developed for determining the charcoal moisture content.

Section 10: Decontamination.

All work surfaces will be cleaned with paper towel at the end of the test and at the end of the day.

Section 11: Designated Areas.

The R³Lab Room 11 and Room 12 framed sections in red in the maps below are designated for charcoal moisture content tasks.



Section 12. Method:

This test method follows all steps of the Standard Test Method for Determination of Total Solids in Biomass ASTM E1756-08 (Method A). Read and understand ASTM 1756-08 before proceeding. For practical purposes, several modifications are implemented and described in the corresponding steps.

3. *Sampling*

According to ASTM 1756-08, the sample is material prepared according to Practice E1757 or extractives-free material prepared according to Test Method E1690. Nonetheless, we do not follow any preparation practice or method and the moisture content analysis is performed immediately after unloading it from the reactor. Experience taught us that charcoal loses moisture when following preparation methods and gets reflected in erratic moisture contents between reproducible experiments and therefore results in uncertain mass balances for reactants and products. A quick unload and an immediate moisture content analysis was found to improve mass balances.

4. An example of the Unloading Form is given in Figure 13.1. The Unloading Form is divided into four tables: Table 1 details the Test Conditions, Table 2 logs data from the Solid Product Bomb Loading, Table 3 data from the Product Moist Mass and Table 4 data for the charcoal moisture content determination. Fill Table 4 following the instructions in section 13.

Section 13. Loading Form

Axially Heated Tubing Bomb Pyrolysis Experiment

Table 1. Test Conditions

Initial Conditions Room Temperature [°C] _____ Room Pressure [mmHg] _____ Reactor Pressure [psig] _____	Final Conditions Room Temperature [°C] _____ Room Pressure [mmHg] _____ Reactor Pressure [psig] _____ After First Sample [psig] _____	Target Pressure [psig] _____ Target HTT [°C] _____
---	--	---

Final Sand Bath Parameters
 Low
 Medium
 High
 Boost

Energy Regulator Setting _____
 Approximate Air Turn Angle [deg] _____

Table 2. Solid Product Bomb Load

	Cork	Reactor	Bentium TC	Reactor Top + Cap	Solid Products	Remaining Products	Ziploc bag	SS Screen	Solid Sample	Aluminum Dish for charcoal MC	Charcoal	Stem	Aluminum dish for SS	Aluminum Tray for charcoal	Cap	mass [g]
1	X															
2	X												X			
3	X	X	X	X	X			X								
4	X	X	X	X	X											
5	X			X									X			
6	X								X							
7	X							X	X							
8	X			X			X									
9	X												X			
10	X					X							X			
11	X		X													
12	X	X	X		X											
13	X	X	X	X	X											
14	X	X			X											
15	X		X													
16	X			X												
17	X													X		
18	X											X				

Last Modified 3/18/2017

Table 3. Product Moist Mass [g]

5-2	0.00
(3-13)-(8-11)	0.00
4-12	0.00
Mass of solid product	0.00
Mass of solid product based on initial weights	0.00

SHADED GREY: WORK FAST & CAREFUL

ASTM procedure E871-82 _____

Table 4. Moisture content charcoal [%, wb]

Aluminum container (15-1)	0.00
Aluminum container + charcoal (16-1)	0.00
16h vacuum oven + 1h cooldown	
2h vacuum oven + 1h cooldown	
2h vacuum oven + 1h cooldown	
2h vacuum oven + 1h cooldown	
2h vacuum oven + 1h cooldown	
Moisture content charcoal [%, wb]	#DIV/0!

Table 4. Moisture content SS [%, wb]

Aluminum container (5-1)	0.00
Aluminum container + SS (6-1)	0.00
16h vacuum oven + 1h cooldown	
1h vacuum oven + 1h cooldown	
1h vacuum oven + 1h cooldown	
1h vacuum oven + 1h cooldown	
1h vacuum oven + 1h cooldown	
Moisture content charcoal [%, wb]	#DIV/0!
Water SS [g]	#DIV/0!

Figure 13.1. Unloading Form

Instructions for Table 4 in Unloading Form

Notice that the first two weights recorded in Table 4 (*Aluminum container* and *Aluminum container + charcoal*) are automatically displayed after filling Table 2 of the Unloading form. The masses of Table 2 were weighted on the analytical balance to the nearest 0.01 g.

The precision of 0.01 g is in accordance with the mass balance precision employed while filling Table 2 even though ASTM 1756-08 requires a precision of 0.0001 g. In addition, the moisture content analysis is performed to the entire sample while ASTM 1756-08 only requires a nominal 0.5 g of sample into the aluminum container. Nonetheless, due to the elimination of preparation methods, an analysis of the full sample is needed to reflect a reliable moisture content of the sample.

1. Place the sample in the vacuum oven at $105 \pm 3^{\circ}\text{C}$ for 16 h. ASTM 1756-08 specifies drying for at least 3 h but not longer than 72 h in a drying oven. A vacuum oven is used to prevent charcoal from burning. As stated on section 2, charcoal fines may heat spontaneously in air. This process is accelerated at increased temperatures and through the addition of water.
2. Remove the sample and the container from the oven and cool in a desiccator equipped with a pressure relief valve for 1 hour. The cooling down period and a relief valve in the desiccator are not specified in the standard. The standard specifies to cool down to room temperature (1 hour has proved to be a reasonable time) and the relief valve was introduced due to the vacuum created in desiccators while charcoal cools down that impedes the opening of the desiccators.
3. Weigh each sample to the nearest 0.0001 mg and record this mass.

After weighing, return the samples to the drying oven at 105°C for 1 h, cool again in the desiccator, and weigh again. Repeat this step until the mass of the samples varies by less than 0.0003 g from the previous weighing. This will be the *valid final mass*.

4. The spreadsheet displays the moisture content of the charcoal calculated as:

$$\text{Moisture Content [\%]} = \frac{\text{Tare and Sample Mass[g]} - \text{Valid final mass [g]}}{\text{Tare and Sample Mass[g]} - \text{Tare Mass[g]}} \times 100$$

Where *Tare and Sample Mass[g]* refers to the *Aluminum container plus charcoal [g]* and the *Tare Mass[g]* refers to the *Aluminum container [g]*.

5. Clean used containers with a paper towel and store them in desiccator. If a new aluminum container is used, place in the drying oven at 105°C for at least one hour. Cool the containers to room temperature in the desiccator.

JOB SAFETY ANALYSIS

Safety Information for the University of Hawaii at Manoa

NAME OF DEPARTMENT: HAWAII NATURAL ENERGY INSTITUTE

Title of Job or Task: Charcoal Moisture content based on ASTM D1756-08

TASK	HAZARDS	CONTROLS
<p>1. Moisture Content Analysis</p>	<p>Charcoal GHS classification: None</p> <p>Charcoal powder and dust may cause eye and skin irritation. Inhalation and ingestion of charcoal dust may cause nose, throat, and gastrointestinal irritation.</p> <p>Crucibles can be dropped</p> <p>Hot vacuum oven (105°C)</p> <p>120 V AC from mains to mass balance, vacuum pump and vacuum oven</p> <p>Vacuum system.</p>	<p>PPE</p> <p>Safety goggles</p> <p>Heat resistant gloves</p> <p>Flame resistant lab coat</p> <p>Covered shoes</p> <p>NIOSH approved particulate mask.</p> <p>Nitrile gloves</p> <p>Long pants</p> <p>Engineered controls</p> <p>Use crucible tongs and carriers to handle hot crucibles</p> <p>Appropriately sized vacuum pump, tubing and connections.</p> <p>Inspect electrical cords, plugs, and receptacles prior to each use.</p>
<p>Required Training:</p> <p>EHSO Lab Safety Training, Read UH Chemical hygiene plan, Specific lab activity training by PI or lab supervisor, Read and understand ASTM D1756-08 for chemical analysis of wood</p>	<p>Required Personal Protective Equipment (PPE)</p> <p>Safety goggles</p> <p>Heat resistant gloves</p> <p>Flame resistant lab coat</p> <p>Covered shoes</p> <p>NIOSH approved particulate mask.</p> <p>Nitrile gloves</p> <p>Long pants</p>	

	charcoal, all methods, JSA's, QRA's and SOP's developed for determining the charcoal moisture content	
Other Information: JSA Completed By: Date Created: OSHA Reference:	See Scott Turn, Trevor Morgan, Lloyd Paredes and Maider Legarra-Arizaleta for more information on Job Hazard Analysis Maider Legarra-Arizaleta, Trevor Morgan, and Scott Turn 04/20/2018 <hr/> <hr/> — For more information about this JSA, contact the <i>University of Hawaii Environmental Health and Safety Office</i> http://www.hawaii.edu/ehso/industrial/ or by phone at 956-3204	

APPENDIX L. SOP and JSA 9: Proximate Analysis

Laboratory Standard Operating Procedures

University of Hawaii at Manoa

Please fill out and place in your Chemical Hygiene Plan

Proximate Analysis

Date: 04/20/2018

Principal Investigator: Scott Q. Turn

Produced By: Maider Legarra Arizaleta, Trevor Morgan and Scott Turn

Room and Building: POST 11/12

Phone Number: PI Scott Turn: 808-956-2346/ POST 11: 808-956-9903 /POST 12: 808-956-3790/

UH Emergency: 808-956-6911 (on campus 66911)/ Emergency: 911

Section 1 Process:

(Check One) Process

Hazardous Chemical

Hazard Class

Summary: This SOP covers the proximate analysis of charcoal. The analysis determines the volatile matter, fixed carbon content and ash content of charcoal following ASTM D1762-84 “Standard Test Method for Chemical Analysis of Wood Charcoal”.

Section 2: Describe Process Hazards, Hazardous Chemical or Hazard Class.

Table 2.1. NFPA Hazard Classification and Exposure limit.^a ACGIH: American Conference of Governmental Industrial Hygienist. ^b TLV-TWA: Threshold Limit Value-Time Weighted Average

Chemical	Health	Fire	Reactivity	Specific	Exposure limit
Charcoal	1	2	1		ACGIH ^a TLV-TWA ^b 2mg/m ³

Charcoal: Charcoal powder and dust may cause eye and skin irritation. Inhalation and ingestion of charcoal dust may cause nose, throat, and gastrointestinal irritation.

Carbon monoxide hazard: Burning charcoal inside without adequate ventilation can kill you. Odorless carbon monoxide is given off upon combustion. NEVER burn charcoal inside homes, vehicles or tents. Char dust is not found on the IARC, OSHA, or NTP carcinogen list. Char dust is produced by charcoal breakage. Thus, the concentration of charcoal dust will vary based on the amount of the breakage. Caution: Wet charcoal may remove oxygen from air causing a potential hazard to workers in a confined space. Reactivity data: Stable under normal temperatures and pressures. May react vigorously or violently when mixed with strong oxidizing agents, especially when heated. Oxidation rate increases with temperature and oxygen availability. Charcoal fines may heat spontaneously in air. This process is accelerated at increased temperatures and through the addition of water.

Elevated Temperature: Internal oven and furnace working surfaces are 105-950°C.

Vacuum System: All the vacuum fittings and tubing are rated appropriately for the size of the vacuum pump.

Mains Electricity: All the electrical connections and cables related to the mass balance, furnace, vacuum oven and vacuum pump are standard 120 V (20 amps) components as provided by the equipment supplier.

Section 3: Personal Protective Equipment.

Safety glasses or goggles, nitrile gloves, heat resistant gloves, flame resistant lab coat, covered shoes, NIOSH-approved particulate mask.

Charcoal: Use a NIOSH-approved respirator under conditions where TLV limits may be exceeded.

Section 4: Engineering Controls.

Charcoal: Use local exhaust or general ventilation to minimize exposure to dust.

Grinding/milling: Ensure glass on the side of the mill is properly positioned and secured. Use the tool provided (not fingers) to feed the charcoal into the mill

Muffle Furnace: Use crucible tongs and carriers to handle hot crucibles

Vacuum Oven: Appropriately sized vacuum pump, tubing and connections.

Mill, Muffle Furnace, Vacuum Pump and Vacuum Oven: No action is required in regard to electricity.

Muffle Furnace: Perform tasks in fume hood and ensure it is operating properly, e.g. with a Kim wipe

Cooling in Desiccator: Use a desiccator with a quarter turn valve to release vacuum

Electricity: Inspect electrical cords, plugs, and receptacles prior to each use.

Section 5: Special Handling and Storage Requirements.

Charcoal: Handling: Wash hands thoroughly after direct contact. Use with adequate ventilation. Minimize dust generation and accumulation. Avoid inhalation and contact with eyes, skin, and clothing. Keep away from heat, sparks and open flames.

Storage: Keep away from heat, sparks, and open flames. Store in a tightly closed container away from oxidizing materials. Keep in a well-ventilated cool dry area.

Section 6: Spill and Accident Procedures.

Charcoal: Remove all sources of ignition. To avoid generating dusty conditions, use a vacuum cleaner to collect the material. Or carefully pick up the material and place it into a clean dry container and cover for disposal. Wash residual to on-site treatment area, where appropriate.

Notice that charcoal may react vigorously or violently when mixed with strong oxidizing agents, especially when heated. Oxidation rate increases with temperature and oxygen availability. Charcoal fines may heat spontaneously in air. This process is accelerated at increased temperatures and through the addition of water.

Small Fire: Fire extinguisher, appropriately trained personnel only. There are fire extinguishers in POST 11 and POST 12 indicated as FE on the floor map below.

Large Fire: Leave the room and call emergency phone (see above).

Section 7: Waste Disposal Procedures.

Reclaim if possible; otherwise dispose of in accordance with all applicable federal, state and local regulations.

Section 8: Special Precautions Animal Use.

Not Applicable

Section 9: Required Approvals:

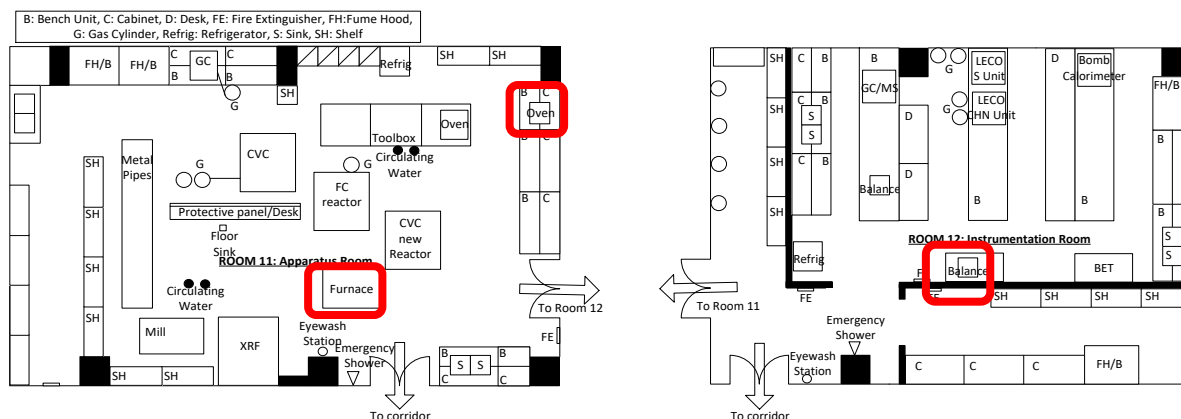
EHSO Lab Safety Training, approval and training from PI or lab supervisor. Read and understand all methods, QRA's, JSA's and SOP's developed for the proximate analysis.

Section 10: Decontamination.

All work surfaces will be cleaned with paper towel at the end of the test and at the end of the day.

Section 11: Designated Areas.

The R³Lab Room 11 and Room 12 framed sections in red in the maps below are designated for proximate analysis tasks.



Section 12. Method:

Sample preparation

1. Cut sample into pieces <1cm with jigsaw
2. Using a series of successively smaller mill screens, grind sample with mill and collect in the receiver jar until all of the material passes a No. 20 mesh screen.
3. Store ground sample in an airtight container

Crucible preparation

1. Heat the muffle furnace to 750°C
2. Using tongs and wearing heat resistant gloves, place 3 empty crucibles and covers in the furnace for 10 min
3. Using tongs and wearing heat resistant gloves, remove the crucibles and covers from the muffle furnace and place them in a desiccator.
4. Allow crucibles to cool for 1 h

Moisture analysis

1. Weigh the crucibles and add to each approximately 1 g, weighed to the nearest 0.0001 g, of the ground sample.
2. Place the crucibles in the vacuum oven at 105°C for 2 h (or overnight if wet). ASTM D1762-84 does not specify the type of oven, a vacuum oven is used to prevent charcoal from burning.
3. Place the dried samples in a desiccator for 1 h and weigh
4. Repeat drying of the sample (steps 2 and 3) in 1 h intervals until a difference of 0.0005g or less is observed between successive weights.

Volatile matter analysis

1. Heat the muffle furnace to 950°C.
2. Preheat the crucibles used for the moisture determination, with lids in place and containing the sample, as follows: with the furnace door open, for 2 min on the outer ledge of the furnace (300°C) and then for 3 min on the edge of the furnace (500°C). Then move the samples to the rear of the furnace for 6 min with the muffle door closed. If possible, watch the samples through a small peep-hole in the muffle door. If sparking occurs, results will be in error (If sparking occurs compare the result with its non-sparking duplicate, if the values are not within 0.5 % the analysis shall be repeated).
3. Cool the samples in a desiccator for 1 h
5. Weigh the samples

Ash analysis

1. Place the lids and the uncovered crucible used for the volatile matter determination, and containing the sample in the muffle furnace at 750°C for 6 h.
2. Cool the crucibles with lids in place in a desiccator for 1 h and weigh.
3. Repeat burning of the sample until a succeeding 1-h period of heating results in a loss of less than 0.0005 g.

Calculate and Report

Calculate the percentage of moisture in the sample as follows:

$$\text{Moisture, \%} = \frac{A - B}{A} 100$$

where:

A = grams of air-dry sample used, and

B = grams of sample after drying at 105°C (Moisture analysis).

Calculate the percentage of volatile matter in the sample as follows:

$$\text{Volatile matter, \%} = \frac{B - C}{B} 100$$

where:

C = grams of sample after heating at 950°C (Volatile Matter analysis).

Calculate the percentage of ash in the sample as follows:

$$\text{Ash, \%} = \frac{D}{B} 100$$

where:

D = grams of residue (Ash analysis).

Report all results to the first decimal place. Values for duplicate determinations should agree within the following:

Constituent Determined	Permissible Differences Between Duplicates, %
Moisture	0.1
Volatile matter	0.5
Ash	0.1

JOB SAFETY ANALYSIS

Safety Information for the University of Hawaii at Manoa

NAME OF DEPARTMENT: HAWAII NATURAL ENERGY INSTITUTE

Title of Job or Task: Proximate Analysis based on ASTM D1762-84

TASK	HAZARDS	CONTROLS
1. Sample Preparation	Charcoal GHS classification: None Charcoal powder and dust may cause eye and skin irritation. Inhalation and ingestion of charcoal dust may cause nose, throat, and gastrointestinal irritation. Sharp cutting blade in the grinder/mill 120 V AC from mains to grinder/mill.	PPE Safety goggles Nitrile gloves Flame resistant lab coat NIOSH-approved particulate mask Long pants Engineered controls Ensure glass on the side of the mill is properly position and secured. Use the tool provided (not fingers) to feed the charcoal into the mill Inspect electrical cords, plugs, and receptacles prior to each use.
2. Transporting crucibles in desiccator	Desiccator can be dropped	PPE Safety goggles Nitrile gloves Flame resistant lab coat Covered shoes Long pants
3. Moisture analysis	Charcoal GHS classification: None	PPE Safety goggles

	<p>Charcoal powder and dust may cause eye and skin irritation. Inhalation and ingestion of charcoal dust may cause nose, throat, and gastrointestinal irritation.</p> <p>Crucibles can be dropped Hot vacuum oven (105°C) 120 V AC from mains to mass balance, vacuum pump and vacuum oven Vacuum system.</p>	<p>Heat resistant gloves Flame resistant lab coat Covered shoes Long pants</p> <p>Engineered controls Use crucible tongs and carriers to handle hot crucibles Appropriately sized vacuum pump, tubing and connections. Inspect electrical cords, plugs, and receptacles prior to each use.</p>
4. Volatile matter and ash analysis	<p>Charcoal GHS classification: None Charcoal powder and dust may cause eye and skin irritation. Inhalation and ingestion of charcoal dust may cause nose, throat, and gastrointestinal irritation.</p> <p>Hot furnace oven (750 to 950°C) Sample releases volatile gases While cooling in desiccator, a vacuum may be created 120 V AC from mains to furnace and mass balance</p>	<p>PPE Safety goggles Heat resistant gloves Flame resistant lab coat Covered shoes Long pants</p> <p>Engineered controls Use crucible tongs and carriers to handle hot crucibles Perform tasks in fume hood and ensure it is operating properly Use a desiccator with a quarter turn valve to release vacuum Inspect electrical cords, plugs, and receptacles prior to each use.</p>
5. Crucible preparation	<p>Hot furnace oven (750°C) While cooling in desiccator, a vacuum may be created 120 V AC from mains to furnace and mass balance</p>	<p>PPE Safety goggles Heat resistant gloves Flame resistant lab coat Covered shoes Long pants</p> <p>Engineered controls Use crucible tongs and carriers to handle hot crucibles</p>

<p style="text-align: center;">Other Information: JSA Completed By: Date Created: OSHA Reference:</p>			<p>Perform tasks in fume hood and ensure it is operating properly</p> <p>Use a desiccator with a quarter turn valve to release vacuum</p> <p>Inspect electrical cords, plugs, and receptacles prior to each use.</p>
	<p>Required Training: EHSO Lab Safety Training, Read UH Chemical hygiene plan, Specific lab activity training by PI or lab supervisor, Read and understand ASTM D1762-84 for chemical analysis of wood charcoal , all methods, QRA's, JSA's and SOP's developed for the proximate analysis.</p>	<p>Required Personal Protective Equipment (PPE) Safety goggles Heat resistant gloves Flame resistant lab coat Covered shoes NIOSH-approved particulate mask Nitrile gloves Long pants</p>	
	<p>See Scott Turn, Trevor Morgan, Lloyd Paredes and Maider Legarra-Arizaleta for more information on Job Hazard Analysis</p> <p>Maider Legarra-Arizaleta, Daylan Siemman, Trevor Morgan and Scott Turn</p> <p>04/20/2018</p> <p>_____</p> <p>For more information about this JSA, contact the <i>University of Hawaii Environmental Health and Safety Office</i> http://www.hawaii.edu/ehso/industrial/ or by phone at 956-3204</p>		

APPENDIX M. SOP and JSA 10: Replacing and Operating Gas

Cylinders

Laboratory Standard Operating Procedures

University of Hawaii at Manoa

Please fill out and place in your Chemical Hygiene Plan

Replacing and Operating Gas Cylinders Date: 4/20/2018

Principal Investigator: Scott Turn

Produced By: Maidier Legarra

Room and Building: POST 11/12

Phone Number: PI Scott Turn: 808-956-2346/ POST 11: 808-956-9903 /POST 12: 808-956-3790/ UH Emergency: 808-956-6911 (on campus 66911)/ Emergency: 911

Section 1 Process:

(Check One) Process

Hazardous Chemical

Hazard Class

Summary:

One gas cylinder of helium is used as a carrier gas for the MicroGC instrument, the outlet pressure from the cylinder regulator to the MicroGC is 80 psig (5.5 bar-g).

One gas cylinder of nitrogen is used for the wall heated tubing bomb (WHTB) experiment.

Section 2: Describe Process Hazards, Hazardous Chemical or Hazard Class.

Asphyxiation: Simple asphyxiation is the primary hazard associated with inert gases (helium and nitrogen in this case). Because inert gases are colorless and odorless, they can escape into the atmosphere undetected and quickly reduce the concentration of oxygen below the level necessary to support life (when the oxygen concentration is reduced below 19.5%).

The calculation below shows that an accidental release of a full He or N₂ cylinder into POST 11 would not be capable of reducing the oxygen level below the hazardous limit of 19.5%.

POST 11 has an approximate volume of 521.22 m³ (V_{POST 11, approx} = 14.6 m x 8.5 m x 4.2 m). The room filled with air at 1 atm and ~20 °C equates to 21,694 moles of air composed of ~ 79% N₂ and ~21% O₂, i.e., 17,138 moles of nitrogen and 4,556 moles of oxygen as shown by equations 1.1 and 1.2 (ideal gas equation):

$$n_{N_2, initial} = \frac{0.79 \text{ atm } 521,220L}{0.082 \frac{\text{atm } L}{\text{mol } K} 293 K} = 17,138 \text{ mol} \quad 1.1$$

$$n_{O_2, initial} = \frac{0.21 \text{ atm } 521,220L}{0.082 \frac{\text{atm L}}{\text{mol K}} 293 K} = 4,556 \text{ mol} \quad 1.2$$

The release of a full *Airgas* helium or nitrogen cylinder into POST 11 would change the composition and concentration of gas in the room. A full *Airgas* helium or nitrogen cylinder with a specified maximum volume of 304 ft³ at STP (equal to 8.61 m³ at STP) would release 352 moles of helium or nitrogen as given by equation 1.3. (Note: 8.61 m³ of nitrogen at STP are compressed to a cylinder volume of 0.0421 m³ at a maximum cylinder pressure of 3000 psi at 25 °C, see eq 1.4).

$$n_{He \text{ or } N_{2, released}} = \frac{1 \text{ atm } 8,610L}{0.082 \frac{\text{atm L}}{\text{mol K}} 298 K} = 352 \text{ mol} \quad 1.3$$

$$\cdot V_1(\text{at } 25 \text{ }^\circ\text{C and } 3000 \text{ psi}) = \frac{14.7 \text{ psi} \cdot 8,61 \text{ m}^3}{3000 \text{ psi}} = 0.0421 \text{ m}^3 = 42.1 L \quad 1.4$$

After the release of a full helium cylinder into POST 11, the composition of the air would be 17138 moles of nitrogen, 4556 moles of oxygen and 352 moles of helium. After the release of a full nitrogen cylinder into POST 11, the composition of the air would be 17490 moles of nitrogen (17138 moles+352 moles) and 4556 moles of oxygen.

In both cases, the room oxygen concentration after the release of helium or nitrogen full cylinder is 20.67 % which is above the hazardous level of 19.5%. The oxygen concentration would remain above the hazardous level, even if the two cylinders were to simultaneously vent into the lab space. Notice that these calculations are somewhat simplistic; this assumes instantaneous and complete mixing of the leaked contaminant and the entirety of the room's air.

High Pressure: All compressed gases are potentially hazardous because of the high pressure stored inside the cylinder (even low pressure cylinders). A sudden release of pressure can cause injuries by propelling a cylinder or whipping a line. Gases under pressure may explode if heated. Contact with rapidly expanding gas may cause burns or frostbite.

Improper Handling of Cylinders: Compressed gas cylinders are heavy and awkward to handle. Improper handling of cylinders could result in sprains, strains, falls, bruises, and broken bones. Other hazards such as cold burns could occur if gases accidentally escape from the cylinder due to mishandling.

Section 3: Personal Protective Equipment.

Safety glasses, flame resistant lab coat, covered shoes, safety shoes and leather work gloves are recommended when handling cylinders

Section 4: Engineering Controls.

The use of oxygen monitoring equipment in the vicinity of the gas cylinders is strongly recommended for enclosed areas where inert gases are being used, especially in small areas that are not well ventilated. The MicroGC and helium gas cylinder are located next to one another in POST 11, the nitrogen cylinder is located next to the WHTB in POST 11 too. This is a large laboratory (approx. 14.6 m x 8.5 m x 4.2 m) with good ventilation (air conditioning, air recirculation and extraction). It has been determined that accidental release of a full helium or nitrogen cylinder

into POST 11 would reduce the oxygen concentration in the room to 20.67 % which is above the hazardous level of 19.5 % (see Section 2).

Excess 'flow restrictor' valve in the line from the nitrogen cylinder to the WHTB and from the helium cylinder to the MicroGC installed to prevent excessive release of nitrogen and helium into the environment.

Electricity: Inspect electrical cords, plugs, and receptacles prior to each use.

Section 5: Special Handling and Storage Requirements.

- Only trained and approved personnel are allowed to move gas cylinders.
- All cylinder movement should be done with a compressed gas cylinder cart.
- Always secure the cylinders when in storage or use. Cylinders secured with a chain or strap must have the chain or strap attached 2/3 of the way up on the cylinder.
- Compressed gas cylinders should not be subjected to any mechanical shock that could cause damage to their valves or pressure relief devices.
- Cylinders should not be dropped, dragged, slid, or used as rollers for moving material or other equipment.
- When in storage, empty or full the caps must be on and the labels viewable. Cylinder caps should not be removed until the cylinder is secured in place and ready for use. Cylinder caps perform two functions:
 - Protecting the valve on the top of the cylinder from damage if it is knocked over;
 - Ventilating the gas out of both sides, and minimizing the likelihood that the cylinder will topple when gas is accidentally released through the valve.
- Cylinders should be stored upright and secured at all times.
- Cylinders should not be stored near radiators or other heat sources, and places where they could come into contact with any electrical apparatus or circuits, and corrosion due to weather or chemicals.
- Cylinders should not be exposed to sparks, flames, or temperatures above 125°F.
- Gases should be used and stored only in a well-ventilated area.
- Never store gases for longer than one year without use.

Section 6: Leaking and Accident Procedures.

Handling of leaking cylinders: Most leaks occur at the valve in the top of the cylinder and may involve the valve threads, valve stem, valve outlet, or pressure relief devices. No action shall be taken involving any personal risk or without suitable training. Evacuate surrounding areas. Keep unnecessary and unprotected personnel from entering. Avoid breathing gas. Provide adequate ventilation. Wear appropriate respirator (Self-Contained Breathing Apparatus SCBA) when ventilation is inadequate.

Small spill: Shutoff source of gas. Stop leak if without risk. Contact emergency personnel (see Phone number information above) if necessary.

Large spill: Call supplier for emergency contact information (AirGas 24-hour phone 1-866-734-3438). Whenever a large or uncontrollable leak occurs, evacuate the area/building and immediately call X6-6911 from internal UH phones or 911 otherwise.

Personnel should not attempt to repair a leaking cylinder. Where action can be taken, trained personnel should move the cylinder to an isolated, well-ventilated area when it is safe to do so.

Section 7: Waste Disposal Procedures.

Unused product/ empty container: When returning an empty cylinder to the vendor, close the valve and cap the cylinder before shipment. Leave 25-30 psig of residual pressure in the cylinder, when possible.

Disposal: For emergency disposal, secure the cylinder and slowly discharge gas to the atmosphere in a well ventilated area or outdoors.

Section 8: Special Precautions Animal Use.

NA.

Section 9: Required Approvals:

- Only approved personnel are allowed to change the gas cylinder connected to the MicroGC or WHTB instruments, contact Scott Turn or Trevor Morgan for approval.
- EHSO Lab Safety Training.
- MicroGC Operation Method for helium cylinder, Experiment Performance and Unloading and Disassembly of the WHTB for nitrogen cylinder, Quantitative Risk Assessment (QRA), Job Safety Analysis (JSA) and Standard Operating Procedure (SOP).

Section 10: Decontamination.

NA.

Section 11: Designated Areas.

The instrument is set up in POST 11. The working area is the same place where the instruments (MicroGC and WHTB) are located.

JOB SAFETY ANALYSIS

Safety Information for the University of Hawaii at Manoa

NAME OF DEPARTMENT: HAWAII NATURAL ENERGY INSTITUTE

Title of Job or Task: Replacing & Operating Gas Cylinder (Micro-GC) - POST 11

TASK	HAZARDS	CONTROLS
<p>1. Helium cylinder used as carrier gas for a MicroGC instrument.</p> <p>Nitrogen cylinder used for the WHTB volume evaluation, for the WHTB leak testing, for purging air from the WHTB and for WHTB pressurization.</p>	<p>Compressed Helium H280 – Contains gas under pressure; may explode if heated.</p> <p>OSHA-H01 – May displace oxygen and cause rapid suffocation.</p> <p>Heavy helium cylinder.</p> <p>Compressed Nitrogen H280 – Contains gas under pressure; may explode if heated.</p> <p>OSHA-H01 – May displace oxygen and cause rapid suffocation.</p> <p>Heavy nitrogen cylinder.</p>	<p>PPE Safety glasses, flame resistant lab coat, covered shoes. Leather gloves and safety shoes are recommended when handling cylinders</p> <p>Engineered controls General lab ventilation should be sufficient to control worker exposure to airborne contaminants (POST-11).</p> <p>Store cylinder in a segregated and approved area. Store cylinder away from direct sunlight in a dry, cool and well-ventilated area. Keep container tightly closed and sealed until ready for use. Cylinders should be stored upright, with valve protection cap in place, and firmly secured to prevent falling or being knocked over.</p> <p>Cylinder temperatures should not exceed 52 °C (125 °F). Avoid contact with eyes, skin and clothing. Avoid breathing gas. Do not puncture or incinerate container. Use equipment rated for cylinder pressure.</p>

Other Information: JSA Completed By:: Date Created: OSHA Reference:			Protect cylinders from physical damage; do not drag, roll, slide, or drop. Use a suitable hand truck for cylinder movement. Install excess flow restrictors on all gas cylinders actively used in the experiment.	
	Required Training: EHSO Lab Safety Training. Read UH Chemical Hygiene Plan. Specific lab activity training by PI or lab supervisor. Read and understand all methods, QRA's, JSA's and SOP's developed for replacing and operating gas cylinders	Required Personal Protective Equipment (PPE) Safety glasses, flame resistant lab coat, covered shoes. Leather gloves and safety shoes are recommended when handling cylinders		
	See Scott Turn, Trevor Morgan, Lloyd Paredes and Maider Legarra-Arizaleta for more information on Job Hazard Analysis Maider Legarra-Arizaleta April 20, 2018 <hr/> For more information about this JSA, contact the <i>University of Hawaii Environmental Health and Safety Office</i> http://www.hawaii.edu/ehso/industrial/ or by phone at 956-3204			

APPENDIX N. Proximate Analysis Reproducibility Study

A certified reference charcoal with known values of fixed-carbon, volatile matter and ash content would be a suitable feedstock material for validating the proximate analysis techniques employed in the WHTB carbonization experiments. Unfortunately, such material could not be found for purchase. Instead, the following three standard materials were employed in this study: The first standard was a Kiawe wood charcoal from Maui (Hawaiian charcoal co. Wailuku, Maui) bought from the store with unknown proximate analysis values. Around half a kilogram of Kiawe charcoal was ground to a particle size below 0.2 mm and was homogenized by rolling and shaking its container for over one hour. The second standard was a coal certified reference material (Leco CRM, Prox-Plus coal 502-680) with the following specified proximate analysis values: volatile matter – $18.4\% \pm 0.3\%$, ash – $9.03\% \pm 0.13\%$, fixed carbon – $72.6\% \pm 0.3\%$. The third standard was another coal certified reference material (ARMI CRM, Prox-X Coal (IARM HC30800A), certificate #: HC30800A-07242008-IARM-F) with specified proximate analysis values of: volatile matter – $35\% \pm 1\%$, ash – $23.9\% \pm 0.1\%$, fixed carbon – $42\% \pm 2\%$.

Since the amounts of both certified reference materials (CRMs) were limited (around 50 grams of each sample), the influence of a number of variables on the proximate analysis results was studied using the Kiawe charcoal (lab standard). The CRMs were subsequently used to validate the proximate analysis technique and to determine which version of the method is best suited to our application. In this way, the number of tests that used the costly CRMs was kept to a minimum. Table N.1 displays an outline of the conditions and goal of the proximate analysis tests undertaken for this study. The bullet points below provide a detailed description of each set of test conditions (variables studied and levels), including tables showing the proximate analysis

results for each test and summarizes the conclusions regarding the most suitable conditions based on the results.

Table N.1. Outline of the experimental conditions and goal for the proximate analysis reproducibility study.

Method and sample	Oven/Furnace	Crucibles in furnace (#)	Sample per crucible (g)	Crucible type	Repeats (#)	Goal
Moisture Content Analysis on Kiawe charcoal	Vacuum oven	3	1	Glass	2	Determine crucible type for moisture content analysis
		3	1	Ceramic	2	
Method 300C-500C-950C-6 mins on Kiawe charcoal	Small furnace	3	1	Ceramic	2	Determine accuracy for proximate analysis values (fC, VM and ash) with method used in preliminary experiments
Method 950C- 6 mins on Kiawe charcoal	Small/ Large furnace	3	1	Ceramic	2	Determine accuracy for proximate analysis values (fC, VM and ash) with new method
		9	1	Ceramic	1	Determine the influence of the number of crucibles loaded in the furnace
		3	0.5	Ceramic	2	Determine the influence of the sample amount per crucible
		3	0.25	Ceramic	2	
Method 20C-950C-100C on Kiawe charcoal	Small/ Large furnace	3	1	Ceramic	1	Determine accuracy for proximate analysis values (fC, VM and ash) of the modified method
Modified Method 950C-100C on Kiawe charcoal	Small/ Large furnace	3	1	Ceramic	1	Determine accuracy for proximate analysis values (fC, VM and ash) of the modified method
Method 950C- 6 mins on Kiawe charcoal	Small/ Large furnace	3	1	Ni-Cr	2	Determine the influence of crucible type
Method 950C- 6 mins on CRM Prox-Plus coal 502-680	Small/ Large furnace	3	1	Ni-Cr	1	Validate the method with a CRM
Method 950C- 6 mins on CRM Prox-Plus coal 502-680	Small/ Large furnace	3	0.5	Ni-Cr	1	Validate the method and lower sample loading with a CRM

Table N.2. Outline of the experimental conditions and goal for the proximate analysis reproducibility study (Continued).

Method and sample	Oven/Furnace	Crucibles in furnace (#)	Sample per crucible (g)	Crucible type	Repeats (#)	Goal
Method 950C- 6 mins on CRM Prox-X Coal	Small/Large furnace	3	1	Ni-Cr	1	Validate the method with a second CRM
Method 950C- 6 mins on CRM Prox-X Coal	Small/Large furnace	3	0.5	Ni-Cr	1	Validate the method and lower sample loading with a second CRM

- Determine the type of crucibles employed for moisture content analysis. Levels: Glass and ceramic.**

Since proximate analysis calculations of volatile matter, ash and fixed-carbon contents are derived on a dry basis, the moisture content of each sample was determined by ASTM E871-82²⁰⁵. Moisture and proximate analysis can be determined simultaneously using material from the same batch and the volatile matter, ash and fixed-carbon values later corrected for moisture.

Charcoal samples are dried in crucibles placed in a vacuum oven at 105°C as described in ASTM E1756-08²⁰⁸. Glass and ceramic crucibles were tested. The results displayed in Table N.2 indicated that ceramic crucibles are more appropriate as the weights recorded were stable and moisture values of seven different samples were consistent. In contrast, the use of glass crucibles showed unstable weights. It was thought that this instability was due to electrostatic charge building up on the glassware, however the stability did not improve after removing the electrostatic charge and the moisture values showed considerable uncertainty.

Table N.3. Results of moisture content analysis of Kiawe charcoal loaded in two different types of crucibles.

Date	170303	170306	170313	170303	170306			170313		
Oven/ Furnace	Vacuum Oven									
Method	Moisture Content Analysis									
Crucibles	Glass	Glass	Glass	Ceramic	Ceramic			Ceramic		
Sample	Kiawe charcoal									
Mass ₀ [g] ^a	0.9908	1.5736	1.2401	1.2579	1.3256	1.3140	1.4917	1.3292	1.2607	1.1066
MC ^b [%]	6.4	6.9	7.3	7.2	7.2	7.2	7.2	7.2	7.2	7.2
^a . Mass ₀ : Initial wet sample mass ^b . MC: Moisture content										

- Proximate analysis method and furnace size. Levels: (1) Method 300-500-950°C-6 mins, (2) Method 950°C- 6 mins, (3) Modified method 20-950-100°C and (4) Modified method 950-100°C:**

Four methods were tested

- Method 300-500-950°C-6 mins:* This method used the small furnace model (Thermolyne 1300 Model FB 1315M) and was applied to charcoals produced in preliminary WHTB experiments that carbonized oak and cellulose. The standard ASTM-D1762-84²⁰⁹ was followed. First the charcoal was dried. Then, it was devolatilized in three steps—(1) for 2 minutes on the outer ledge of the furnace at around 300°C with the furnace door open, (2) for 3 minutes on the edge of the furnace at around 500°C with the door open and (3) at the rear of the furnace at 950°C for 6 minutes with the muffle door closed. Finally, the charcoal was ashed at 750°C for a minimum of 6 hours. The use of this procedure often resulted in dropped crucibles and loss of experimental samples due to the difficulties of moving and

placing the crucibles in the different locations in a stable manner during the first two steps of devolatilization.

- *Method 950°C- 6 mins:* Proximate analysis was performed by following standards ASTM E872-82(2013)²⁰⁰ and ASTM E830-87(1996)²⁰¹. This method devolatilizes the sample in a single step at 950°C for 6 minutes (ASTM E872-82(2013)²⁰⁰, the standard for coal samples) and ashes it at 750°C for a minimum of 6 hours (ASTM E830-87(1996),²⁰¹ the standard for refuse derived fuel). This method removed the more problematic steps during devolatilization of the earlier method minimizing sample losses and improving practicality.
- *Modified method 20-950-100°C:* A modified version was also tested. In this method, the furnace (Fisher Scientific Isotemp muffle furnace model 58, cat. # 10-650-58) was programmed to heat the samples from room to 950°C at the maximum specified heating rate allowed by the furnace (200°C /min). Samples were held at 950°C for 6 minutes and subsequently cooled down to 100°C to prevent moisture pick-up. The goal was to perform char devolatilization overnight and to offer the possibility to remove the samples on the following day.
- *Modified method 950-100°C:* In this method, samples were introduced in the furnace (Fisher Scientific Isotemp muffle furnace model 58, cat. # 10-650-58) already heated to 950°C, were held for 6 minutes and subsequently cooled down to 100°C to prevent moisture pick-up.

In all methods, volatile matter, ash and fixed-carbon contents are calculated as follows: The volatile matter is estimated by difference between the dried and the devolatilized charcoal, the ash content between the dried and ashed charcoal, and finally, the fixed-carbon content is calculated on a dry basis by subtracting all the other constituents percentages from 100%, that is to say, $\%fC = 100 - \%VM - \%ash_{char}$.

The results displayed in Table N.3 indicates that the method 950°C- 6 mins—as opposed to the method 300-500-950°C-6 mins—displayed around 2-3% higher volatile matter content values (20.9-21.6% vs. 18.6-19.1%), and similar ash contents of around 2%. Compared to the modified method 20-950-100°C, the 950°C- 6 mins method showed radically higher volatile matter values (20.9-21.6% versus 3.6-3.9%). And finally, compared to the modified method 950-100°C, the 950°C- 6 mins method estimated somewhat lower volatile matter contents (20.9-21.6% versus 25.2-28%).

Sub-section *Validation with certified reference materials (CRMs)* below presents the proximate analysis results of the coal reference materials with the 950°C- 6 mins method, the results show good accuracy when compared to the certified values. Therefore, it seems that the method used in preliminary experiments 300-500-950°C-6 mins is likely to slightly underestimate the volatile matter content (and slightly overestimate the fixed-carbon content), the modified method 20-950-100°C result in proximate analysis values that greatly deviate from the actual values with significant underestimations of the volatile matter contents, while the modified method 950-100°C somewhat overestimates the volatile matter content.

The low devolatilization degree observed in the modified method 20-950-100°C was the result of the furnace heating profile. In this method, the furnace was programmed to ramp from room temperature to 950°C at 200°C/min and ramp down to 100°C after 6 min at 950°C. Nonetheless, the 200°C/min heating rate was unachievable. The actual furnace temperature could not match the temperature set point specified by the program resulting in actual heating rates considerably lower than 200°C/min especially when approaching higher temperatures. When the cool down step began, the actual furnace temperature had never reached the 950°C target. The result was the removal of just a tiny amount of volatiles from the sample.

To check whether the modified method 20-950-100°C was worth exploring, another modified method (950-100°C) was tested. Three charcoal samples were inserted in the oven at 950°C. After exactly 6 minutes, the furnace temperature was set to 100°C. In this method, a very slow cool down stage was observed (it took almost 5 hours for the furnace to cool down from 950 to 120°C). As a result, the sample was exposed to temperatures close to 950 C for an extended period of time which probably partially combusted the sample and therefore resulted in overestimated volatile matter values. In conclusion, the method selected for the proximate analysis evaluation in WHTB experimental samples is method 950°C- 6 mins as it gave the most accurate fixed-carbon, volatile matter and ash values. Modified methods were discarded since the calculated values do not reflect the true values.

Table N.4. Results of proximate analysis tests of Kiawe charcoal analysed using several methods.

Date	170307			170307			170307			170314			170323			170324		
Oven/ Furnace	Small Furnace			Small Furnace			Large Furnace			Large Furnace			Large Furnace			Large Furnace		
Method	Method 300-500-950°C-6 mins			Method 300-500-950°C-6 mins			Method 950°C-6 mins			Method 950°C-6 mins			Modified method 20-950-100°C			Modified method 950-100°C		
Crucibles	Ceramic			Ceramic			Ceramic			Ceramic			Ni-Cr ^f			Ni-Cr ^f		
Sample	Kiawe charcoal																	
Mass ₀ [g] ^a	0.92 89	0.89 84	0.93 79	1.22 81	0.96 30	1.17 19	0.81 29	0.91 07	0.98 67	0.91 90	1.02 04	1.18 11	0.99 00	0.93 66	1.04 66	1.13 72	1.01 51	0.96 88
MC ^{b,c} [%]	7.2	7.2	7.2	7.2	7.2	7.2	7.2	7.2	7.2	7.2	7.2	7.2	7.2	7.2	7.2	7.2	7.2	7.2
VM ^d [%]	18.6	18.9	18.7	18.9	19.1	19.0	21.4	21.6	20.9	21.2	20.9	21.0	3.9	3.6	3.7	25.3	25.2	28.0
Ash [%]	2.11	2.03	2.11	2.12	1.95	1.93	2.11	2.18	2.15	1.98	2.05	2.11	NA ^g	NA ^g	NA ^g	NA ^g	NA ^g	NA ^g
fC ^e [%]	79.3	79.1	79.2	79.0	78.9	79.1	76.4	76.2	77.0	76.8	77.1	76.9	NA ^g	NA ^g	NA ^g	NA ^g	NA ^g	NA ^g
<p>^a. Mass₀: Initial wet sample mass</p> <p>^b. MC: Moisture content</p> <p>^c. Moisture content analysis was performed on a different charcoal sample from the same batch. VM, fC and ash have been corrected using this value.</p> <p>^d. VM: Volatile Matter</p> <p>^e. fC: fixed Carbon</p> <p>^f. Note that the modified method used nickel-chromium crucibles instead of ceramic. It was determined that the crucible type did not present a significant difference in the results (see section <i>Crucible types. Levels: Ceramic and nickel-chromium</i>).</p> <p>^g. NA: Not Available</p>																		

- **Number of crucibles in furnace: Levels: 3 crucibles in furnace and 9 crucibles in furnace.**

In order to determine whether proximate analysis could be performed on multiple samples simultaneously, nine samples were analyzed together. All nine analysis showed similar fixed-carbon, volatile matter and ash contents to one-another (see Table N.4), the values were also consistent to the three-sample tests shown previously in Table N.3. For example, volatile matter contents of the 9-sample test ranged from 19.9 to 21.6% whereas the volatile matter in the 3-sample tests varied from 20.9 to 21.6%.

Note: ceramic crucibles were used for these tests which meant each sample was introduced in to the furnace one by one prolonging the time the furnace was open. This resulted in the furnace temperature dropping below 950 C. It is likely that minimizing the time the furnace remains open during sample introduction would improve the standard deviation of volatile matter and fixed-carbon contents. This could be accomplished by placing several crucibles in the furnace at the same time using a tray to hold multiple crucibles. Thus, crucibles made out of a Ni-Cr alloy were tested. This type of crucible can be held in custom-made Ni-Cr trays. Each tray holds 3-cruciblesthat can be inserted in the furnace in a single step which simplifies and reduces the time of the analysis.

Table N.5. Results of nine proximate analysis tests of Kiawe charcoal analyzed simultaneously.

Date	170310								
Oven/ Furnace	Large Furnace								
Method	Method 950°C-6 mins								
Crucibles	Ceramic								
Sample	Kiawe charcoal								
Mass ₀ [g] ^a	0.8578	1.0195	1.2666	0.9789	1.4977	1.1851	1.1594	1.4004	1.7497
MC ^{b,c} [%]	7.2	7.2	7.2	7.2	7.2	7.2	7.2	7.2	7.2
VM ^d [%]	21.6	20.8	21.0	21.5	20.3	20.5	20.5	20.3	19.9
Ash [%]	1.998	2.019	2.025	1.949	2.022	1.882	2.082	2.093	2.063
fC ^e [%]	76.4	77.1	76.9	76.6	77.7	77.6	77.4	77.7	78.1
^a . Mass ₀ : Initial wet sample mass ^b . MC: Moisture content ^c . Moisture content analysis was performed in a different charcoal sample from the same batch. VM, fC and ash have been corrected using this value. ^d . VM: Volatile Matter ^e . fC: fixed Carbon									

- **Amount of sample per crucible. Levels : 1, 0.5 and 0.25 g per crucible**

In addition to analyzing 1g samples per crucible as specified by the ASTM, lower sample mass loadings were also subjected to proximate analysis. The goal is to determine whether and how much the sample amount can be reduced without influencing the volatile matter, fixed-carbon and ash content results. Due to the limited amounts of charcoal produced during the WHTB experiments, reduced loadings would be beneficial as more experimental sample would remain for other types of analysis.

The fixed-carbon, volatile matter and ash values calculated from the analysis of 0.5 and 0.25 g of sample per crucible are presented in Table N.5. Reducing the mass loading appears to result in higher mass losses during the devolatilization step. The analysis of 0.5 g of sample per crucible showed volatile matter contents of 20.9 -22.8% and the analysis of 0.25 g of sample per crucible presented contents of 23.4-26.3%. These values compare to a volatile matter content of 20.9-21.6% observed when the specified loading of 1 g of sample per crucible was analyzed. In

conclusion, differences in results between analysis of 0.5 g of sample per crucible and 1 g were small or negligible but became larger when the amount analyzed was reduced to 0.25 g. The subsection below *Validation with certified reference materials (CRMs)* confirms that reducing the mass loadings from 1 to 0.5 g per crucible does not have a significant impact on the proximate analysis values calculated for the two certified reference materials.

Table N.6. Results of proximate analysis tests of various mass loadings of Kiawe charcoal.

Date	170314			170316			170314			170316			170321		
Oven/ Furnace	Large Furnace VM. Small furnace ash			Large Furnace VM. Large furnace ash			Large Furnace VM. Small furnace ash			Large Furnace VM. Small furnace ash			Large Furnace VM. Small furnace ash		
Method	Method 950°C-6 mins			Method 950°C-6 mins			Method 950°C-6 mins			Method 950°C-6 mins			Method 950°C-6 mins		
Crucibles	Ceramic			Ceramic			Ceramic			Ceramic			Ceramic		
Sample	Kiawe charcoal														
Mass ₀ [g] ^a	0.5472	0.5541	0.5950	0.4172	0.5133	0.5395	0.6275	0.5395	0.2952	0.2396	0.3193	0.2790	0.2341	0.2791	
MC ^{b,c} [%]	7.2	7.2	7.2	7.2	7.2	7.2	7.2	7.2	7.2	7.2	7.2	7.2	7.2	7.2	
VM ^d [%]	22.2	22.6	NA ^f	22.8	21.6	22.1	20.9	22.4	NA ^f	24.3	24.0	24.1	26.3	23.4	
Ash [%]	2.067	2.100	NA ^f	1.937	1.973	2.256	2.180	2.124	NA ^f	2.023	2.159	2.085	1.611	2.161	
fC ^e [%]	75.7	75.3	NA ^f	75.3	76.4	75.7	77.0	75.4	NA ^f	73.6	73.9	73.8	72.1	74.5	
<p>^a. Mass₀: Initial wet sample mass ^b. MC: Moisture content ^c. Moisture content analysis was performed in a different charcoal sample from the same batch. VM, fC and ash have been corrected using this value. ^d. VM: Volatile Matter ^e. fC: fixed Carbon ^f. NA: Not Available</p>															

- **Crucible types. Levels: Ceramic and nickel-chromium.**

Two types of crucibles were tested for the proximate analysis: ceramic and nickel-chromium. Ceramic ones are specified by the ASTM standards and were used in preliminary experiments. The Ni-Crones can be mounted in a manufactured Ni-Cr tray that can hold three crucibles at once and therefore introduces practical advantages such as reducing the time to place and remove crucibles from the furnace or improving the stability of the crucibles. Table N.6 shows the proximate analysis results of samples loaded in Ni-Cr crucibles. Using the Ni-Cr crucibles, instead of ceramic, does not have an effect on the proximate analysis values and improves the practicality of the proximate analysis. Note: It is essential to have crucible lids loosely placed over the crucible during the devolatilization step. If the lids are fitted too tightly it can result in pressure build-up in the crucibles that ultimately causes the lids and sample to be violently ejected.

Table N.7. Results of proximate analysis tests of Kiawe charcoal analysed in Ni-Cr crucibles.

Date	170316			170324		
Oven/Furnace	Large Furnace VM and ash			Large Furnace VM		
Method	Method 950°C-6 mins			Method 950°C-6 mins		
Crucibles	Ni-Cr			Ni-Cr		
Sample	Kiawe charcoal					
Mass ₀ [g] ^a	0.9324	0.9895	1.0529	0.9691	0.7758	1.0939
MC ^{b,c} [%]	7.2	7.2	7.2	7.2	7.2	7.2
VM ^d [%]	20.9	20.8	20.9	21.2	21.3	21.5
Ash [%]	2.484	2.373	2.271	2.234	2.249	2.147
fC ^e [%]	76.6	76.8	76.8	76.6	76.5	76.3
^a . Mass ₀ : Initial wet sample mass ^b . MC: Moisture content ^c . Moisture content analysis was performed in a different charcoal sample from the same batch. VM, fC and ash have been corrected using this value. ^d . VM: Volatile Matter ^e . fC: fixed Carbon						

- **Validation with certified reference materials (CRMs).**

Method 950°C-6 mins with Ni-Cr crucibles was validated by two coal certified reference materials (CRMs): Prox-Plus coal 502-68 with the following specified proximate analysis values: volatile matter – 18.4%±0.3%, ash – 9.03%±0.13%, fixed carbon – 72.6%±0.3%, and Prox-X Coal (IARM HC30800A) with specified proximate analysis values of: volatile matter – 35%±1%, ash – 23.9%±0.1%, fixed carbon – 42%±2%.

Sample loadings of 0.5 and 1 g per crucible were tested for both CRMs. That is, a total of four different set of conditions were tested (2 samples plus 2 mass loadings). All analysis showed close agreement with the coal certifications (see Table N.7). In the case of CRM Prox-Plus Coal (502-680), the analysis of 1 g of sample appeared to slightly underestimate the amount of volatiles while the analysis of 0.5 g of sample slightly overestimated it. The tests using 0.5g samples gave values closer to the certified values. In the case of CRM Prox-X Coal (IARM HC30800A), both the 1 g and 0.5g analysis slightly overestimated the amount of volatiles with values a little bit higher from 0.5 g samples. Both samples also slightly underestimated the fixed carbon content. The 0.5 g samples displayed better reproducibility for both the fixed carbon and ash and were closer to the certified values.

Based on the results, it was concluded that a 0.5 g of sample per crucible was an appropriate loading to perform proximate analysis. This amount results in accurate values and at the same time, leaves a generous amount of additional experimental sample for performing other analysis.

Table N.8. Results of proximate analysis tests of various mass loadings of certified reference coal materials.

Date	170321			170314			170328			170328		
Oven/ Furnace	Large Furnace VM/Small furnace ash			Large Furnace VM/Small furnace ash			Large Furnace VM/Small furnace ash			Large Furnace VM/Small furnace ash		
Method	Method 950°C-6 mins			Method 950°C-6 mins			Method 950°C-6 mins			Method 950°C-6 mins		
Crucibles	Ni-Cr			Ni-Cr			Ni-Cr			Ni-Cr		
Sample	CRM Prox-Plus Coal (502-680)			CRM Prox-Plus Coal (502-680)			Prox-X Coal (IARM HC30800A)			Prox-X Coal (IARM HC30800A)		
Mass _o [g]] ^a	1.149 1	1.129 5	0.981 1	0.466 7	0.444 4	0.620 9	1.025 9	0.976 0	0.933 9	0.470 7	0.519 1	0.516 4
MC ^{b,c} [%]	0.6	0.6	0.6	0.6	0.6	0.6	1.9	1.9	1.9	1.9	1.9	1.9
VM ^d [%]	17.8	17.9	17.9	18.7	18.7	18.6	36.0	35.9	35.6	36.5	36.4	36.8
Ash [%]	9.068	9.074	9.073	NA ^f	9.212	9.007	23.40 5	25.44 7	25.21 9	23.69 7	23.96 2	23.73 2
fC ^e [%]	73.1	73.1	73.0	NA ^f	72.1	72.4	40.6	38.6	39.1	39.8	39.6	39.5
^a . Mass _o : Initial wet sample mass ^b . MC: Moisture content ^c . Moisture content analysis was performed in a different charcoal sample from the same batch. VM, fC and ash have been corrected using this value. ^d . VM: Volatile Matter ^e . fC: fixed Carbon ^f . NA: Not Available												

APPENDIX O. MATLAB code CVC model 1

```
function main

t=0:1:15000; % s time scale
% initialconditions:
x1_o=10; %x1_o=Mw_o=100g
x2_o=0; %x2_o=Mc_o=0g
x3_o=0; %x3_o=Mt_o=0g
x4_o=0; %x4_o=Mg_o=0g
x5_o=298 ;%x5_o=T=25 degree C= 298K
x6_o=100; %x6_o=P=1 atm=100 kPaapprox.
[t,x]=ode45( @rhs, t, [x1_o x2_o x3_o x4_o x5_o x6_o] );
figure(1);
plot(t,x(:,1), 'r',t,x(:,2), 'b',t,x(:,4), 'g',t,x(:,3), 'y', 'linewidth',2);
xlabel('time[s]'); ylabel('Yields[wt%]');
legend('show') ;
legend('Wood', 'Char', 'Gas', 'Tar')

figure(2);
subplot(1,2,1)
plot(t,x(:,5), 'linewidth',2);
xlabel('time[s]'); ylabel('Temperature [oC]');

subplot(1,2,2)
plot(t,x(:,6), 'linewidth',2)
xlabel('time[s]'); ylabel('Pressure [kPa]');
x(15000,6)
x(15000,4)
x(15000,2)
end

function dxdt=rhs(t,x)
%x1_o=Mw=100g
%x2_o=Mc=0g
%x3_o=Ct=0g
%x4_o=Cg=0g
%Kinetic data k1-k3: Thurner and Mann (1981), k4 Liden et al. and k5 Di
%Blasi 1993

Mwo=10;
A1 = 1.43E4;%s^(-1)
A2 = 4.13E6;%s^(-1)
A3 = 7.38E5;%s^(-1)
E1 = 88.6; %kJ/mol
E2 = 112.7; %kJ/mol
E3 = 106.5; %kJ/mol
A4=4.28E6;%s^(-1)
A5=1E5;%s^(-1)
```

```

E4=107.5;%kJ/mol
E5=107.5;%kj/mol
R=8.314E-3;%kJ/molK

k1=A1*exp(-E1/R/x(5));
k2=A2*exp(-E2/R/x(5));
k3=A3*exp(-E3/R/x(5));
k4=A4*exp(-E4/R/x(5));
k5=A5*exp(-E5/R/x(5));
Wg=44; %g/mol molecular weight non-condensable gas
Wt=200; %g/mol molecular weight tar
tw=0.0021; %m wall thickness 0.083 in in m
k_ss=0.019;%kW/mk thermal conductivity stainless steel at 225C
Rad=0.0127;%m reactor radius 1 in in m
L=0.1524; %m reactor length 6 in in m
A_ss=2*pi()*Rad*L; %m^2 Area reactor
V=pi()*Rad^2*L; %m^3 Volume reactor
Vwo=0.2*V; % Initial Volume solid
cp1 = 1.5E-3 ;%kJ/gKcpw Lee et al. (1976)

cp4 = 1.1E-3; %kJ/g K cpg Di Blasi (1993a)
cp2 = 1.5E-3;% kJ/gK cpc Lee et al. (1976)
cp3=1.1E-3; %kJ/gK cpt Di Blasi (1993a)
Ts=573;%K Temperature sandbath
r1=k1*x(1)/V;
r2=k2*x(1)/V;
r3=k3*x(1)/V;
r4=k4*x(3)/V;
r5=k5*x(3)/V;
h1=0.418;%kJ/g Chan et al.
h2=0.418;%kJ/g Chan et al.
h3=0.418;%kJ/g Chan et al.
h4=-0.042;%kJ/g Koufopoulos et al.
h5=-0.042;%kJ/g Koufopoulos et al.

dxdt_1 = -(k1+k2+k3)*x(1);
dxdt_2 = k3*x(1) + k5*x(3);
dxdt_3 = k2*x(1) -k4*x(3)-k5*x(3);
dxdt_4 = k1*x(1) +k4*x(3);
denom=x(1)*cp1+x(2)*cp2+x(3)*cp3+x(4)*cp4-R*V*(x(4)/Wg+x(3)/Wt)/(V-
Vwo*(x(1)+x(2))/Mwo);
Qcond=k_ss/tw*A_ss*(Ts-x(5));
Qreac=V*(r1*(-h1)+r2*(-h2)+r3*(-h3)+r4*(-h4)+r5*(-h5));
Alpha=(1/Wg*dxdt_4+1/Wt*dxdt_3)/(V-
Vwo*(x(1)+x(2))/Mwo)+(x(4)/Wg+x(3)/Wt)*Vwo/Mwo*(dxdt_1+dxdt_2)/(V-
Vwo*(x(1)+x(2))/Mwo)^2;
dxdt_5=(Qcond+Qreac+V*R*x(5)*Alpha)/denom;

dxdt_6=(R*x(5)*(dxdt_4/Wg+dxdt_3/Wt)+R*dxdt_5*(x(4)/Wg+x(3)/Wt))/(V-
Vwo*(x(1)+x(2))/Mwo)+(x(4)/Wg+x(3)/Wt)*R*x(5)*Vwo/Mwo*(dxdt_1+dxdt_2)/(V-
Vwo*(x(1)+x(2))/Mwo)^2;

dxdt=[dxdt_1; dxdt_2; dxdt_3; dxdt_4; dxdt_5;dxdt_6];
end

```

APPENDIX P. Temperature, pressure and product distribution history profiles at various heat transfer coefficients predicted by CVC model 1

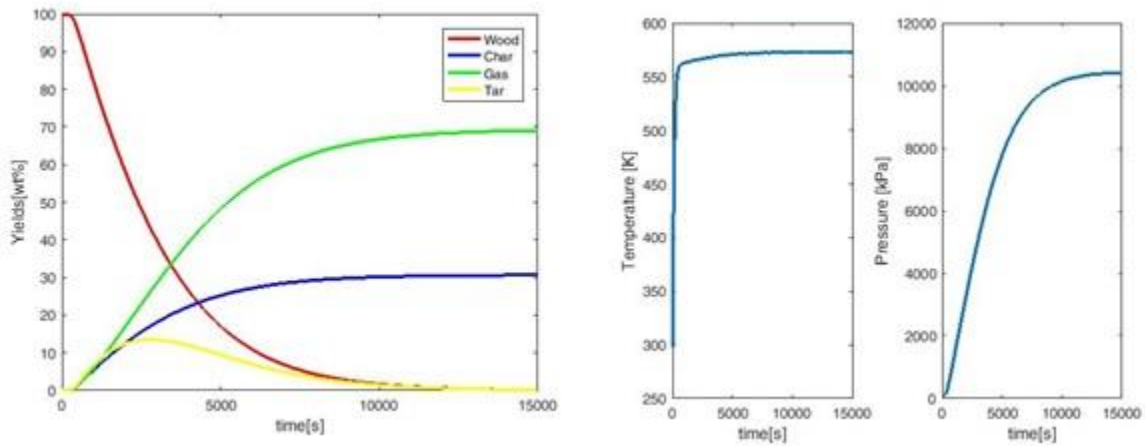


Figure P.1. History profiles of product yields (Left) and pressure and temperature (Right) predicted by CVC model 1 using a heat transfer coefficient of 10^{-3} kW/K. The rest of the model parameters are given in Table 7.2.

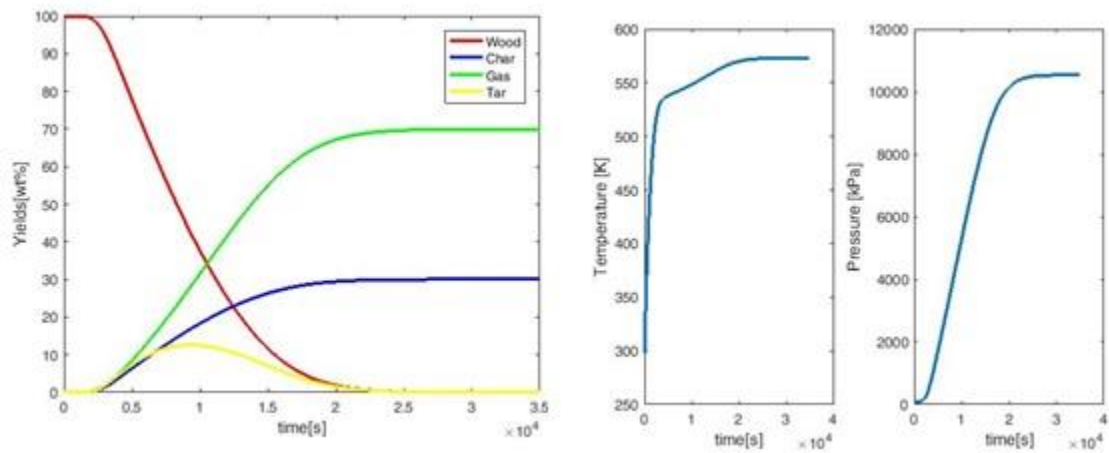


Figure P.2. History profiles of product yields (Left) and pressure and temperature (Right) predicted by CVC model 1 using a heat transfer coefficient of 10^{-4} kW/K. The rest of the model parameters are given in Table 7.2.

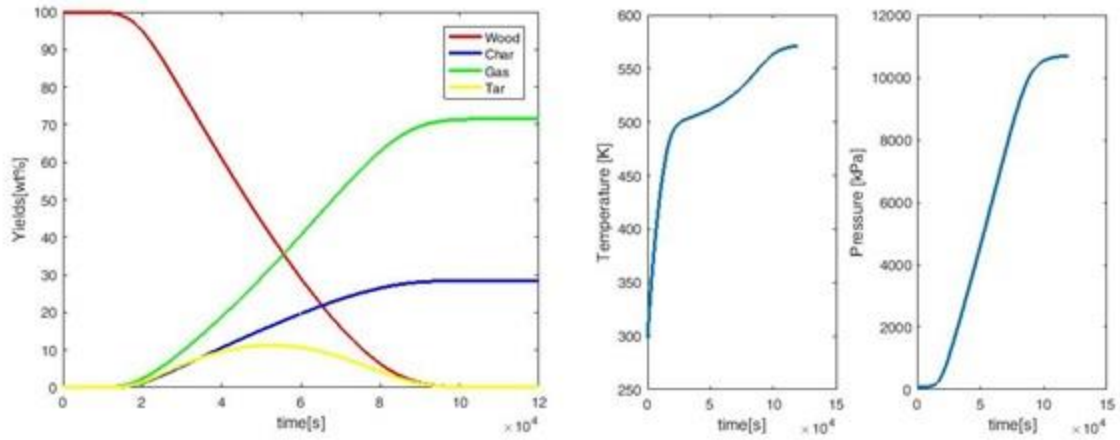


Figure P.3. History profiles of product yields (Left) and pressure and temperature (Right) predicted by CVC model 1 using a heat transfer coefficient of 10^{-5} kW/K. The rest of the model parameters are given in Table 7.2.

APPENDIX Q. MATLAB code CVC model 2

```
function main

t=0:1:15000; % s time scale
% initial conditions:
x1_o=10; %x1_o=Mw_o=10g
x2_o=0; %x2_o=Mc1_o=0g
x3_o=0; %x3_o=MG1_o=0g
x4_o=0; %x4_o=Mc2_o=0g
x5_o=0; %x5_o=MG2_o=0g
x6_o=298 ; %x6_o=T=25 degree C= 298K
x7_o=100; %x7_o=P=1 atm=100 kPaapprox.
[t,x]=ode45( @rhs, t, [x1_o x2_o x3_o x4_o x5_o x6_o x7_o] );
figure(1);
plot(t,x(:,1), 'r',t,x(:,2)+x(:,4), 'b',t,x(:,3)+x(:,5), 'g', 'linewidth',2);
xlabel('time[s]'); ylabel('Yields[wt%]');
legend('show') ;
legend('Wood','Char',' Volatiles')

figure(2);
subplot(1,2,1)
plot(t,x(:,6), 'linewidth',2);
xlabel('time[s]'); ylabel('Temperature [oC]');

subplot(1,2,2)
plot(t,x(:,7), 'linewidth',2)
xlabel('time[s]'); ylabel('Pressure [kPa]');

end

function dxdt=rhs(t,x)
%x1_o=Mw_o=10g
%x2_o=Mc1_o=0g
%x3_o=MG1_o=0g
%x4_o=Mc2_o=0g
%x5_o=MG2_o=0g
%x6_o=T=25 degree C= 298K
%x7_o=P=1 atm=100 kPaapprox.
%Kinetic data k1-k3
Mwo=10;
A1 = 9.973E-5;%s^(-1)
D1 = 17254.4; %K
L1 = -9061227;%K^2
A2 = 1.068E-3;%s^(-1)
D2 = 10224.4;%K
L2 = -6123081;%K^2
A3 = 5.7E5;%s^(-1)
E3 = 81; %kJ/mol
R=8.314E-3;%kJ/molK
```

```

k1=A1*exp(D1/x(6)+L1/x(6)^2);
k2=A2*exp(D2/x(6)+L2/x(6)^2);
k3=A3*exp(-E3/R/x(6));
Wg=200; %g/mol molecular weight volatiles
tw=0.0021; %m wall thickness 0.083 in in m
k_ss=0.019;%kW/mk thermal conductivity stainless steel at 225C
Rad=0.0127;%m reactor radius 1 in in m
L=0.1524; %m reactor length 6 in in m
A_ss=2*pi()*Rad*L; %m^2 Area reactor
V=pi()*Rad^2*L; %m^3 Volume reactor
Vwo=0.2*V; % InitialVolumesolid
cp1 = 1.5e-3 ;%kJ/gKcpw
cp2 = 1.5e-3 ;%kJ/gK cpc1
cp3 = 1.1E-3; %kJ/g K cpg1
cp4 = 1.5e-3 ;%kJ/gK cpc2
cp5=1.1E-3; %kJ/gK cpg2
Ts=573;%K Temperature sandbath
r1=k1*x(1)/V;
r2=k2*x(1)/V;
r3=k3*x(2)/V;

h1=0.418;%kJ/g
h2=0.418;%kJ/g
h3=-0.042;%kJ/g
delta=1.45;
dxdt_1 = -(k1+k2)*x(1);
dxdt_2 = k2*x(1) -k3*x(2);
dxdt_3 = k1*x(1) -k3*x(2);
dxdt_4 = delta*k3*x(2);
dxdt_5 = (2-delta)*k3*x(2);
denom=x(1)*cp1+x(2)*cp2+x(3)*cp3+x(4)*cp4+x(5)*cp5-
R*V*(x(3)+x(5))/Wg)/(V-Vwo*(x(1)+x(2)+x(4))/Mwo);
Qreac=V*(r1*(-h1)+r2*(-h2)+r3*(-h3));
Alpha=1/Wg*(dxdt_3+dxdt_5)/(V-
Vwo*(x(1)+x(2)+x(4))/Mwo)+((x(3)+x(5))/Wg*Vwo/Mwo*(dxdt_1+dxdt_2+dxdt_4))/(V-
Vwo*(x(1)+x(2)+x(4))/Mwo)^2;
Qcond=k_ss/tw*A_ss*(Ts-x(6));
dxdt_6=(Qcond+Qreac+V*R*x(6)*Alpha)/denom;
dxdt_7=(R*x(6)*(dxdt_3+dxdt_5)/Wg+R*dxdt_6*(x(3)+x(5))/Wg)/(V-
Vwo*(x(1)+x(2)+x(4))/Mwo)+((x(2)+x(5))/Wg*R*x(6)*Vwo/Mwo*(dxdt_1+dxdt_2+dxdt_
4))/(V-Vwo*(x(1)+x(2)+x(4))/Mwo)^2;
dxdt=[dxdt_1; dxdt_2; dxdt_3; dxdt_4; dxdt_5;dxdt_6;dxdt_7];
end

```

APPENDIX R. Temperature, pressure and product distribution history profiles at various heat transfer coefficients predicted by CVC model 2

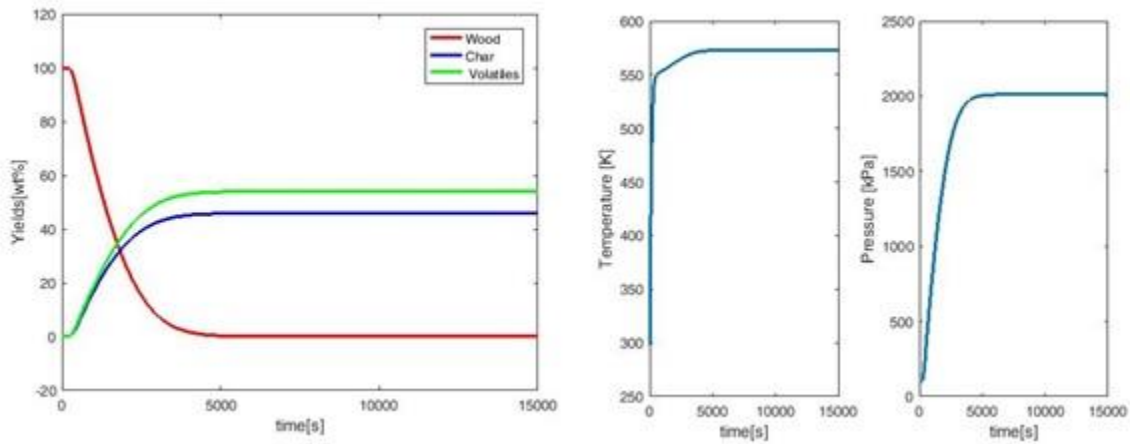


Figure R.1. History profiles of product yields (Left) and pressure and temperature (Right) predicted by CVC model 2 using a heat transfer coefficient of 10^{-3} kW/K. The rest of the model parameters are given in Table 7.4.

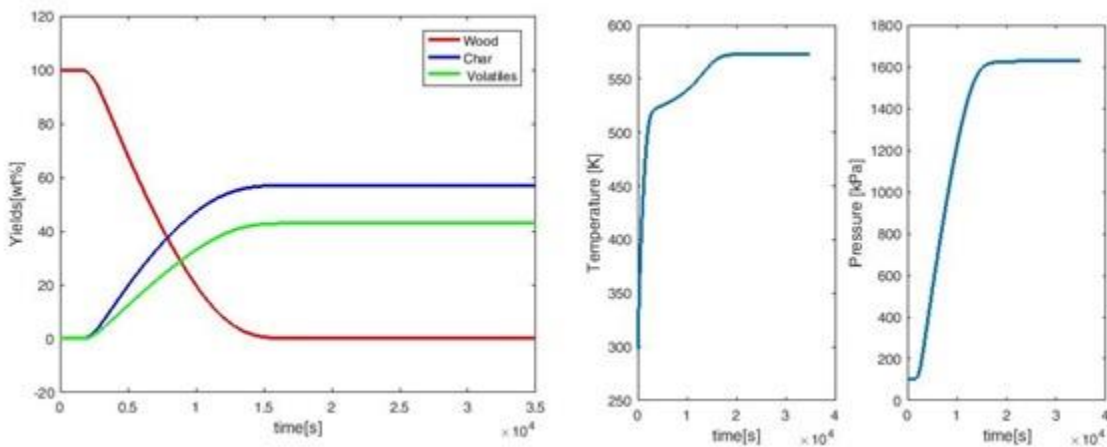


Figure R.2. History profiles of product yields (Left) and pressure and temperature (Right) predicted by CVC model 2 using a heat transfer coefficient of 10^{-4} kW/K. The rest of the model parameters are given in Table 7.4.

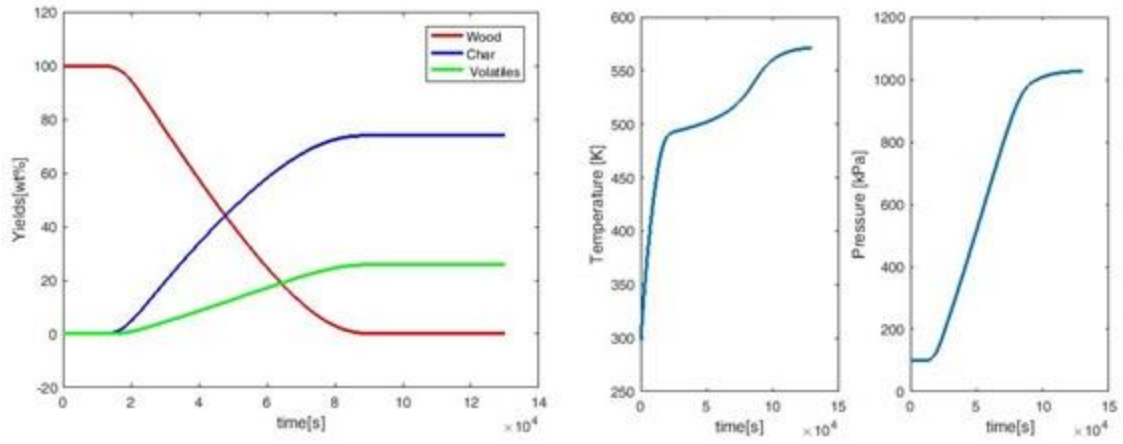


Figure R.3. History profiles of product yields (Left) and pressure and temperature (Right) predicted by CVC model 2 using a heat transfer coefficient of 10^{-5} kW/K. The rest of the model parameters are given in Table 7.4.

BIBLIOGRAPHY

- (1) Cama, T.; Henry, D. Trump: We Are Getting out of Paris Climate Deal | TheHill. June 1, 2017.
- (2) EC. Paris Agreement | Climate Action https://ec.europa.eu/clima/policies/international/negotiations/paris_en (accessed Mar 8, 2018).
- (3) Crooks, E. Business and World Leaders Criticise Trump's Paris Exit. *Financ. times* **2017**.
- (4) Zhang, H.-B.; Dai, H.-C.; Lai, H.-X.; Wang, W.-T. U.S. Withdrawal from the Paris Agreement: Reasons, Impacts, and China's Response. *Adv. Clim. Chang. Res.* **2017**, *8* (4), 220–225.
- (5) Bendix, A. The Global Reaction to Trump's Climate-Change Decision - The Atlantic. *Atl.* **2017**.
- (6) McBride, J. The Consequences of Leaving the Paris Agreement | Council on Foreign Relations <https://www.cfr.org/backgrounder/consequences-leaving-paris-agreement> (accessed Mar 8, 2018).
- (7) CNBC. Environmental groups react to Trump's decision to withdraw from Paris Agreement <https://www.cnbc.com/2017/06/02/environmental-groups-react-to-trumps-decision-to-withdraw-from-paris-agreement.html> (accessed Mar 8, 2018).
- (8) Trømborg, E.; Leistad, Ø. IEA Bioenergy Task 40 – Country Report 2009 for Norway. 2009.
- (9) Skreiberg, Ø. <https://www.sintef.no/projectweb/biocarb/a-potential-revolution-in-the-norwegian-bioenergy-future>.
- (10) <http://oilprice.com/Alternative-Energy/Biofuels/Waste-Wood-Norway-Taps-into-a-Huge-Source-of-Biomass-Fuel.html>. 2013.
- (11) Eikeland, J.; Monsen, B. E.; Modahl, I. S. Reducing CO₂ Emissions in Norwegian Ferroalloy Production in COM 2001. 2001.
- (12) BioCarb+ Research | Hawaii Natural Energy Institute <https://www.hnei.hawaii.edu/projects/biocarb-research> (accessed Jun 17, 2018).
- (13) EDMST; Carnegie Mellon University. History of the Energy System <http://environ.andrew.cmu.edu/m3/s3/01history.shtml#> (accessed Mar 9, 2018).
- (14) Walker, N. *Biomass: Fueling Change*; Crabtree Publishing Company, 2007.
- (15) Fuller, R. J.; Aye, L. Human and Animal Power – The Forgotten Renewables. *Renew. Energy* **2012**, *48* (Supplement C), 326–332.

- (16) Rodrigue, J. P.; Comtois, C.; Slack, B. *The Geography of Transport Systems*; Taylor & Francis, 2016.
- (17) Maschio, G.; Koufopoulos, C.; Lucchesi, A. Pyrolysis, a Promising Route for Biomass Utilization. *Bioresour. Technol.* **1992**, *42* (3), 219–231.
- (18) Demirbas, A.; Arin, G. An Overview of Biomass Pyrolysis. *Energy Sources* **2002**, *24* (5), 471–482.
- (19) Lohri, C. R.; Rajabu, H. M.; Sweeney, D. J.; Zurbrügg, C. Char Fuel Production in Developing Countries – A Review of Urban Biowaste Carbonization. *Renew. Sustain. energy Rev.* **2016**, *59*, 1514–1530.
- (20) Chhiti, Y.; Kemiha, M. Thermal Conversion of Biomass, Pyrolysis and Gasification. *Int. J. Eng. Sci.* **2013**, *2* (3), 75–85.
- (21) Antal *, M. J. J.; Mochidzuki, K.; Paredes, L. S. Flash Carbonization of Biomass. *Ind. Eng. Chem. Res.* **2003**, *42* (16), 3690–3699.
- (22) Nunoura, T.; Wade, S. R.; Bourke, J. P.; Antal, M. J. Studies of the Flash Carbonization Process. 1. Propagation of the Flaming Pyrolysis Reaction and Performance of a Catalytic Afterburner. *Ind. Eng. Chem. Res.* **2006**, *45* (2), 585–599.
- (23) Czernik, S. Fundamentals of Charcoal Production. In *IBI Conference on Biochar, Sustainability and Security.*; 2008.
- (24) Grønli, M. Pyrolysis and Charcoal. *Present. Biokarboniseringsseminarium* **2010**.
- (25) Williams, S.; Higashi, C.; Phothisantikul, P.; Wesenbeeck, S. Van; Jr, M. J. A. The Fundamentals of Biocarbon Formation at Elevated Pressure: From 1851 to the 21st Century. *J. Anal. Appl. Pyrolysis* **2014**, No. 0.
- (26) Wesenbeeck, S. Van; Higashi, C.; Legarra, M.; Wang, L.; Michael Jerry Antal, J. Biomass Pyrolysis in Sealed Vessels. Fixed-Carbon Yields from Avicel Cellulose That Realize the Theoretical Limit. *Energy & Fuels* **2016**, *30* (1), 480–491.
- (27) Legarra, M.; Morgan, T.; Turn, S. Q.; Wang, L.; Skreiberg, Ø.; Antal, M. J. Carbonization of Biomass in Constant-Volume Reactors. *Energy & Fuels* **2017**.
- (28) van der Stelt, M. J. C.; Gerhauser, H.; Kiel, J. H. A.; Ptasinski, K. J. Biomass Upgrading by Torrefaction for the Production of Biofuels: A Review. *Biomass and Bioenergy* **2011**, *35* (9), 3748–3762.
- (29) Shankar Tumuluru, J.; Sokhansanj, S.; Hess, J. R.; Wright, C. T.; Boardman, R. D. A Review on Biomass Torrefaction Process and Product Properties for Energy Applications. *Ind. Biotechnol.* **2011**, *7* (5), 384–401.
- (30) Peng, J. H.; Bi, H. T.; Sokhansanj, S.; Lim, J. C. A Study of Particle Size Effect on Biomass Torrefaction and Densification. *Energy & Fuels* **2012**, *26* (6), 3826–3839.
- (31) Hoekman, S. K.; Broch, A.; Robbins, C. Hydrothermal Carbonization (HTC) of

- Lignocellulosic Biomass. *Energy Fuels* **2011**, *25*, 1802–1810.
- (32) Libra, J.; Ro, K.; Kammann, C.; Funke, A.; Berge, N.; Neubauer, Y.; Titirici, M.-M.; Fühner, C.; Bens, O.; Kern, J.; et al. *Hydrothermal Carbonization of Biomass Residuals: A Comparative Review of the Chemistry, Processes and Applications of Wet and Dry Pyrolysis*; 2011; Vol. 2.
- (33) Kim, D.; Yoshikawa, K.; Park, K. Y. Characteristics of Biochar Obtained by Hydrothermal Carbonization of Cellulose for Renewable Energy. *Energies* **2015**, *8* (12), 12412.
- (34) Reza, M. T.; Becker, W.; Sachsenheimer, K.; Mumme, J. Hydrothermal Carbonization (HTC): Near Infrared Spectroscopy and Partial Least-Squares Regression for Determination of Selective Components in HTC Solid and Liquid Products Derived from Maize Silage. *Bioresour. Technol.* **2014**, *161*, 91–101.
- (35) Xu, Q.; Qian, Q.; Quek, A.; Ai, N.; Zeng, G.; Wang, J. Hydrothermal Carbonization of Macroalgae and the Effects of Experimental Parameters on the Properties of Hydrochars. *ACS Sustain. Chem. Eng.* **2013**, *1* (9), 1092–1101.
- (36) *Colophon Technology Watch*; Ravindranathan Thampi, K., Wubben, E., Nuhoff-Isakhanyan, G., Eds.; 2015.
- (37) Wannapeera, J.; Worasuwanarak, N. Upgrading of Woody Biomass by Torrefaction under Pressure. *J. Anal. Appl. Pyrolysis* **2012**, *96*, 173–180.
- (38) Chiamonti, D.; Prussi, M.; Nistri, R.; Pettorali, M.; Rizzo, A. M. Biomass Carbonization: Process Options and Economics for Small Scale Forestry Farms. *Energy Procedia* **2014**, *61*, 1515–1518.
- (39) Antal, M. J.; Grønli, M. The Art, Science, and Technology of Charcoal Production. *Ind. Eng. Chem. Res.* **2003**, *42* (8), 1619–1640.
- (40) Food of the United Nations. FAO Forestry Department, Agriculture Organization. Simple Technologies of Charcoal Making. *FAO For. Pap.* **41** **1987**.
- (41) Smith, K. R.; Pennise, D. M.; Khummongkol, P.; Chaiwong, V.; Ritgeen, K.; Zhang, J.; Panyathanya, W.; Rasmussen, R. A.; Khalil, M. A. K.; Thorneloe, S. A. Greenhouse Gases from Small-Scale Combustion Devices in Developing Countries. Phase III: Charcoal-Making Kilns in Thailand. *US Environ. Prot. Agency, Off. Res. Dev. Washingt. DC* **1999**.
- (42) Mok, W. S. L.; Antal, M. J.; Szabo, P.; Varhegyi, G.; Zelei, B. Formation of Charcoal from Biomass in a Sealed Reactor. *Ind. Eng. Chem. Res.* **1992**, *31* (4), 1162–1166.
- (43) Domac, J.; Trossero, M.; Siemons, R. *Industrial Charcoal Production: Water Management*. FAO, TCP: 3101; Rome, 2008.
- (44) Kempegowda, R. S.; Skreiberg, Ø.; Tran, K.-Q. Biocarbonization Process for High Quality Energy Carriers: Techno-Economics. *Energy Procedia* **2017**, *105*, 628–635.
- (45) Foley, G. *Charcoal Making in Developing Countries*; Earthscan, International Institute for

- Environment and Development, 1986.
- (46) *Industrial Charcoal Making*; Food Agriculture Organization of the United Nations, 1985.
 - (47) Krevelen, D. W.; Schuyer, J. *Coal Science Aspects of Coal Constitution*; Elsevier, 1957.
 - (48) Budai, A.; Zimmerman A R; Cowie A L; Webber J B; Singh B P; Glaser B; Masiello C A; Andersson D; Shields F; Lehmann J; et al. *Biochar Carbon Stability Test Method: An Assessment of Methods to Determine Biochar Carbon Stability | International Biochar Initiative*; 2013.
 - (49) Solomon, P. R. Relation between Coal Aromatic Carbon Concentration and Proximate Analysis Fixed Carbon. *Fuel* **1981**, *60* (1), 3–6.
 - (50) Tran, K.-Q.; Alonso, M. Z.; Wang, L.; Skreiberg, Ø. Simultaneously Boosting the Mass and Fixed-Carbon Yields of Charcoal from Forest Residue via Atmospheric Carbonization. *Energy Procedia* **2017**, *105*, 787–792.
 - (51) European Biochar Certificate - Guidelines for a Sustainable Production of Biochar. European Biochar Foundation (EBC). Arbaz, Switzerland 2016.
 - (52) Van Wesenbeeck, S.; Wang, L.; Ronsse, F.; Prins, W.; Skreiberg, Ø.; Antal, M. J. Charcoal “Mines” in the Norwegian Woods. *Energy & Fuels* **2016**, *30* (10), 7959–7970.
 - (53) Fuwape, J. A. Carbonization of Five Short Rotation Tropical Tree Species. *Dev. Thermochem. Biomass Convers.* **1997**, *1*.
 - (54) Violette, M. No Title. *Ann. Chim. Phys.* **1853**, *32*, 304.
 - (55) Varhegyi, G.; Jr., M. J. A.; Szekely, T.; Till, F.; Jakab, E.; Szabo, P. Simultaneous Thermogravimetric-Mass Spectrometric Studies of the Thermal Decomposition of Biopolymers. 2. Sugarcane Bagasse in the Presence and Absence of Catalysts. *Energy & Fuels* **1988**, *2* (3), 273–277.
 - (56) Wang, L.; Skreiberg, Ø.; Gronli, M.; Specht, G. P.; Antal Jr, M. J. Is Elevated Pressure Required to Achieve a High Fixed-Carbon Yield of Charcoal from Biomass? Part 2: The Importance of Particle Size. *Energy & Fuels* **2013**, *27* (4), 2146–2156.
 - (57) Antal, M. J.; Allen, S. G.; Dai, X.; Shimizu, B.; Tam, M. S.; Grønli, M. Attainment of the Theoretical Yield of Carbon from Biomass. *Ind. Eng. Chem. Res.* **2000**, *39* (11), 4024–4031.
 - (58) Van Wesenbeeck, S.; Higashi, C.; Legarra, M.; Wang, L.; Antal, M. J. Biomass Pyrolysis in Sealed Vessels. Fixed-Carbon Yields from Avicel Cellulose That Realize the Theoretical Limit. *Energy and Fuels* **2016**, *30* (1).
 - (59) Morgan, T. J.; Kandiyoti, R. Pyrolysis of Coals and Biomass: Analysis of Thermal Breakdown and Its Products. *Chem. Rev.* **2014**, *114* (3), 1547–1607.
 - (60) Stiles, H. N.; Kandiyoti, R. Secondary Reactions of Flash Pyrolysis Tars Measured in a Fluidized Bed Pyrolysis Reactor with Some Novel Design Features. *Fuel* **1989**, *68* (3), 275–

282.

- (61) Blasi, C. Di; Branca, C.; Masotta, F.; Biase, E. De. Experimental Analysis of Reaction Heat Effects during Beech Wood Pyrolysis. *Energy & Fuels* **2013**, *27* (5), 2665–2674.
- (62) Blasi, C. Di; Branca, C.; Sarnataro, F. E.; Gallo, A. Thermal Runaway in the Pyrolysis of Some Lignocellulosic Biomasses. *Energy & Fuels* **2014**, *28* (4), 2684–2696.
- (63) Mok, W. S.-L.; Antal, M. J. Effects of Pressure on Biomass Pyrolysis. II. Heats of Reaction of Cellulose Pyrolysis. *Thermochim. Acta* **1983**, *68* (2), 165–186.
- (64) Zaror, C. A.; Hutchings, I. S.; Pyle, D. L.; Stiles, H. N.; Kandiyoti, R. Secondary Char Formation in the Catalytic Pyrolysis of Biomass. *Fuel* **1985**, *64* (7), 990–994.
- (65) Palmer, R. C. Effect of Pressure on Yields of Products in the Destructive Distillation of Hardwood. *J. Ind. & Eng. Chem.* **1914**, *6* (11), 890–893.
- (66) Frolich, P. K.; Spalding, H. B.; Bacon, T. S. Destructive Distillation of Wood and Cellulose under Pressure. *Ind. Eng. Chem.* **1928**, *20* (1), 36–40.
- (67) Pindoria, R. V; Megaritis, A.; Messenböck, R. C.; Dugwell, D. R.; Kandiyoti, R. Comparison of the Pyrolysis and Gasification of Biomass: Effect of Reacting Gas Atmosphere and Pressure on Eucalyptus Wood. *Fuel* **1998**, *77* (11), 1247–1251.
- (68) Shafizadeh, F. Pyrolytic Reactions and Products of Biomass. In *Fundamentals of thermochemical biomass conversion*; Overend, R. P., Milne, T. A., Mudge, L. K., Eds.; Springer Netherlands: Dordrecht, 1985; pp 183–217.
- (69) Antal *, M. J. J.; Croiset, E.; Dai, X.; DeAlmeida, C.; Mok, W. S. L.; Norberg, N.; Richard, J.-R.; Majthoub, M. Al. High-Yield Biomass Charcoal. *Energy & Fuels* **1996**, *10* (3), 652–658.
- (70) Lédé, J.; Li, H. Z.; Villermaux, J.; Martin, H. Fusion-like Behaviour of Wood Pyrolysis. *J. Anal. Appl. Pyrolysis* **1987**, *10* (4), 291–308.
- (71) Lédé, J.; Blanchard, F.; Boutin, O. Radiant Flash Pyrolysis of Cellulose Pellets: Products and Mechanisms Involved in Transient and Steady State Conditions. *Fuel* **2002**, *81* (10), 1269–1279.
- (72) Dauenhauer, P. J.; Colby, J. L.; Balonek, C. M.; Suszynski, W. J.; Schmidt, L. D. Reactive Boiling of Cellulose for Integrated Catalysis through an Intermediate Liquid. *Green Chem.* **2009**, *11* (10), 1555–1561.
- (73) Mettler, M. S.; Vlachos, D. G.; Dauenhauer, P. J. Top Ten Fundamental Challenges of Biomass Pyrolysis for Biofuels. *Energy Environ. Sci.* **2012**, *5*, 7797–7809.
- (74) Cetin, E.; Gupta, R.; Moghtaderi, B. Effect of Pyrolysis Pressure and Heating Rate on Radiata Pine Char Structure and Apparent Gasification Reactivity. *Fuel* **2005**, *84* (10), 1328–1334.
- (75) Newalkar, G.; Iisa, K.; D’Amico, A. D.; Sievers, C.; Agrawal, P. Effect of Temperature, Pressure, and Residence Time on Pyrolysis of Pine in an Entrained Flow Reactor. *Energy &*

Fuels **2014**, 28 (8), 5144–5157.

- (76) Illerup, J. B.; Rathmann, O. CO₂ Gasification of Wheat Straw, Barley Straw, Willow and Giganteus. *Roskilde, Denmark Riso Natl. Lab.* **1996**.
- (77) Serio, M. A.; Solomon, P. R.; Heninger, S. G. Coal Pyrolysis in a High Pressure Entrained Flow Reactor. *Prepr. Pap., Am. Chem. Soc., Div. Fuel Chem.:(United States)* **1986**, 31 (CONF-8609181-).
- (78) Punsuwan, N.; Tangsathitkulchai, C. Product Characterization and Kinetics of Biomass Pyrolysis in a Three-Zone Free-Fall Reactor. *Int. J. Chem. Eng.* **2014**, 2014.
- (79) Diebold, J. Workshop Summary. In *Specialists' workshop on fast pyrolysis of biomass proceedings*; Copper Mountain, Colorado, 1980; pp 3–6.
- (80) Kosstrin, H. M. Direct Formation of Pyrolysis Oil from Biomass. In *Specialists' workshop on fast pyrolysis of biomass proceedings*; Copper Mountain, Colorado, 1980; pp 105–121.
- (81) Morgan, T. J.; Turn, S. Q.; George, A. Fast Pyrolysis Behavior of Banagrass as a Function of Temperature and Volatiles Residence Time in a Fluidized Bed Reactor. *PLoS One* **2015**.
- (82) Morgan, T. J.; Turn, S. Q.; Sun, N.; George, A. Fast Pyrolysis of Tropical Biomass Species and Influence of Water Pretreatment on Product Distributions. *PLoS One* **2016**, 11 (3), 1–27.
- (83) Li, C.; Suzuki, K. Tar Property, Analysis, Reforming Mechanism and Model for Biomass Gasification—An Overview. *Renew. Sustain. energy Rev.* **2009**, 13 (3), 594–604.
- (84) Herod, A. A.; Bartle, K. D.; Morgan, T. J.; Kandiyoti, R. Analytical Methods for Characterizing High-Mass Complex Polydisperse Hydrocarbon Mixtures: An Overview. *Chem. Rev.* **2012**, 112 (7), 3892–3923.
- (85) Scott, D. S.; Legge, R. L.; Piskorz, J.; Majerski, P.; Radlein, D. Fast Pyrolysis of Biomass for Recovery of Specialty Chemicals. In *Developments in Thermochemical Biomass Conversion*; Springer, 1997; pp 523–535.
- (86) Lede, J.; Diebold, J. P.; Peacocke, G. V. C.; Piskorz, J. The Nature and Properties of Intermediate and Unvaporized Biomass Pyrolysis Materials. *Dev. Thermochem. Biomass Convers.* **1997**, 27–42.
- (87) Peacocke, G. V. C. Ablative Pyrolysis of Biomass. PhD Thesis, The University of Aston in Birmingham (UK), 1994.
- (88) Piskorz, J.; Scott, D. S.; Radlein, D. Mechanisms on the Fast Pyrolysis of Biomass—Comments on Some Sources of Confusion. In *Frontiers of Pyrolysis: Biomass Conversion and Polymer Recycling*; Breckenridge, USA, 1995.
- (89) Jarvis, M. W.; Haas, T. J.; Donohoe, B. S.; Daily, J. W.; Gaston, K. R.; Frederick, W. J.; Nimlos, M. R. Elucidation of Biomass Pyrolysis Products Using a Laminar Entrained Flow Reactor and Char Particle Imaging. *Energy & Fuels* **2010**, 25 (1), 324–336.

- (90) Gonenc, Z. S.; Gibbins, J. R.; Katheklakis, I. E.; Kandiyoti, R. Comparison of Coal Pyrolysis Product Distributions from Three Captive Sample Techniques. *Fuel* **1990**, *69* (3), 383–390.
- (91) Biagini, E.; Simone, M.; Tognotti, L. Characterization of High Heating Rate Chars of Biomass Fuels. *Proc. Combust. Inst.* **2009**, *32* (2), 2043–2050.
- (92) Pastor-Villegas, J.; Durán-Valle, C. J.; Valenzuela-Calahorro, C.; Gómez-Serrano, V. Organic Chemical Structure and Structural Shrinkage of Chars Prepared from Rockrose. *Carbon N. Y.* **1998**, *36* (9), 1251–1256.
- (93) Fraga-Araujo, A. R. Pyrolytic Decomposition of Lignocellulosic Materials. PhD Thesis, Imperial College of Science, Technology and Medicine, London, 1990.
- (94) Martin, C. E.; Purdy, K. R.; Dubayeh, S. A.; Kerr, C. P.; Garr, T. D. The Effect of Carbonization Heating Rate on Charcoal and Active Carbon Yields. *Appl. Biochem. Biotechnol.* **1991**, *28* (1), 21–32.
- (95) Angin, D. Effect of Pyrolysis Temperature and Heating Rate on Biochar Obtained from Pyrolysis of Safflower Seed Press Cake. *Bioresour. Technol.* **2013**, *128*, 593–597.
- (96) Chen, D.; Zhou, J.; Zhang, Q. Effects of Heating Rate on Slow Pyrolysis Behavior, Kinetic Parameters and Products Properties of Moso Bamboo. *Bioresour. Technol.* **2014**.
- (97) Chan, W. C. R.; Kelbon, M.; Krieger-Brockett, B. Single-Particle Biomass Pyrolysis: Correlations of Reaction Products with Process Conditions. *Ind. Eng. Chem. Res.* **1988**, *27* (12), 2261–2275.
- (98) Antal, M. J. J.; Mok, W. S. L.; Varhegyi, G.; Szekely, T. Review of Methods for Improving the Yield of Charcoal from Biomass. *Energy & Fuels* **1990**, *4* (3), 221–225.
- (99) Pindoria, R. V.; Megaritis, A.; Messenbock, R. C.; Dugwell, D. R.; Kandiyoti, R. Comparison of the Pyrolysis and Gasification of Biomass: Effect of Reacting Gas Atmosphere and Pressure on Eucalyptus Wood. *Fuel* **1998**, *77*, 1247–1251.
- (100) Shafizadeh, F. Utilization of Biomass by Pyrolytic Methods. *TAPPI For. Biol./Wood Chem. Conf., Madison* **1977**.
- (101) Reed, T. B.; Diebold, J. P.; Desrosiers, R. Perspectives in Heat Transfer Requirements and Mechanisms for Fast Pyrolysis. *Spec. Work. fast pyrolysis biomass Proc.* **1980**.
- (102) Lewellen W. A. Howard J. B., P. C. P. Cellulose Pyrolysis Kinetics and Char Formation Mechanism. *Fire Explos. 16th Symp. Combust. Combust. Inst.* **1976**, 1471–1480.
- (103) Bradbury, A. G. W.; Sakai, Y.; Shafizadeh, F. A Kinetic Model for Pyrolysis of Cellulose. *J. Appl. Polym. Sci.* **1979**, *23* (11), 3271–3280.
- (104) Zanzi, R.; Sjöström, K.; Björnbom, E. Rapid High-Temperature Pyrolysis of Biomass in a Free-Fall Reactor. *Fuel* **1996**, *75* (5), 545–550.
- (105) Biagini, E.; Tognotti, L. Characterization of Biomass Chars: Reactivity and Morphology of Chars Obtained in Different Conditions. *Int. J. Energy a Clean Environ.* **2005**, *6* (4).

- (106) Stubington, J. F.; Sumaryono. Release of Volatiles from Large Coal Particles in a Hot Fluidized Bed. *Fuel* **1984**, *63* (7), 1013–1019.
- (107) Suuberg, E. M. Rapid Pyrolysis and Hydropyrolysis of Coal. PhD Thesis, Massachusetts Institute of Technology (MIT): Boston, MA, 1977.
- (108) Kandiyoti, R.; Herod, A.; Bartle, K. D.; Morgan, T. J. *Solid Fuels and Heavy Hydrocarbon Liquids: Thermal Characterization and Analysis*; Elsevier Science, 2016.
- (109) Gonenc, S.; Sunol, A. K. Pyrolysis of Coal. In *Coal: Resources, Properties, Utilization, Pollution*; Kural, O., Ofset, O., Eds.; Istanbul, 1994.
- (110) Di Blasi, C. Kinetic and Heat Transfer Control in the Slow and Flash Pyrolysis of Solids. *Ind. Eng. Chem. Res.* **1996**, *35* (1), 37–46.
- (111) Demirbas, A. Effects of Temperature and Particle Size on Bio-Char Yield from Pyrolysis of Agricultural Residues. *J. Anal. Appl. Pyrolysis* **2004**, *72* (2), 243–248.
- (112) Beaumont, O.; Schwob, Y. Influence of Physical and Chemical Parameters on Wood Pyrolysis. *Ind. Eng. Chem. Process Des. Dev.* **1984**, *23* (4), 637–641.
- (113) Gábor Várhegyi, *; Szabó, P.; Till, F.; Zelei, B.; Michael Jerry Antal, J.; Dai, X. TG, TG-MS, and FTIR Characterization of High-Yield Biomass Charcoals. *Energy & Fuels* **1998**, *12* (5), 969–974.
- (114) Bennadji, H.; Smith, K.; Serapiglia, M. J.; Fisher, E. M. Effect of Particle Size on Low-Temperature Pyrolysis of Woody Biomass. *Energy & Fuels* **2014**, *28* (12), 7527–7537.
- (115) Machado, J. G. M. da S.; Osório, E.; Vilela, A. C. F. Reactivity of Brazilian Coal, Charcoal, Imported Coal and Blends Aiming to Their Injection into Blast Furnaces. *Mater. Res.* **2010**, *13*, 287–292.
- (116) Várhegyi, G.; Szabó, P.; Mok, W. S.-L.; Antal, M. J. Kinetics of the Thermal Decomposition of Cellulose in Sealed Vessels at Elevated Pressures. Effects of the Presence of Water on the Reaction Mechanism. *J. Anal. Appl. Pyrolysis* **1993**, *26* (3), 159–174.
- (117) Wang, L.; Skreiberg, Ø.; Van Wesenbeeck, S.; Grønli, M.; Antal, M. J. Experimental Study on Charcoal Production from Woody Biomass. *Energy & Fuels* **2016**, *30* (10), 7994–8008.
- (118) Bai, X.; Xue, Y. Transport and Secondary Reactions of Depolymerized/Deconstructed Species. In *Fast Pyrolysis of Biomass – Advances in Science and Technology # 8538*; Brown, R. C., Wang, K., Eds.; 2017; pp 57–78.
- (119) Krumm, C.; Pfaendtner, J.; Dauenhauer, P. J. Millisecond Pulsed Films Unify the Mechanisms of Cellulose Fragmentation. *Chem. Mater.* **2016**, *28* (9), 3108–3114.
- (120) Bai, X.; Johnston, P.; Sadula, S.; Brown, R. C. Role of Levoglucosan Physicochemistry in Cellulose Pyrolysis. *J. Anal. Appl. Pyrolysis* **2013**, *99*, 58–65.
- (121) Bai, X.; Johnston, P.; Brown, R. C. An Experimental Study of the Competing Processes of Evaporation and Polymerization of Levoglucosan in Cellulose Pyrolysis. *J. Anal. Appl.*

- Pyrolysis* **2013**, *99*, 130–136.
- (122) Hosoya, T.; Kawamoto, H.; Saka, S. Different Pyrolytic Pathways of Levoglucosan in Vapor- and Liquid/Solid-Phases. *J. Anal. Appl. Pyrolysis* **2008**, *83* (1), 64–70.
- (123) Ningbo, G.; Baoling, L.; Aimin, L.; Juanjuan, L. Continuous Pyrolysis of Pine Sawdust at Different Pyrolysis Temperatures and Solid Residence Times. *J. Anal. Appl. Pyrolysis* **2015**, *114*, 155–162.
- (124) Mohamed, A. R.; Hamzah, Z.; Daud, M. Z. M.; Zakaria, Z. The Effects of Holding Time and the Sweeping Nitrogen Gas Flowrates on the Pyrolysis of EFB Using a Fixed-Bed Reactor. *Procedia Eng.* **2013**, *53*, 185–191.
- (125) Mayor, J. R.; Williams, A. Residence Time Influence on the Fast Pyrolysis of Loblolly Pine Biomass. *J. Energy Resour. Technol.* **2010**, *132* (4), 041801.
- (126) Wang, Y.; Hu, Y.; Zhao, X.; Wang, S.; Xing, G. Comparisons of Biochar Properties from Wood Material and Crop Residues at Different Temperatures and Residence Times. *Energy & Fuels* **2013**, *27* (10), 5890–5899.
- (127) Ling, C. K.; Kyin, E. H.; Hua, L. S.; Chen, L. W.; Yee, C. Y. Yield and Calorific Value of Bio Oil Pyrolysed from Oil Palm Biomass and Its Relation with Solid Residence Time and Process Temperature. *Asian J. Sci. Res.* **2015**, *8* (3), 351–358.
- (128) Lin, Y.; Yan, W.; Sheng, K. Effect of Pyrolysis Conditions on the Characteristics of Biochar Produced from a Tobacco Stem. *Waste Manag. Res.* **2016**, *34* (8), 793–801.
- (129) Ronsse, F.; van Hecke, S.; Dickinson, D.; Prins, W. Production and Characterization of Slow Pyrolysis Biochar: Influence of Feedstock Type and Pyrolysis Conditions. *GCB Bioenergy* **2013**, *5* (2), 104–115.
- (130) McKendry, P. Energy Production from Biomass (Part 1): Overview of Biomass. *Bioresour. Technol.* **2002**, *83* (1), 37–46.
- (131) Bajpai, P. Structure of Lignocellulosic Biomass. In *Pretreatment of Lignocellulosic Biomass for Biofuel Production*; 2016; pp 7–12.
- (132) Stefanidis, S. D.; Kalogiannis, K. G.; Iliopoulou, E. F.; Michailof, C. M.; Pilavachi, P. A.; Lappas, A. A. A Study of Lignocellulosic Biomass Pyrolysis via the Pyrolysis of Cellulose, Hemicellulose and Lignin. *J. Anal. Appl. Pyrolysis* **2014**, *105*, 143–150.
- (133) Yang, H.; Yan, R.; Chen, H.; Zheng, C.; Lee, D. H.; Liang, D. T. In-Depth Investigation of Biomass Pyrolysis Based on Three Major Components: Hemicellulose, Cellulose and Lignin. *Energy Fuels* **2006**, *20* (1), 388–393.
- (134) Raveendran, K.; Ganesh, A.; Khilar, K. C. Pyrolysis Characteristics of Biomass and Biomass Components. *Fuel* **1996**, *75* (8), 987–998.
- (135) Ounas, A.; Aboulkas, A.; El harfi, K.; Bacaoui, A.; Yaacoubi, A. Pyrolysis of Olive Residue and Sugar Cane Bagasse: Non-Isothermal Thermogravimetric Kinetic Analysis. *Bioresour.*

- Technol.* **2011**, *102* (24), 11234–11238.
- (136) Stenseng, M.; Jensen, A.; Dam-Johansen, K. Investigation of Biomass Pyrolysis by Thermogravimetric Analysis and Differential Scanning Calorimetry. *J. Anal. Appl. Pyrolysis* **2001**, *58–59*, 765–780.
- (137) Rao, T. R.; Sharma, A. Pyrolysis Rates of Biomass Materials. *Energy* **1998**, *23* (11), 973–978.
- (138) Manyà, J. J.; Velo, E.; Puigjaner, L. Kinetics of Biomass Pyrolysis: A Reformulated Three-Parallel-Reactions Model. *Ind. Eng. Chem. Res.* **2003**, *42* (3), 434–441.
- (139) Orfão, J. J. M.; Antunes, F. J. A.; Figueiredo, J. L. Pyrolysis Kinetics of Lignocellulosic Materials—three Independent Reactions Model. *Fuel* **1999**, *78* (3), 349–358.
- (140) Koufopoulos, C. A.; Lucchesi, A.; Maschio, G. Kinetic Modelling of the Pyrolysis of Biomass and Biomass Components. *Can. J. Chem. Eng.* **1989**, *67* (1), 75–84.
- (141) Miller, R. S.; Bellan, J. A Generalized Biomass Pyrolysis Model Based on Superimposed Cellulose, Hemicellulose and Lignin Kinetics. *Combust. Sci. Technol.* **1997**, *126* (1–6), 97–137.
- (142) Antal, M. J. . In *Advances in Solar Energy Vol. 2*; Boer, K. W., Duffie, J. A., Eds.; American Solar Energy Society: New York, 1983; pp 175–239.
- (143) Worasuwannarak, N.; Sonobe, T.; Tanthapanichakoon, W. Pyrolysis Behaviors of Rice Straw, Rice Husk, and Corncob by TG-MS Technique. *J. Anal. Appl. Pyrolysis* **2007**, *78* (2), 265–271.
- (144) Wang, G.; Li, W.; Li, B.; Chen, H. TG Study on Pyrolysis of Biomass and Its Three Components under Syngas. *Fuel* **2008**, *87* (4–5), 552–558.
- (145) Hosoya, T.; Kawamoto, H.; Saka, S. Pyrolysis Behaviors of Wood and Its Constituent Polymers at Gasification Temperature. *J. Anal. Appl. Pyrolysis* **2007**, *78* (2), 328–336.
- (146) Hosoya, T.; Kawamoto, H.; Saka, S. Influence of Inorganic Matter on Wood Pyrolysis at Gasification Temperature. *J. Wood Sci.* **2007**, *53* (4), 351–357.
- (147) Wang, S.; Guo, X.; Wang, K.; Luo, Z. Influence of the Interaction of Components on the Pyrolysis Behavior of Biomass. *J. Anal. Appl. Pyrolysis* **2011**, *91* (1), 183–189.
- (148) Mackay, D. M.; Roberts, P. V. The Dependence of Char and Carbon Yield on Lignocellulosic Precursor Composition. *Carbon N. Y.* **1982**, *20* (2), 87–94.
- (149) Akhtar, J.; Saidina Amin, N. A Review on Operating Parameters for Optimum Liquid Oil Yield in Biomass Pyrolysis. *Renew. Sustain. Energy Rev.* **2012**, *16* (7), 5101–5109.
- (150) Shafizadeh, F.; DeGroot, W. F. Thermal Analysis of Forest Fuels. In *Fuels and energy from renewable resources*; Tillman, D. A., Sarkanen, K. V, Anderson, L. L., Eds.; Academic Press: New York, 1977; pp 95–114.

- (151) Jin, W.; Singh, K.; Zondlo, J. Pyrolysis Kinetics of Physical Components of Wood and Wood-Polymers Using Isoconversion Method. *Agriculture* **2013**, *3* (1), 12–32.
- (152) Haykiri-Acma, H.; Yaman, S. Thermogravimetric Investigation on the Thermal Reactivity of Biomass During Slow Pyrolysis. *Int. J. Green Energy* **2009**, *6* (4), 333–342.
- (153) Biagini, E.; Tognotti, L. Characterization of Biomass Chars. In *Proceedings of the seventh international conference on energy for clean environment*; Lisbon, Portugal, 2003.
- (154) Antal, M. J.; Mok, W. S. L.; Varhegyi, G.; Szekeley, T. Review of Methods for Improving the Yield of Charcoal from Biomass. *Energy & Fuels* **1990**, *4* (3), 221–225.
- (155) Sonobe, T.; Worasuwannarak, N. Kinetic Analyses of Biomass Pyrolysis Using the Distributed Activation Energy Model. *Fuel* **2008**, *87* (3), 414–421.
- (156) Tumuluru, J.; Sokhansanj, S.; Wright, C.; Boardman, R. A Review on Biomass Classification and Composition, Co-Firing Issues and Pretreatment Methods. ASABE American Society of Agricultural and Biological Engineers Annual International Meeting: Louisville, Kentucky, 2011.
- (157) Raveendran, K.; Ganesh, A.; Khilar, K. C. Influence of Mineral Matter on Biomass Pyrolysis Characteristics. *Fuel* **1995**, *74* (12), 1812–1822.
- (158) Tang, W. K.; Eickner, H. W. Effect of Inorganic Salts on Pyrolysis of Wood, Cellulose and Lignin Determined by Differential Thermal Analysis. 1968.
- (159) Encinar, J. M.; Beltrán, F. J.; Ramiro, A.; González, J. F. Catalyzed Pyrolysis of Grape and Olive Bagasse. Influence of Catalyst Type and Chemical Treatment. *Ind. Eng. Chem. Res.* **1997**, *36* (10), 4176–4183.
- (160) Nik-Azar, M.; Hajaligol, M. R.; Sohrabi, M.; Dabir, B. Mineral Matter Effects in Rapid Pyrolysis of Beech Wood. *Fuel Process. Technol.* **1997**, *51* (1–2), 7–17.
- (161) Qiu, H.-X.; Richards, G. N. Attempted Removal of Metal Ions and Subsequent Vacuum Pyrolysis of Barks from Five Species of Softwoods. *J. Wood Chem. Technol.* **1989**, *9* (2), 251–263.
- (162) Shafizadeh, F.; Furneaux, R. H.; Cochran, T. G.; Scholl, J. P.; Sakai, Y. Production of Levoglucosan and Glucose from Pyrolysis of Cellulosic Materials. *J. Appl. Polym. Sci.* **1979**, *23* (12), 3525–3539.
- (163) Shafizadeh, F.; Chin, P. S. Thermal Deterioration of Wood. In *Wood Technology: Chemical Aspects. Vol. 43*; 1977; pp 57–81.
- (164) Fang, P.; McGinnis, G. D. Flash Pyrolysis of Hollocellulose from Loblolly Pine Bark. In *Thermal uses and properties of carbohydrates and lignins*; Shafizadeh, F., Sarkanen, K. V., Tillman, D. A., Eds.; Academic Press, 1976; pp 37–47.
- (165) Pan, W.-P.; Richards, G. N. Influence of Metal Ions on Volatile Products of Pyrolysis of Wood. *J. Anal. Appl. Pyrolysis* **1989**, *16* (2), 117–126.

- (166) Gray, M. R.; Corcoran, W. H.; Gavalas, G. R. Pyrolysis of a Wood-Derived Material. Effects of Moisture and Ash Content. *Ind. Eng. Chem. Process Des. Dev.* **1985**, *24* (3), 646–651.
- (167) Richards, G. N.; Zheng, G. Influence of Metal Ions and of Salts on Products from Pyrolysis of Wood: Applications to Thermochemical Processing of Newsprint and Biomass. *J. Anal. Appl. Pyrolysis* **1991**, *21* (1–2), 133–146.
- (168) Nassar, M. M.; Bilgesu, A.; MacKay, G. D. M. Effect of Inorganic Salts on Product Composition during Pyrolysis of Black Spruce. *Wood fiber Sci.* **2007**, *18* (1), 3–10.
- (169) Pütün, E. Catalytic Pyrolysis of Biomass: Effects of Pyrolysis Temperature, Sweeping Gas Flow Rate and MgO Catalyst. *Energy* **2010**, *35* (7), 2761–2766.
- (170) Zhou, L.; Yang, H.; Wu, H.; Wang, M.; Cheng, D. Catalytic Pyrolysis of Rice Husk by Mixing with Zinc Oxide: Characterization of Bio-Oil and Its Rheological Behavior. *Fuel Process. Technol.* **2013**, *106*, 385–391.
- (171) Kabakçı, S. B.; Hacibektaşoğlu, Ş. Catalytic Pyrolysis of Biomass. In *Pyrolysis*; Mohamed Samer, Ed.; InTech, 2017.
- (172) Zabeti, M.; Nguyen, T. S.; Lefferts, L.; Heeres, H. J. In Situ Catalytic Pyrolysis of Lignocellulose Using Alkali-Modified Amorphous Silica Alumina. *Bioresour. Technol.* **2012**, *118*, 374–381.
- (173) Mihalcik, D. J.; Mullen, C. A.; Boateng, A. A. Screening Acidic Zeolites for Catalytic Fast Pyrolysis of Biomass and Its Components. *J. Anal. Appl. Pyrolysis* **2011**, *92* (1), 224–232.
- (174) Iisa, K.; Stanton, A. R.; Czernik, S. *Production of Hydrocarbon Fuels from Biomass by Catalytic Fast Pyrolysis*; Golden, CO, 2012.
- (175) Zhang, H.; Xiao, R.; Jin, B.; Shen, D.; Chen, R.; Xiao, G. Catalytic Fast Pyrolysis of Straw Biomass in an Internally Interconnected Fluidized Bed to Produce Aromatics and Olefins: Effect of Different Catalysts. *Bioresour. Technol.* **2013**, *137*, 82–87.
- (176) Huang, W.; Gong, F.; Fan, M.; Zhai, Q.; Hong, C.; Li, Q. Production of Light Olefins by Catalytic Conversion of Lignocellulosic Biomass with HZSM-5 Zeolite Impregnated with 6 Wt.% Lanthanum. *Bioresour. Technol.* **2012**, *121*, 248–255.
- (177) Galgano, A.; Blasi*, C. Di. Modeling Wood Degradation by the Unreacted-Core-Shrinking Approximation. *Ind. Eng. Chem. Res.* **2003**, *42* (10), 2101–2111.
- (178) Koufopoulos, C. A.; Papayannakos, N.; Maschio, G.; Lucchesi, A. Modelling of the Pyrolysis of Biomass Particles. Studies on Kinetics, Thermal and Heat Transfer Effects. *Can. J. Chem. Eng.* **1991**, *69* (4), 907–915.
- (179) Blasi, C. Di. Heat, Momentum and Mass Transport through a Shrinking Biomass Particle Exposed to Thermal Radiation. *Chem. Eng. Sci.* **1996**, *51* (7), 1121–1132.
- (180) Hagge, M. J.; Bryden, K. M. Modeling the Impact of Shrinkage on the Pyrolysis of Dry Biomass. *Chem. Eng. Sci.* **2002**, *57* (14), 2811–2823.

- (181) Lu, H.; Ip, E.; Scott, J.; Foster, P.; Vickers, M.; Baxter, L. L. Effects of Particle Shape and Size on Devolatilization of Biomass Particle. *Fuel* **2010**, *89* (5), 1156–1168.
- (182) Chan, W.-C. R.; Kelbon, M.; Krieger, B. B. Modelling and Experimental Verification of Physical and Chemical Processes during Pyrolysis of a Large Biomass Particle. *Fuel* **1985**, *64* (11), 1505–1513.
- (183) Babu, B. V.; Chaurasia, A. S. Heat Transfer and Kinetics in the Pyrolysis of Shrinking Biomass Particle. *Chem. Eng. Sci.* **2004**, *59* (10), 1999–2012.
- (184) Di Blasi, C. Modeling and Simulation of Combustion Processes of Charring and Non-Charring Solid Fuels. *Prog. Energy Combust. Sci.* **1993**, *19* (1), 71–104.
- (185) Haseli, Y. Modeling Combustion of Single Biomass Particle, Eindhoven University, 2012.
- (186) Babu, B. V. Biomass Pyrolysis: A State-of-the-Art Review. *Biofuels, Bioprod. Biorefining* **2008**.
- (187) Hawley, L. F. Wood Distillation. *Chem. Cat. Co. New York* **1923**.
- (188) Grønli*, M. G.; Melaaen, M. C. Mathematical Model for Wood Pyrolysis Comparison of Experimental Measurements with Model Predictions. *Energy & Fuels* **2000**, *14* (4), 791–800.
- (189) Chorley, J.; Ramsay, W. On the Destructive Distillation of Wood. *J. Soc. Chem. Ind.* **1892**, *11*, 395–403, 872–874.
- (190) Klason, P.; Heidenstam, G.; Norlin, E. Untersuchungen Zur Holzverkohlung. I. Die Trockene Destillation Der Cellulose. *Z. Angew. Chem.* **1909**, *25*, 1205.
- (191) Klason, P.; Heidenstam, G. V; Norlin, E. Teoretiska Undersokningar Rorande Kolning Af Ved. I. Om Torrdestillation of Cellulosa. *Ark. Kemi, Miner. Geol.* **1908**, *3*.
- (192) Klason, P.; Heidenstam, G. V; Norlin, E. No Title. *Ark. kemi Min. och Geol.* **1910**, *27*, 1252.
- (193) Milosavljevic, I.; Oja, V.; Suuberg, E. M. Thermal Effects in Cellulose Pyrolysis: Relationship to Char Formation Processes. *Ind. Eng. Chem. Res.* **1996**, *35* (3), 653–662.
- (194) Arseneau, D. F. Competitive Reactions in the Thermal Decomposition of Cellulose. *Can. J. Chem.* **1971**, *49* (4), 632–638.
- (195) Rath, J.; Wolfinger, M. G.; Steiner, G.; Krammer, G.; Barontini, F.; Cozzani, V. Heat of Wood Pyrolysis. *Fuel* **2003**, *82* (1), 81–91.
- (196) Roberts, A. F. The Heat of Reaction during the Pyrolysis of Wood. *Combust. Flame* **1971**, *17* (1), 79–86.
- (197) Ramiah, M. V. Thermogravimetric and Differential Thermal Analysis of Cellulose, Hemicellulose, and Lignin. *J. Appl. Polym. Sci.* **1970**, *14* (5), 1323–1337.
- (198) Alves, S. S.; Figueiredo, J. L. Pyrolysis Kinetics of Lignocellulosic Materials by Multistage

- Isothermal Thermogravimetry. *J. Anal. Appl. Pyrolysis* **1988**, *13* (1), 123–134.
- (199) Kilzer, F. J.; Broido, A. Speculations on the Nature of Cellulose Pyrolysis. **1965**.
- (200) ASTM E872 - 82(2013), Standard Test Method for Volatile Matter in the Analysis of Particulate Wood Fuels. 2013.
- (201) ASTM E830-87(1996), Standard Test Method for Ash in the Analysis Sample of Refuse-Derived Fuel . ASTM International: West Conshohocken, PA 1996.
- (202) ASTM E777-17, Standard Test Method for Carbon and Hydrogen in the Analysis Sample of Refuse-Derived Fuel. ASTM International: West Conshohocken, PA, 2017 2017.
- (203) ASTM E775-15, Standard Test Methods for Total Sulfur in the Analysis Sample of Refuse-Derived Fuel. ASTM International: West Conshohocken, PA 2015.
- (204) ASTM E778-15, Standard Test Methods for Nitrogen in Refuse-Derived Fuel Analysis Samples. ASTM International: West Conshohocken, PA 2015.
- (205) ASTM E871-82(2013), Standard Test Method for Moisture Analysis of Particulate Wood Fuels. 2013.
- (206) Vassilev, S. V.; Baxter, D.; Andersen, L. K.; Vassileva, C. G.; Morgan, T. J. An Overview of the Organic and Inorganic Phase Composition of Biomass. *Fuel* **2012**, *94*, 1–33.
- (207) ASTM D1576-13, Standard Test Method for Moisture in Wool by Oven-Drying. 2013.
- (208) ASTM E1756 - 08(2015) Standard Test Method for Determination of Total Solids in Biomass. 2015.
- (209) ASTM D1762-84, Standard Test Method for Chemical Analysis of Wood Charcoal. ASTM International: West Conshohocken, PA 2013.
- (210) Legarra, M.; Morgan, T.; Turn, S.; Wang, L.; Skreiberg, Ø.; Antal, M. J. *Carbonization of Biomass in Constant-Volume Reactors*; 2018; Vol. 32.
- (211) Ziegler, E. N.; Brazelton, W. T. Mechanism of Heat Transfer to a Fixed Surface in a Fluidized Bed. *Ind. Eng. Chem. Fundam.* **1964**, *3* (2), 94–98.
- (212) Koufopoulos, C. A.; Lucchesi, A.; Maschio, G. Kinetic Modelling of the Pyrolysis of Biomass and Biomass Components. *Can. J. Chem. Eng.* **1989**, *67* (1), 75–84.
- (213) Thurner, F.; Mann, U. Kinetic Investigation of Wood Pyrolysis. *Ind. Eng. Chem. Process Des. Dev.* **1981**, *20* (3), 482–488.
- (214) Font, R.; Marcilla, A.; Verdu, E.; Devesa, J. Kinetics of the Pyrolysis of Almond Shells and Almond Shells Impregnated with Cobalt Dichloride in a Fluidized Bed Reactor and in a Pyroprobe 100. *Ind. Eng. Chem. Res.* **1990**, *29* (9), 1846–1855.
- (215) Liden, A. G.; Berruti, F.; Scott, D. S. A Kinetic Model for the Production of Liquids from the Flash Pyrolysis of Biomass. *Chem. Eng. Commun.* **1988**, *65*, 207–221.

- (216) Blasi, C. Di. Analysis of Convection and Secondary Reaction Effects Within Porous Solid Fuels Undergoing Pyrolysis. *Combust. Sci. Technol.* **1993**, *90* (5), 315–340.
- (217) Wagenaar, B. M.; Prins, W.; van Swaaij, W. P. M. Flash Pyrolysis Kinetics of Pine Wood. *Fuel Process. Technol.* **1993**, *36* (1), 291–298.
- (218) Nunn, T. R.; Howard, J. B.; Longwell, J. P.; Peters, W. A. Product Compositions and Kinetics in the Rapid Pyrolysis of Sweet Gum Hardwood. *Ind. Eng. Chem. Process Des. Dev.* **1985**, *24* (3), 836–844.
- (219) The Energy Balance for Chemical Reactors
<https://www.scribd.com/document/381428810/The-Energy-Balance-for-Chemical-Reactors> (accessed Jun 12, 2018).
- (220) Thermal Conductivity of common Materials and Gases
https://www.engineeringtoolbox.com/thermal-conductivity-d_429.html (accessed Mar 29, 2018).
- (221) Lee, C. K.; Chaiken, R. F.; Singer, J. M. Charring Pyrolysis of Wood in Fires by Laser Simulation. *Symp. Combust. Elsevier* **1977**, *16* (1), 1459–1470.
- (222) Bjoerseth, A.; Ramdahl, T. (eds. . *Handbook of Polycyclic Aromatic Hydrocarbons, Volume 2, Emission Sources and Recent Progress in Analytical Chemistry*; Marcel Dekker, Inc., New York, NY, 1985.
- (223) Van de Kamp, W.; De Wild, P.; Zielke, U.; Suomalainen, M. Tar Measurement Standard for Sampling and Analysis of Tars and Particles in Biomass Gasification Product Gas. *Energy Res. Cent. Netherlands* **2005**.
- (224) Oesch, P.; Leppämäki, E.; Ståhlberg, P. Sampling and Characterization of High-Molecular-Weight Polyaromatic Tar Compounds Formed in the Pressurized Fluidized-Bed Gasification of Biomass. *Fuel* **1996**, *75* (12), 1406–1412.
- (225) Liu, Z.; Balasubramanian, R. Upgrading of Waste Biomass by Hydrothermal Carbonization (HTC) and Low Temperature Pyrolysis (LTP): A Comparative Evaluation. *Appl. Energy* **2014**, *114*, 857–864.
- (226) Thunman, H.; Niklasson, F.; Johnsson, F.; Leckner, B. Composition of Volatile Gases and Thermochemical Properties of Wood for Modeling of Fixed or Fluidized Beds. *Energy & Fuels* **2001**, *15* (6), 1488–1497.
- (227) Richard, N.; Thunman, H. *General Equations for Biomass Properties*. Available at https://www.researchgate.net/profile/Henrik_Thunman/publication/237809816; 2002.
- (228) Sadhukhan, A. K.; Gupta, P.; Saha, R. K. Modelling and Experimental Studies on Pyrolysis of Biomass Particles. *J. Anal. Appl. Pyrolysis* **2008**, *81* (2), 183–192.
- (229) Koufopoulos, C. A. Modelling of the Pyrolysis of Lignocellulosic Materials, Dept. Chem. Engineering, Nat. Tech. Univ. Athens, 1989.

- (230) Charles Becht, I. V. *PROCESS PIPING. The Complete Guide to ASME B31.3 (Charles Becht IV)*; 2002.
- (231) <https://www.swagelok.com/downloads/webcatalogs/en/ms-01-107.pdf>.
- (232) Callahan, F. J. *Swagelok Tube Fitter's Manual*; 1993.
- (233) ASTM E2930-13, Standard Practice for Pressure Decay Leak Test Method. 2013.